.TURBULENT CONVECTIVE PHENOMENA IN

STRAIGHT, RECTANGULAR-SECTIONED DIFFUSERS

by

Devraj Sharma

Thesis submitted for the degree of
Doctor of Philosophy
in the Faculty of Engineering
University of London
.and
for the Diploma of Membership
of Imperial College

Mechanical Engineering Department
Imperial College
London, S.W.7.   September, 1974

ABSTRACT

A numerical method for solving the partial differential equations which govern the transport of mass, momentum, energy, etc. in three-dimensional, confined, boundary-layer flows, is described. The extension of this procedure to handle flows confined in straight ducts of axially-varying cross-section, is presented. The method is shown to be flexible, economical and reasonably accurate in predicting two classes of laminar-flow problems.

A simple turbulence model, akin to the mixing-length hypothesis of two-dimensional boundary-layer situations, is proposed and used in conjunction with the above-mentioned numerical procedure, in predicting fully-turbulent flows in ducts and diffusers. The inadequacies of this model are highlighted and an already-existing two-equation model of turbulence is used to overcome these. This more complex model, is then used to make predictions of turbulent, unstalled flow in straight, rectangular-sectioned diffusers under a large variety of conditions. A few heat-transfer predictions are also reported. In all these situations, detailed comparisons with experimental and analytical evidence, are provided. The favourable nature of these comparisons lend support to the use and development of this prediction procedure as an engineering design tool.

A modest program of experimental research into three-dimensional, turbulent flows in diffusers is also reported. Measurements of static pressure and mean-velocity profiles are made with simple pitot probes. Rectangular-sectioned diffusers of inlet aspect ratio 1 : 1 are considered, and a limited range of included angles and Reynolds numbers covered. The data thus obtained, are used to provide partial corroborative evidence of the prediction procedure mentioned above.

The program of research, both theoretical and experimental, reported in this Thesis is intended as a demonstration of the capability of the numerical calculation procedure. It is not intended to be a detailed investigation of the physical nature of turbulent flows in unstalled diffusers.

PREFACE

This Thesis presents the major part of my research activities during the period 1969 - 1972. These activities centered around the development of a numerical procedure for solving the partial differential equations governing the three-dimensional boundary-layer flow of fluids; they also included the validation of this procedure in predicting turbulent flows in rectangular-sectioned diffusers.

Upon my arrival at the Mechanical Engineering Department of Imperial College, I spent several months in acquainting myself with the two separate numerical methods then in existence for predicting two-dimensional boundary-layer and recirculating flows. It was felt at that time, that such an acquaintance would be the logical first step in the process of developing a method for three-dimensional boundary-layer flows. The task of the latter development was undertaken jointly by David G. Tatchell and myself, under the supervision of Dr. A.D. Gosman and Professor D.B. Spalding. Simultaneously, Dr. R.M. Curr working under the supervision of Professor Spalding was seeking to develop a similar procedure using an alternative formulation of the problem.

It was felt right from the start, that the primitive variables, i.e. velocity components and static pressure, would be the most convenient dependent variables of the differential equations for the solution of which, a numerical procedure was sought. The choice of the grid system and the manner of discretization of the differential equations, were arrived at after much experimentation. Progress however, was very slow and after almost a year, a research group was formed to attempt, through joint effort, at a speedy solution to the problem. This group consisted of Professor Spalding, Drs. A.D. Gosman and L.S. Caretto, David Tatchell and myself. The efforts of this group proved fruitful and gave birth, early in 1971, to the SIVA scheme, described by Caretto, Curr and Spalding [9] . A companion paper by Curr, Sharma and Tatchell [16] presented predictions made with this procedure, of some laminar flows in ducts.

While this procedure was being tested further, Dr. S.V. Patankar joined the group with the intention of developing a method, similar to SIVA, for predicting three-dimensional, external boundary-layer flows. His work resulted in the development of the SIMPLE algorithm, suitable for both internal and external flows. At this stage, I spent some time in close collaboration with Dr. Patankar, participating in the development and testing of a computer program embodying SIMPLE. The tests were also used to compare the capabilities of the two numerical schemes. The comparisons confirmed the expectation that for otherwise identical conditions, the non-iterative SIMPLE scheme would prove to be more economical than the iterative SIVA scheme. I therefore decided to adopt SIMPLE for the subsequent part of my research activities. The results of some of these activities were presented at the First Indian National Conference on Heat and Mass Transfer in Madras in December 1971.

Once the calculation procedure was ready and tested, I followed some suggestions made by Dr. Patankar in devising a simple turbulence model, suitable for use in predicting three-dimensional, turbulent flows in diffusers. Whilst this model was being tested,I devoted the major part of my attention to the experimental program. Over a period of four months, I was able to design the rig, have it fabricated, assembled and commissioned; I then performed a limited range of measurements on rectangular-sectioned diffusers. The data obtained from these measurements, as well as others reported in the literature, were then used by me to compare with numerical predictions. Some of these comparisons brought out the inadequacies of the simple turbulence model.

By this time, the $k \sim \epsilon$ two-equation model of turbulence had come into extensive use in the Mechanical Engineering Department. I therefore set about using this model with the calculation procedure and was able to convince myself of its superiority over the simple model. Confirmation of this fact was achieved by repeating the predictions made earlier, and making detailed comparisons with experimental data. Some unpublished work in this respect was made available to me by Dr. S. Masuda of Keio University, Japan. When this task was completed in October 1972, strained financial circumstances compelled me to take on an engagement of full-time research in the Mechanical Engineering Department. The pres-

entation of this Thesis has consequently been delayed.

I must now express my gratitude to all who provided help, in tangible and intangible ways, during the period of my PhD research activities. Professor Spalding has, at all times, been a source of boundless inspiration; his close involvement with almost all stages of the work resulted in the detection and avoidance of many profitless routes in the achievement of the main goals. His criticisms, though severe, were always constructive. I have learnt a lot from his own adherence to exacting standards, though emulating it has been far from easy.

Dr. Patankar, who was responsible for my coming to Imperial College, has been generous with patient explanations, advice and encouragement when I was most in need. David Tatchell and I worked in close co-operation over many months;this partnership with him has been, for me, a helpful influence. Drs. Gosman, Runchal, Caretto and Wolfshtein, all participated in discussions which proved very valuable to me.

During the course of my experimental program, Fred Bell, Bob King and Laury Allen were always free with help, advice and jokes which made for speedy execution of the program. I cannot thank enough Miss M. P. Steele who smoothed over so many adminstrative problems, and whose friendship has been so valuable to me. My thanks are also due to Miss E. M. Archer for cheerfully allowing me unlimited use of the Library facilities.

To my parents and to Doris Reim, I shall always be indebted; their encouragement meant more to me than I can express.

CONTENTS

LIST OF FIGURES

15

CHAPTER 1

INTRODUCTION

1.1 The problem considered

In this Thesis is described, a procedure for predicting steady, three-dimensional, turbulent flows confined within ducts whose cross-sectional area varies with axial position in a prescribed manner. The prediction procedure is composed of a numerical scheme for solving the partial differential equations which govern the transport of mass, momentum and energy in such flows, and a hypothesis for modelling the turbulence. A feature common to the flows considered, is the existence of a predominant direction of flow. This is one of the features which is used here to classify such flows as three-dimensional boundary layers.

Validation of the prediction procedure is achieved by comparing predicted results with experimental and analytical evidence, over a range of flow situations. Such validation, in this Thesis, is restricted to constant-property, laminar and fully-turbulent flows in the inlet region of straight, rectangular-sectioned ducts and diffusers. The effects of a variety of conditions upon such flows, are examined.

1.2 Practical relevance

The ability to predict the detailed nature of three-dimensional confined flows, and the distributions of energy and matter transported by them is often a matter of practical importance; whether it be for the optimal design of equipment in which they occur, or to aid the understanding of their effects upon the immediate environment, as in effluent transport by rivers.

The kind of flows outlined above abound in engineering practice. Examples may be found in the air-intake passages of many aircraft engines, in fluids transported in ducts of irregular cross-sections,

which may on occasions be coiled in some regular or arbitrary fashion, in river flows and other similar circumstances. Illustrations of a few such situations are provided in figure (1.2-1).
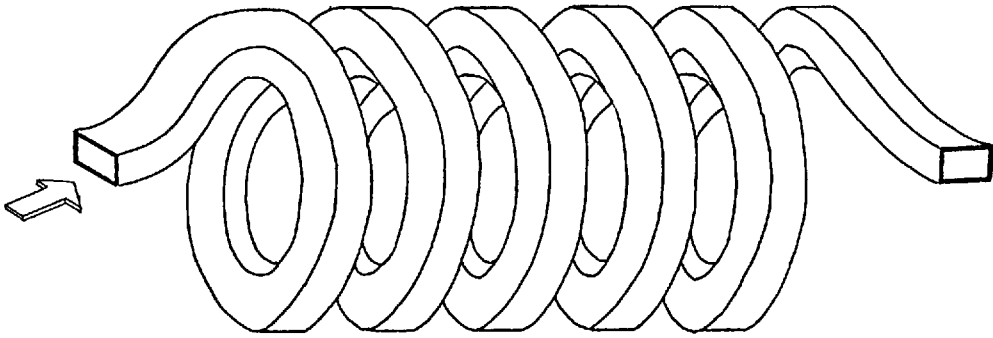
(a)   Flow through coiled ducts.
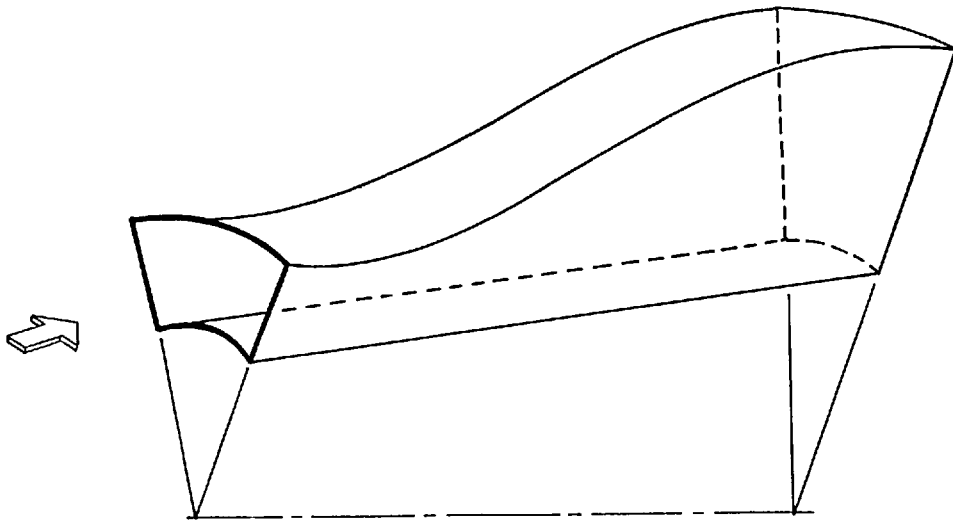
(b)   Flow through annular diffusers.
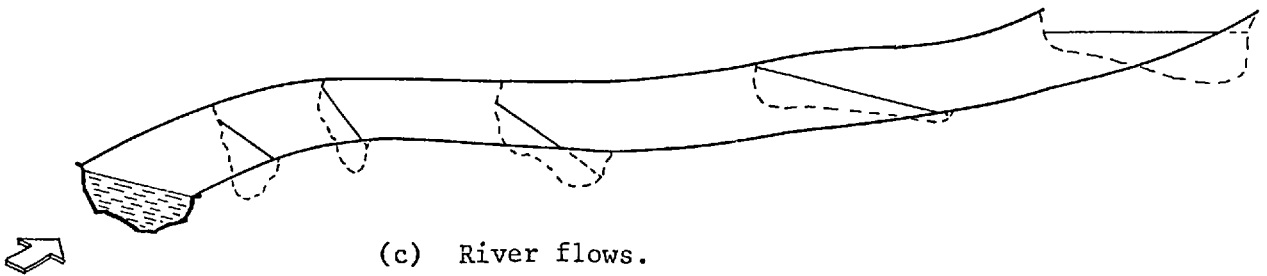
(c)   River flows.

Fig.(1.2.1)   Examples of three-dimensional boundary-layer flows.

1.3   The three-dimensional boundary layer

The term "three-dimensional boundary layer", has been applied
in the literature to a limited class of external flows adhering to
walls (see, for example, Rosenhead /50/). In this Thesis however, fol-
lowing recent practice (Caretto et. al. / 9/ , Patankar and
Spalding / 45/), the definition of the term is generalised to include
a wide range of flow situations of which, the class of external flows
mentioned above, form a part. The physical characteristics of flows
which permit this generalisation are summarised as follows.

Three-dimensional flows which can be classified as boundary
layers, posses the following two features:

1)   There should exist, one predominant direction of
       flow; this shall hereinafter be referred to as the PFD.

2)   Events downstream of any location along the PFD,
       should have <u>no</u> influences upstream of this location;
       for example, flow recirculations along the PFD
       should not occur.

The mathematical consequences of this generalisation are described in
detail in Chapter 2.

Flows in ducts and unstalled diffusers of rectangular cross-
section satisfy the above requirements and hence are referred to as
boundary-layer flows. The important difference between these flows and
the external flows referred to above is that whereas in the former full
account is taken of stresses on planes normal to <u>two</u> directions other
than the PFD, only <u>one</u> such direction is considered in the latter. A
second, less important, difference lies in the manner in which the
pressure-gradient along the PFD is related to the flow-field; whereas,
in the internal flows considered here, it is intimately connected with
the flow-field itself, in external flows it is related to conditions
prevailing in regions outside the flow-field, i.e., the so-called
'free-stream'.

1.4   Historical perspective

The work reported in this Thesis is now placed in perspective with respect to work published in the literature, on rectangular-sectioned ducts and diffusers.

1.4.1   Duct flows

Experimental measurements. Measurements of laminar flow-development in rectangular-sectioned ducts have been reported by the following authors. Sparrow et. al. [59] presented data on pressure-drop and axial-velocity profiles for ducts of aspect ratios 2 : 1 and 5 : 1. Goldstein and Kreid [23] reported similar results for the square-sectioned duct. Beavers et. al. [4] obtained pressure-drop data in ducts of aspect ratios ranging from 1 : 1 to 59 : 1. Yu and Sparrow [66] reported similar measurements in duct of aspect ratio 82 : 1, in which one wall was permitted to move longitudinally in a steady manner. Each of these studies was conducted over a range of Reynolds number. Experimental work pertaining to large aspect-ratio ducts, has been listed by Fan and Hwang [18]

Measurements of pressure-drop and friction factors for turbulent flow in rectangular-sectioned ducts, have been reviewed by Harnett et. al. Since this work was published, more detailed measurements have been reported by Ahmed [1] , Ahmed and Brundrett [2] , and others; a detailed list of such studies is available in Tatchell [60]. As part of   a study of diffusers, several authors reported measurements of pressure-drop and profiles of axial velocity, across the two centre-planes of ducts, i.e. zero-angle diffusers. These authors include Masuda et.al [38] , Wolf and Johnstone [65], and Masuda [37]; their measurements were obtained in the inlet region of ducts of aspect ration 2 : 1, 4 : 1 and 2 : 1 respectively, and covered a range of inlet   turbulence intensities and velocity distributions.

Analytical studies. Several authors have presented analytical results for constant-property, laminar flow development in straight ducts, with aspect ratio as parameter; among these are Han [25] , Lundgren et. al. [36] , Fleming and Sparrow [20] , and Wiginton and Dalton [64].

Their approaches consisted essentially of analytical integrations of linearized forms of the axial momentum equation, in conjunction with an integral continuity equation. The difference between the above approaches, lies in the manner in which the axial momentum equation is linearized. Miller /41/ has applied a numerical procedure, valid for fully three-dimensional flows, to laminar flow in the entrance region of a square-sectioned duct. With the exception of Ahmed /1/ , analyses of turbulent three-dimensional duct flows do not appear to have been reported in the literature.

1.4.2   Diffuser flows

Experimental measurements. The study of turbulent flows confined within rectangular diffusers has formed the subject of numerous publications. A review of the substantial proportion of these published results, has been made by Reneau et. al. /47/ . Detailed measurements have been made of the various flow regimes within diffusers from un-stalled flow (e.g. Carlson /10/), through transitory stall (e.g. Smith and Kline /56/) and fully-developed stall (e.g. Chin and Kline /14/), to jet flow. The unstalled flow regime has been subject to extensive investigation. The effects of inlet aspect ratio were measured by Johnstone and Powars /32/ who also reviewed the earlier work in this area. The effects of different wall shapes on straight, rectangular-sectioned diffusers were studied by Carlson et.al./11/ ; Norbury /42/ reported measurements of pressure-recovery and centre-line velocity decay in a trumpet-shaped diffuser. Experimentally-determined values of geometries that provided maximum pressure-recovery with little or no stall were published by Sovran and Klomp /57/ .

Several authors have reported studies of the effects of a variety of conditions at the inlet to diffusers upon their performance. These include Bradley and Cockrell /5/ , and Waitman et. al. / 62/. Particular attention has been paid to the effects of shear flow at inlet to diffusers by Horlock and Lewis /31/ , Masuda et. al. /38/ , Wolf and Johnstone /65/ and others.

Improvements in diffuser performance by tangential injection of fluids have been affected by Fiedler and Gessner [19] . Similar results were reported by Furuya et. al.[22] and Rockwell [48] who studied the effects of extraction of fluid from regions of low momentum within diffusers.

The flow patterns within curved, rectangular-sectioned diffusers were first observed by Fox and Kline [21] . Subsequently these results were augmented by Sagi et. al. [52] . Numerous observations, both qualitative and quantitative, have been reported of the performance of diffusers of arbitrary shape used in engineering practice; the work by Sakurai [53] is one example.

Detailed measurements of heat transfer in rectangular-sectioned diffusers have been sparingly reported. Ellison [17] , obtained measurements of temperature profiles and Stanton number in a low aspect ratio diffuser. Similar results were obtained by 'Hool as quoted by Carmichael and Pustintsev [12] .

Analytical investigations. The analyses of turbulent flow within rectangular-sectioned diffusers, have been restricted mainly to the momentum-integral type. Cocanover et. al. [15] provide one such method and indicate how this may be applied to diffusers of several geometric configurations. Modifications to momentum-integral methods in order to handle special circumstances have been reported by several authors (e. g. Bradley and Cockrell [5] , Wheeler and Johnstone [63] etc.), but none appear to be generally applicable to all geometric shapes, inlet conditions or aspect ratios.

Horlock and Lewis [31] , and Livesey and Turner [35] , provide interesting potential flow methods to take account of shear flow within large aspect-ratio diffusers. They appear however to suffer from the same deficiencies as the above.

1.4.3   Numerical calculation procedures

Numerical procedures for the integration of the partial differential equations of convective motion have been reported by several

authors. Patankar and Spalding /44/ , presented a scheme designed for two-dimensional boundary layers. Gosman et. al. /24/ reported a method applicable to two-dimensional recirculating flows.

In recent years, several authors have published numerical methods designed to make calculations of two- and three-dimensional steady and unsteady flows. Among these are Harlow and Welch /28/ , Chorin /13/ , and Amsden and Harlow /3/ .

A procedure for solving the equations of three-dimensional boundary-layer motion, was first reported by Caretto et. al. /9/ . This procedure was used to make predictions of some laminar, confined flows which were reported by Curr et. al. /16/ . Subsequently, a method designed to solve the identical problem was developed by Patankar and Spalding /45/ . It is an extension of this procedure that has been used in the present work.

Two reviews of existing calculation procedures for steady, three-dimensional, external boundary layers have been made. They are due to Patankar /43/ and Wheeler and Johnstone /63/ .

1.4.4   Mathematical models of turbulence

Dating from Prandtl's mixing-length hypothesis, numerous authors have applied simple algebraic models to the prediction of turbulent, confined flows, e.g. Hinze /30/ . In a recent review, Launder and Spalding /33/ trace the development of turbulence modelling in internal flows.

Present day turbulence models are necessarily complex; they require, in general, the solution of partial differential equations governing the transport of turbulence quantities. Such equations have been derived by several authors and have been reported by Harlow and Nakayama /27/ , Rodi /49/ , Harlow /26/ and others. Multiple-equation turbulence models have been successfully applied to a variety of flow situations (e.g. Launder and Spalding /34/). One such model, requiring the solution of two equations, has been adapted for use in the present work.

1.5   Strategy of the present investigation

This Thesis reports both theoretical and experimental investigations of three-dimensional, turbulent flows confined within rectangular-sectioned ducts and diffusers. The strategy adopted for this work is summarised as follows:

1) Predictions were first obtained of several laminar
   flow situations. These predictions were compared
   with available experimental and analytical evidence
   in order to validate the numerical calculation pro-
   cedure.

2) Extension of this calculation procedure was made to
   permit its application to flows within ducts with
   axially-varying cross-sections.

3) A mathematical model of turbulence was developed
   and tested in its ability to predict fully-turbu-
   lent flows in the above geometric configurations.

4) Validation of the prediction procedure consisting
   of the numerical calculation procedure and the
   mathematical model of turbulence was carried out.

The path followed in implementing the above strategy is summarised as follows:

1) Performance of a thorough review of the existing
   information on three-dimensional duct and diffuser
   flows; collection and collation of this information
   was achieved in a manner suitable for making compari-
   sons with predictions.

2) Comparison of numerical predictions of laminar flows
   with available information in order to permit an assess-
   ment, of the accuracy of the solutions as well as the
   stability and convergence rates of the calculation pro-
   cedure, to be made.

3) Identification, from the literature review, of areas wherein experimental investigations into three-dimensional diffuser flows, might profitably be made. Conducting such studies to obtain data useful in performing validation tests on as many aspects of the prediction procedure as possible.

4) Conducting such validation exercises by comparing predictions of a wide range of flow situations with analytical and experimental evidence collected from independent sources.

1.6   Layout of the Thesis

The rest of this Thesis is divided into four parts. In Part I, comprising Chapters 2, 3 and 4, a detailed description of the theoretical work, is provided. This includes a derivation of the differential equations, their numerical discretization procedure and a description of the manner of solution of the resulting algebraic equations, which form the subject matter of Chapters 2 and 3. Chapter 4 confines itself to details of the two models of turbulence used in this work.

The experimental program undertaken in this work, is described in Part II. Details of the objectives of this program, and the design, fabrication and use of the apparatus used therein are provided in Chapter 5. In Chapter 6, an evaluation of the data obtained in the experimental investigation, is made.

The prediction of a wide range of laminar and turbulent flow situations as well as an assessment of the turbulence models used, form the subject matter of Part III. Accordingly, while Chapter 7 describes predictions of laminar flows, comparison of predictions with experimental and analytical results for turbulent flow, are provided in Chapter 8. In Chapter 9, a summary is made of the work performed, conclusions thereof are drawn and suggestions made for future work.

Part IV comprises a list of references, a description of the nomenclature used in this Thesis and four Appendices. The latter contains information supplementary to the theoretical work descri'.ed in Part I as well as tabulated forms of experimental data obtained from the program described in Part II.

PART   I

Theoretical Investigation

CHAPTER 2

THE MATHEMATICAL PROBLEM

2.1   Introduction

This chapter describes the formulation of the mathematical prob-
lem. The description consists first of a brief derivation of the par-
tial differential equations which govern the transport of mass, momen-
tum, energy and other scalar fluid properties in steady three-dimen-
sional boundary-layer flows. In this derivation, the equations of three-
dimensional fluid motion expressed in cartesian-tensor form, are used
to arrive at a set of equations represented in a quasi-orthogonal cur-
vilinear co-ordinate system. Next, the initial and boundary conditions
on the dependent variables of this equation set, that are required to
be specified, are described. Following this, the physical hypotheses
necessary to complete the problem specification, are detailed. Finally,
a summary is provided of the approximations involved in arriving at the
mathematical description of the problem.

2.2   The governing differential equations

The partial differential equations which govern steady, three-
dimensional motion of fluids can be expressed as follows:

Continuity

$$\frac{\partial (\rho U_i)}{\partial x_i} = 0 \qquad\qquad , \; (2.2.1)$$

transport of momenta (three components, j)

$$\frac{\partial (\rho U_i U_j)}{\partial x_i} = \rho U_j - \frac{\partial \sigma_{ij}}{\partial x_i} \qquad\qquad , \; (2.2.2)$$

transport of scalar fluid property, ϕ

$$\frac{\partial(\rho U_i \phi)}{\partial x_i} = s^\phi - \frac{\partial J_{\phi,i}}{\partial x_i} \qquad , (2.2.3)$$

where the symbols are defined as follows:

U_i $\equiv$ velocity component in each of the three co-ordinate directions, i ;

x_i $\equiv$ corresponding co-ordinate axis;

U_j $\equiv$ momentum per unit mass transported along the jth direction;

σ_{ij} $\equiv$ complete stress tensor;

s^{U_j} $\equiv$ source (and/or sink) of U_j;

ϕ $\equiv$ transported scalar fluid property;

s^ϕ $\equiv$ source (and/or sink) of ϕ;

$-J_{\phi,i}$ $\equiv$ flux of ϕ along the ith direction;

and $\rho \equiv$ fluid density.

The conventional Newtonian approximations are now made concerning the diffusion of momenta and other properties, ϕ. Accordingly, the following relations are applied to equations (2.2.2) and (2.2.3) respectively.

$$-\sigma_{ij} = -p\,\delta_{ij} + \mu\left\{\frac{\partial U_i}{\partial x_j} + \frac{\partial U_j}{\partial x_i}\right\} \qquad , (2.2.4)$$

$$-J_{\phi,i} = \Gamma_\phi \frac{\partial \phi}{\partial x_i} \qquad , (2.2.5)$$

where $p \equiv$ static pressure;

δ_{ij} , the Kronecker - delta function;

$\mu \equiv$ dynamic viscosity of the fluid;

$\Gamma_\phi \equiv$ coefficient in the "diffusion-law" (2.2.5),

defined by :

$$\Gamma_\phi = \frac{\mu}{Pr_\phi} \qquad , \ (2.2.6)$$

Pr_ϕ , being the Prandtl/Schmidt number appropriate to the transport of ϕ .

2.2.1 The boundary-layer approximations

The mathematical consequences of the generalised definition given to three-dimensional boundary layers in Chapter 1, are considered in this section.

1) Let there exist a predominant direction to the flow represented by equations (2.2.1) to (2.2.3); furthermore, let this direction (PFD) be aligned with the x_1-direction.

2) The requirement that, along this direction, downstream conditions have no influence upon upstream events implies that:

a) The *diffusion* fluxes of momentum, energy and other scalar properties along the PFD are negligible. Thus:

$$\tilde{\sigma}_{x_1 j} \approx 0 \qquad \qquad , \ a) \Big\}$$

$$J_{\phi, x_1} \approx 0 \qquad \qquad , \ b) \Big\} \qquad (2.2.7)$$

b) The downstream pressure-field has negligible influence upon upstream flow conditions.

It is the satisfaction of the latter requirement that necessitates the deliberate introduction of an inconsistency in the treatment of pressure. The nature of this inconsistency is discussed at length by Caretto et. al. / 9 / , and Patankar and Spalding / 45 / .Here it is merely noted that the pressure-gradient appearing in the x_1-direction

(i.e. PFD) momentum equation is presumed to be de-coupled from the pressure-gradients appearing in the momentum equations corresponding to the x_2 and x_3 directions. This practice is a necessary step towards making x_1 a truely "one-way" co-ordinate, i.e. one along which upstream conditions determine down-stream events but not vice versa. Accordingly, the pressure-gradients driving the three velocity components are expressed as follows:

x_1 - direction: $\qquad -\dfrac{\partial \bar{p}}{\partial x_1}$

x_2 - and x_3 - directions: $-\dfrac{\partial p}{\partial x_2}$, and $-\dfrac{\partial p}{\partial x_3}$ respectively.

The implications of this de-coupling upon the solution procedure are elaborated in Chapter 3.

When the afore-mentioned conditions 1) and 2) are applied to equations (2.2.2) and (2.2.3), there results a set of parabolic equations. It is the parabolic nature of these equations which permits the freedom to employ marching-integration procedures for their solution.

The representation of flows within ducts whose cross-sections vary with axial position, cannot conveniently be achieved through such parabolic equations expressed in orthogonal co-ordinate systems. It is to overcome this inconvenience that the set of derived equations is recast in terms of a curvilinear quasi-orthogonal co-ordinate system.

2.2.2 A curvilinear co-ordinate system

The curvilinear system of co-ordinates chosen for use in the present work, is quasi-orthogonal. It is stipulated that whereas two of the co-ordinate axes (i.e. x_2 and x_3) maintain mutual orthogonality throughout the flow-field, the third (i.e. x_1) is permitted to depart from orthogonality with respect to the other two, within specified limits. It is demonstrated below that these limits are consistent with the boundary-layer approximations defined above.

The elements of the curvilinear system (ξ, η, ζ) are defined in terms of orthogonal, cartesian co-ordinates (for convenience represented here as (x, y, z)), as follows:

$$\xi \approx x \qquad\qquad , \qquad \text{a)}$$

$$\eta \equiv \frac{y - y_S}{y_N - y_S} \qquad , \qquad \text{b)}$$

$$\text{and} \quad \zeta \equiv \frac{z - z_W}{z_E - z_W} \qquad , \qquad \text{c)}$$

$$(2.2.8)$$

The definitions (2.2.8) can best be appreciated with reference to figure (2.2.1). The subscripts N, S, E, and W, refer respectively to the North, South, East and West boundaries of the calculation domain in the y~z plane. The co-ordinates η and ζ are mutually orthogonal for all values of ξ. Furthermore, planes of constant-ξ are approximated as planes of constant-x.

The components of velocity U, V and W are now defined as follows: V and W are normal to the x~z and x~y planes respectively, i.e. are aligned with the η and ζ co-ordinate directions. U is normal to constant-ξ planes, but is permitted to depart from alignment with ξ by small angles; the limits of this inclination are prescribed below. The following mathematical consequences result from the above definitions.

The co-ordinates (ξ, η, ζ) satisfy the general relationships:

$$\frac{\partial}{\partial x} = \frac{\partial}{\partial \xi} \cdot \frac{\partial \xi}{\partial x} + \frac{\partial}{\partial \eta} \cdot \frac{\partial \eta}{\partial x} + \frac{\partial}{\partial \zeta} \cdot \frac{\partial \zeta}{\partial x}$$

$$\frac{\partial}{\partial y} = \frac{\partial}{\partial \xi} \cdot \frac{\partial \xi}{\partial y} + \frac{\partial}{\partial \eta} \cdot \frac{\partial \eta}{\partial y} + \frac{\partial}{\partial \zeta} \cdot \frac{\partial \zeta}{\partial y}$$

$$\frac{\partial}{\partial z} = \frac{\partial}{\partial \xi} \cdot \frac{\partial \xi}{\partial z} + \frac{\partial}{\partial \eta} \cdot \frac{\partial \eta}{\partial z} + \frac{\partial}{\partial \zeta} \cdot \frac{\partial \zeta}{\partial z}$$

$$(2.2.9)$$

calculation
domain

Fig.(2.2.1)   Illustration of the quasi-orthogonal co-ordinate
              system; the circled characters represent the
              North, South, East and West boundaries of the
              calculation domain.

It can be deduced that, on applying the definitions (2.2.8) to these
relationships, the effect of non-orthogonality of the ξ - co-ordinate
with respect to η and ζ , are negligible only if the following con-
ditions are satisfied:

$$\frac{d\xi}{dx} \approx 1 \qquad , \quad \text{a)}$$

$$\text{and} \quad \frac{d\eta}{dx} , \frac{d\zeta}{dx} \ll 1 \qquad . \quad \text{b)} \qquad (2.2.10)$$

Since the conditions (2.2.10 b) are similar to the relationships (2.2.7),
it is concluded that the set of assumptions embodied in (2.2.10) are
consistent with those of (2.2.7). The definitions (2.2.8) along with the
conditions (2.2.10), thus permit the transport equations to be expressed
in curvilinear co-ordinates, whilst retaining their boundary-layer
character.

A useful digression is made here. The conditions (2.2.10 b) are
related to the area-ratio variation along the axes of diffuser flows.
It is well-known that this variation must be small, to maintain the un-
stalled flow regime within diffusers. Since stall, or axial-flow re-
circulation violates the conditions required for boundary-layer flows,
the above conditions are consistent with the physical nature of dif-
fuser flows examined in this Thesis.

2.2.3   The general transport equations in curvilinear co-ordinates

The approximations of Section (2.2.1) along with the definitions
of Section (2.2.2) when applied to the general equations (2.2.1)   to
(2.2.3), result in a set of differential equations that govern three-
dimensional, boundary-layer flows in ducts with axial-variations in
cross-section. Recognising the similarity of equations (2.2.2) and
(2.2.3), this set is expressed in a general form as follows:

continuity

$$\frac{\partial(\rho U)}{\partial\xi} + \frac{1}{(y_N - y_S)}\frac{\partial}{\partial\eta}\left\{\rho V - \rho U\left[\frac{dy_S}{dx} + \eta\frac{d(y_N - y_S)}{dx}\right]\right\}$$

$$+ \frac{1}{(z_E - z_W)}\frac{\partial}{\partial\zeta}\left\{\rho W - \rho U\left[\frac{dz_W}{dx} + \zeta\frac{d(z_E - z_W)}{dx}\right]\right\}$$

$$= 0 \qquad , \quad (2.2.11)$$

transport of fluid property, ϕ

$$\frac{\partial(\rho U \phi)}{\partial\xi} + \frac{1}{(y_N - y_S)}\frac{\partial}{\partial\eta}\left\{\left(\rho V - \rho U\left[\frac{dy_S}{dx} + \eta\frac{d(y_N - y_S)}{dx}\right]\right)\phi\right\}$$

$$+ \frac{1}{(z_E - z_W)}\frac{\partial}{\partial\zeta}\left\{\left(\rho W - \rho U\left[\frac{dz_W}{dx} + \zeta\frac{d(z_E - z_W)}{dx}\right]\right)\phi\right\}$$

$$= S_\phi + \frac{1}{(y_N - y_S)^2}\frac{\partial}{\partial\eta}\left\{\Gamma_\phi\frac{\partial\phi}{\partial\eta}\right\} + \frac{1}{(z_E - z_W)^2}\frac{\partial}{\partial\zeta}\left\{\Gamma_\phi\frac{\partial\phi}{\partial\zeta}\right\} \quad (2.2.12)$$

In the above equation, ϕ is taken to represent any fluid property transported by the flow, <u>including</u> the three components of momenta per unit mass, U, V and W. The detailed nature of the equations for each such property is provided in Appendix A 1. In the above equations the quantities within square brackets are consequences of the curvilinear nature of the geometry confining the flow.

2.3 Auxiliary information

In addition to the set of equations represented by (2.2.11) and (2.2.12), the complete specification of the mathematical problem of three-dimensional boundary layers requires:

a) Initial conditions, i.e. initial values of dependent variables corresponding to the position of the co-ordinate along the PFD (i.e. ξ) at which solutions to the set of equations are begun.

b) Boundary conditions, i.e. conditions of all the
dependent variables at the E, W, N and S boundaries,
as a function of ξ .

c) Auxiliary relationships, which allow the density,
diffusion coefficients, sources and sinks in each
of the equations, to be computed in terms of the
dependent variables of these equations, over the
entire flow-field.

The auxiliary information supplied to the solution procedure in the
present work is described in Chapter 3 and Appendix A 1.

2.4   Summary

The contributions of this chapter may be summarised as
follows:

1) A derivation is provided of the partial differential
equations which govern the transport of mass, momen-
tum, energy etc. in three-dimensional boundary-layer
flows.

2) These equations are represented in terms of a curvi-
linear, quasi-orthogonal co-ordinate system. This
practice makes convenient, the representation of
flows within ducts with moderate variations in cross-
section with axial position.

3) The auxiliary information required to complete the
problem specification is enumerated.

It is left to seek a solution procedure for this mathematical
problem. Such a procedure is described in Chapter 3.

CHAPTER 3

THE SOLUTION PROCEDURE

3.1   Introduction

In this chapter, details are provided of a numerical scheme reported by Patankar and Spalding [45] , for the solution of the mathematical problem described in Chapter 2. The common features of this scheme termed SIMPLE (for Semi-Implicit Method for Pressure-Linked Equations), with that proposed by Caretto et. al. [9] and called SIVA (for Simultaneous Variable Adjustment) are first described. Then, following a brief outline of the SIVA algorithm, a more detailed account is given of the SIMPLE algorithm. A series of unpublished tests performed by the author has indicated that the latter procedure is more economical for use in confined-flow situations than the former. It is for this reason that the SIMPLE procedure was used throughout this work.

The layout of the rest of this chapter is as follows: Section 2 reports the procedures adopted in the discretizations of equations (2.2.11) and (2.2.12). The computational structures of the SIVA and SIMPLE schemes, with attention to the differences between them, are outlined in Section 3. In Section 4, the manner of incorporation of auxiliary information into the computational procedure, is briefly outlined. Remarks on the convergence rates and stability of the procedure, and assessments of the accuracy of the results obtained, are made in Section 5 . A brief summary concludes the chapter.

3.2   The discretization procedure

The first step in the development of a numerical scheme for solving equations (2.2.11) and (2.2.12), is to obtain discretized equivalents for them. This is described in the following sections.

3.2.1 The grid system

The numerical grid used consists of:

a) A system of intersecting, orthogonal grid lines in
the $\eta \sim \zeta$ planes. No restrictions are placed upon
the spacing between the lines in any given direc-
tion.

b) Planes of constant ξ , at which solutions are ob-
tained, are arrived at by taking successive in-
crements along the ξ (i.e. PFD) direction. There
is again no intrinsic restriction placed upon the
manner of these increments, hereafter termed the
forward step size, $\Delta\xi$. The limits on the size of
the forward step are governed by considerations of
stability and accuracy of the numerical procedure.

In obtaining the predictions reported in this Thesis, the spacings be-
tween the grid lines a) as well as the forward step sizes b) were non-
uniform. Details of the grid dispositions used are provided in Appen-
dix A3.

3.2.2 Location of variables on the gird

The intersections of the grid lines mentioned above are termed
grid nodes. All the fluid properties with the exception of the velocity
components V and W, are presumed to be located at such grid nodes. The
velocity V is presumed to be located exactly midway between grid nodes
in the η-direction and velocity W similarly located along the ζ-di-
rection. Figure (3.2.1) indicates the grid system in the $\eta \sim \zeta$ plane,
superposed upon which are the locations where variables are stored. This
"staggered" location of variables is similar to that reported by other
workers (e.g. Amsden and Harlow [3]). Such "staggering" of variable
locations possesses two advantages:

a) Velocity components V and W are stored at just the
points at which they are required when mass balances

are made over the control volume surrounding each
grid node; also, their location makes convenient the
calculation of convective contributions to the bal-
ance of ϕ over such control volumes.
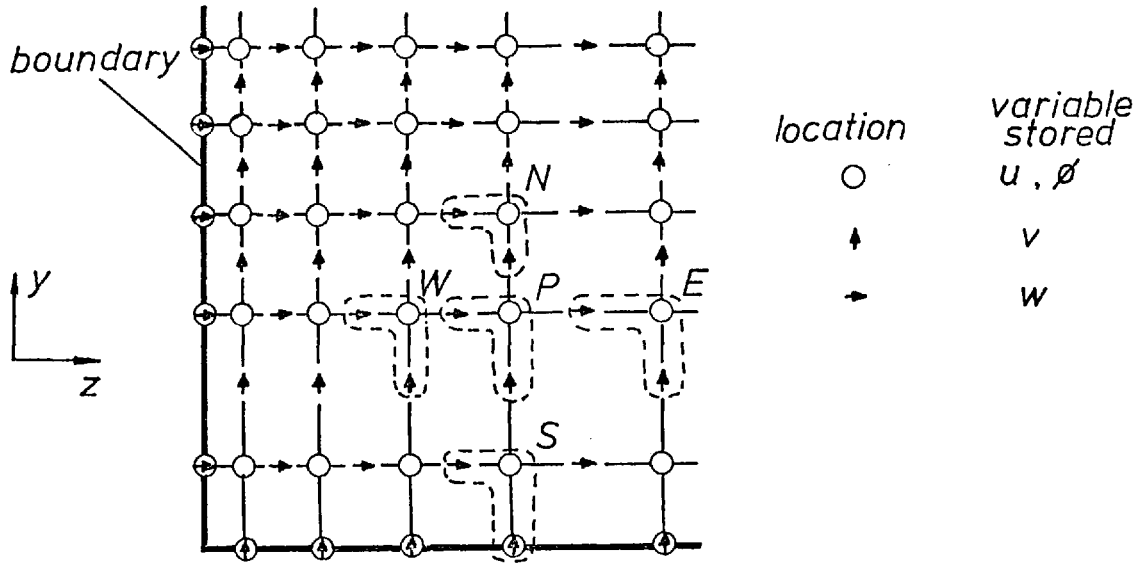
Fig.(3.2.1) Staggered location of variables.

b) Pressures, stored at the grid nodes themselves, en-
sure ease in the calculation of pressure-gradients
that affect the V and W momentum equations.

In the algebra connected with the discretization procedure, when
a variable is required at points other than those at which it is located,
averages of neighbouring values are used to arrive at the value of the
variable at that point.

3.2.3 The control volumes

The control volume surrounding each grid node P, indicated in
figure (3.2.2), has two faces that coincide with two constant $-\xi$ planes.
One of these, at which integrations of the partial differential equations

are to be performed, is designated the downstream (D) station.
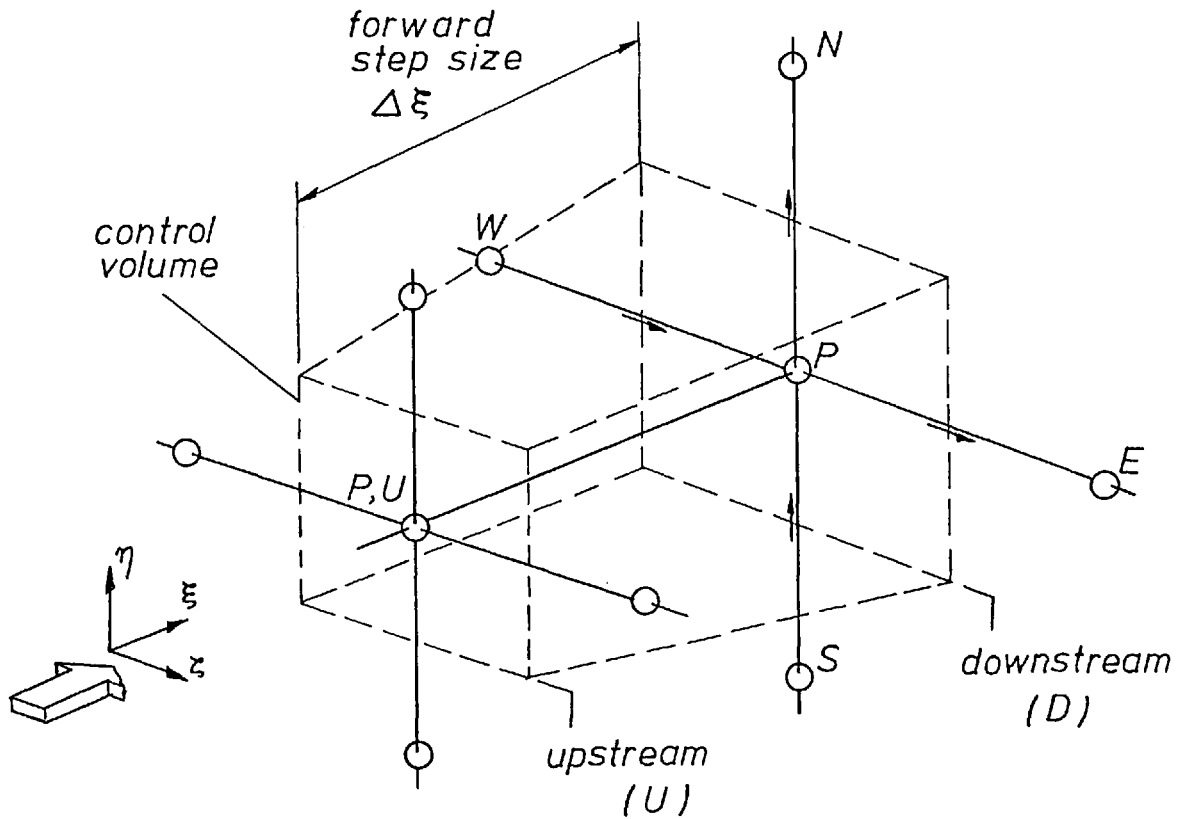
Fig.(3.2.2)   Finite - difference control volume.

The other faces are so located that, the velocity components giving rise to convective fluxes along the η and ζ directions, are located on the faces themselves. Figure (3.2.3), illustrates this point, with reference to a cross-section of the control volume in the $\xi \sim \eta$ plane. It is over such control volumes, that balances of U, ϕ and mass are made in the calculation procedure. Similar control volumes, resulting from the "staggering" of locations on the grid, are defined to surround the locations of the V and W velocity components. Three sets of control volumes, are thus identifiable over the entire calculation domain.
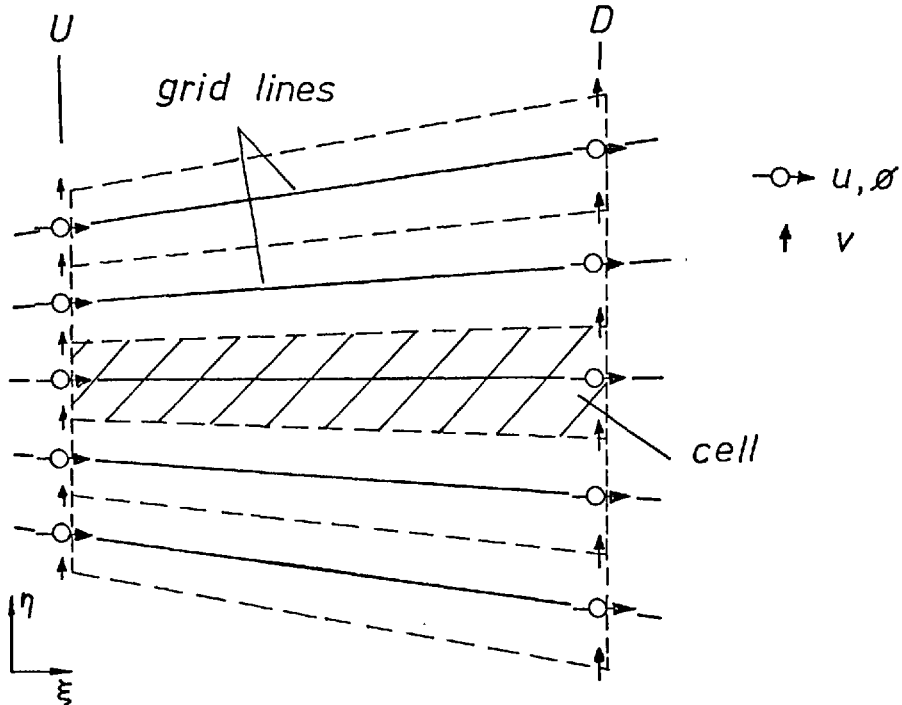
Fig.(3.2.3) Control volume when the grid expands to accomodate
             exactly the diffuser shape. Note the inclination
             of the U-velocity arrow with grid lines.

3.2.4   The near-boundary region

A slight modification to the variable-location and control-
volume definitions is made in the region of boundaries of the calcu-
lation domain. Such boundaries are positioned along lines passing through
points where the velocity components normal to the boundaries are lo-
cated. The modification to the variable-location concept lies in speci-
fying grid nodes, corresponding to the above velocity locations, to be
located at the boundaries as well. This modification, clearly observable
in figure (3.2.1), results in a change in control-volume definitions.
The control volumes corresponding to the near-boundary velocities, V in
the case of N and S and W in the case of E and W boundaries, are now
fifty per cent larger than their value within the rest of the flow-
field, for a uniform grid disposition. Figure (3.2.4) illustrates the
near-boundary control volumes.

near-boundary
V-control volume
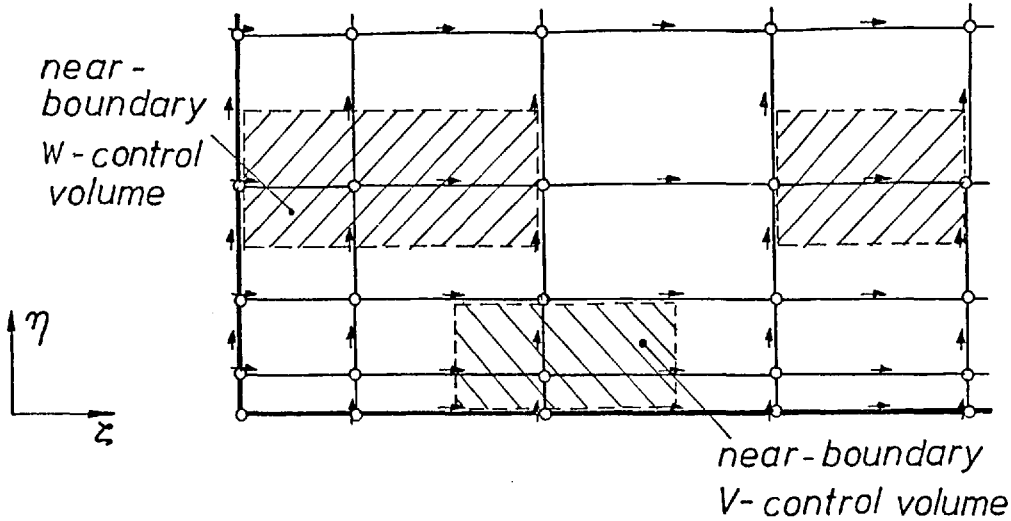
Fig. (3.2.4) The near-boundary modification
to control volumes.

3.2.5 The discretized equation

The manner in which the discretized forms of the equation
set (2.2.12) is arrived at is as follows. Integrations of the partial
differential equation governing the transport of each variable are
performed, for each location of the variable, over the control volume
that encloses this location. These integrations are performed after
making presumptions about the manner in which the variable is distrib-
uted between grid nodes. All variables were presumed so to vary,
linearly in the η - and ζ -directions and in step-wise fashion along
the ξ -direction. The result of these operations is an algebraic
equation for each grid location, representing the discretized form of
the balance of the variable, over the control volume corresponding to
that location. For a general dependent variable ϕ , this equation takes
the form:

$$\left\{ c_P^\xi \phi_P - c_{P,U}^\xi \phi_{P,U} \right\} + \left\{ c_\eta^\eta \left[\phi_N + \phi_P \right] - c_s^\eta \left[\phi_P + \phi_S \right] \right\}$$

$$+ \left\{ c_e^\zeta \left[\phi_E + \phi_P \right] - c_w^\zeta \left[\phi_P + \phi_W \right] \right\} = S^\phi +$$

$$\left\{ D_\eta^\eta \left[\phi_N - \phi_P \right] - D_s^\eta \left[\phi_P - \phi \right] \right\}$$

$$+ \left\{ D_e^\zeta \left[\phi_E - \phi_P \right] - D_w^\zeta \left[\phi_P - \phi_W \right] \right\} \qquad \cdot (3.2.1)$$

Here, C's are appropriate to convective contributions,
  D's the diffusive, and S the source (and/or sink)
    contributions to the balance of ϕ.

The subscripts are associated with pointson the grid system
and superscripts to the co-ordinate directions for which the coefficient
is appropriate.

Before proceeding to define the terms of equation (3.2.1),
attention is drawn to the manner of discretization of the convective
terms in the η- and ζ-directions. In this Thesis, two approaches,
leading essentially to the same results, have been successfully used.

The problem lies in calculating the value of a variable at the
face of a control volume, that is convected across that face. For example,
considering figure (3.2.5), it is required to determine the
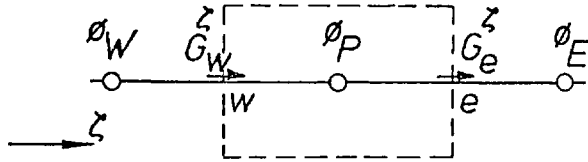
Fig.(3.2.5)

value of ϕ that is convected across face w by the mass-velocity G_w^ζ.
Simple averaging schemes often lead to severe problems of convergence,
often delaying it or even causing divergence of calculation procedures
for convective flows (e.g. Burggraf [8]). Several authors (e.g. Gosman
et. al. [24] , Spalding [58]) have proposed remedial measures.

One of these measures consists of using forward or backward
differencing for the convective term along any given direction depending
upon whether the local convective flux is positive (i.e. forward) or
negative (i.e. backward). This is expressed algebraically as:

$$\phi_w = \frac{1}{2}\left[\phi_W \left\{ G_w^\zeta + |G_w^\zeta| \right\} + \phi_P \left\{ G_w^\zeta - |G_w^\zeta| \right\} \right] \qquad ,(3.2.2)$$

where,   the $G's$ represent the ζ-direction mass-valocities
at the w-location.

Thus, the value of ϕ at w is ϕ_W or ϕ_P depending upon whether G_W is
positive or nagative. The upwind-differencing practice was adopted with
the SIVA scheme.

A second, hybrid method of discretizing the convective terms
in equation (2.2.12), was used with the SIMPLE algorithm. Designated as
the high-lateral-flux modification, its application to two-dimensional
flows is discussed in detail in the book by Patankar and Spalding [44] .
This method, consisting of a modification of the coefficients of the
discretized equation, and called the high-lateral-flux modification, is
described below.

The coefficients of equation (3.2.1) are now defined, with
reference to figure (3.2.6).
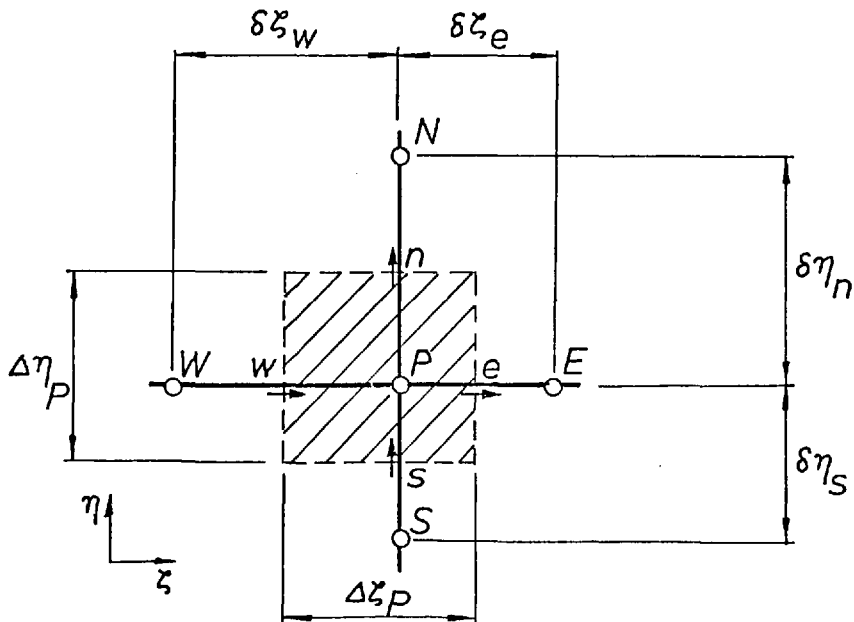
Fig.(3.2.6)   Grid nomenclature for discretization
procedure.

$$c^{\xi}_{P,U} = (\rho U)_{P,U} \, \Delta\eta_{P,U} \, \Delta\zeta_{P,U} \qquad , (a)$$

$$c_j^{\eta} = \left\{ \rho V - \rho U \left[\frac{dy_s}{dx} + \eta \frac{d(y_N - y_s)}{dx} \right] \right\}_j \Delta \zeta_P \Delta \xi \qquad , (b)$$

$$c_i^{\zeta} = \left\{ \rho W - \rho U \left[\frac{dz_w}{dx} + \zeta \frac{d(z_E - z_w)}{dx} \right] \right\}_i \Delta \eta_P \Delta \xi \qquad , (c)$$

$$C_P^{\xi} = c_{P,U}^{\xi} + c_n^{\eta} - C_s^{\eta} + c_e^{\zeta} - c_w^{\zeta} \qquad , (d)$$

$$D_j^{\eta} = \Gamma_{\phi j} \frac{\Delta \zeta_P \Delta \xi}{\delta \eta_j} \qquad , (e)$$

$$D_i^{\zeta} = \Gamma_{\phi i} \frac{\Delta \eta_P \Delta \xi}{\delta \zeta_i} \qquad , (f)$$

$$S^{\phi} = (s^{\phi})_P \Delta \xi \Delta \eta_P \Delta \zeta_P \qquad , (g)$$

$$\left. \begin{array}{c} \\ \\ \\ \\ \\ \\ \\ \end{array} \right\} (3.2.3)$$

where, Δ's , and δ's   represent the widths of control-volume faces and internodal distances respectively,

i and j stand for locations (e, w) and (n, s) respectively,

$\Delta \xi$ is the forward step size,

and S^{ϕ} is the integrated form of the source (and/or sink) of ϕ .

On rearranging the terms of equation (3.2.1), one obtains:

$$\sum_{i=E,W,N,S,P_U} A_i' \phi_P = \sum_{i=E,W,N,S} A_i' \phi_i + S_P^{\phi} \qquad , \qquad (3.2.4)$$

where:

$$A_E' = D_e^{\zeta} - \tfrac{1}{2} c_e^{\zeta} \qquad , (a)$$

$$A_W' = D_w^{\zeta} + \tfrac{1}{2} c_w^{\zeta} \qquad , (b)$$

$$A_N' = D_n^{\eta} - \tfrac{1}{2} c_n^{\eta} \qquad , (c)$$

$$A_S' = D_s^{\eta} + \tfrac{1}{2} c_s^{\eta} \qquad , (d)$$

$$A_{P,U}' = C_{P,U}^{\xi} \qquad , (e)$$

$$S_P^{\phi} = S^{\phi} + C_{P,U}^{\xi} \phi_{P,U} \qquad , (f)$$

$$\left. \begin{array}{c} \\ \\ \\ \\ \\ \\ \end{array} \right\} (3.2.5)$$

It is possible for the convective contribution C of the coefficient A' to become large on occasion, resulting in the coefficient becoming negative and causing physically implausible results when equation (3.2.4) solved with such coefficients. The hybrid scheme mentioned above, is introduced to overcome this possibility. It consists of modifying all coefficients of the form D_j^i as follows:

$$\bar{D}_j^i \equiv \frac{1}{2}\left\{ D_j^i + \left|\frac{1}{2}C_j^i\right| + \left| D_j^i - \left|\frac{1}{2}C_j^i\right|\right| \right\} \qquad , (3.2.6)$$

where, $|a|$ signifies that the modulus of a is under consideration. The effect of the above modification upon the calculation procedure is similar to that of relation (2.2.2).

3.3. The computational algorithm

The purpose of a computational algorithm here is to solve equations of the form (3.2.4) for all the p, U, V, W and ϕ simultaneously, at the downstream ξ station. Furthermore, since the equations are non-linear, the coefficients A_i' being functions of the dependent variables themselves, the algorithm must provide effective means of computing these coefficients. Having completed the solutions at the downstream (D) station, a forward step in the ξ direction is to be taken and the procedure repeated. It is the repetition of this process along the positive- ξ direction that allows the algorithm to be termed the marching-integration technique. Two such techniques are described here.

3.3.1 SIVA scheme

The SIVA scheme is essentially an iterative one. The central idea of this scheme may be described thus: If the pressure-field were known, the momentum equations would be uncoupled and could be solved individually using some scheme for solving algebraic equations. Furthermore, the velocity-field obtained in this manner would satisfy the continuity equation everywhere. Therefore, in the SIVA procedure, since the pressures are not known in advance, guessed or estimated values of pressures are used to obtain a first estimate of the velocity-field;

thereafter this being is used to obtain a <u>new</u> pressure field, that would bring the velocity-field into conformity with the continuity equation. The <u>iterative</u> repetition of this process until the continuity and momenta are deemed to be satisfied, according to pre-determined criteria, concludes the calculation at one station. A forward step is taken and procedure repeated.

During each iterative cycle at a given station, the algebraic discretised equations are rendered linear by maintaining constant the coefficients A_i' and the source term S_p^{ϕ}. Furthermore, in the SIVA scheme, the grid is swept in such a fashion that point-by-point solutions are obtained for each variable by the use of a Gauss-Siedel procedure. At each point, a cluster of five variables is simultaneously adjusted (hence the name SIVA), to allow the satisfaction of five algebraic balance equations. With reference to figure (3.2.6), these variables are: P_p, V_n, V_s, W_e and W_w. The adjustment is affected through algebraic manipulations of five equations of the form (3.2.1). The simultaneity is introduced to take additional account of the strong interlinkages between the continuity equation and the momentum equations along the η and ζ directions. Details of the algebra associated with the SIVA procedure are described by Caretto et. al. [9] .

3.3.2 SIMPLE scheme

The SIMPLE scheme, while performing essentially the same fundtion, departs from SIVA in several important respects. Central to this scheme is the idea of seeking a non-iterative marching integration procedure that takes full advantage of the boundary-layer character of the flow-field. To this end, in this scheme as in SIVA, a guessed field of pressures is used to arrive at a first approximation to the velocity-field. It differs from SIVA, however, in the following respects:

a) The continuity relation is used to arrive at <u>corrections</u> to the guessed pressure-field.

b) The velocity-field is corrected simultaneously
so as to satisfy approximate algebraic forms of
the momentum equations.

c) The coefficients A_i' are evaluated from values
of variables prevailing at the upstream station.
Thus the boundary-layer character of the problem,
is invoked to linearise the discretized equations.

d) The source term S_P^{ϕ} is linearised by using partly
upstream and partly downstream values of ϕ . The
details of this linearisation are provided in
Appendix A3.

e) The linearised algebraic equations are solved thus:
two sweeps, one in the η- and one in the ζ-direction,
of the standard tri-diagonal matric algorithm (TDMA)
are employed. This involves, for equation (3.2.4),
in ϕ_E and ϕ_W being presumed constant during the
η-direction sweep, and ϕ_N and ϕ_S presumed constant
for the ζ-direction sweep.

The following algebraic manipulations illustrate the application of
SIMPLE to the solution of confined flows in ducts of axially-varying
area.

1) First the discretized froms of the continuity and
momentum equations are expressed as follows:

continuity

$$\left\{ G_e^{\zeta} - G_w^{\zeta} \right\} \Delta \eta_P \Delta \xi + \left\{ G_{\eta}^{\eta} - G_{\jmath}^{\eta} \right\} \Delta \zeta_P \Delta \xi$$

$$= \left\{ G_{P,U}^{\xi} \Delta \eta_{P,U} \Delta \zeta_{P,U} - G_P^{\xi} \Delta \eta_P \Delta \zeta_P \right\} \quad , \quad (3.3.1)$$

Momentum

ξ -direction

$$U_P = \sum_{i=E,W,N,S} A_i^U U_i + S_P^U + D_P^U \left\{ \frac{\partial \bar{p}}{\partial \xi} \right\} \qquad , \; (3.3.2)$$

η -direction

$$V_P = \sum_{i=E,W,N,S} A_i^V V_i + S_P^V + D_P^V \left\{ P_P - P_S \right\} \qquad , \; (3.3.3)$$

ζ -direction

$$W_P = \sum_{i=E,W,N,S} A_i^W W_i + S_P^W + D_P^W \left\{ P_P - P_W \right\} \; , \; (3.3.4)$$

Here, G_i^j represents the mass velocity along direction- j at location i . For example:

$$G_b^\eta = (\rho V)_b - \left\{ \rho U \left[\frac{dy_s}{dx} + \eta \frac{d(y_N - y_s)}{dx} \right] \right\}_b \qquad \cdot \; (3.3.5)$$

$\Delta \eta_{P,U}$ and $\Delta \zeta_{P,U}$ represent the upstream values of these quantities.

S_P^ϕ represents the source (and/or sink) of each ϕ excluding the pressure-gradient term.

A_i^ϕ denotes coefficients of the form :

$$A_i^\phi = \frac{A_i^{\phi\prime}}{\sum\limits_{i=E,W,N,S,P_U} A_i^{\phi\prime}} \qquad , \qquad (3.3.6)$$

and,

$$D_P^U = - \Delta \xi \, \Delta \eta_P \, \Delta \zeta_P \qquad \qquad , \; (a)$$

$$D_P^V = - \Delta \xi \, \Delta \zeta_P \qquad \qquad , \; (b) \qquad \left.\begin{array}{c} \\ \\ \\ \end{array}\right\} \; (3.3.7)$$

$$D_P^W = - \Delta \xi \, \Delta \eta_P \qquad \qquad . \; (c)$$

2) Assuming for the moment that $\left(\frac{\partial \bar{p}}{\partial \xi}\right)$ is known, and equation (3.3.2) has been solved to obtain the downstream values of U, the first approximations to V and W are determined from:

$$V_P^* = \sum_{i = E,W,N,S} A_i^V V_i^* + S_P^V + D_P^V\{p_P^* - p_S^*\} , \qquad (3.3.8)$$

and

$$W_P^* = \sum_{i = E,W,N,S} A_i^W W_i^* + S_P^W + D_P^W\{p_P^* - p_W^*\}, \qquad (3.3.9)$$

where the 'starred' values represent velocities corresponding to the guessed pressure-field, p^*. These starred values will not, in general, satisfy the continuity equation (3.3.1), but will give rise to a net mass source at P, i.e. $\dot{m}_P$, defined by:

$$\dot{m}_P = \left\{ G_n^{\eta *} - G_s^{\eta *} \right\} \Delta\xi \Delta\zeta_P + \left\{ G_e^{\zeta *} - G_\omega^{\zeta *} \right\} \Delta\xi \Delta\eta_P$$

$$+ \left\{ G_P^\xi \Delta\eta_P \Delta\zeta_P - G_{P,U}^\xi \Delta\eta_{P,U} \Delta\zeta_{P,U} \right\} \qquad . \quad (3.3.10)$$

3) It is required now to obtain corrections to the velocities and pressures so as to reduce this mass source to zero. To this end, the pressure-field is expressed as:

$$p = p^* + p' \qquad , \quad (3.3.11)$$

where p' represents the correction to be applied. The corresponding corrections to velocities are:

$$V_P = V_P^* + D_P^V \{ p_P' - p_S' \} \qquad , \quad (a) \Big\}$$
$$W_P = W_P^* + D_P^W \{ p_P' - p_W' \} \qquad . \quad (b) \Big\} \qquad (3.3.12)$$

It is emphasised here that in arriving at these velocity corrections, terms of the form:

$$\sum_{i = E,W,N,S} A_i^V (V_i - V_i^*) \qquad \text{and} \qquad \sum_{i = E,W,N,S} A_i^W (W_i - W_i^*)$$

have been neglected, thus introducing further linearisations

in the procedure. The inaccuracies thus introduced are more than compensated for by the savings in computational effort, for when the correct solution has been obtained, the contributuion of such terms is, in any case, zero.

The substitution of equations (3.3.12 a) and (3.3.12 b) into equation (3.3.10), results in an equation, for pressure-correction of the form:

$$ p_P' \; = \; \sum_{i\,=\,E,W,N,S} A_i^{p'} \, p_i' \;\; + \;\; S_P^{p'} \qquad , \quad (3.3.13) $$

where the $A's$ involve $\rho's$, $D's$ and other geometric quantities appearing in equation (3.3.10), and the mass source, $\dot{m}_P$, has been incorporated into $S_P^{p'}$. It is from solutions to this equation, that corrected values of pressures and velocities V and W are arrived at.

4) The foregoing steps were based on the assumptions that $\left(\frac{\partial \bar{p}}{\partial \xi}\right)$ was known and that equation (3.3.2) could be solved for $U's$. The procedure adopted for calculating $\left(\frac{\partial \bar{p}}{\partial \xi}\right)$ and the $U's$ is as follows:

● A first estimate of $U's$ is obtained by using a guessed value of pressure-gradient, $\left(\frac{\partial \bar{p}}{\partial \xi}^*\right)$ in

$$ U_P^* \; = \; \sum_{i\,=\,E,W,N,S} A_i^U \, U_i^* \;\; + \;\; S_P^U \;\; + \;\; D_P^U \left\{ \frac{\partial \bar{p}^*}{\partial \xi} \right\} \qquad . \; (3.3.14) $$

● This preliminary velocity field will imply a total mass-flow rate within the duct given by

$$ \dot{m}^* \; = \; \sum_{all\ P} \rho \, U_P^* \, \Delta \eta_P \, \Delta \zeta_P \qquad \qquad . \; (3.3.15) $$

● The difference between the true mass-flow rate $\dot{m}$ and this value is used to arrive at corrections to the pressure-gradient. In order to do this, the following definitions

are made:

$$\frac{\partial \bar{p}}{\partial \xi} \equiv \frac{\partial \bar{p}^*}{\partial \xi} + \frac{\partial \bar{p}'}{\partial \xi} \qquad , \ (a) \qquad (3.3.16)$$

and,

$$U_P \equiv U_P^* + D_P^U \left\{ \frac{\partial \bar{p}'}{\partial \xi} \right\} \qquad . \ (b)$$

Since it is required that:

$$\dot{m} = \sum_{all\ P} \rho U_P \, \Delta \eta_P \, \Delta \zeta_P \qquad , \ (3.3.17)$$

the following relation is obtained by substituting equation (3.3.16 b) into (3.3.17):

$$\frac{\partial \bar{p}'}{\partial \xi} = \frac{\dot{m} - \sum_P \rho U_P^* \, \Delta \eta_P \Delta \zeta_P}{\sum_P \rho D_P^U \, \Delta \eta_P \, \Delta \zeta_P} \qquad . \ (3.3.18)$$

This provides the necessary correction to pressure-gradient and consequently to the velocity-field U .

5) Once, the corrected velocity field has been obtained, solutions to the equation (3.2.4) for any other dependent variable ϕ , are obtained in a straight-forward manner.

Steps 1) to 5) complete the operations at a given downstream station. A forward step is then taken and the process repeated, until the region of interest within the ducts, is covered.

3.4   Incorporation of auxiliary information

3.4.1   Initial conditions

Initial conditions of all variables can be supplied to the calculation procedure in a simple manner. For example, a distribtuion of experimentally-determined velocities at the inlet to a duct may be supplied as a function of grid position. So also, may the static-pressure and temperature distributions. In fact, the choice of grid dispositions at the initial station is sometimes dictated by the necessity of accurately representing known distributions of velocity and/or temperature.

3.4.2 Boundary conditions

An important feature of the calculation procedure is the ease
with which hydrodynamic boundary conditions can be applied. When solving
for the starred velocity-field, the actual boundary conditions for vel-
ocities are expected to be close to their true values. Thus, corrections
are not required to be made to boundary velocities. Consequently, the
gradients of p' normal to a boundary must be zero. In addition to imper-
vious wall boundaries, boundaries of the calculation domain might at
times be planes of symmetry. For example, advantage might be taken of
symmetry in duct geometry and/or inlet conditions to perform calculations
for a quadrant of a rectangular-sectioned duct. In this event, at the two
symmetry-plane boundaries, the velocity component normal to it as well as
the gradients of all other quantities normal to it are set to zero. Some-
times the gradient of a quantity rather than its value (like heat flux),
may be required to be specified at a boundary. On such occasions, the
discretized equation for the control volumes adjacent to such boundaries
are adjusted to accommodate the supplied boundary flux. Examples of the
boundary-condition incorporation are provided in Chapters 7 and 8.

3.4.3 Other auxiliary information

In the present instance, uniform-property flows only, are con-
sidered and hence, density and laminar viscosity are supplied as constant
values. The diffusion coefficient in turbulent flow is determined, as des-
cribed in Chapter 4, from a turbulence model. The sources and sinks of all
variables are computed at each grid node, and represent an average of
values prevailing over the control volume surrounding the node. Appen-
dix A.1 provides a list of the source/sink terms in tabulated form.

3.5 Remarks on the numerical procedure

The numerical calculation procedure described above has been em-
bodied into computer program, written in the FORTRAN-IV language.
Details of the use (on a CDC machine) of this computer

program are presented in Appendix A3.

3.5.1 Accuracy of procedure

Analytical exact solutions were, in general, not available to confirm the accuracy of the numerical results obtained by the calculation procedure. Assessments of accuracy of predictions, in each of the cases presented in this Thesis, was therefore made in the following manner: Tests were conducted to determine the dependency of solutions upon grid size. To this end, solutions were obtained with successive refinements of grid-size, i.e. reductions in the spacing between grid nodes in the η - and ζ -directions, as well as the forward step size $\Delta\xi$. When solutions were observed, in respect of several details, to be unaffected by further refinements, they were presumed to be grid-independent. The predictions reported in Part III of this Thesis, were obtained with grids corresponding to this situation. Figures (3.5.1) and (3.5.2) provide illustrations of grid-dependency tests for one laminar and one turbulent flow-situation respectively. Details of grids and forward step-sizes used for the predictions reported in this Thesis are provided in Appendix A3.

3.5.2 Stability

The linearisation procedures described in Section 3.3, do not permit the SIMPLE scheme to be unconditionally stable. However, detailed tests to trace all the factors influencing stability and to devise remedial measures to improve the same, were not found to be necessary. The most influential factor affecting stability, was found to be the size of the forward step, $\Delta\xi$. By restricting the maximum step size to values presented in Appendix A3, stable solutions were, in all cases reported in this Thesis, obtained without recourse to iterations or other special measures.
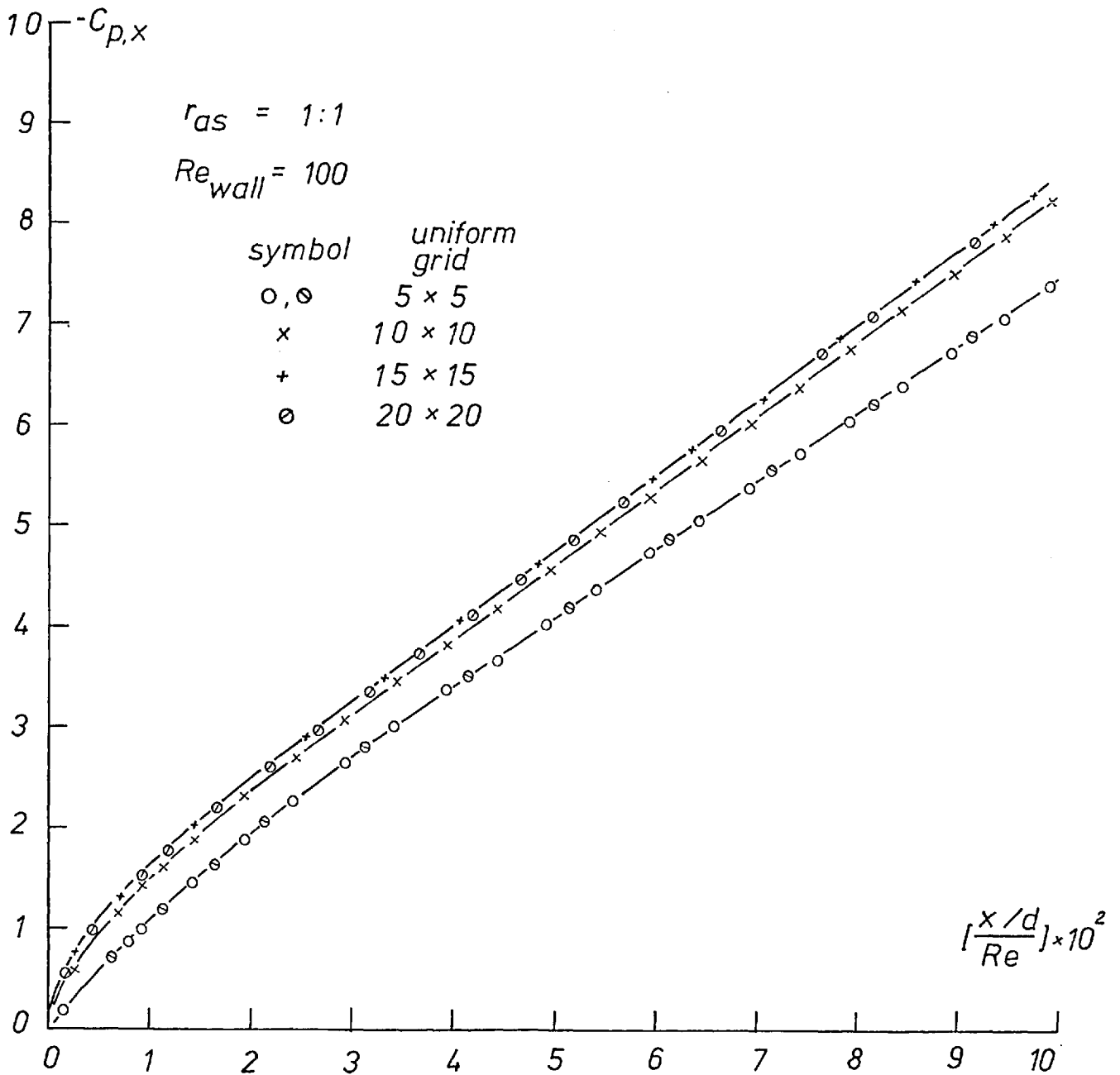
Fig.(3.5.1) Effect of grid size on predictions. Laminar flow in a
rectangular-sectioned duct with one moving wall.
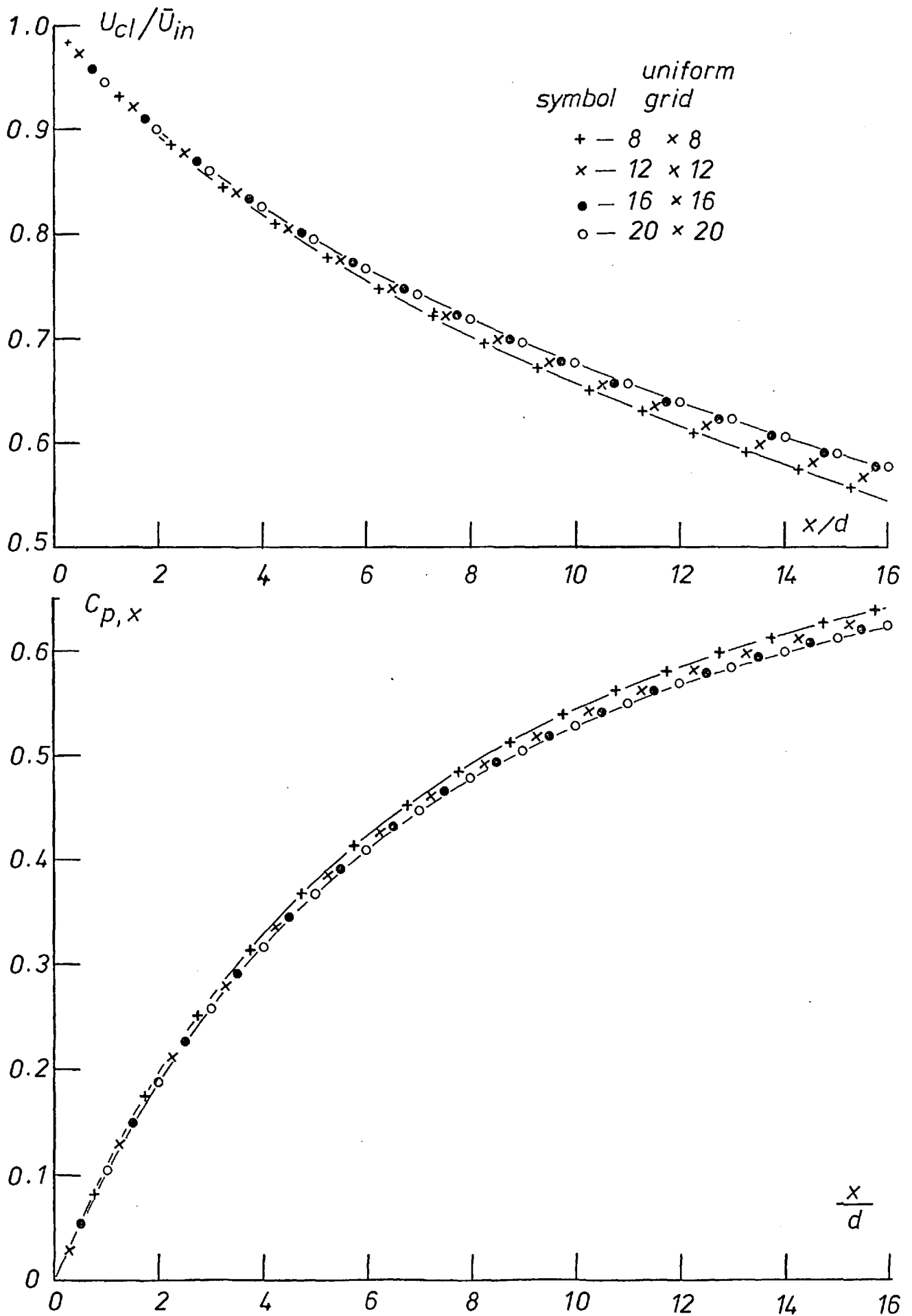
Fig.(3.5.2)   Effect of grid size on predictions.. Turbulent flow in a
rectangular-sectioned diffuser.

3.5.3 Convergence

Convergence of the SIMPLE solution procedure was monotonic for all the situations considered in this Thesis. A minimum number of one pair of TDMA sweeps at each calculation plane, one each in the η- and ζ - directions, was deemed sufficient, for each dependent variable with the exception of pressure correction, to obtain convergent solutions. Three pairs of TDMA sweeps were found to be necessary for the pressure-correction equation. Calculations of residuals of the algebraic equations made at frequent intervals, enabled a check to be made during the calculation procedure, of convergence rates. Such checks invariably indicated monotonic and speedy convergence.

The errors introduced by the various linearisations into the solutions are similar to the truncation errors in any finite-difference scheme and hence could be reduced to given acceptable levels by reductions in the size of the forward steps.

3.6 Concluding remarks

Two numerical procedures for the solution of three-dimensional boundary-layer equations have been outlined. One of them, a semi-implicit scheme, as applied to confined flows, is described in some details. Remarks are made on the stability and accuracy of this procedure and the accuracy of the solutions obtained by its use. Predictions of several laminar flow situations made by this procedure are reported in Chapter 7.

CHAPTER 4

MATHEMATICAL MODELLING OF TURBULENCE

4.1 Introduction

In this chapter the mathematical nature of the problem of model-
ling turbulence in three-dimensional boundary-layer flows, is first out-
lined. Two independent approaches to the solution of this problem are
then described. The similarity between the two approaches lies in the
use of the eddy- or turbulent-viscosity concept. In this concept, the
turbulent stresses are represented by a turbulent viscosity and an ef-
fective mean-velocity gradient. The differences between the two ap-
proaches are fundamental. In the first, a set of simplifying assumptions,
similar to the mixing-length hypothesis of two-dimensional flows, is
used to obtain algebraic expressions for the turbulent viscosity; this
quantity being composed of an empirically-derived mixing-length and an
effective velocity gradient. In the second, more complex, approach a
pair of partial differential equations that govern the transport of
turbulence quantities, is solved. From the resulting distributions of
these quantities, the turbulent viscosity is calculated.

The particular attention paid to turbulence in the immediate
vicinity of wall boundaries, is also described in this chapter. The
complex nature of this problem is not sought to be modelled; however,
it is presumed that in the region close to a wall, the profiles of the
velocity components parallel to the wall, obey the well-known semi-log-
arithmic law. The computational economy achieved by such a presumption
is emphasised.

Some mathematical consequences of the above-mentioned models of
turbulence are described in Appendix A3. The prediction of turbulent
flows, by the use of these models in conjunction with the numerical sol-
ution procedure described in Chapter 3, is reported in Chapter 8.

4.2   The mathematical problem

It is first necessary, in defining the mathematical problem, to seek expressions for the turbulent transport of momentum and other scalar fluid properties. Following conventional practice (e.g. Hinze [30]), this is achieved as follows: The instantaneous value of any scalar fluid property, ϕ , may be expressed as the sum of a time-averaged or macro-scale component and a fluctuating or micro-scale component, thus:

$$\phi = \bar{\phi} + \phi'$$

, (4.2.1)

It is emphasised here that ϕ may represent each of the three momenta per unit mass, U_j , static pressure p , or any other transported fluid property. Considering steady flows (in the macro-scale sense only), when the relationship (4.2.1) is substituted into the general form of the transport equation (2.2.3), and an average over large times is taken, the following equation results:

$$\frac{\partial(\overline{\rho U_i \bar{\phi}})}{\partial x_i} = \mathcal{S}^{\bar{\phi}} - \frac{\partial \bar{J}_{\phi,i}}{\partial x_i} - \frac{\partial(\overline{\rho U_i'\phi'})}{\partial x_i}$$

, (4.2.2)

where, the overbars represent time-averaged values and symbols retain their earlier meaning. In what follows, the overbars over the time-averaged values of velocities and ϕ are removed and the fluctuating components of the velocities are represented by lower-case letters.

The mathematical nature of the the so-called "closure" problem is to cast equation (4.2.2) into a form that has as dependent variable, the time-averaged property, ϕ ; i.e. a functional relationship of the form

$$- \overline{\rho u_i'\phi'} = f(U_i, \phi)$$

, (4.2.3)

is sought. The physical nature of the problem is to devise such a relationship with the aid of available experimental information on the effects of turbulence upon macro-scale motion, and vice versa.

The subject of turbulence is replete with attempts to 'close' the mathematical problem posed above for a variety of flow situations. Some of these attempts have proved successful for simple situations, whilst proving inadequate under more complex conditions. Others, have withstood, with some measure of success, the tests of generality and versatility (e.g. Rodi [49]). Albeit, there exist tested models of turbulence for two-dimensional flow situations. The present attempt is to devise a model for three-dimensional boundary-flows and to test its validity. Thus, an expression of the form (4.2.3) is sought; the nature of the expression being such as to enable it to be simply incorporated into the computational scheme. It is to this end, that, in both models of turbulence described here, the so-called eddy-viscosity hypothesis is retained.

4.3   A simple model of turbulence

In order to illustrate the derivation of a simple turbulence model, consideration is given to the turbulent transport of momentum per unit mass. Modelling of the transport of other scalar fluid properties, is then merely stated. For the transport of momentum per unit mass, the quantities ϕ and ϕ' in expression (4.2.3) are replaced respectively by U_j and u_j . The problem then resolves itself into seeking an expression for the turbulent, or Reynolds stresses, $-\rho\overline{u_i u_j}$. Such an expression, similar to that proposed by Boussinesq (see Hinze [30]), relates the turbulent stresses to the mean velocity gradient, via a proportionality factor, as follows:

$$-\rho\overline{u_i u_j} \;=\; \rho\, \nu_t \left\{ \frac{\partial U_i}{\partial x_j} + \frac{\partial U_j}{\partial x_i} \right\} - \frac{2}{3} k \delta_{ij} \qquad , \quad (4.3.1)$$

where: k , is the turbulence energy $\left(\equiv \tfrac{1}{2} \overline{u_i u_i} \right)$,

δ_{ij} , the Kronecker delta function,

and ν_t , the proportional factor, called the eddy- or turbulent viscosity,

is used here.

The purpose of the simple turbulence model is to devise an algebraic expression for ν_t , based upon the geometric and flow characteristics of the situations under consideration.

The algebraic expression for turbulent viscosity is arrived at as follows: it is hypothesised that this quantity is related to a length scale of turbulence and an effective mean-velocity gradient thus:

$$\nu_t \;=\; \ell^2 \left[\left\{ \frac{\partial U_i}{\partial x_j} + \frac{\partial U_j}{\partial x_i} \right\} \frac{\partial U_i}{\partial x_j} \right]^{\frac{1}{2}} \qquad , \quad (4.3.2)$$

where,

$\ell \;\equiv\;$ the turbulence length scale,

and , the quantities in square brackets are summed over the three directions i for each component j .

The above expression can be seen to reduce to the well-known Prandtl's mixing-length formula, for two-dimensional boundary-layer flows, and thus may be considered to be a generalisation of the same.

In attempting to 'close' the problem via the effective viscosity hypothesis, the length scale ℓ has been introduced as a further un-known quantity. The closure would thus be complete were ℓ to be specified in some manner. Fortunately, past experience and experimental evidence suggest methods of doing so for simple confined flows. For two-dimensional flows the practice consists of relating the length scale to a "mixing-length" which in turn is typical of a given geometric con-figuration. For example, when turbulent flow within a circular pipe has reached its hydrodynamically fully-developed state, the distribution of the length scale is well-known (e.g. Schlichting [67]).

For three-dimensional flows within ducts, the length scale dis-tribution can be cast in the form of simple algebraic expressions re-lated to the geometric configuration of the ducts. One such expression, due to Buleev [7] , relates the length scale at each point in the

cross-section of a duct, to the distance of the point from walls in its neighbourhood, thus:

$$\ell = c_\mu \frac{1}{\pi} \int_D \frac{1}{\delta} d\Omega$$

, (4.3.3)

where c_μ ≡   a constant (here taken as 0.44),

δ ≡   distance of a point from a wall along direction Ω,

and D ≡   the domain of integration, i.e. the cross-section of the duct.

For circular pipes, the length scale distribution obtained from the formula (4.3.3) is remarkably close to that obtained by Nikuradse (see Schlichting [67]) from measurements of velocity profiles (Fig.(4.3.1)).
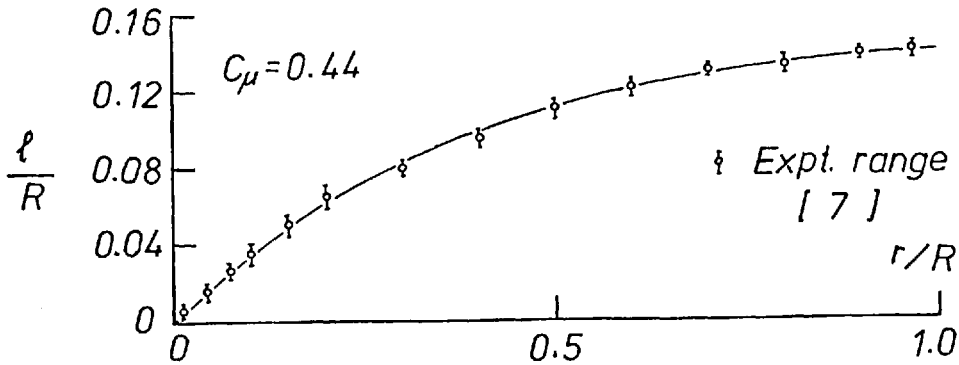
Fig.(4.3.1) Length scale distribution in a circular pipe.

The length scale distribution in rectangular-sectioned ducts, obtained from the formula (4.3.3.) and used in the present work, is expressed

as follows:

$$\ell = \frac{2 c_\mu \, y_1 \, y_2 \, z_1 \, z_2}{\left\{ y_1 z_1 \sqrt{y_2^2 + z_2^2} + y_1 z_2 \sqrt{y_2^2 + z_1^2} + y_2 z_1 \sqrt{y_1^2 + z_2^2} + y_2 z_2 \sqrt{y_1^2 + z_1^2} \right\}}$$

, (4.3.4)

where $\quad y_1, y_2 \equiv$ distances of a point $P(y,z)$
from one pair of walls parallel
to the z-direction,

and $\quad z_1, z_2 \equiv$ distances of P from the pair of
walls prallel to the y-direction.

For a duct of aspect ratio 2 : 1, expression (4.3.4) results in a length scale distribtuion represented in figure (4.3.2).
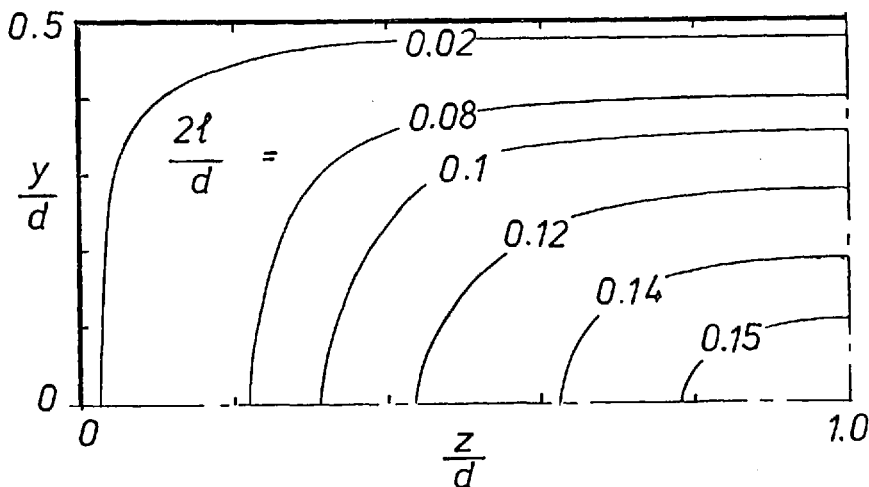
Fig.(4.3.2) Length scale distribution in a rectangular-
sectioned duct of r_{as} = 2 : 1.

In order to extend the application of expression (4.3.4) to flows confined in ducts of axially-varying, cross-sectional area, four additional parameters are introduced into it. This results in an expression of the form:

$$\ell = \ell \{ y, z \, ; \, \alpha_E, \alpha_W, \alpha_N, \alpha_S \}$$

, (4.3.5)

where, the $\alpha's$ represent slopes of the four walls E, W, N and S.

The set of expressions (4.3.1) to (4.3.5) taken together represent the 'closure' of the problem posed in Section 4.2. The implications of thus closing the problem upon the partial differential equations governing the transport of momentum, are detailed in Appendix A2. It will be seen from this that no change occurs in the form of these equations, thus enhancing the computational efficiency while solving them.

It has long been recognised that complex, three-dimensional, transient turbulence phenomena occur in the vicinity of wall boundaries to fluid flow. The turbulence model described above does not claim to model these phenomena. Furthermore, the needs of economy do not permit realistic numerical computations to be performed, in the close proximity of walls from the laminar sublayer to the fully-turbulent region of flows. Consequently, special practices are adopted in modelling the turbulence that prevails in such regions. As this treatment has features essential to the complex model of turbulence described next, it is described along with other common features, in the latter part of this chapter.

4.4   A two-equation turbulence model

Research into the mathematical modelling of turbulence has, in recent years, led to the use of multi-equation turbulence models. By this is meant the practice of solving partial differential equations governing the transport of turbulence quantities whose distributions provide sufficient detailed information to 'close' the problem posed in Section 4.2, with realism. Such equations have been derived by several authors (e.g. Harlow and Nakayama [27]); the use of these and similar equations for predicting a variety of turbulent flows has been reviewed by Launder and Spalding [34] , Harlow [26] and others.

Turbulence models which require the solution of two transport equations have been successfully applied to two-dimensional flow situations (e.g. Rodi [49]). The necessity for two equations is dictated largely by the need for describing both the intensity and the scale of

turbulence, in any flow situations. Several two-equation models for predicting confined flow situations have been described by Launder and Spalding *[33]* . One such model, in which transport equations for turbulence energy k , and its rate of dissipation ε are solved is used in a form applicable to three-dimensional boundary-layer flows, in the present work.

The quantity k is defined as follows:

$$k \equiv \tfrac{1}{2} \overline{u_i u_i} \qquad , \quad (4.4.1)$$

and ε is its rate of dissipation. The turbulent viscosity hypothesis is retained in this model. The turbulent stresses are related to the mean velocity gradient, as before, by the expression (4.3.1), and the expression for turbulent viscosity used is an extension of the Prandtl-Kolmogorov formula (see Rodi *[49]*):

$$\mu_t = \rho C_D \frac{k^2}{\varepsilon} \qquad , \quad (4.4.1)$$

where C_D is a constant. The length scale of turbulence in this model, is obtained from:

$$\ell = C_D \frac{k^{\frac{3}{2}}}{\varepsilon} \qquad , \quad (4.4.2)$$

The partial differential equations governing the transport of k and ε in three-dimensional boundary-layer flows are represented as follows*:

$$\frac{\partial(\rho U k)}{\partial x} + \frac{\partial(\rho V k)}{\partial y} + \frac{\partial(\rho W k)}{\partial z} = G - \rho \varepsilon + \frac{\partial}{\partial y}\left\{\Gamma_k \frac{\partial k}{\partial y}\right\}$$
$$+ \frac{\partial}{\partial z}\left\{\Gamma_k \frac{\partial k}{\partial z}\right\} \qquad , \quad (4.4.3)$$

---

*These equations represent an extension of those reported by Launder and Spalding *[33]* , based upon a rationale similar to that used in deriving the equations of Chapter 2.

$$\frac{\partial(\rho U \varepsilon)}{\partial x} + \frac{\partial(\rho V \varepsilon)}{\partial y} + \frac{\partial(\rho W \varepsilon)}{\partial z} = C_1 G \frac{\varepsilon}{k} - C_2 \rho \frac{\varepsilon^2}{k}$$

$$+ \frac{\partial}{\partial y}\left\{\Gamma_\varepsilon \frac{\partial \varepsilon}{\partial y}\right\} + \frac{\partial}{\partial z}\left\{\Gamma_\varepsilon \frac{\partial \varepsilon}{\partial z}\right\} \quad , \quad (4.4.4)$$

where $\quad G \quad \equiv \quad$ generation of turbulence energy,

$\quad \Gamma_k, \Gamma_\varepsilon \quad \equiv \quad$ diffusion coefficients of k and ε respectively,

and $\quad C_1, C_2 \quad \equiv \quad$ are constants of the turbulence model.

Equations (4.4.3) and (4.4.4) may be expressed in quasi-orthogonal co-ordinates in a manner identical to that described in Chapter 2. The final form of the equations used in this work is tabulated in Appendix A1, along with the expression used for G as well as the constants mentioned in this chapter.

4.5   The effective viscosity

The turbulent viscosity, determined from either of the two models described above, is then used to determined the overall or 'effective' viscosity, from:

$$\mu_{eff} = \mu + \mu_t \qquad , \quad (4.5.1)$$

The effective exchange coefficient for the diffusion of all other scalar fluid properties ϕ , is written simply as:

$$\Gamma_{eff, \phi} = \frac{\mu}{Pr_{,\phi}} + \frac{\mu_t}{Pr_{t,\phi}} \qquad , \quad (4.5.2)$$

where, $Pr_{,\phi}$ and $Pr_{t,\phi}$ are the laminar and turbulent Prandtl/Schmidt

numbers respectively, for the diffusion of fluid property, ϕ . Values of $Pr_{t,\phi}$ used in this Thesis and tabulated below, are those developed and used in recent works*.

No	ϕ	$Pr_{t,\phi}$
1	U	1.0
2	V	1.0
3	W	1.0
4	k	1.0
5	ε	1.3
6	T	0.9

Table (4.5.1)

The effective viscosity now replaces the fluid viscosity and the effective transport coefficient for ϕ , the normal transport coefficient, in the appropriate transport equation.

4.6   The near-wall region

Although turbulent flow in the immediate vicinity of walls is complicated by a large number of factors, it is generally recognised that sufficiently far away from the wall, i.e. in the fully-turbulent region, the velocity profile exhibits similar characteristics under a number of conditions. This "universal" feature has been used to cast the velocity profile into the well-known, semi-logarithmic 'law':

$$\frac{U - U_W}{U_{\tau}} = \frac{1}{K} \ln \left[E U_{\tau} \, \delta \rho / \mu \right] \qquad , \quad (4.6.1)$$

with: U $\equiv$ the velocity component parallel to the wall;

U_W $\equiv$ velocity of the wall (i.e. $(U-U_W)$ denotes the relative velocity);

*See Launder & Spalding [33] .

U_τ ≡   is the shear velocity,
              defined below;

κ, E ≡   are log-law constants
              (here, values of 0.42 and 9.0
              respectively, have been used);

δ ≡   is the normal distance from
              the wall;

and ρ, μ are the fluid density and
              laminar viscosity, respectively.

It is this relationship that is applied in the present work as a bound-
ary condition for velocity components parallel to and adjacent to wall
boundaries of the flow (Fig. (4.6.1)). The difference between the two
models, in the application of equation (4.6.1), lies in the manner in
which U_τ is calculated.
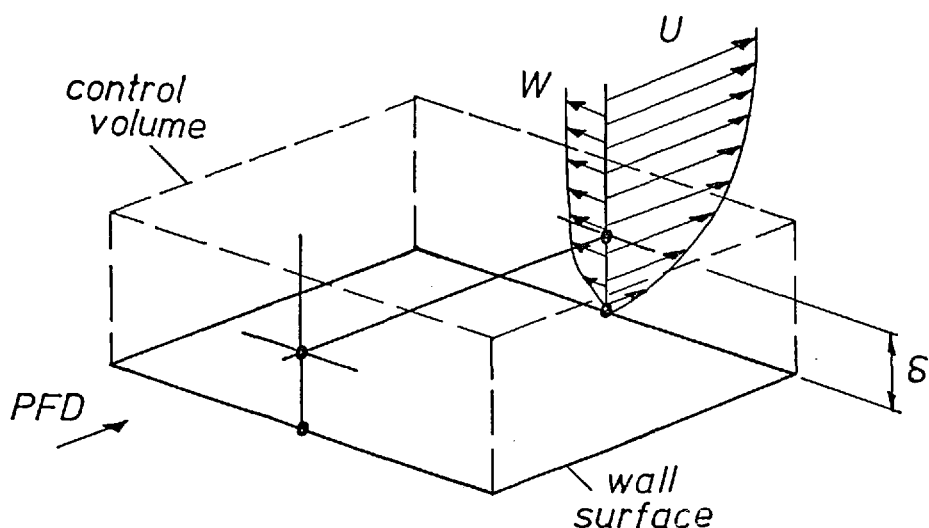
Fig.(4.6.1) Representation of velocity profiles in the
            neighbourhood of walls.

In the simple turbulence model, the definition

$$U_\tau \equiv \sqrt{\tau_w/\rho} \qquad , \quad (4.6.2)$$

where τ_w denotes the wall shear stress, is used. At each axial station, equation (4.6.1) is used in an iterative manner for each wall boundary until a convergent value of U_τ is obtained. The computational details of this and the following practice are provided in Appendix A3.

In the two-equation turbulence model U_τ is defined as follows:

$$U_\tau \equiv C_D^{\frac{1}{4}} k^{\frac{1}{2}} \qquad , \quad (4.6.3)$$

where k represents the value of turbulence energy in the near-wall region. Account is taken of the behaviour of k and ε in the near-wall region, in an empirical manner. The diffusion of k near walls is known to be small (Rodi [49]) and is neglected, while full account is taken of the generation, dissipation and convection of k . The value of ε is obtained from a lin-ear-length-scale-near-walls presumption. The computational aspects of this treatment are described in Appendix A3.

The above-mentioned practices complete the treatment of the near-wall region in modelling the turbulent transport of momentum. Figure (4.6.2) shows a graphical representation of equation (4.6.1) along with experimental data. The data correspond to experimental measurements made on a flat plate with a shear-flow velocity profile (corresponding to case B, (Fig. 8.3.21) of Chapter 8). Equation (4.6.1) is seen to represent the data fairly well.

The analyses of other variables with respect to their behaviour in the neighbourhood of walls, leads to the conclusion that relation-ships similar to (4.6.1) may be devised. One such relationship used for a general variable, ϕ , in the present work, is as follows:

$$\frac{\phi - \phi_w}{\left\{\dfrac{\dot{\phi}_w''}{\rho U_\tau}\right\}} = \frac{1}{\kappa} \ln\left[E \delta U_\tau \rho/\mu \right] + P_\phi \qquad , \quad (4.6.4)$$

where: $\dot{\phi}_W''$ ≡   , represent the approriate ϕ-flux
at the wall;

and P_ϕ ≡   denotes a function relating the smooth-
ness of the wall to the diffusion of ϕ
through it ; the following functional
of P_ϕ was used in the present work
(e.g. see Patankar and Spalding [44]):

$$P_\phi = 9.24 \left\{ \frac{Pr_\phi}{Pr_{t,\phi}} - 1 \right\} \left\{ \frac{Pr_\phi}{Pr_{t,\phi}} \right\}^{-0.25} \qquad . \ (4.6.5)$$
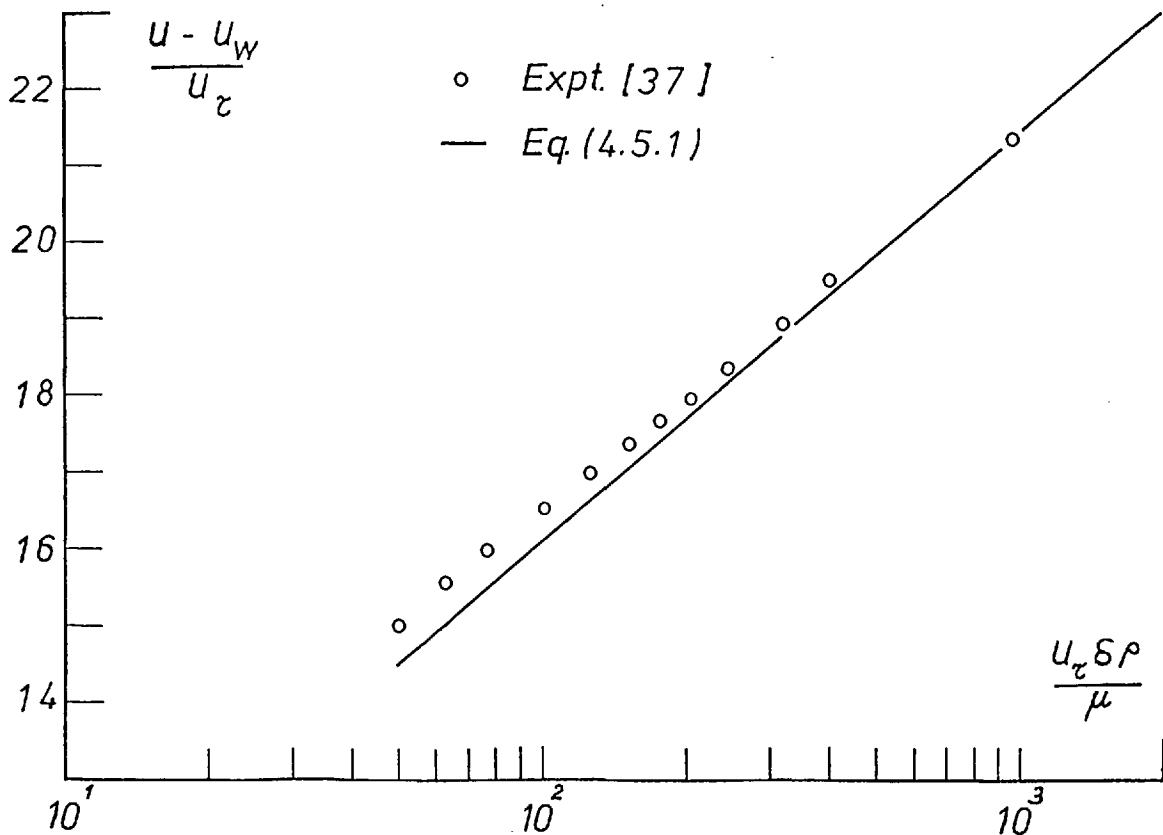
Fig.(4.6.2)   Illustration of the semi - logarithmic law of the wall.

4.7   Summary and concluding remarks

1)   Two methods for the mathematical modelling of turbulence in
three-dimensional boundary-layer flows have been described in this chap-
ter; one is a simple model akin to the mixing-length hypothesis of two-
dimensional flows. The other is a two-equation model, in which transport
equations are solved for turbulence energy, k and its dissipation
rate, ε .

2)   The method of turbulence modelling adopted here is as follows:

•   The turbulent stresses, $-\overline{\rho u_i u_j}$ are related to time-averaged
velocity gradients and an exchange coefficient, by analogy with the
molecular viscosity concept.

•   In both models described here, the concept of this exchange
coefficient, i.e. turbulent viscosity μ_t , is retained. However,
the manner of arriving at it is different in each case. In the simple
model, the turbulent viscosity is expressed in terms of an effective
path length, i.e. length scale of turbulence, and an effective vel-
ocity gradient. In the complex model, the turbulent viscosity is
arrived at from values of kinetic energy and its rate of dissipation,
obtained by solving equations governing their transport.

3)   Adopted in the above manner, turbulence modelling leads to
partial differential equations governing time-averaged fluid motion
identical in form to equations (2.1.7) to (2.1.10) for laminar flows,
with the exception that the laminar diffusion coefficient is replaced
by an effective diffusion coefficient.

4)   The above modelling would be inappropriate to regions adjacent
to wall boundaries of the flow. Thus special attention is paid to such
regions where steep gradients of fluid properties generally occur. Wall
flux relationships are devised which use well-authenticated experimental
information as a basis.

5)   Some of the mathematical consequences of the turbulent-viscosity assumption are derived in Appendix A2, and computational details in Appendix A3.

6)   The predictions of fully-turbulent flows in ducts and diffusers made with the turbulent models are described in Chapter 8, where an assessment of their relative capability is also made.

PART II

Experimental Program

CHAPTER 5

EXPERIMENTAL INVESTIGATION OF TURBULENT

FLOWS IN RECTANGULAR-SECTIONED DIFFUSERS

5.1 Introduction

In this chapter the objectives of, and the motivation for the
program of experimental investigation are first outlined. The criteria
which helped to determine the choice of the geometric configuration
adopted for the program, as well as the measurement devices used, are
enumerated. The design and fabrication of elements of the rig, includ-
ing details of its permanent features as well as improvements to the
whole assembly, are then reported. Commissioning, testing and routine
running of the rig presented no serious difficulties and are described
only in brief. The measuring devices chosen were simple; however, the
manufacture of the probes used had some novel and interesting features.
Thus, these are described in some detail.No special data-logging or
data-reduction devices were adopted. The experimental data are reduced
to convenient non-dimensional form and are presented mainly as tables
in Appendix A4. In conclusion, an assessment is provided of the quality
of the data obtained.

5.2 Motivation and general objectives

The paucity of experimental data on confined, three-dimensional
boundary-layer flows pin-pointed the need for information to test the
validity of the prediction procedure described in Part I of this Thesis.
Furthermore, this information was required in a configuration which
possessed all the essential physical features of situations occuring
in engineering practice, with little of the esential geometric com-
plexity so common in real life. This would, it was felt, then enable
both the numerical calculating procedure as well as the turbulence model
incorporated in it, to be adequately tested. Breadth, rather than depth,
it was decided, would be the keynote of the investigation.The short
time available placed a natural restriction upon this motivation.

The primary object of the present investigation was thus to obtain experimental data for a range of geometric and hydrodynamic parameters. Three secondary objectives at this stage were: first, testing of the efficacy of the turbulence model and thereby suggesting future lines of development. Second, provision of useful data in an area of engineering interest, preferably and within the knowledge of the author, hitherto unexplored. Third, testing the mathematical assumptions made in deriving the differential equations (2.1.7) to (2.1.10).

Several tertiary objectives of an educative nature, suggested themselves during the course of the investigation. Gaining familiarity with measurement techniques and developing a feel for the care required in obtaining reliable data, proved immensely satisfying to the author.

5.2.1   Specific objectives

Taking the above-mentioned considerations into account, it was decided that measurements of pressure and velocity fields would be made in straight diffusers of rectangular cross-sections. Further, it was decided for convenience that attention was to be restricted to the situation where two walls were retained parallel and the other two used in constructing diffusers of varying included angles. This is the situation commonly referred to in the literature as "two-dimensional" diffusers. However, in order to ensure three-dimensionality of the flow-field, the aspect ratio of the test-section at inlet was chosen to be unity.

Measurements were to be made with simple equipment; static and total-head probes were considered sufficient for this purpose and standard types of micro-manometers were to be used. The various elements of the rig were designed in accordance with these objectives.

5.3   Design and fabrication of equipment

Figures (5.3.1) and (5.3.2) show the complete assembly of the rig from different angles. In the former, only those elements of the assembly which do not constitute standard laboratory equipment, are

① Bell mouth

② Screens

③ Honeycomb

④ Contraction section

⑤ Test section

⑥ Traversing gear

⑦ Blower

⑧ Motor

⑨ Connecting section

⑩ Rectangular-to-circular connecting diffuser

⑪ Break in support frame to reduce vibration transmission
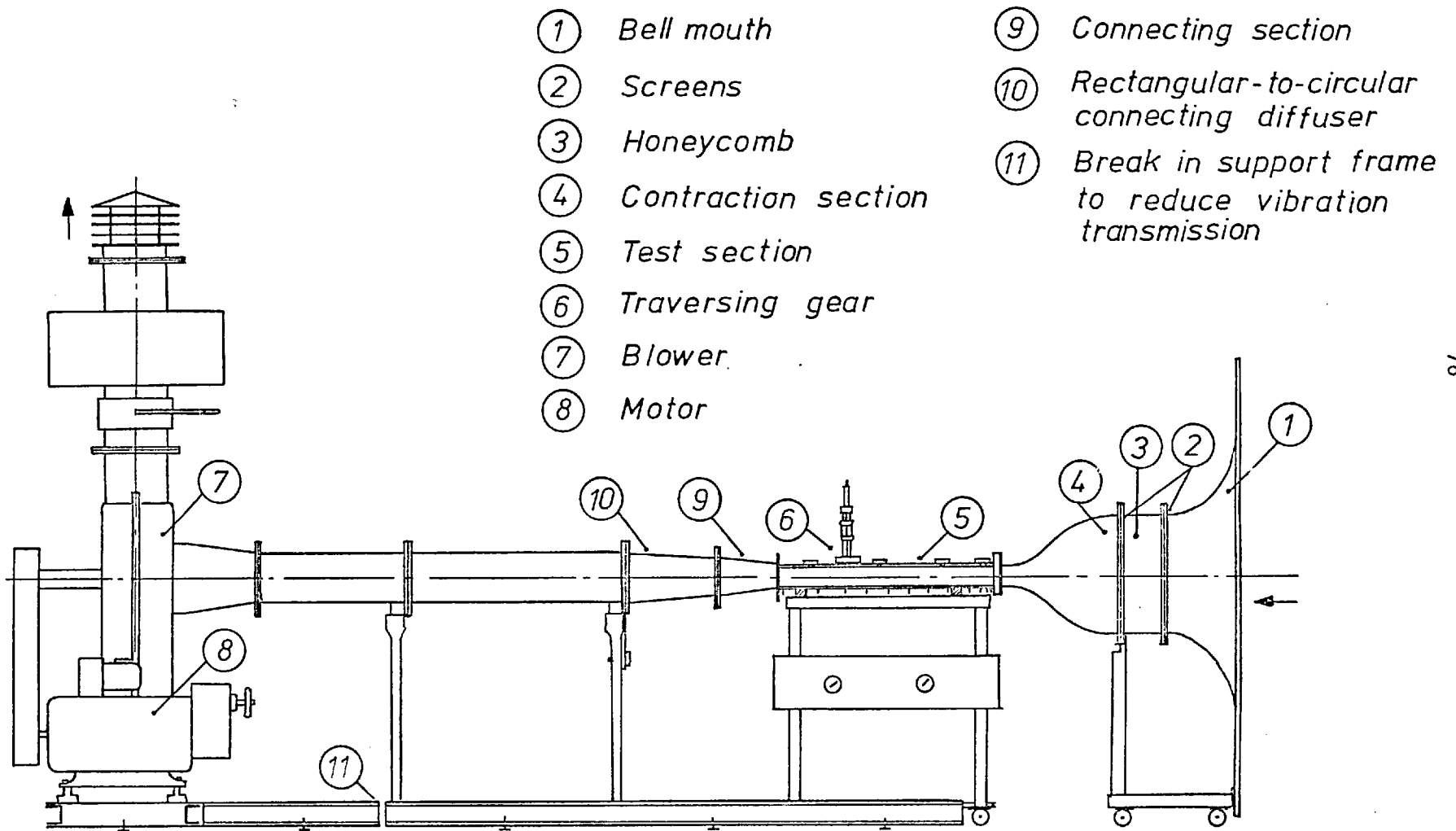
Fig.(5.3.1) Assembled view of experimental rig.
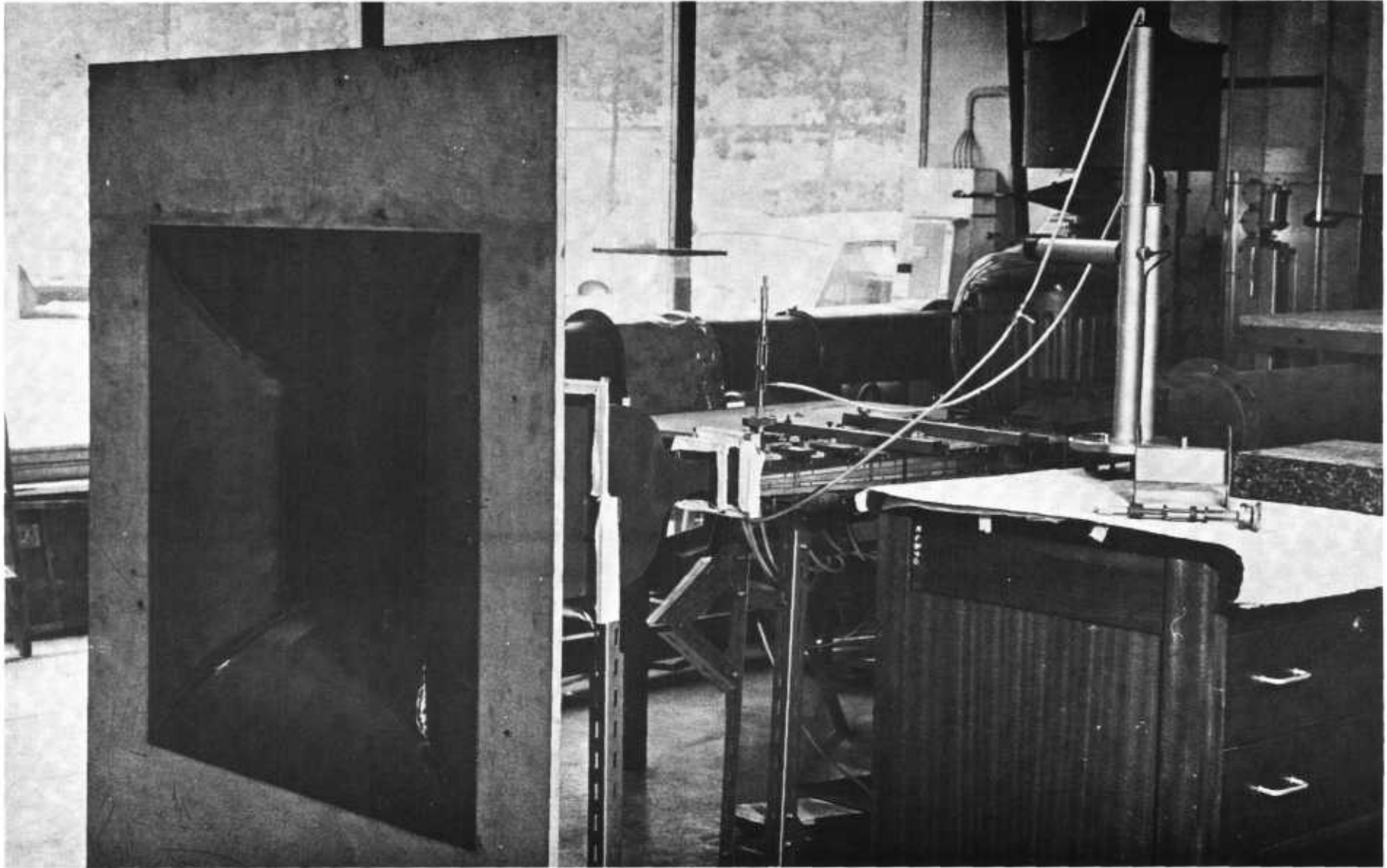
Fig.(5.3.2) Experimental rig.

described in detail in the following sections.

5.3.1 The test section

In order to keep the test-section to a compact size and yet provide information up to stations reasonably far downstream of the inlet, the cross-section at inlet was chosen to be 2 in. (50.8 mm) square, and the test-section itself 800 mm long. Thus, a length-to-diameter ratio of approximately sixteen was attainable and was considered sufficient to provide data on diffusers in the unstalled region, over a wide range of included angles.

The side-walls of the test-section were manufactured from 12 mm thick Perspex sheets. This was done so as to enable visual checks of various kinds to be performed. The roof and floor were machined from precision-rolled Aluminium sheets, also 12 mm thick. The manufacturer's specifications of both Perspex and Aluminium sheeting, indicated surface roughness elements and/or waviness factors of less than 0.01 %. The roof of the diffuser was accurately machined in four separate pieces such that, when finally in place, the gap between two neighbouring pieces allowed sliders of T-shaped cross-sections to fit snugly while permitting a smooth sliding motion. There were four such gaps accommodating sliders , as well as four circular holes accurately reamed and rendered burr-free on the roof of the diffuser. When not in use, these holes as well as similar ones on the sliders, were blocked with Perspex plugs machined to fit tightly. Measurements were made with probes that passed through similar plugs with holes appropriate to the probe size, drilled through their axes. Care was taken, by a lapping operation, to ensure a step-free smooth inner surface on the diffuser roof, whatever the nature of the plug used. The floor of the test-section had 13 holes, 0.25 mm in diameter, precision-drilled into the measuring surface at predetermined positions along the centreline. The spacing between these holes used to measure wall values of static pressure, was chosen such that more holes were placed in regions where a steep variation in pressure was anticipated than in regions where the variation was expected to be moderate. On the under side of the diffuser floor, these holes were connected to holes of

larger diameter into which were fitted brass tubing to form pressure pick-ups.

The test-section was assembled with the roof and floor securely connected, by means of a number of flat-headed 4 mm screws, to an additional pair of fixed side walls, also of Perspex as shown in Fig. (5.3.3). This was done, in each case, after the swivelling pair of side-walls had been adjusted into position to achieve the desired included angle. Strips of double-sided sticky tape on the top and bottom edges of these side walls, permitted an adequate air-tight seal between the roof and floor to be maintained. The complete assembly, when in position on the rig, was further clamped at two points along the diffuser axis to a pair of hollow Aluminium square-sections, to prevent sagging. Care was taken to ensure that when thus assembled, the sliders could be smoothly moved and clamped in any desired position. The clamps used were U-shaped and manufactured from 13 mm thick Aluminium sheeting. They served the dual purpose of holding the roof-sections together as well as enabling the sliders to be securely clamped and made immobile in any required position. In each instance, the test-section was checked and burrs or steps due to mis-alignments, carefully lapped away to ensure flat, smooth internal surfaces. Finally, flanges were screwed onto the external surfaces of the test-section, at inlet and outlet, to enable it to be connected to the contraction section and tail-end diffuser respectively.

The swivelling of the side walls was achieved through the use of a simple hinge arrangement as shown in Fig. (5.3.4). Dowel pins attached to fixed portions of the side walls, fitted into appropriately located holes in the roof-section at inlet. As seen in the figure, the side walls swivel about the axes of these dowel pins. The entrance section to the diffuser for all included angles is presumed to be the plane that includes these axes. Care was taken to smooth any rough edges caused by the swivelling action, with plastecene.

slider-T

fixed side
wall

slot in plate screwed to
base to secure side
walls in position

150

320

plan

80

connector to
contraction
section

u-connectors
holding roof together

roof

connector to
tail-end diffuser

inlet
section

floor

50

800

elevation
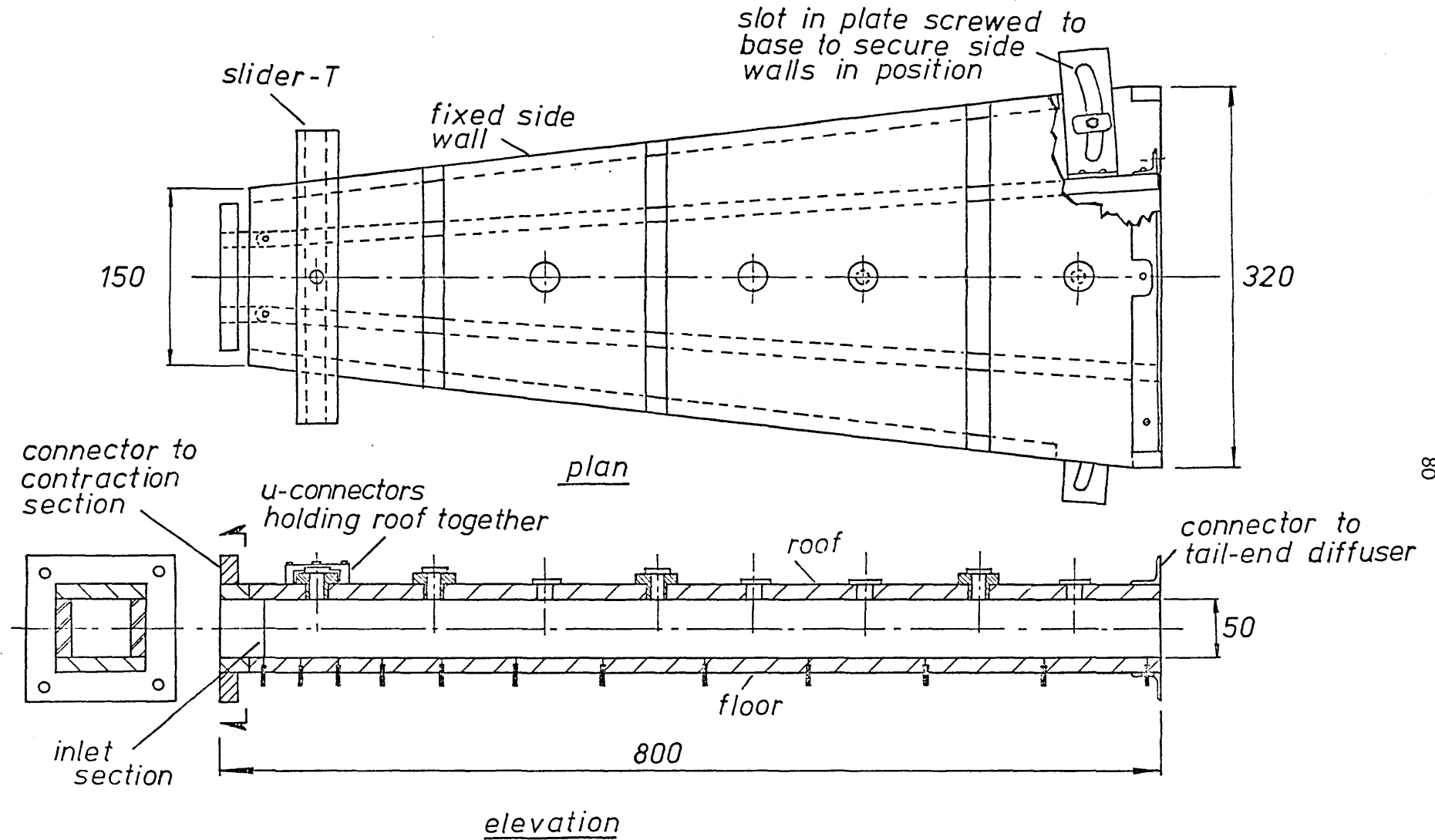
Fig.(5.3.3)   Assembled view of the test section.
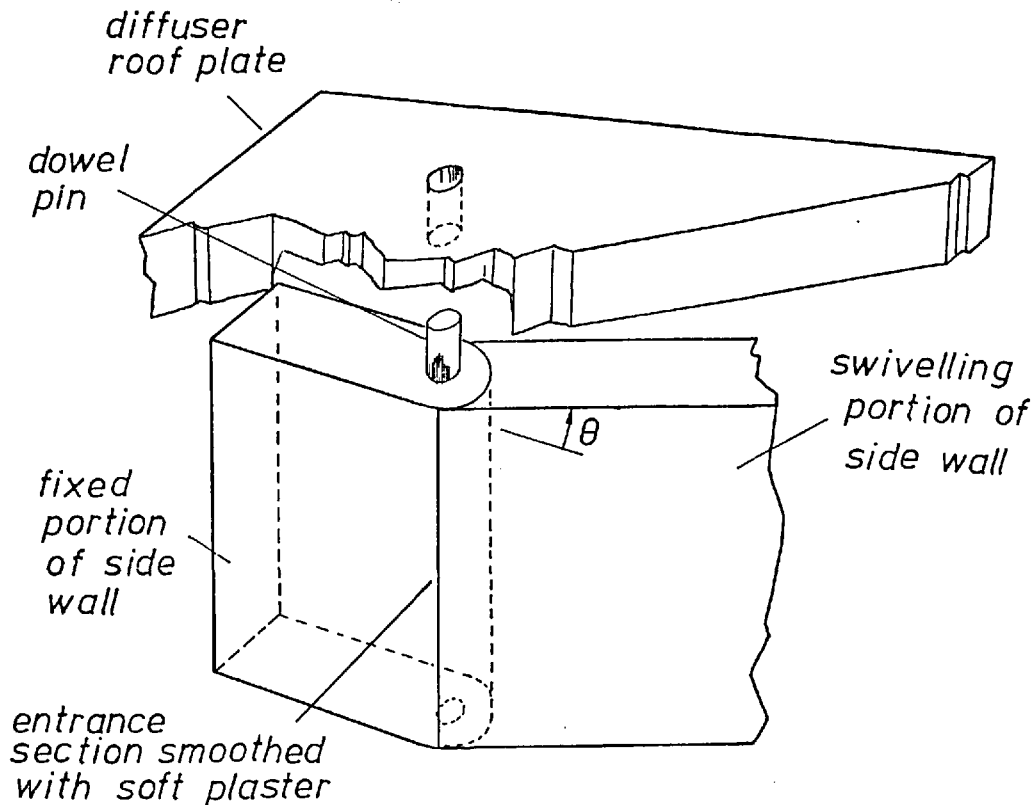
Fig.(5.3.4) Details of arrangement for swivelling
            diffuser side walls.

5.3.2 Contraction and Bell-mouth sections

The design of the contraction section was based upon information reported by Bradshaw and Pankhurst [6] . It was recognised that provisions for flow acceleration to yield uniform velocity distributions and the prevention of local flow reversals in the axial direction are, on occasion, opposing aims. It was decided in the present instance to overcome these difficulties by the use of a large contraction ratio (36 : 1) together with a reasonably smooth contour to the four walls of the contraction. Correspondingly, a symmetrical contraction, 300 mm square at its inlet end reduced to 50 mm square at its outlet end, over a length of 450 mm, was fabricated from sheet metal and treated with rust-proof paint. The internal surfaces were polished and plastecene used to smooth over any burrs, left over from welding, on the internal

corners. A flange was provided at each end.

At the larger end, the flange was connected to a similar one on a straight connecting piece, also constructed of sheet metal, which housed the flow-straightening devices. These devices consisted of two 20-mesh screens made of 28 swg copper wire and possessing an open-area ratio of 0.59, one at either end. Sandwiched between these two was a honey-comb section made of Aluminium foil. As described by Bradhurst and Pankhurst [6] , this system was expected to remove any flow ir-regularities and enabled uniform flow to be obtained at inlet to the test-section.

One end of the above-mentioned connecting-section was attached to a bell-mouth section to provide a smooth entry to the contraction section. Starting from 300 mm square at its outlet end, this bellmouth had sides flared out symmetrically to 500 mm square at its inlet end over a length of 200 mm.

The bellmouth and contraction sections are shown in Figure (5.3.5). Also shown are connecting sections. Several were ducts of 50 mm square cross-section and varying lengths fabricated of sheet metal. These were used to obtaining varying thicknesses of inlet boundary layers at the entrance to the test-section. The tail-end diffuser shown served as a connecting piece between the test-section and the permanent portions of the rig.

From laboratory tests on set-ups similar to the bellmouth-con-traction section assembly described above, it was observed that the level of turbulence at inlet to the test-section was uniformly low; it was estimated to be below 0.3 %.

5.3.3   Tail-end connecting sections

The intake manifold of the blower, to which the test-section was to be attached, had a circular cross-section, 220 mm in diameter. Thus, connecting pieces were required to match the rectangular cross-sections at the tail-end of the test-section with the circular cross-section of
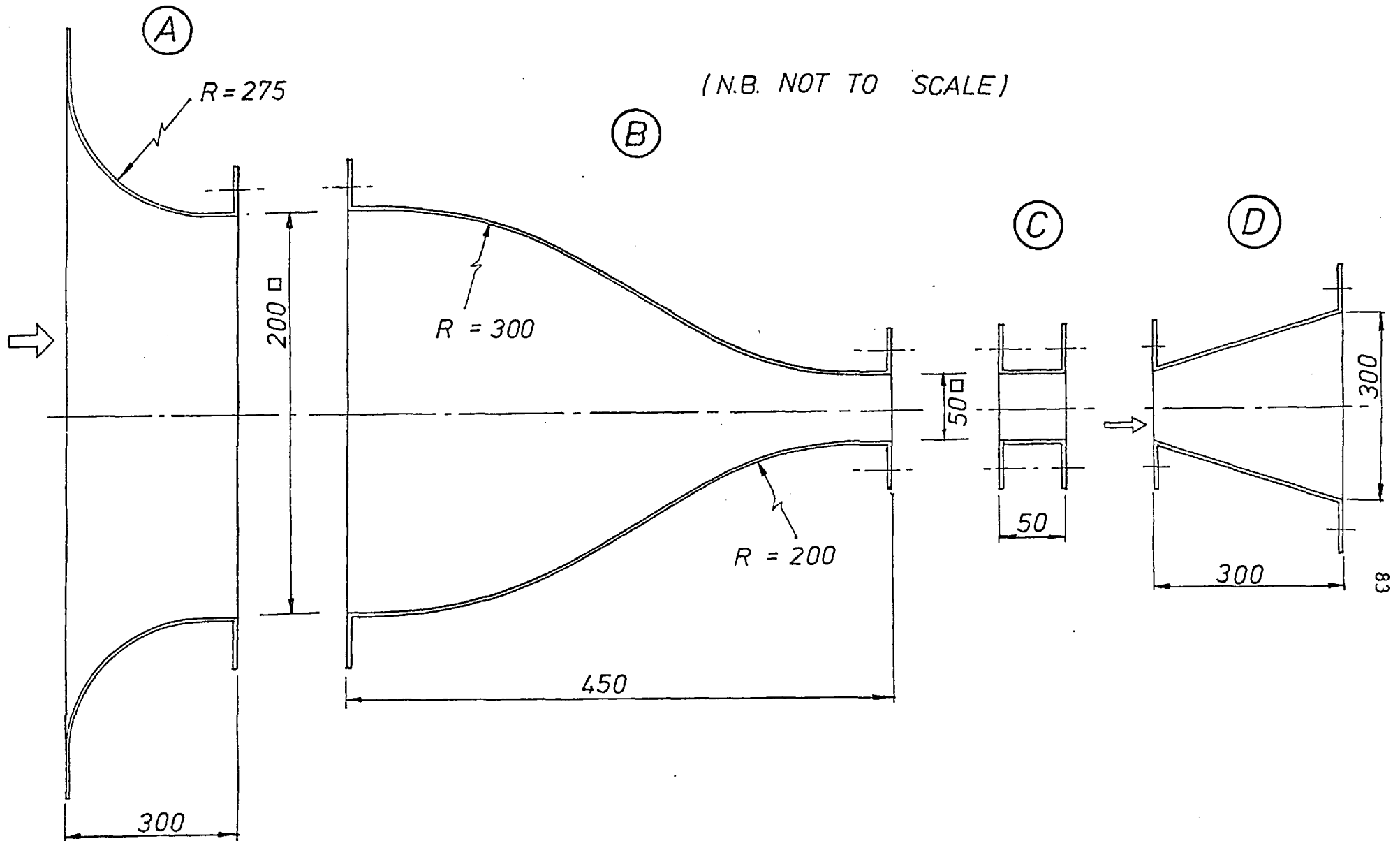
Fig.(5.3.5) Details of the Bellmouth (A), Contraction-section (B), and connecting sections (C) and (D).

the intake manifold. This was achieved in two stages: first a sheet
metal element was fabricated to fit the cross-section of the intake
manifold on one end and ending in a 200 mm x 160 mm rectangular cross-
section on the other. Four other connecting pieces were fabricated,
each on one end and on the other having rectangular sections to accom-
modate end-planes of the test-section corresponding to a limited range
of included angles.

Connections between the various elements of the rig was affected
through flanges lined with rubber to ensure an adequate air seal, to
reduce vibration transmission and to enable small adjustments to be
made to the alignment of the rig. The flanges were secured with 9.5 mm
bolts throughout. The assembly was mounted on a test bed fabricated
from slotted angle-irons and mounted on castor wheels. This set-up per-
mitted ease of movement of the assembly when changes were to be affected
in the geometric configuration of the test-section. It also served to
reduce the transmission of machine vibration. Vibration was further
damped through the use of a rubber bellows section between two portions
of the intake manifold.

5.4   The traversing gear

The T-sectioned sliders (Fig.(5.3.6)) with the probe holes had
provisions for the mounting of the probe-traversing mechanism. This con-
sisted of a recess surrounding each probe hole, into which the base of
the traversing mechanism could be securely screwed. The sliders them-
selves, were accurately machined from brass bar-stock. Particular care
was taken to ensure that the probe holes were drilled and reamed such
that their axes were exactly normal to the direction of sliding. The
above-mentioned base of the traversing gear was also capable of being
screwed on directly to the external surface of the roof of the test
section, at four points.

The traversing mechanism itself, Figure (5.3.7) consisted of
two Aluminium discs separated by and rigidly attached to which were
three silver-steel rods 160 mm in length. These rods were located on a
circle of 32 mm diameter and were 120° apart. A platform supporting the

50 mm travel micrometer

slider assembly

probe holder

T-slider

perspex bush

probe

probe-holder

base screwed on to T-slider or diffuser roof
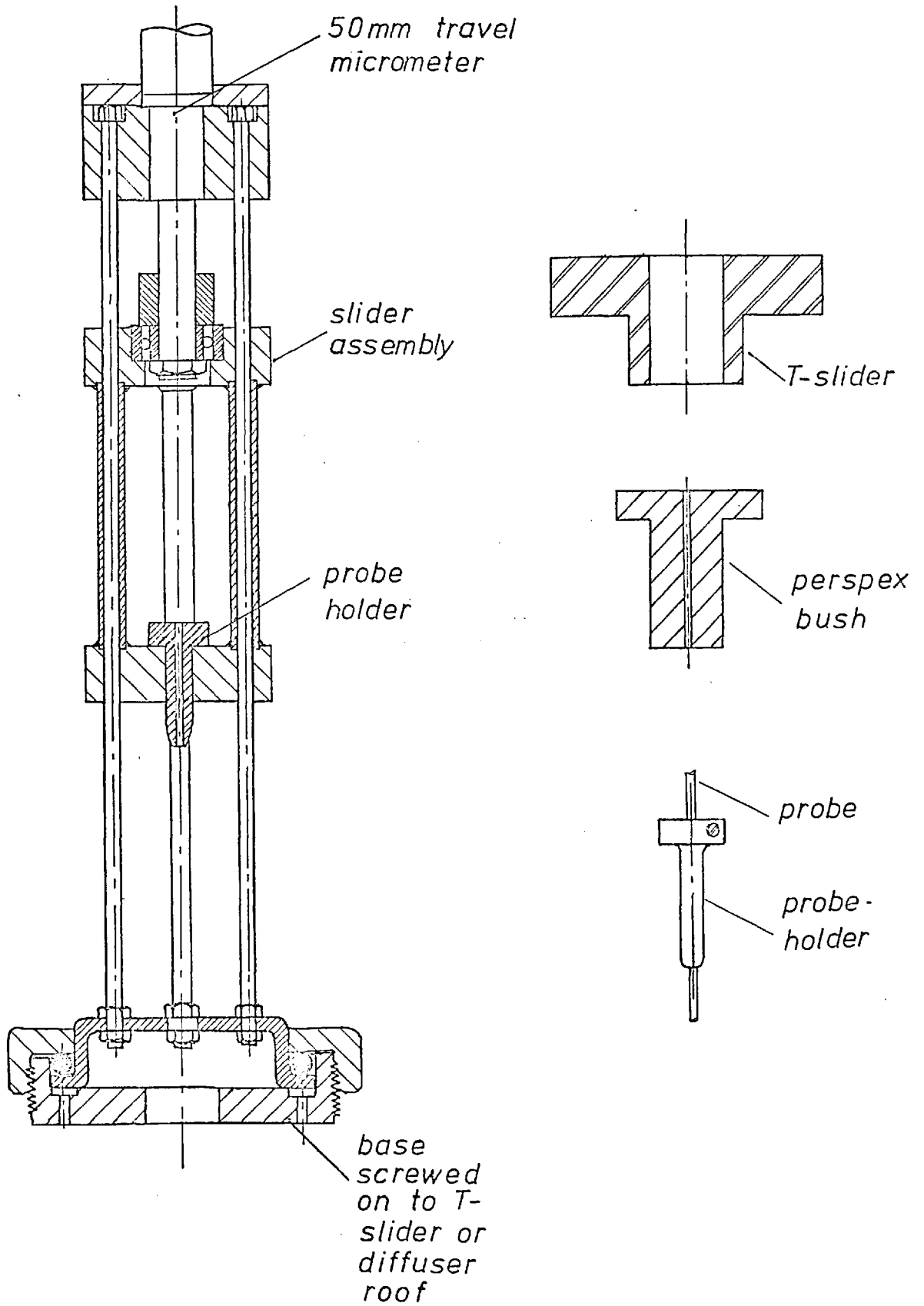
Fig.(5.3.7) Assembly showing details of probe-traversing gear.

probe was capable of sliding vertically along the rods. This platform
consisted of two discs 38 mm in diameter, machined from Duralumin bar-
stock, separated by and attached to which were three hollow brass cyl-
inders 30 mm in length. These cylinders provided smooth sliding-fit
guides for the steel rods and had their axes coincident with those of
the latter. The probe-holder, made of brass, could be rotated about the
vertical axis and secured at any orientation. The probe passed through
a hole drilled along the axis of the probe-holder and could, in turn,
be rigidly fixed to the probe-holder by a set-screw. The disc at the
top end of the traversing mechanism, supported a 50 mm travel, Moore
and Wright, precision micrometer. The stem of the micrometer was con-
nected to the top of the platform, through a journal bearing as shown in
the figure. This arrangement enabled the platform to be raised or lowered
accurately through the use of the micrometer screw, with the minimum of
slip or backlash. To eliminate backlash altogether, traverses were, in
all cases, made in one direction only.
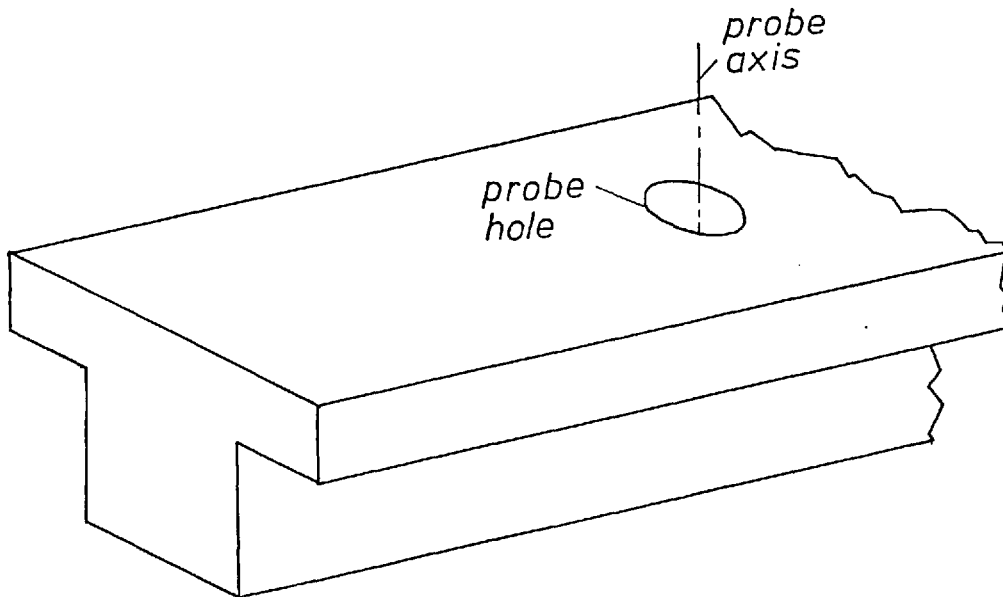
Fig.(5.3.6)   T - sectioned slider.

The disc at the bottom of the mechanism rested within a re-
cessed brass base mentioned earlier and acted as a support to the
traversing gear assembly. The base itself, was threaded externally and
when a corresponding cap was screwed on the assembly was held rigidly
in the recess located on the base. A rubber O-ring, placed between the

cap and the bottom disc, ensured an even pressure on the disc at all times.

5.5   Measuring devices

Simplicity and ease of measurement were the over-riding criteria which decided the use of pitot probes in conjunction with hydrostatic micro-manometers for the measurement of static and total pressures throughout the test-section.

The size of the cross-section of the test-section precluded the use of combined pitot-static probes which tended to be too large and hence caused unacceptable disturbances to the flow. Hence, small-bore probes were used to measure static and total pressures separately. Such probes of several sizes and shapes were constructed of fine-bore hypodermic, stainless-steel tubing. After a series of tests both for purposes of calibration and to determine their reliability, strength and ease of use, a set of probes was finally chosen to make the measurements reported in this Thesis. These are represented in Figure (5.5.1). The set A were used for routine measurements, B for measurements across the inlet cross-section and C for qualitative observations of flow pattern.

Trials indicated that simple cold bending could produce right-angled bends in hypodermic tubing with great accuracy and without causing weakening or pinching of the tubes. Composite probes were constructed by attaching small O.D. tubing to the bores of large diameter tubes to produce the requisite length and shape. The connexion was in all cases cemented with Araldite; approximately 12 hours were allowed for, for the glue to harden in an oven heated to a low temperature. When tested these joints proved both air-tight and strong. This done, the connexions were smoothed over externally with fine-grained sandpaper and polished to give a smooth transition in diameters. In each case, a pair of probes, one each for static and total pressure measurement, was fashioned to identical dimensions. This ensured identical flow-blockage effects when the probes were inserted into the test-section.

The manufacture of static-head probes presented some interesting
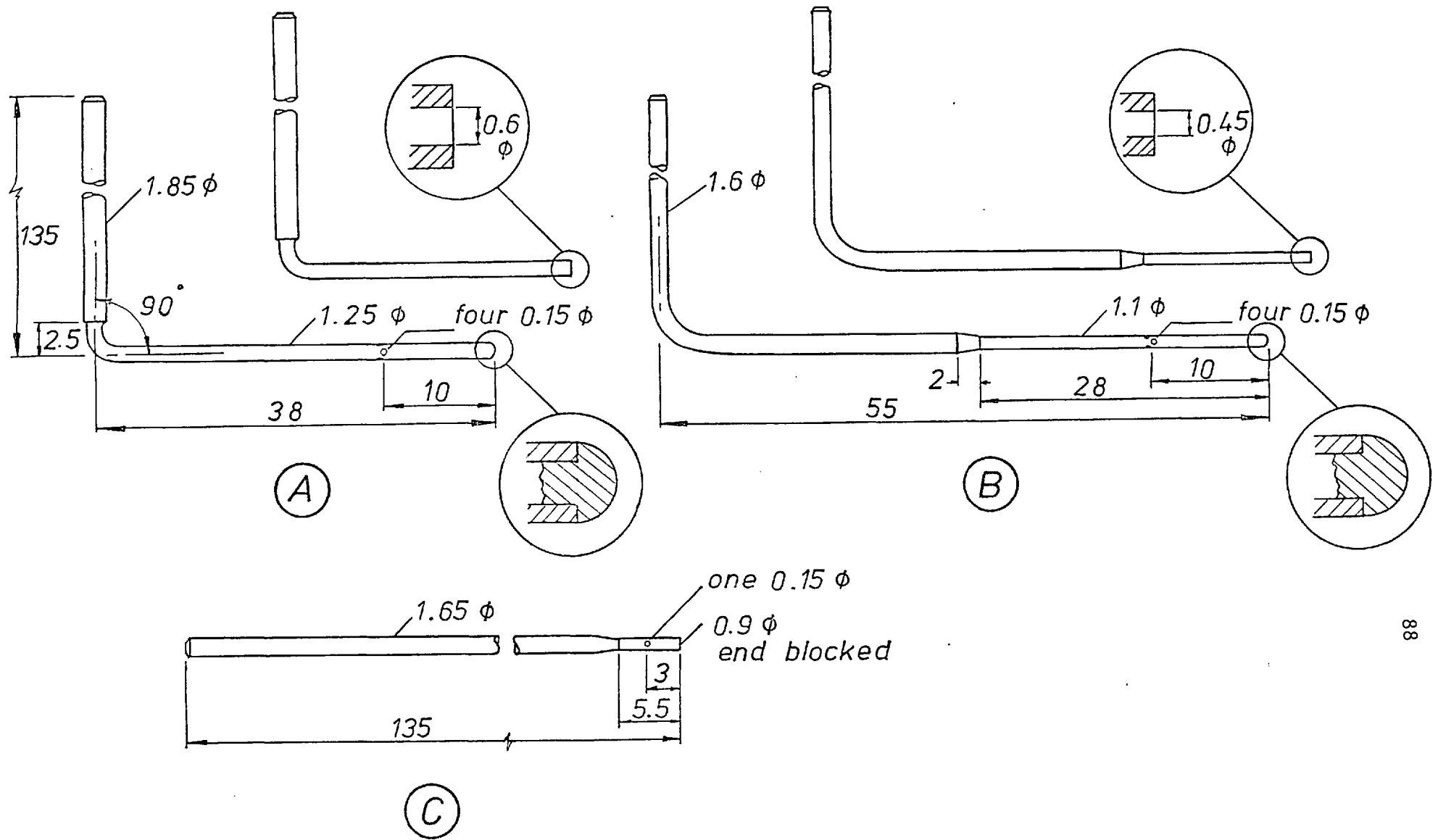
Fig.(5.5.1)   Details of probes used : (A)- all stations other than inlet; (B)- at inlet station; and
(C)- flow - reversal testing probe.

problems; to these, it is believed, some novel solutions were devised. The major problem was the creation of burr-free, circular holes on the periphery of the hypodermic tubing. This took on fairly serious proportions since the OD of most tubing used was of the order of 1 mm. The location of four symmetric holes of small diameter on such tubing, could not be achieved by drilling. Besides being expensive in drills, time and tubing, the resulting holes proved unsatisfactory. The problem was overcome through the use of the spark-erosion process. The method adopted was as follows:

First, thin copper strands, each less than 0.125 mm in diameter were extracted from ordinary electric fluxes. One end of such a strand was clamped to a precision vice; at the other, a steady pull was exerted. This resulted in the drawing out of the strand and served the dual purpose of reducing the diameter still further and of stiffening of the strand due to work-hardening. Approximately 40 mm lengths of these hardened strands were held in pin-chucks and used as electrodes in an S.M.D. Electric Discharge Machine. Figure (5.5.2) illustrates the set-up used:
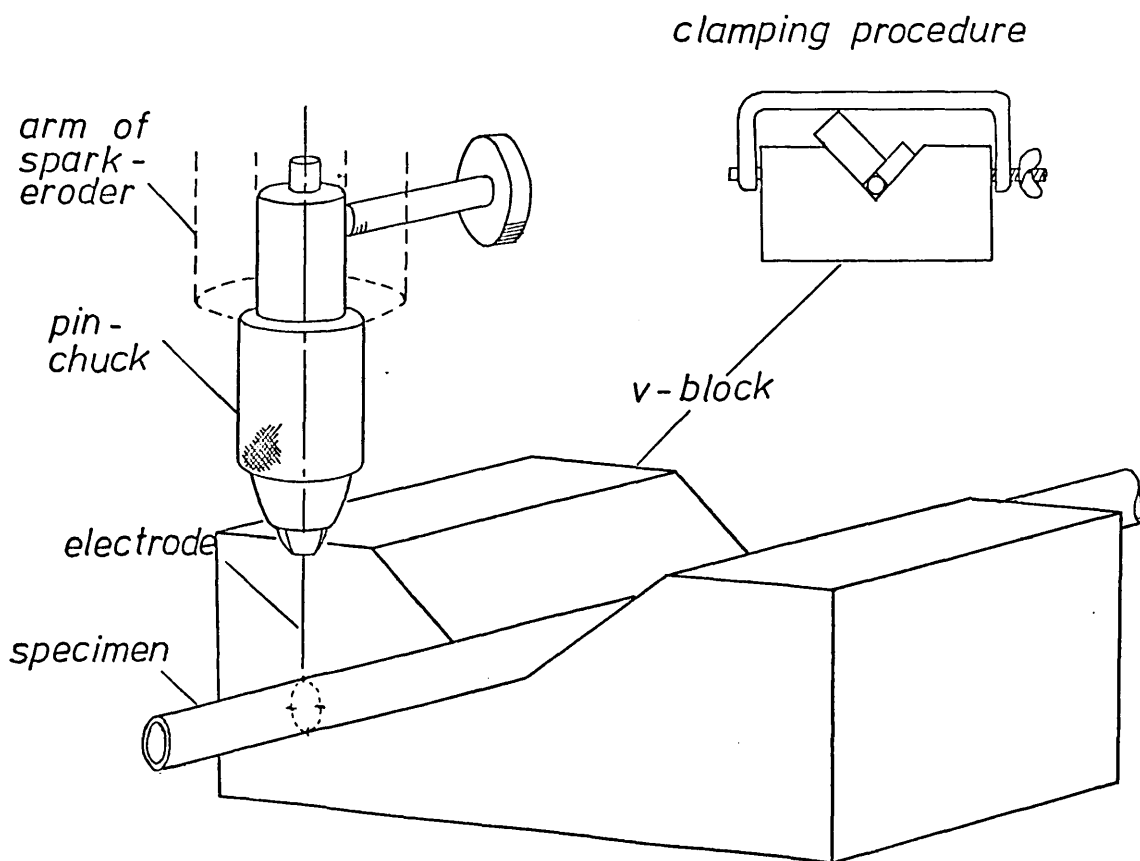
Fig.(5.5.2) Assembly for spark - erosion
of hypodermic tubing.

The specimen tubing were placed horizontally on a V-block and clamped firmly to it. Through scribing on dye-stains, painted on the tubing, the location at which a hole was to be bored was marked on this tubing. A disc graduated in degrees, attached to the tubing at its far end could be used to rotate the tubing through a predetermined interval, whenever more holes than one were required in the same plane. The entire assembly was then immersed in a bath, integral to the discharge machine, filled with paraffin. The elbow of the arm to which the pin-chuck holding the electrode was affixed, was first crudely adjusted to position the electrode roughly above the point marked on the tube. A servo-motor connected to a cross-member on the arm was then switched on to lower this member slowly until the electrode was just in contact with the specimen tubing. At this point, the position of the arm was corrected manually, until the electrode was aligned exactly with the required point. The discharge system was then connected up and the spark-erosion process initiated. Through trial and error it was determined that a capacitance value of 0.001 mF and a resistance of $8200\,\Omega$ produced the best results. Approximately ten minutes sufficed for the creation of each hole. The completion of this process was indicated clearly by the ejection of debris and air bubbles from the bore of the tubing into the clear paraffin of the bath. Circulation of paraffin through the tubing enhanced the removal of debris and made more regular the erosion process. It was found useful for the small-bore tubing to increase this circulation artificially by the use of a hand pump from time to time. The graduated disc was then rotated through a predetermined angle and the procedure repeated as many times as was required. Since the tubes were of small diameter, care was taken to stagger the position of these holes axially by a small amount, to reduce excessive weakening of tubing at the plane were the holes were located. In all cases, the centre-lines of these holes were not staggered more than half the O.D. of the tubing.

Examination under a microscope revealed that the holes generated by the afore-mentioned procedure were perfectly circular, free from burrs and other imperfections and in almost all instances were less than 0.2 mm in diameter. The ends of all static pressure probes were then blocked off with a glob of Araldite and when this had dried and set, it was lapped to a hemispherical shape to streamline the flow in the vicinity of the

probe tip. Total pressure probes needed no special treatment beyond the honing of the ends to render them flat and exactly perpendicular to the probe axis.

Probe set B (Fig. (5.5.1) was used to measure distributions of static and total pressure across the inlet plane of the test-section. This was necessitated by the design of the sliders whose width required a minimum distance of 46 mm from the centre of the measuring hole to the inlet plane. Set A was used for measurements at all other planes.

Static and total pressures were transmitted to and registered by Betz-type micromanometers graduated in millimeters. 6 mm bore Poly-thene tubing was used to transmit pressures from the probes to the mano-meter. These manometers were found to be reliable and accurate, though the large response times associated with their use, detracted somewhat from their convenience. Periodic checks were conducted to ensure that all connexions associated with measurement of pressures were airtight at all times.

5.6   Commissioning, testing and running of rig

a)   Air-tightness

The rig was commissioned with both side walls of the test-sec-tion in a zero-angle position to form a square-sectioned duct. Connec-tions between the various elements of the rig were sealed with a cloth tape and tests were made to detect leaks; the joints proved air-tight. The plugs covering probe holes and the slider-roof section contacts were similarly checked. A slightly loose contact between one of the sliders and the roof of the test-section was corrected with silicone grease. To test the side wall-roof contacts, a little chalk dust was sprinkled on the test-section floor and was observed to be undisturbed when compressed air was blown towards it from the annular space between the fixed and swivelling side walls. Finally, with the blower switched on to its full capacity, small amounts of smoke were introduced into the above-mentioned annular space. These were seen to be undisturbed and were not sucked into the test-section at any point.

b)   Vibration

Initially, the rig was seen to vibrate considerably, especially with the blower at its maximum capacity. Bolts connecting elements of the rig, were tightend and a rubber bellows was introduced between two sections of the intake mainfold of the blower. While this reduced the vibration considerably, it was not eliminated entirely. The major avenue of vibration transmission was discovered to be the motor housing. When a breach was affected in this support, using a gas-cutter, no visible vibration was detectible in the test-section.

c)   Calibration

The micromanometers were used to register pressures on a test-tunnel built for purposes of calibration and available in the laboratory. These compared very favourably with standard readings and hence no corrections were applied to values registered by these manometers.

Pressure drop readings at the inlet to the test-section at various positions of the rheostat control of the motor used to run the blower indicated that Reynolds numbers in the range 1×10^5 to 2×10^5 could be attained. For most of the runs reported in this work, a value of approximately 1.4×10^5 was chosen.

The probes themselves, corresponded to standard designs (e.g. Rosenhead $[50]$) and required no calibration.

d)   Cleaning

The inner surfaces of the test-section were constantly cleaned; whenever the geometric configuration was changed, the surfaces of the roof and floor were polished. At regular intervals, all the probes in use were cleaned with acetone. At less frequent intervals all flexible tubing were cleaned and dried before re-use.

e)   Operation

Recordings of pressure static and total were made in several sessions over a period of eight weeks. On each occasion the flow was allowed some time to settle down after the blower was switched on. Readings at any given station were completed before terminating each session. Random checks were made at the start of each session to ensure repeatability of results; in all instances, this was achieved to within 2 %.

5.7   Data recording and reduction

a)   Traversing

There were eight measuring stations for static and total pressures. Four of these, through the use of sliders, enabled distributions over the entire cross-section of the diffusers to be obtained; the remainder enabled pressure profiles across the vertical centreplanes to be measured. In addition, there were thirteen pressure taps on the floor of the test-section which enabled wall static pressures to be measured.

The micrometer on the traversing gear was operated manually, the direction of traverse always being from floor to roof. Horizontal traverses at four stations were achieved through sliding the traversing gear. Graduated steel rulers affixed to the roof and adjacent to the slider were used to measure these traverses; a pointer attached to the base of the gear indicating the distance moved in millimeters. On average, about twenty measuring points were chosen in each direction of traverse.

b)   Data recording and reduction

All data recordings were performed manually; care being taken to allow sufficient time for the micromanometers to respond to changes in flow conditions. Checks at random points were constantly made, for repeatability of recordings. Occasionally, the speed of the motor connected to the blower tended to float, but invariably returned to the speed governed by the rheostat setting on the motor speed control. When-

ever such fluctuations were observed, readings were temporarily sus-
pended.

A small computer program was written to reduce the data to
convenient nondimensional forms. Tables of these are available in
Appendix A4.

5.8 Concluding remarks

Within the limits of the objectives laid out at the beginning
of this chapter, the experimental program undertaken for this thesis
proved successful. The designing of the various elements of the rig
and measuring devices and their manufacture was a matter of a few
months. Commissioning, testing and routine running of the rig occupied
a further couple of months. The data obtained are tabulated in
Appendix A4.

CHAPTER 6

PRESENTATION OF EXPERIMENTAL DATA

6.1   Introduction

It is the purpose of this chapter to present experimental data
obtained by the investigation reported in Chapter 5. A brief description
is provided of the type of measurements made. A simplistic assessment is
made of the consistency, reproducibility and accuracy of the data ob-
tained. The data are used to examine the three-dimensional flow pattern
in rectangular-sectioned diffusers. It is concluded that the limited ob-
jectives of the experimental program were achieved.

6.2   Type of measurements made

6.2.1   Quantitative measurements

Measurements of static pressure and axial-velocity distributions
only were made. This was achieved for three positions of the swivelling
side walls, corresponding to the 0°, 2° and 4° included angles respect-
ively. In addition static pressure recordings were observed from wall
pressure taps, at two further positions corresponding to the 6° and 8°
included angles. Such recordings were also observed with side walls fixed
at the 4° included angle position, for five different flow rates, i.e.
Reynolds numbers. The inlet conditions under all these circumstances
were identical: uniform velocity with a very small boundary-layer growth,
(i.e. $2\delta^{*}/d$ less than 0.01) on all four walls. The intensities of
turbulence at inlet to the test-section were in all cases estimated to
be uniformly low.

There were eight measuring stations. At four of these, the
sliders enabled traverses over the entire cross-section of the test-
section to be made. At the remaining four, traverses in the vertical
direction only could be made along the vertical centreplane of the test-
section. The size of the test-section precluded the use of a combination

pitot-static probe. Consequently traverses were made first with the
static probe and subsequently with the total-head probe at each point
in the flow field for which measurements are reported. Values of local
velocity were obtained from a combination of these results. Mean vel-
ocities corresponding to each different flow rate used, were obtained
by integrating the velocity distribution at inlet to the test-section.
The uniformity of this distribution made this integration relatively
easy. Measurement of flow rate by one other means was carried out. An
orific plate located in the intake manifold of the blower and calibrated
by earlier workers was used to measure the flow rate which was within
2 % of that arrived at by the afore-mentioned procedure. Hence the for-
mer practice was adopted throughout the remainder of this work. Great
care was taken in sealing off points where leaks were expected. The mean
velocity at inlet to the test-section, obtained from the flow rate was
used to normalise velocities obtained at all other points, as well as
static pressures via the dynaic head at inlet. It is these normalised
quantities which are tabulated in Appendix A4.

6.2.2   Qualitative measurements

In addition to the above measurements, it was sought to arrive
at qualitative descriptions of the flow field. To this end, the probe
designated (C) in Figure (5.5.1), was used. For each position of the
side walls, this probe was introduced into the flow through the normal
traversing procedure. At any position in the flow, the probe was rotated
manually through the use of the probe holder (Fig.(5.3.7). At positions
like the central core of the test-section, the reading on the micromano-
meter with the hole aligned along the flow direction, rapidly diminished
when the probe was rotated about its axis through a small angle. When the
rotation was continued this reading returned to its maximum value only
when the probe hole once again returned to its position of alignment with
the flow direction. This indicated that the magnitude of secondary flows
in these regions, was indeed small.

The above procedure proved less sensitive when adopted close to
the four walls; however, such tests always indicated a one-way flow, for
the included angles for which measurements are reported here. When these

tests were continued with the sidewalls positioned at 10° and 12° included angles, some interesting behaviour was observed. In the vicinity of corners of the test section, no predominant flow direction could be detected by the above-mentioned test procedure. Furthermore the recording of the manometer was no longer steady, large fluctuations being observed even with the probe hole aligned with the axis of the test-section. These fluctuations were observed at all four corners in the x/d ranges between 6.1 and 13.2 for the 12° diffuser and 7.45 and 13.2 for the 10° diffuser. This is in qualitative agreement with measurements obtained in two-dimensional diffuser-flows reported by Reneau et. al. [47] .

6.3.   Assessment of data obtained

6.3.1   Consistency and repeatability

Detailed checks on the internal consistency of the data obtained were not made. However, the data recording, performed at different times, of the same geometric situation, revealed almost identical results, in every case. Repeatability was thus ensured in all cases.

6.3.2   Accuracy

The inaccuracy of the micromanometers used in the experiments was less than 0.2 mm of water. The error in measurement of flow rate and hence of mean velocity at inlet to the test-section is estimated at $\pm$ 2 - 3 %. The error in registering total head on the manometer was of the order of 1 - 2 %. Thus the error, both random and systematic, in the normalised velocities presented in Appendix A4, is evaluated to be of the order of $\pm$ 6 %. The errors in the values of pressure-rise coefficients presented are evaluated to be less than this value and of the order of $\pm$ 4 %.

It is believed that the precision of traversing and probe-positioning was of a high order. The error in this respect being of the order of $\pm$ 0.01 mm in the vertical direction and $\pm$ 0.1 mm in the horizontal, i.e. slider, direction. The error in angular displacement

of the swivelling side walls was estimated to be less than 1 %.

6.4 Concluding remarks

1) The simple devices used in measurements reported in this Thesis, have minimised the need for repeated calibration. The maximum errors in the reported values of velocity are estimated to be less than $\pm$ 6 % and those in values of pressure-rise coefficient to be less than $\pm$ 4 %.

2) The quantitative measurements obtained are reasonably reliable and cover a range, which, within the knowledge of the author, has not been reported elsewhere.

3) Qualitative measurements with a special probe have indicated that the flow field in diffusers for which measurements are reported, is essentially one-way. For 10° and 12° diffusers, varying amounts of reverse flow or stall were observed. These were of the unsteady kind and were detected to commence at 7.45 and 6.1 duct-widths respectively, from the inlet.

4) Static pressure traverses indicated that in the bulk of the flow at any given axial station, static pressure was essentially uniform, thus vindicating the assumption to this effect made in Chapter 3.

PART   III

Theoretical Predictions
compared with experi-
mental and analytical
data

CHAPTER 7

PREDICTION OF LAMINAR FLOWS

7.1   Introduction

.   . In this chapter, the results of computations of three-dimen-
sional laminar flows in ducts, are presented. Two classes of flow situ-
ations are considered, the effect of several flow parameters upon each
of these, being separtely studied. Predictions of heat transfer in the
same situations, with two different types of boundary conditions, are
also reported. Wherever possible, comparisons with available analytical
and experimental evidence, are indicated. As a result of these, it is
concluded that the prediction procedure is flexible, and reasonably
accurate in the prediction of duct flows.

7.2   Developing flows in ducts

The problem considered here is one of laminar flow development
in straight, rectangular-sectioned ducts. The ducts are of constant
cross-section, and the velocity distribution at their inlet sections
are presumed uniform, unless available in experimentally determined
form. Predictions of the hydrodynamic features of the problem are des-
cribed below.

7.2.1   Pressure-drop

The pressure drop along the axes of the ducts is expressed as
a coefficient, $-C_{px}$ in terms of the dynamic head at inlet. In Figures
(7.2.1a), (7.2.1b) and (7.2.1c), the effect of aspect ratio upon the
pressure drop, can be observed as a function of distance. This distance
is so normalised, that the results are independent of Reynolds' Number.
The present predictions are represented by firm lines, experimentally-
determined values by appropriate points and the results of other anal-
ses by dashed lines. The characteristic duct width, used both for the
definition of Reynolds numbers and in normalising distance along the
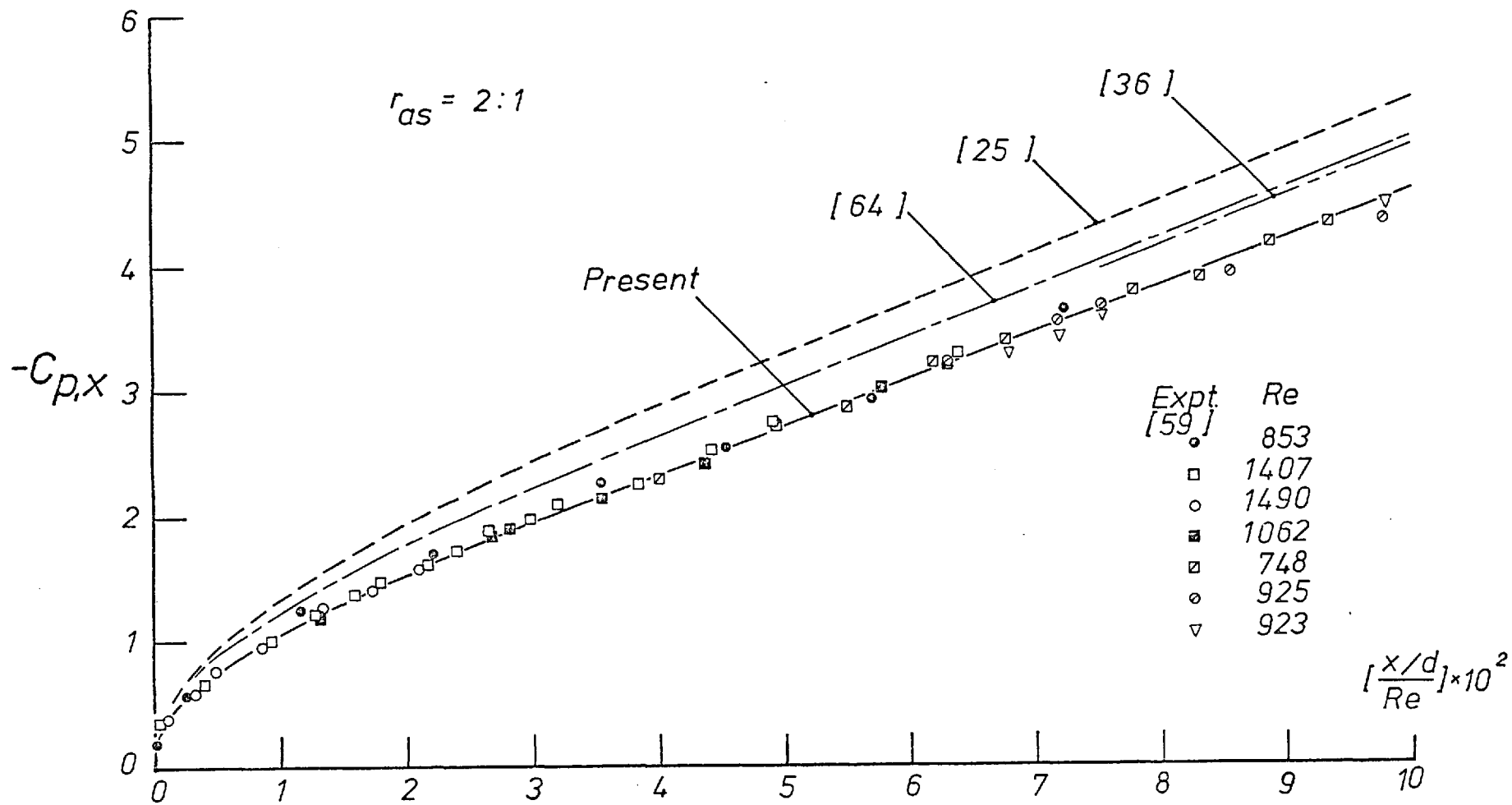
Fig.(7.2.1) (a) Pressure-drop in the entrance section of rectangular-sectioned ducts

$-C_{p,x}$

$r_{as} = 5:1$

[25]

[64]

[36]

Present

Expt.

[4]	Pt.	Re
	○	1063
	△	702

[59]	Pt.	Re
	⊗	1225
	▲	1602
	▽	1686
	□	2149
	◉	2257
	▲	2583
	▼	2708

$[\frac{x/d}{Re}] \times 10^2$
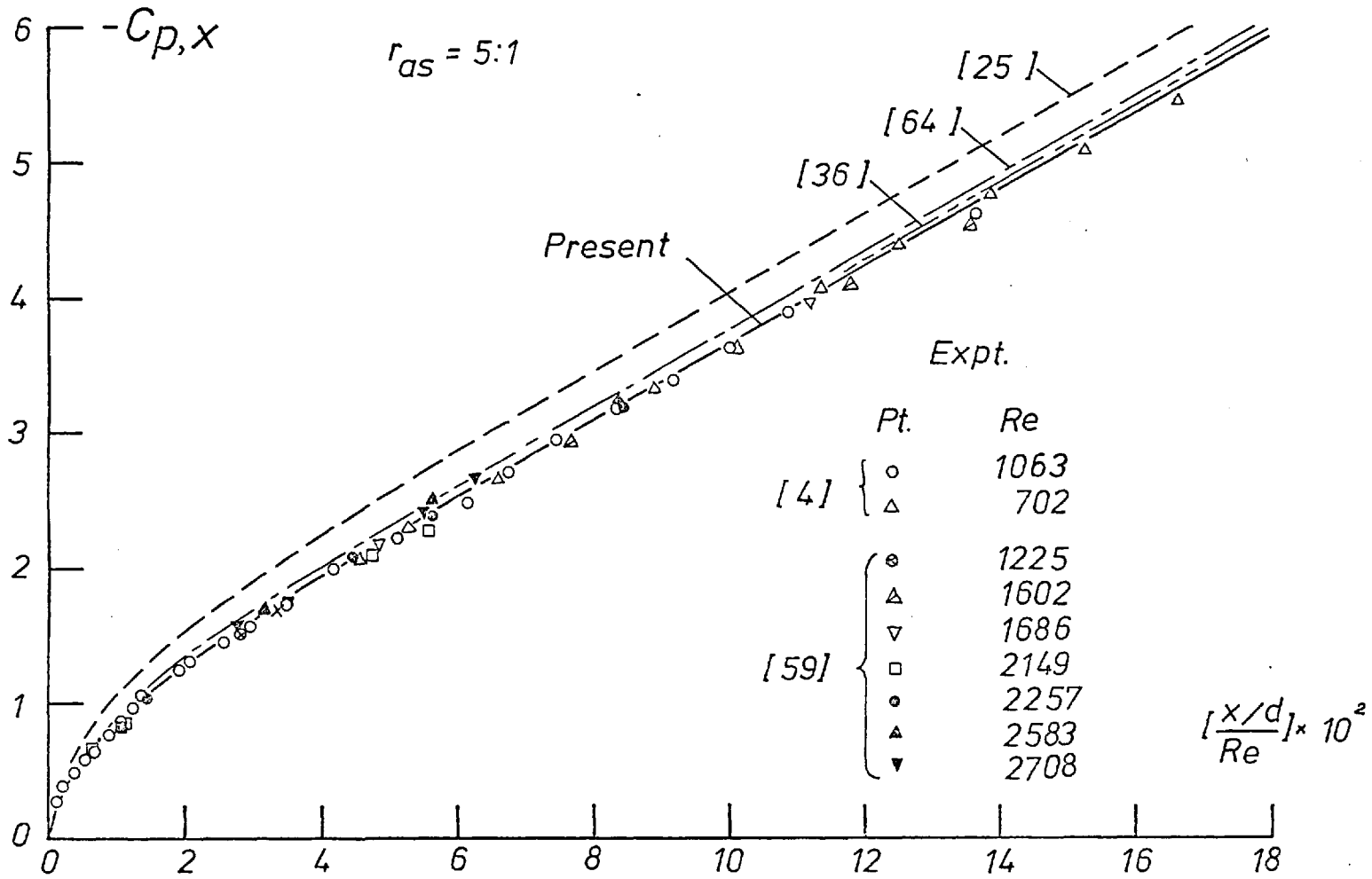
Fig.(7.2.1) (b) Pressure-drop in the entrance region of rectangular-sectioned ducts.

duct axes, is the width of the shorter side of the duct, d . In this way, although the flow rates in each case differ, the influence of the width of the longer side may be clearly observed. For uniform-property laminar flows, the use of the non-dimensional co-ordinate $\left(\frac{x/d}{Re}\right)$ renders the problem Reynolds number independent.

In Fig. (7.2.1a) the numerical calculations can be observed to predict a lower value of pressure drop in a 2 : 1 duct than those predicted by the analyses due to Han $[25]$, Wiginton and Dalton $[64]$ and Lundgren et. al. $[36]$. Furthermore, the prediction is in close agreement with experimental data obtained by Sparrow et. al. $[59]$. In Figs. (7.2.1b) and (7.2.1c), similar results can be observed for a 5 : 1 and a 51 : 1 aspect ratio duct respectively. The experimental data are those measured by Beavers et. al. $[4]$. It is emphasized here that no special practices were adopted in the calculations to procure the close agreement between calculated and experimental values. For the results presented in Fig. (7.2.1c), the assumption of two-dimensionality of flow in the 51 : 1 aspect ratio duct, was checked by performing calculations for the genuinely two-dimensional situation. Differences too small to be plotted, between results for a 51 : 1 and the infinite parallel-plate situation, were observed.

Computations of flows in ducts were continued until the fully-developed situation was reached. The friction factors obtained from the axial pressure-gradient under this circumstance is represented in Figure (7.2.2) and Table (7.2.1). Favourable comparisons can be observed between calculated and experimentally-determined, values of friction factor.

It may thus be concluded that the manner of calculation of pressure gradient along the PFD is a valid one, for favourable pressure gradient situations. It would be reasonable to suppose that an identical procedure may be used for adverse pressure gradient situations as in diffuser flows. Although calculations were made for laminar diffuser flows, no experimental or analytical results were available for com-
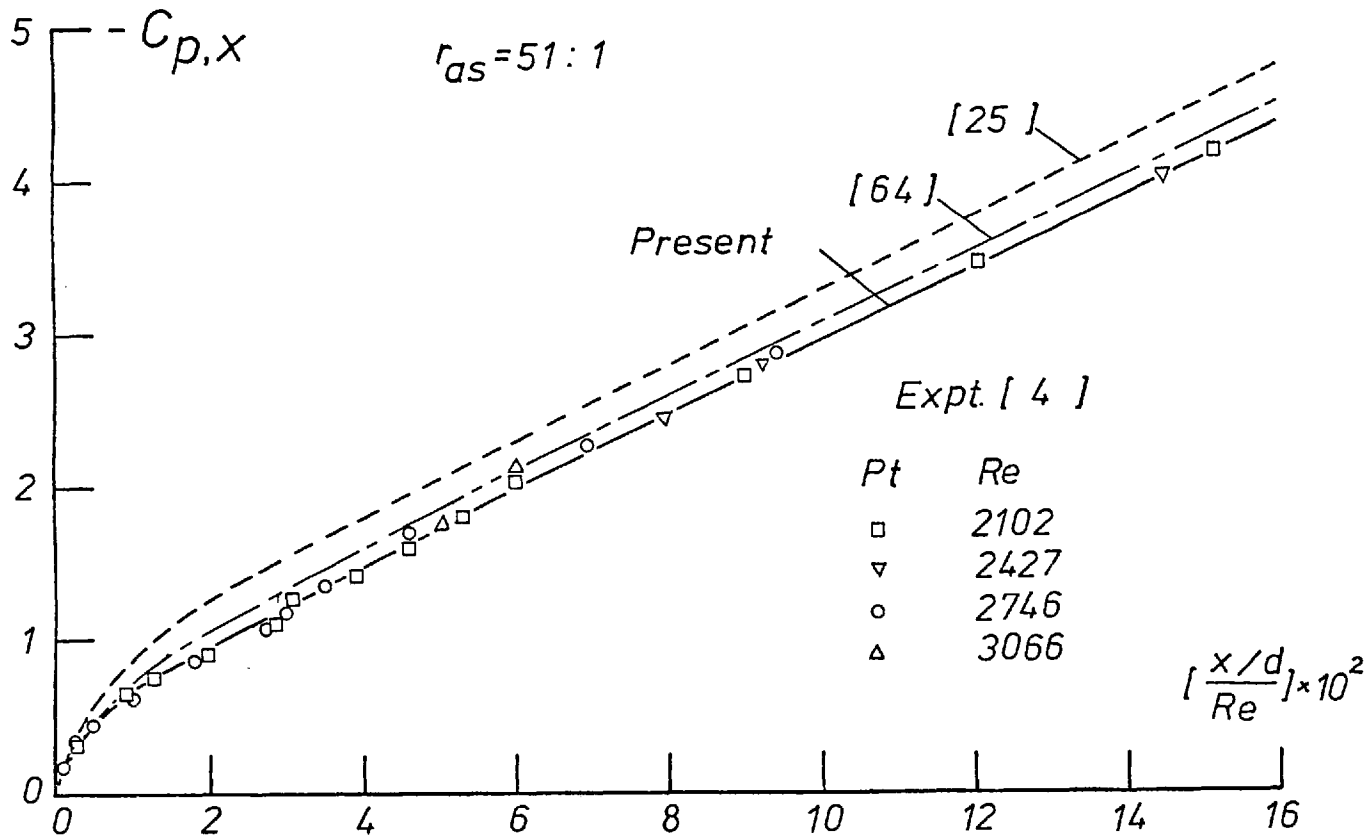
Fig.(7.2.1) (c)   Pressure-drop in the entrance region of rectangular-
sectioned ducts.
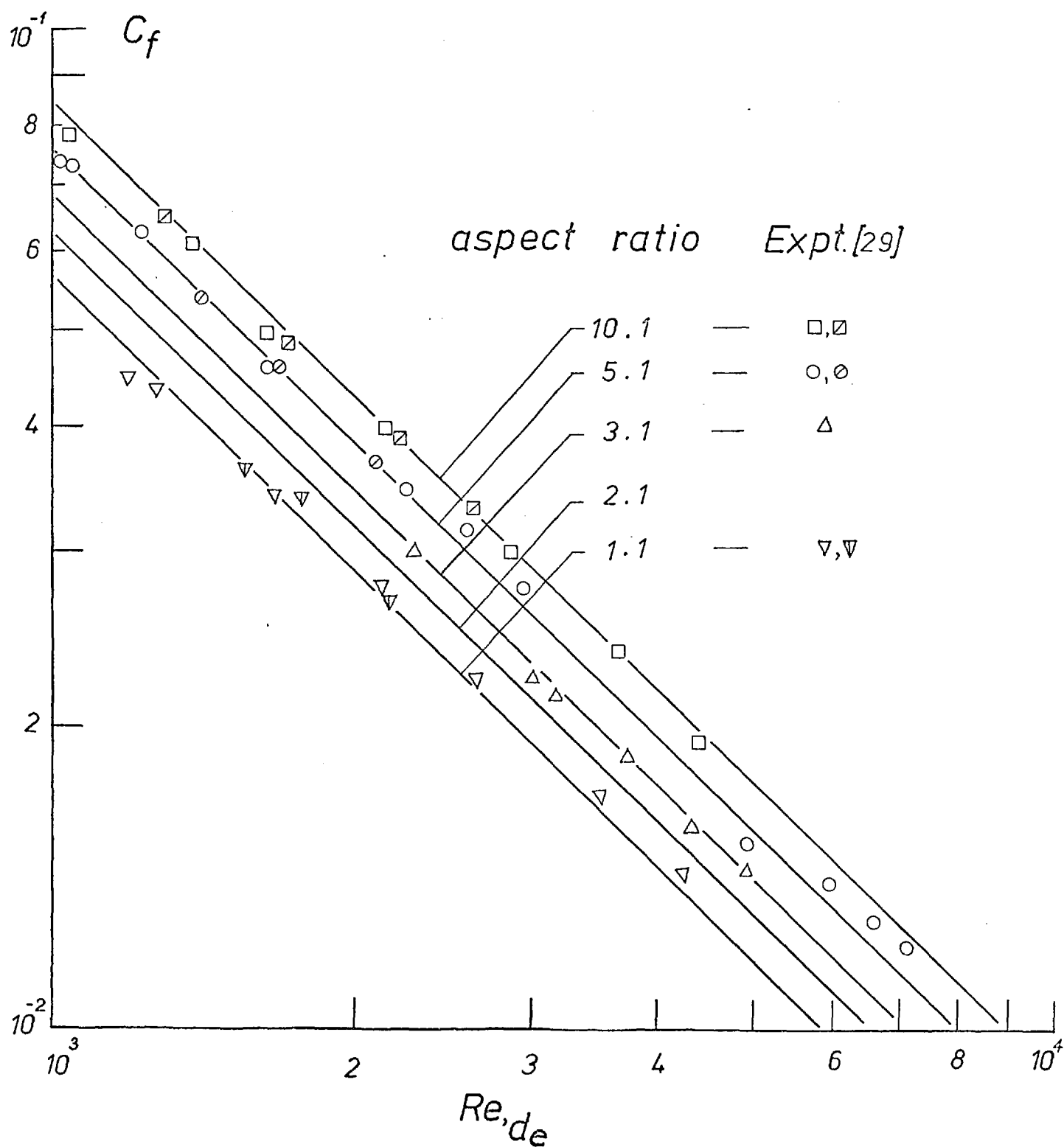
Fig.(7.2.2)   Effect of aspect ratio on laminar friction factor for
fully-developed flow in rectangular-sectioned ducts.

No.	Aspect Ratio r_{as}	Fully-developed centreline velocity $(U/\bar{U}_{in})$				Fully-developed friction factor constant $C \equiv f.Re.$			
		Han [25]	McComas [39]	Fleming and Sparrow [20]	Present	Lundgren et.al. [36]	McComas [39]	Fleming and Sparrow [20]	Present
1	1 : 1	2.0971	2.096	-	2.09	56.91	56.91	-	56.9
2	2 : 1	1.991	1.992	1.99	1.98	62.19	62.19	-	62.2
3	3 : 1	-	-	-	1.86	-	-	-	68.3
4	4 : 1	1.773	1.774	-	1.77	72.93	72.93	-	72.9
5	5 : 1	-	-	1.72	1.70	-	-	76.3	75.6
6	10 : 1	-	1.6003	-	1.60	84.68	84.68	-	85.3
7	: 1	1.50	1.50	1.50	1.50	96.0	96.00	-	95.9

Table (7.2.1)
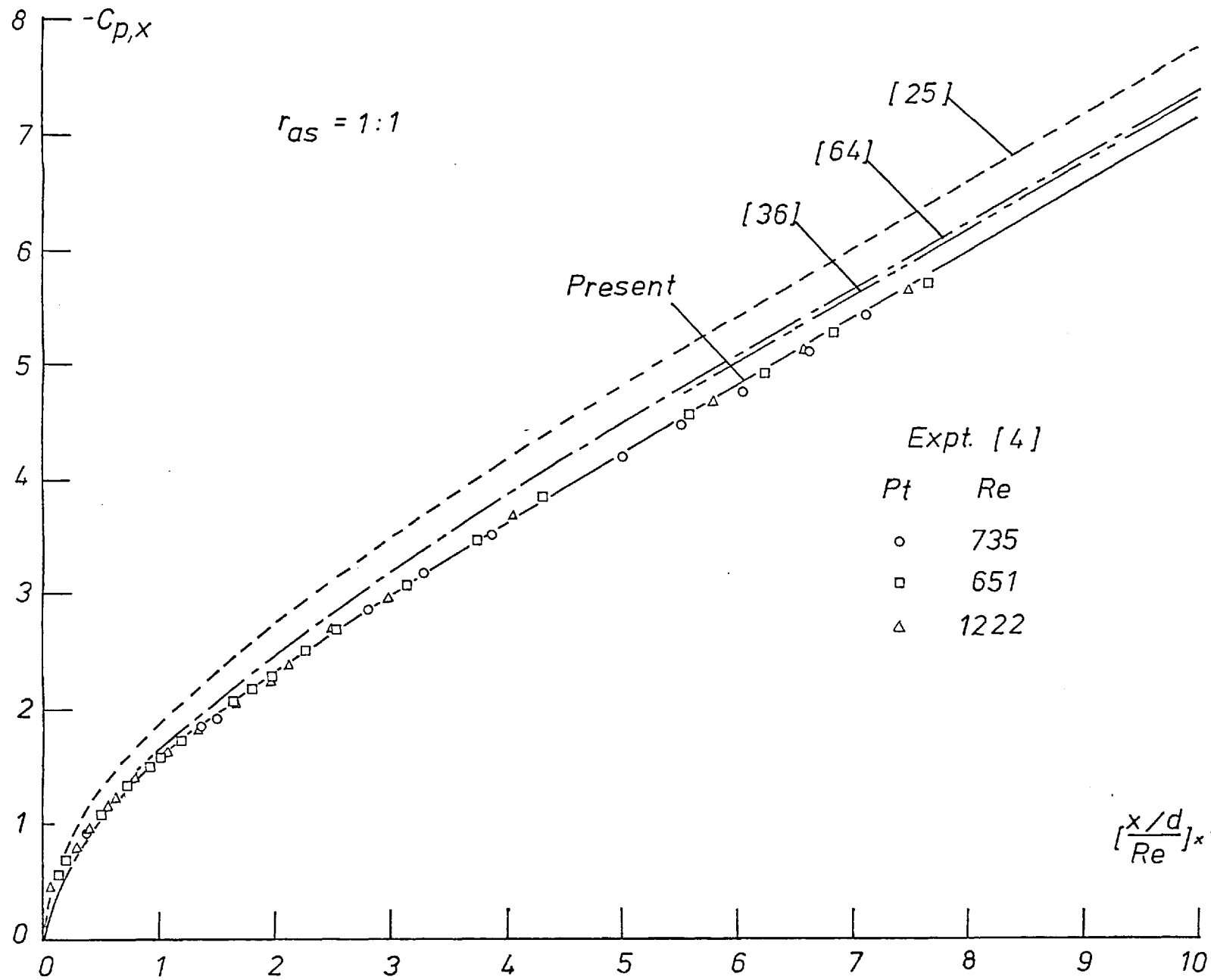
Fig.(7.2.3)   Pressure drop in the entrance region of a square-sectioned duct.

7.2.2 Velocity-profile development

The present procedure yielded, in addition to the pressure-drop results presented above, the associated three-dimensional velocity field. In this section the computed values of velocity distributions are presented and compared with other available information.

Accordingly, in Figure (7.2.4) the predicted increase in velocity along the centreline of a 2 : 1 aspect ratio duct, is presented. The experimentally-measured velocity distributuion at a station close to the actual duct entrance was used as the initial distributuion in the calculation procedure; the distances represented in the following figures are accordingly, measured with reference to this station. The analysis due to Han [25] , uses a linearized form of the momentum equation along the PFD as well as the continuity relation predicts a more rapid rise of velocity than that calculated with the present procedure, as well as that experimentally observed. The detailed velocity distrib ution up to a normalised distance of approximately 13, is represented in Figures (7.2.5a) and (7.2.5b) where comparisons are shown with data obtained by Sparrow et. al. [59] . These indicate clearly the growth and inter-action of the boundary layers on all four walls. Similar results for a 5 : 1 aspect ratio duct are presented in Figures (7.2.6a) and (7.2.6b); the numerical predictions being compared with experimental observations reported by Sparrow et. al. [59] .

It is concluded that predictions of velocity profiles in laminar duct flows have been obtained with reasonable succes. This lends confidence to the proposed prediction of turbulent flows in ducts and diffusers of identical geometric configuration.
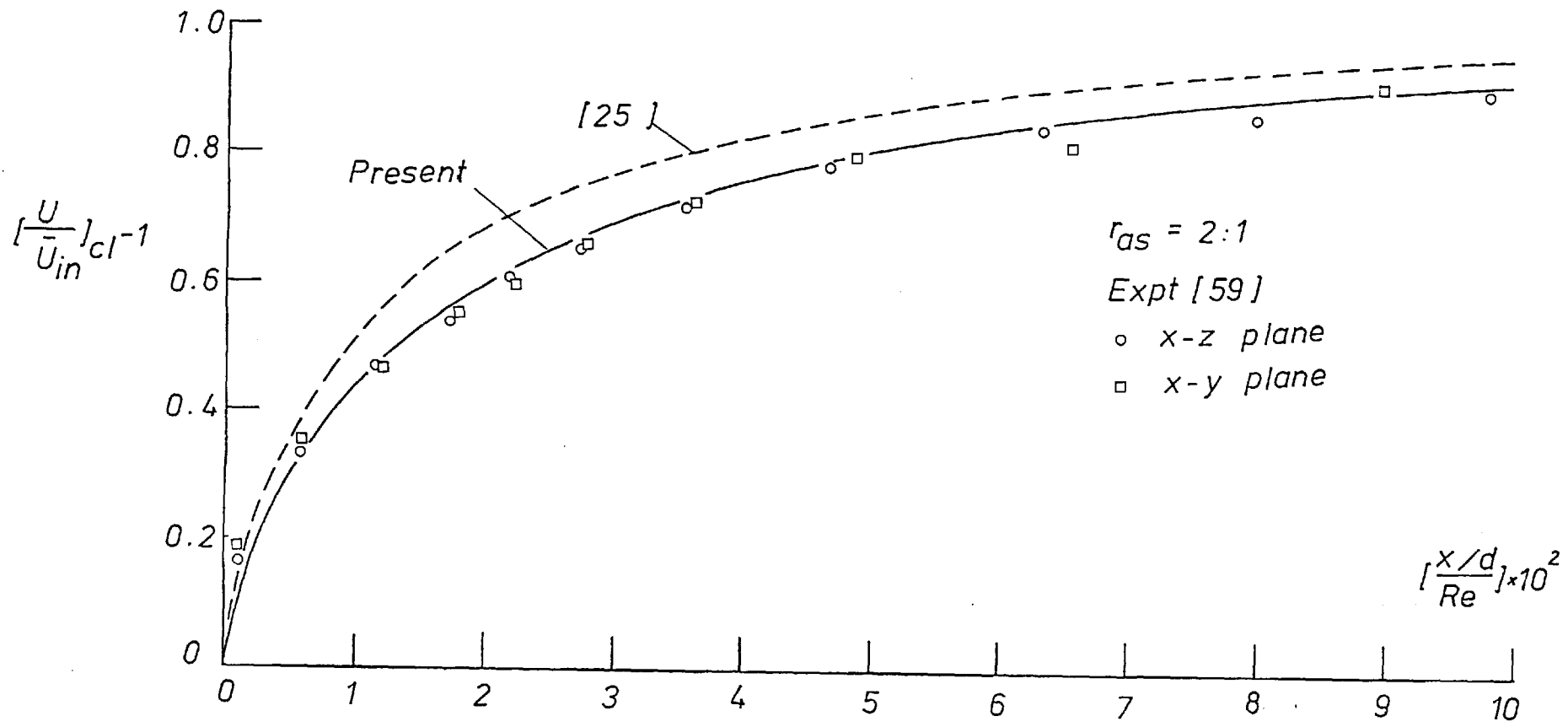
Fig.(7.2.4) Development of centreline velocity in the entrance region of rectangular-sectioned ducts.
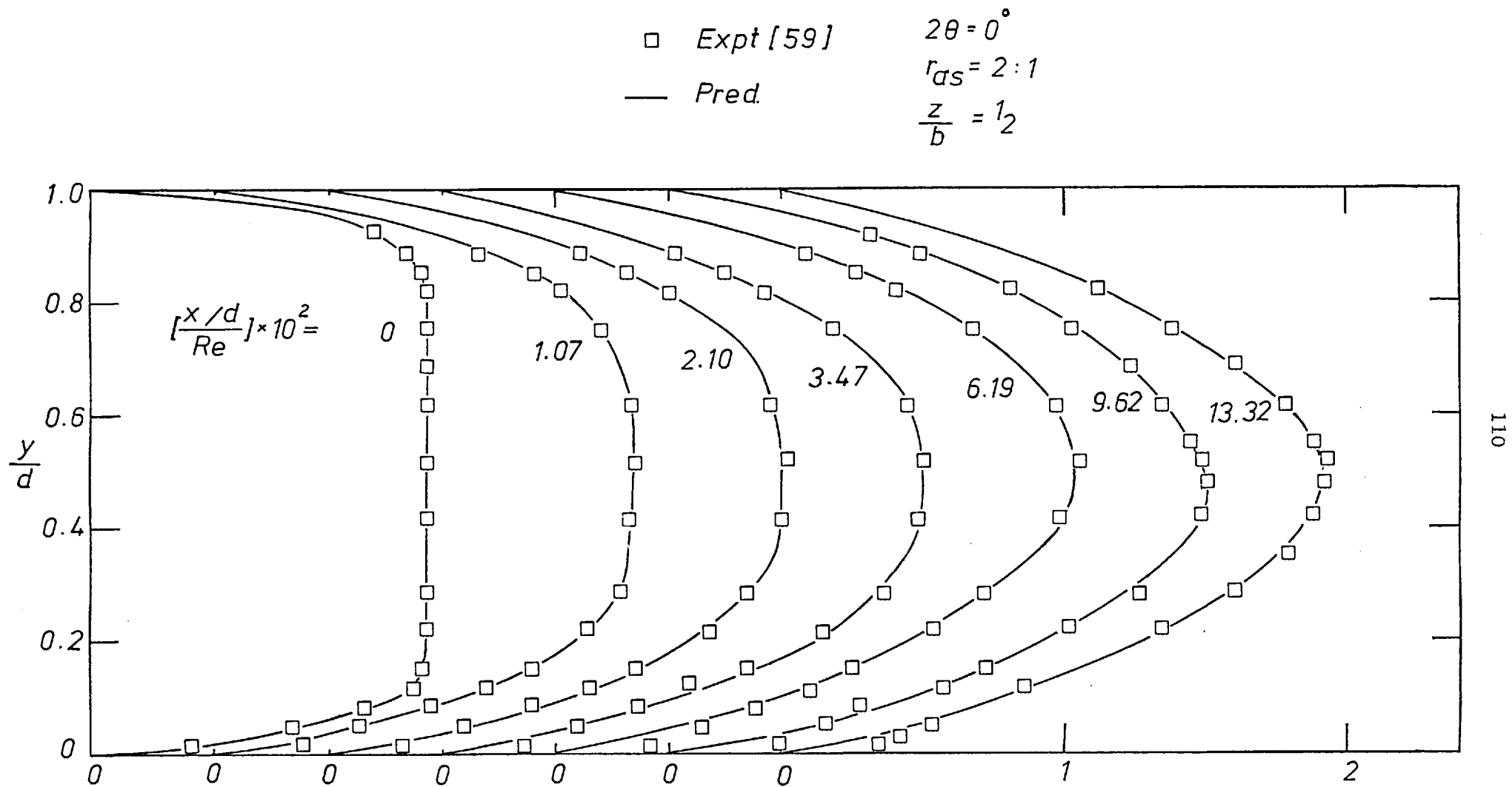
Fig.(7.2.5) (a) Development of velocity (U/U_{in}) profiles across the vertical centreplane of a 2:1 duct.

□ Expt [59]
— Pred.

$2\theta = 0°$
$r_{as}\left(\frac{b}{d}\right) = 2:1$
$\frac{y}{d} = \frac{1}{2}$

Analysis
--- [25]
—·— [64]

$\left[\dfrac{\frac{x}{d}}{Re}\right] \times 10^{2} =$

0   1.10   1.59   4.76   6.44   8.89   11.86

$\frac{z}{b}$

1.0   0.8   0.6   0.4   0.2   0

0   0   0   0   0   1.0   2.0
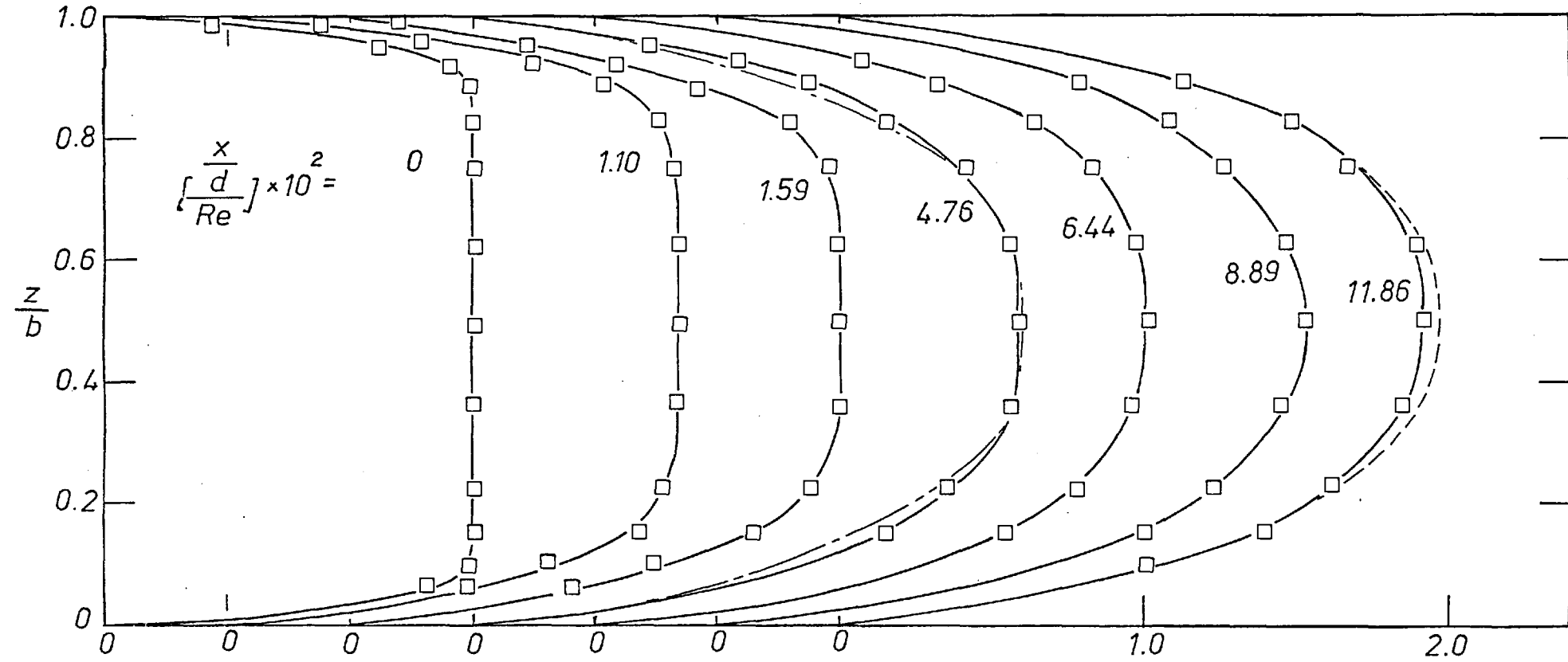
Fig.(7.2.5) (b)   Development of velocity profiles across the horizontal centreplane of a 2:1 duct.
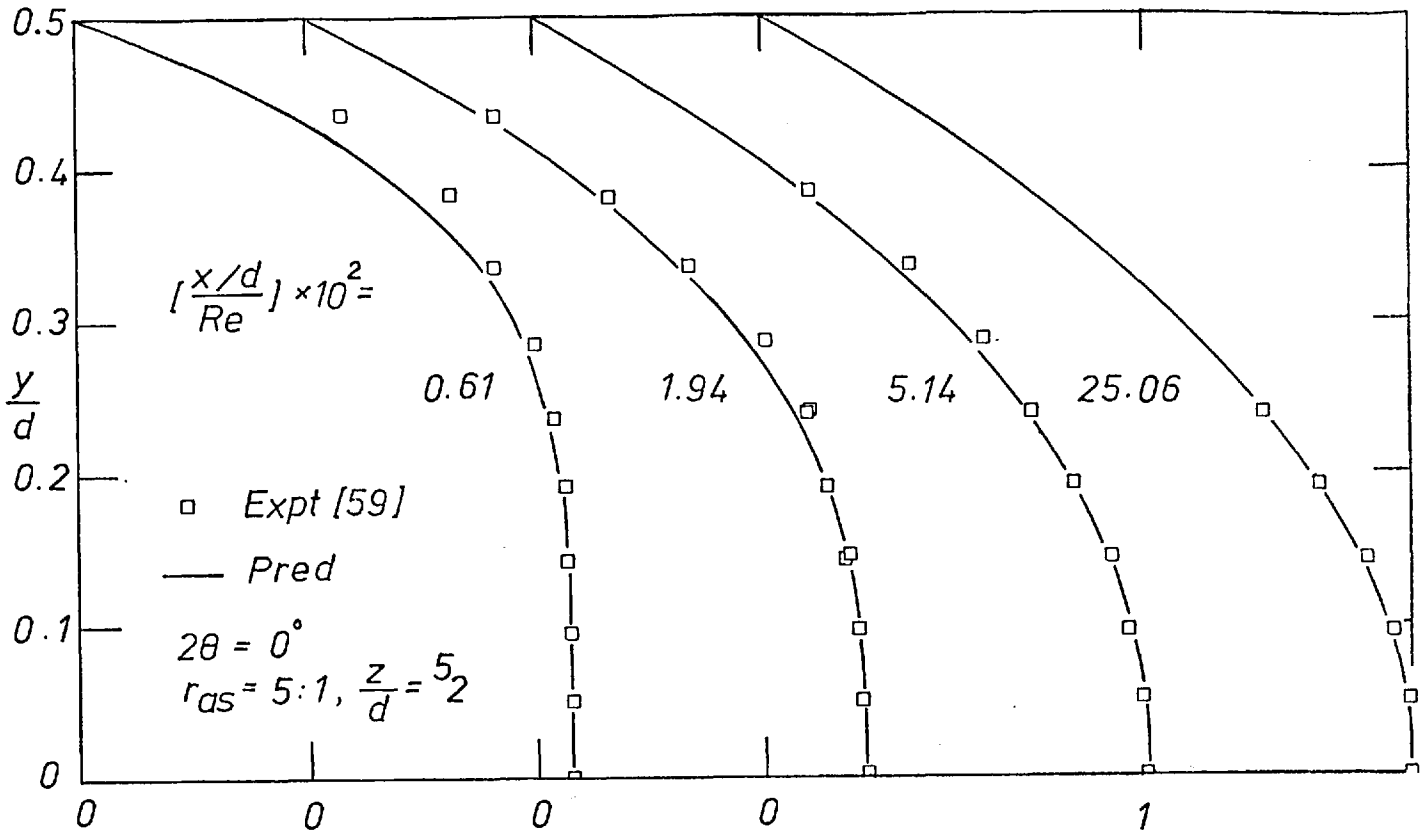
Fig.(7.2.6) (a) Development of velocity (U/U_{in}) profiles across the vertical centreplane of a 5:1 duct.
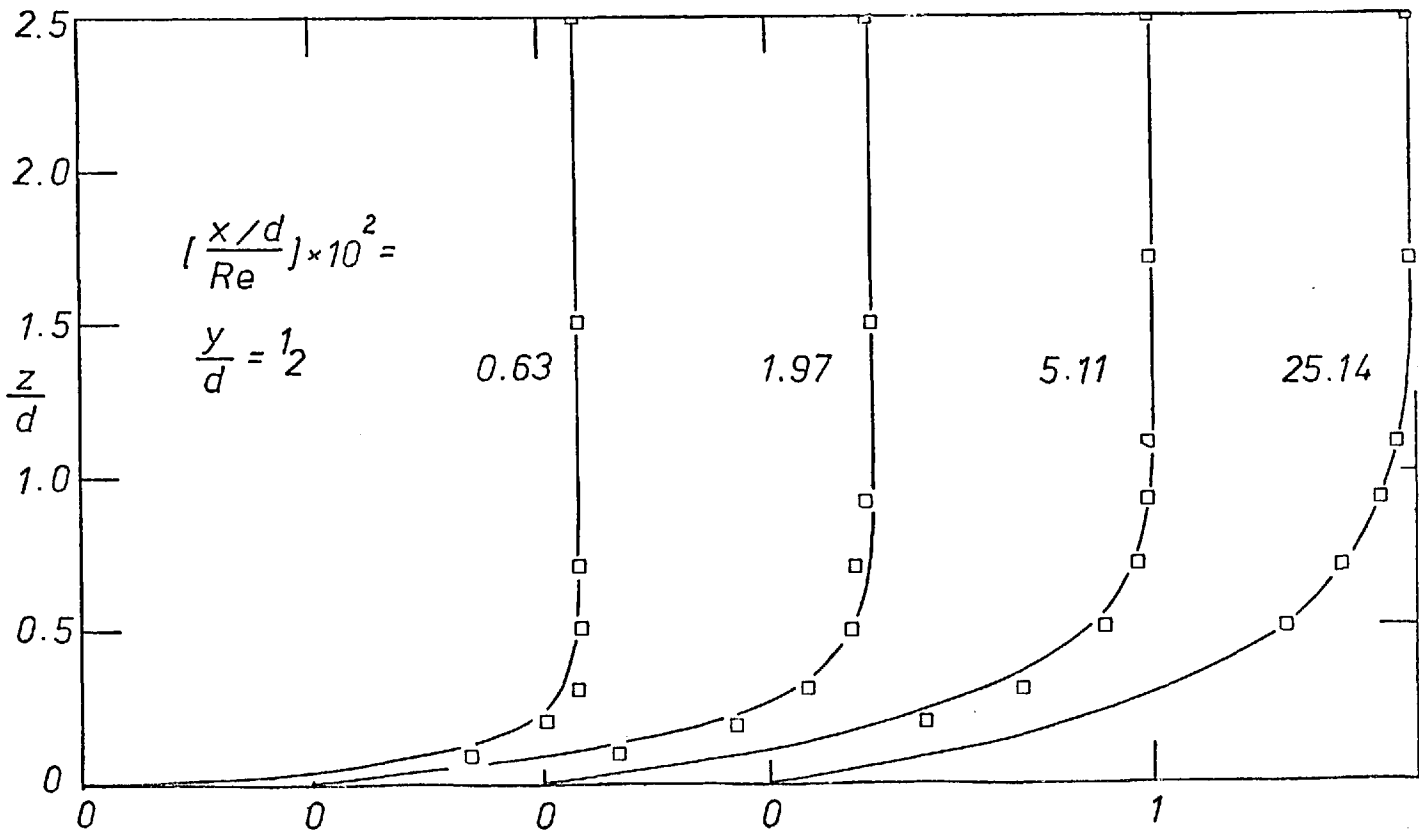
Fig.(7.2.6) (b) Development of velocity profiles across the horizontal centreplanes of a 5:1 duct.

7.3   Flow in rectangular-sectioned ducts with one moving wall

Some of the results reported in this Section has been presented by Sharma and Spalding [55] . They are included here for completeness and as a further evidence of the flexibility of the numberical calculation procedure. Two types of situations are considered here: one in which one of the walls of a rectangular-sectioned duct moves longitudinally (i.e. along the PFD) parallel to itself and another, in which one wall moves laterally again parallel to itself. In both instances, steady movement of the walls alone, is considered. The design of screw-extruders and movement of glass upon its melt during the manufacture of glass sheeting are situations of engineering importance, wherein such analyses would prove useful.

7.3.1   Longitudinal wall movement

Figure (7.3.1) indicates the geometry under consideration. The radius of curvature of the PFD co-ordinate (i.e. ξ) is presumed to be so large that its effects upon the flow may be ignored.

In Figure (7.3.2) the calculated values of pressure drop are compared with experimentally observed values of Yu and Sparrow [66] . The parameter is the ratio of moving-wall to inlet Reynolds numbers (or mean velocities). It can be seen that pressure-drop is reduced by a 'favourably-moving' wall. Within a normalised distance of 5, no re-circulation along the PFD was observed and calculations of this situation presented no problems. The influence of the side walls was marginal due to the large aspect ratio (81 : 1). The radius of curvature (R/d) was also very large (94.72), and so its effects were not included in the calculation.

7.3.2   Lateral wall movement

The situation considered is represented in Figure (7.3.3). Fluid is presumed to enter the duct with a uniform velocity and the effect of
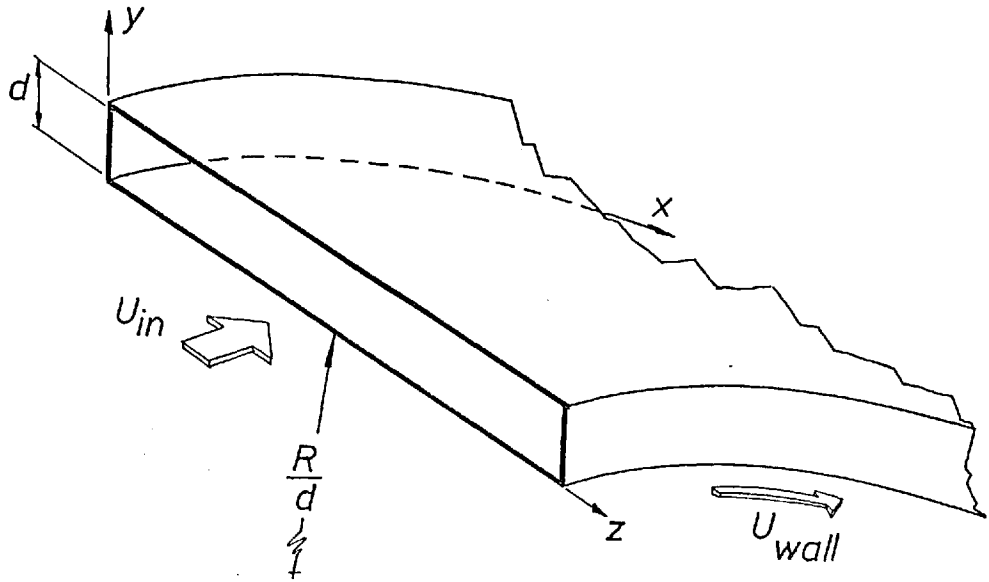
Fig.(7.3.1) 'Moving-wall' geometric configuration. Case 1.
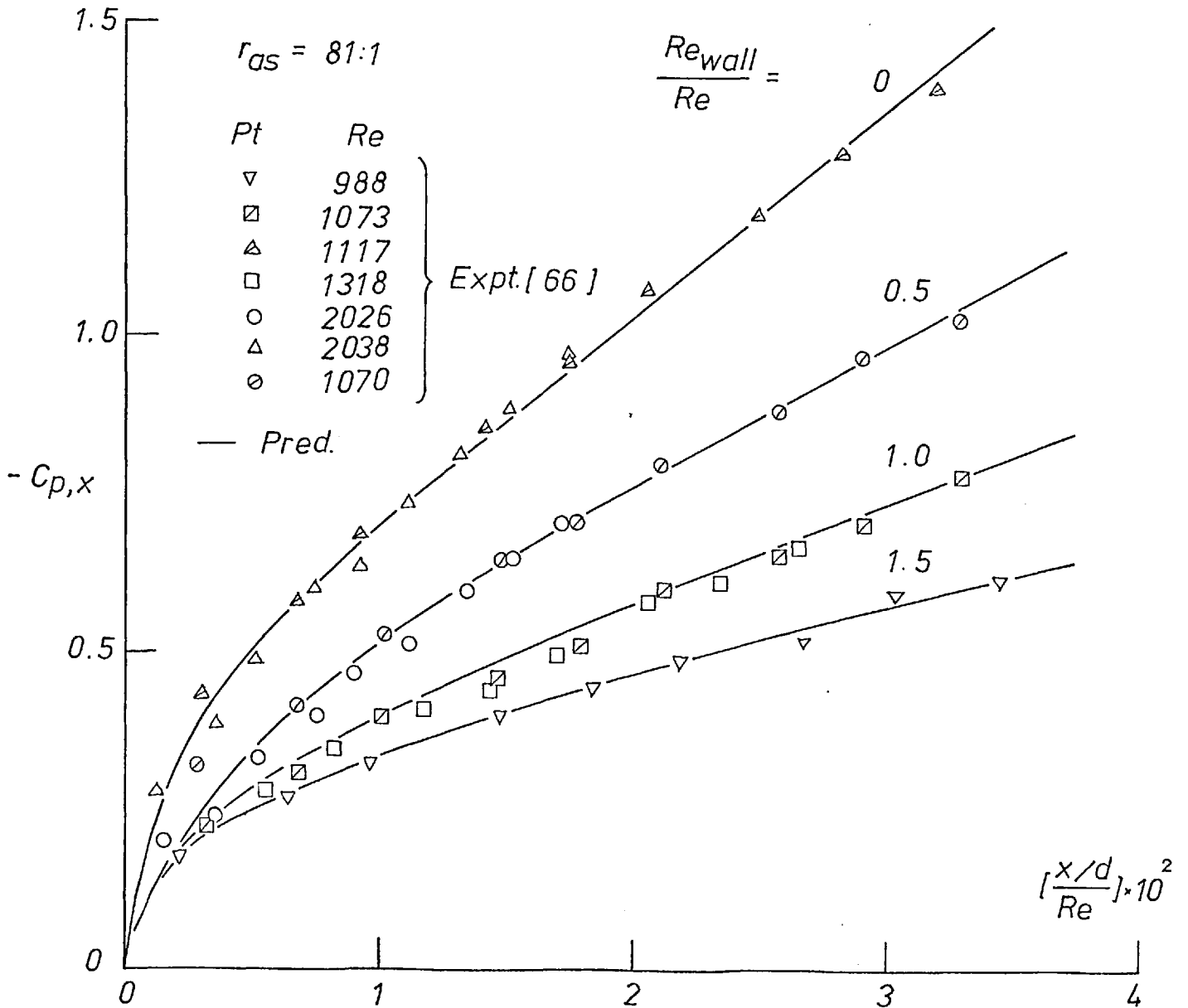
Fig.(7.3.2) Effect of moving wall on pressure drop, Case 1.

the moving wall upon the flow development forms the subject of study.
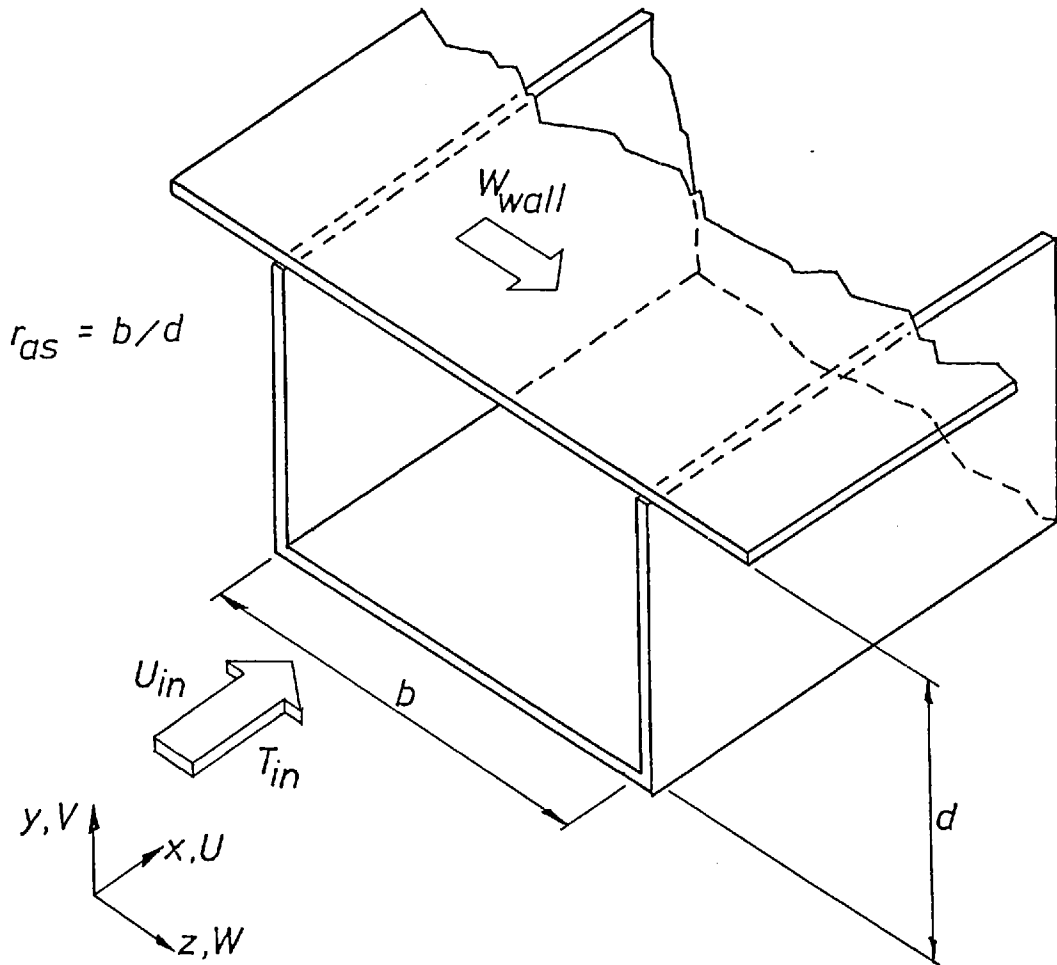
Fig.(7.3.3) 'Moving wall' geometric configuration, Case2.

Thus in Figure (7.3.4) the effect of moving-wall velocity (i.e. Reynolds number) upon the pressure drop in duct of aspect ratio 1 : 1, is presented. Included in the figure are experimental data for the situation when all walls are stationery. It can be observed that a steady increase in pressure drop occurs with increase in wall Reynolds number. However, close to the inlet, i.e. $(X/d)/Re < 0.02$, the flow remains unaffected by the movement of the wall. The effect of aspect ratio upon pressure drop at a given value of wall Reynolds number may be observed in Fig. (7.3.5a).A dimunition in pressure drop occurs with increase in width of the longer side. When the same results are plotted for identical mass flow rates, i.e. hydraulic diameters, it is observed that pressure-drop in fact increases with increase of aspect ratio (Figure (7.3.5b).

Fig.(7.3.4) Effect of moving wall on pressure drop, Case 2.
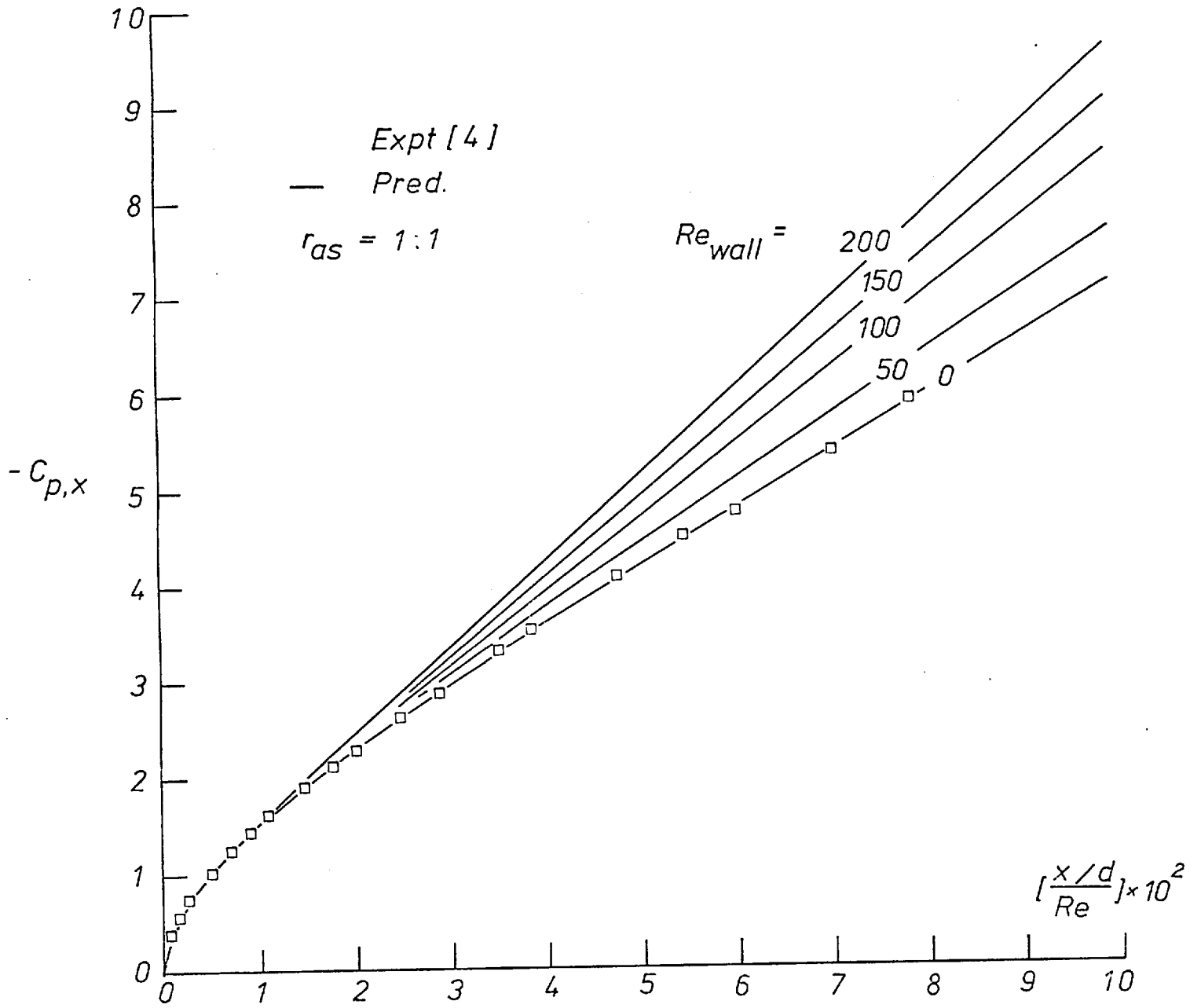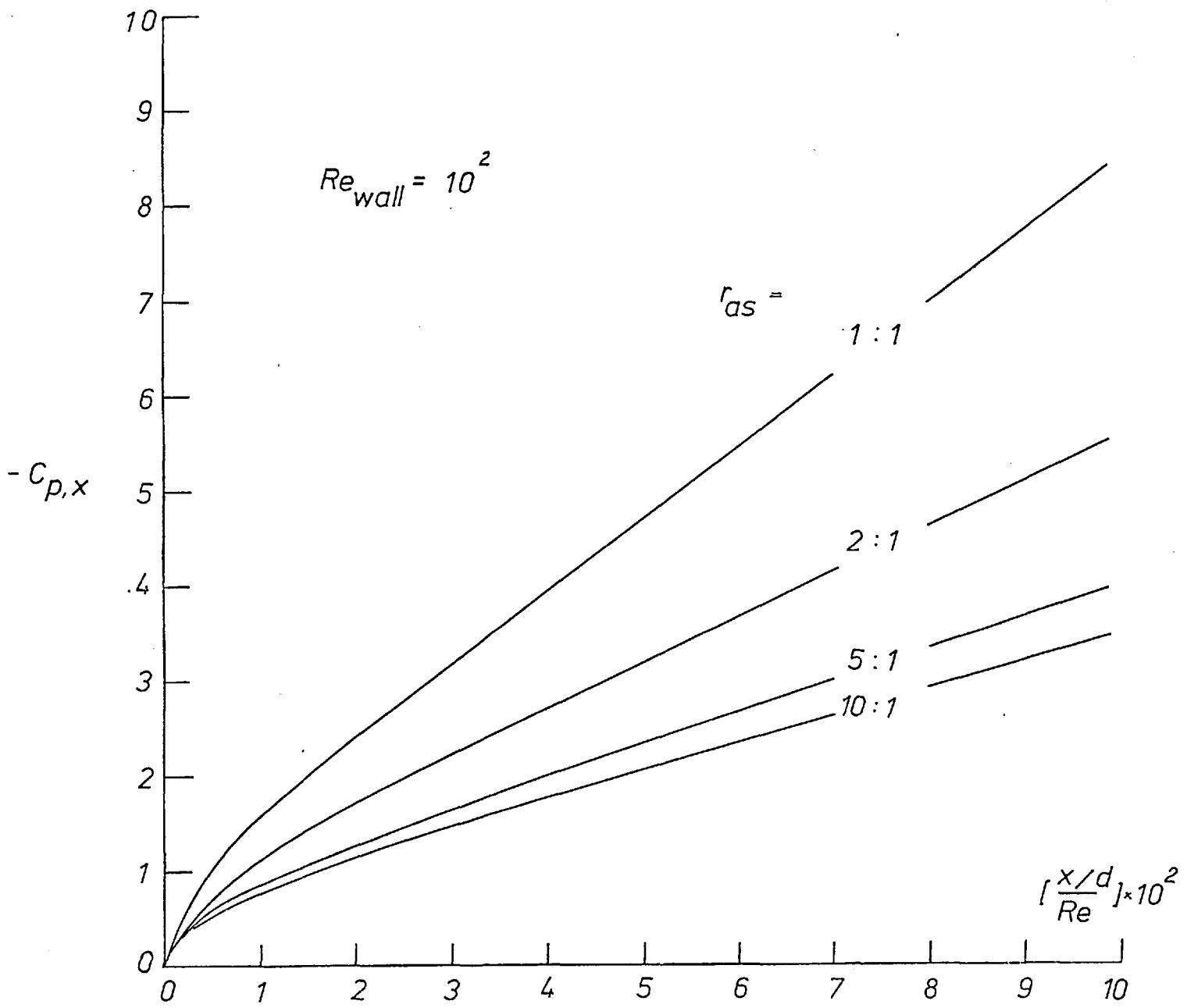
Fig.(7.3.5) Effect of aspect ratio on pressure drop in rectangular-sectioned ducts with one moving wall: Fixed Characteristic width, d.

Fig.(7.3.5) (b) Effect of aspect ratio on pressure drop in rectangular -
sectioned ducts with one moving wall: fixed mass flow rate.

$Re_{wall} = 10^2$

$d_e = \dfrac{2bd}{b+d}$

$r_{as} =$

10:1

5:1

1:1

$-C_{p,x}$

$[\dfrac{x/d_e}{Re}] \times 10^2$
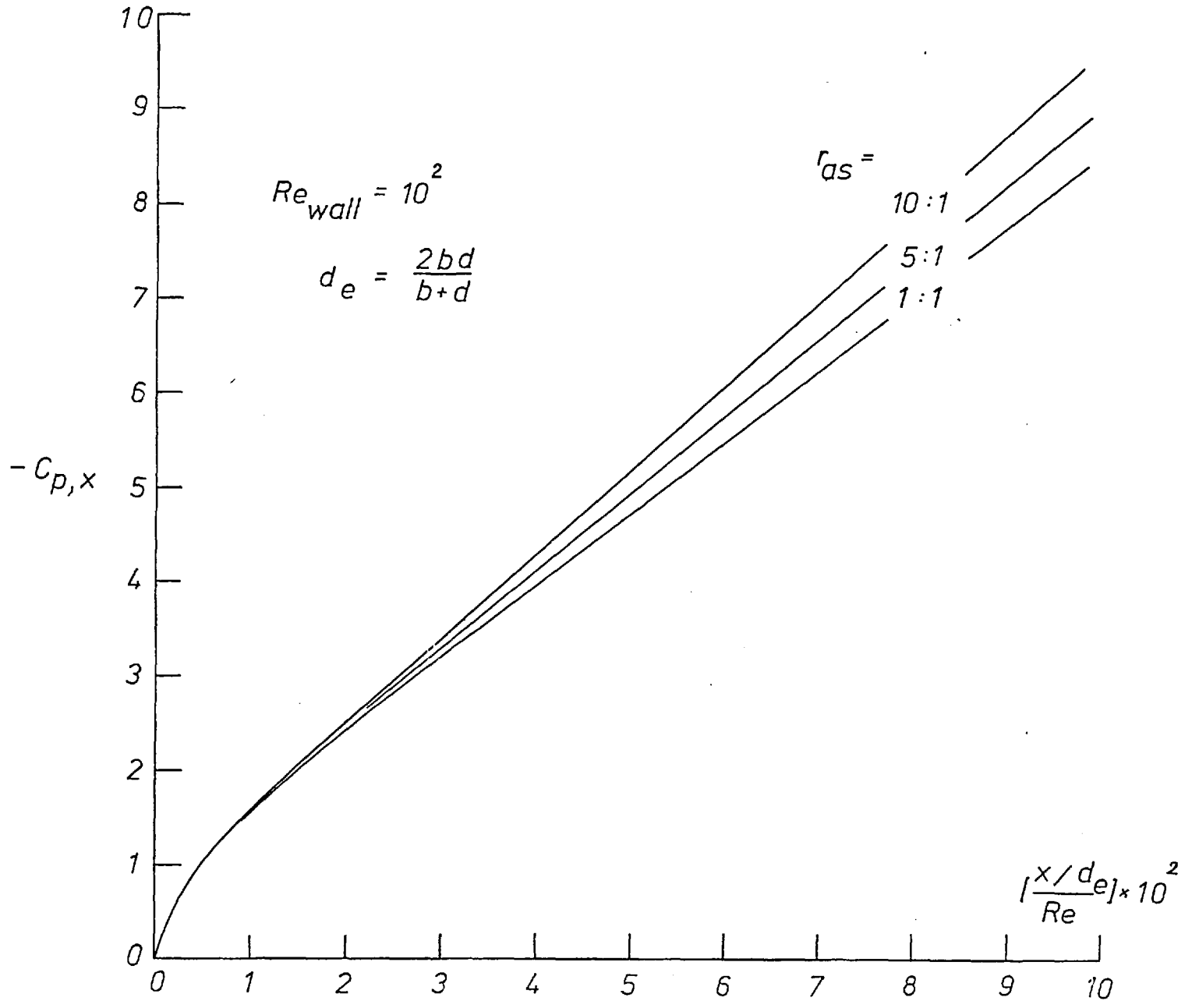
Predictions of velocity distributions are presented in Figures (7.3.6), (7.3.7) and (7.3.8). In the first of these, the calculated maximum-velocity development as affected by the wall Reynolds number, is represented. When the walls are stationary, the calculated values compare favourably with measured values reported by Goldstein and Kreid [23] . In the second, calculated values of axial-velocity contours as affected by the moving wall Reynolds number can be observed; increase in wall velocity is seen to cause a shift in the positions of the vortex centre and the position of maximum velocity. Finally, in figure (7.3.8), the profile across the vertical centreplane of the velocity component parallel to the moving wall, is shown compared with the result of a numerical calculation entirely different from the work reported in this Thesis. It is thus concluded that predictions of this flow situation, consistent with physical reality and available information, have been successfully obtained. In the rest of this chapter, a set of heat transfer predictions are reported as an illustration of the capability of the calculation procedure.
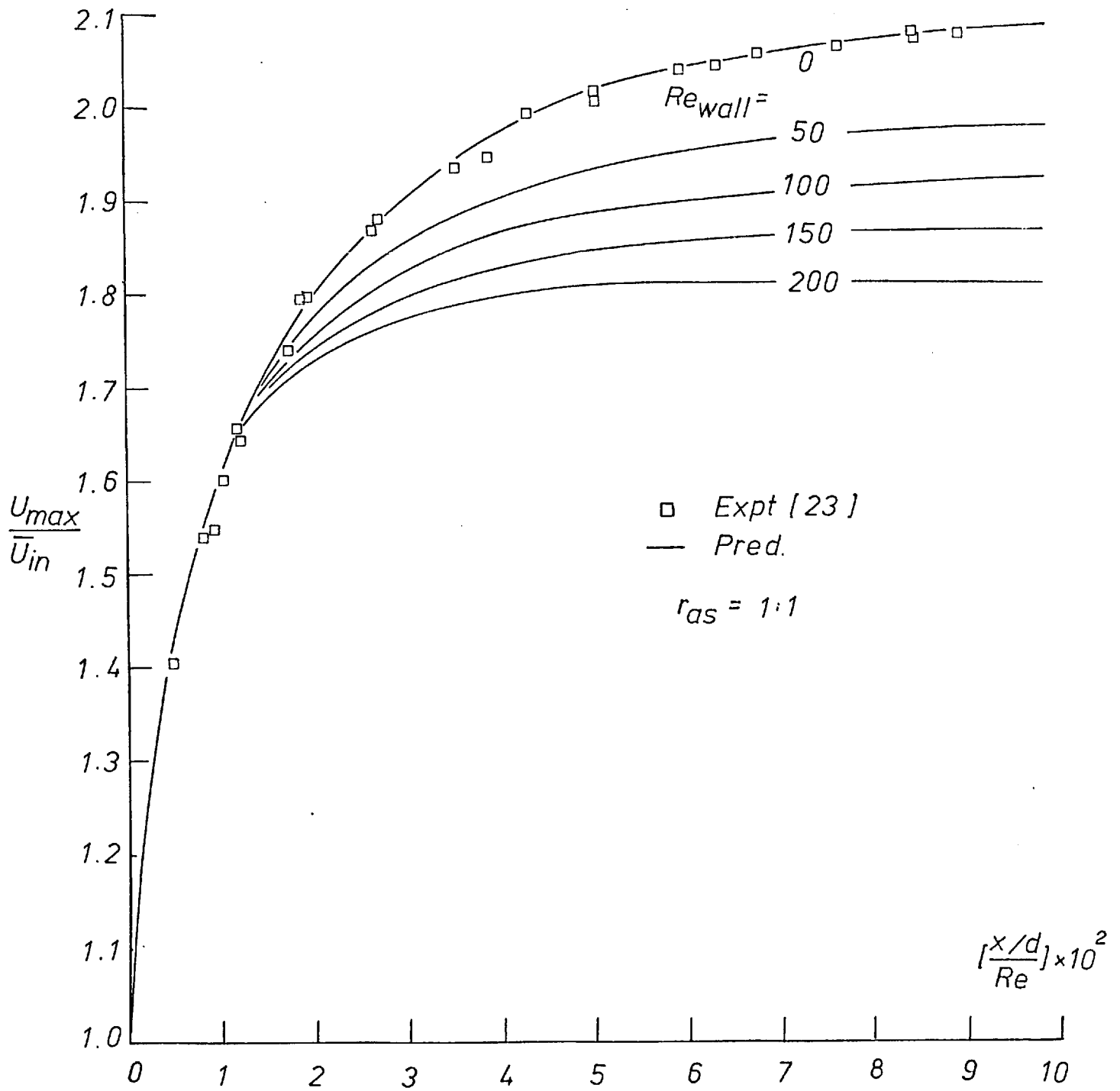
Fig.(7.3.6) Effect of moving wall on development of maximum velocity.

$Re_{wall} = 0$　　　　$= 100$　　　　$= 200$
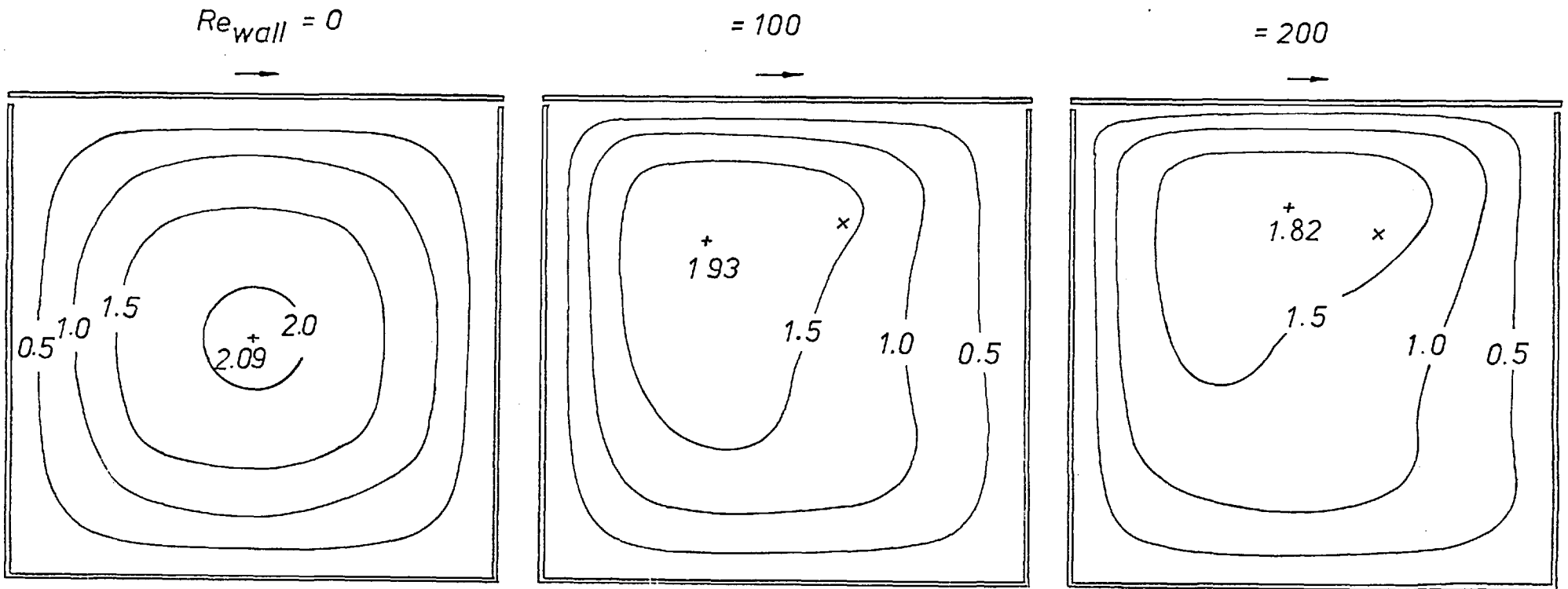
$r_{as} = 1:1$　　　+　maxm. velocity location

$[\dfrac{x/d}{Re}] = 0.1$　　　×　vortex centre

Fig.(7.3.7)　Effect of moving wall on axial velocity (U/U_{in}) contours.　Note: Points of maximum velocity and vortex centres differ.

Fig.(7.3.8) Profile of (W/W_{wall}) across the vertical centreplane for fully-developed flow.

In the figure:

Analysis [8] (dashed line)

Pred (solid line)

$r_{as} = 1:1$

$\frac{z}{d} = \frac{1}{2}$

$Re_{wall} = 10^2$

Axes: vertical axis $\frac{y}{d}$ with values 0, 0.2, 0.4, 0.6, 0.8, 1.0; horizontal axis $\frac{W}{W_{all}}$ with values -1.0, 0, 1.0.

122
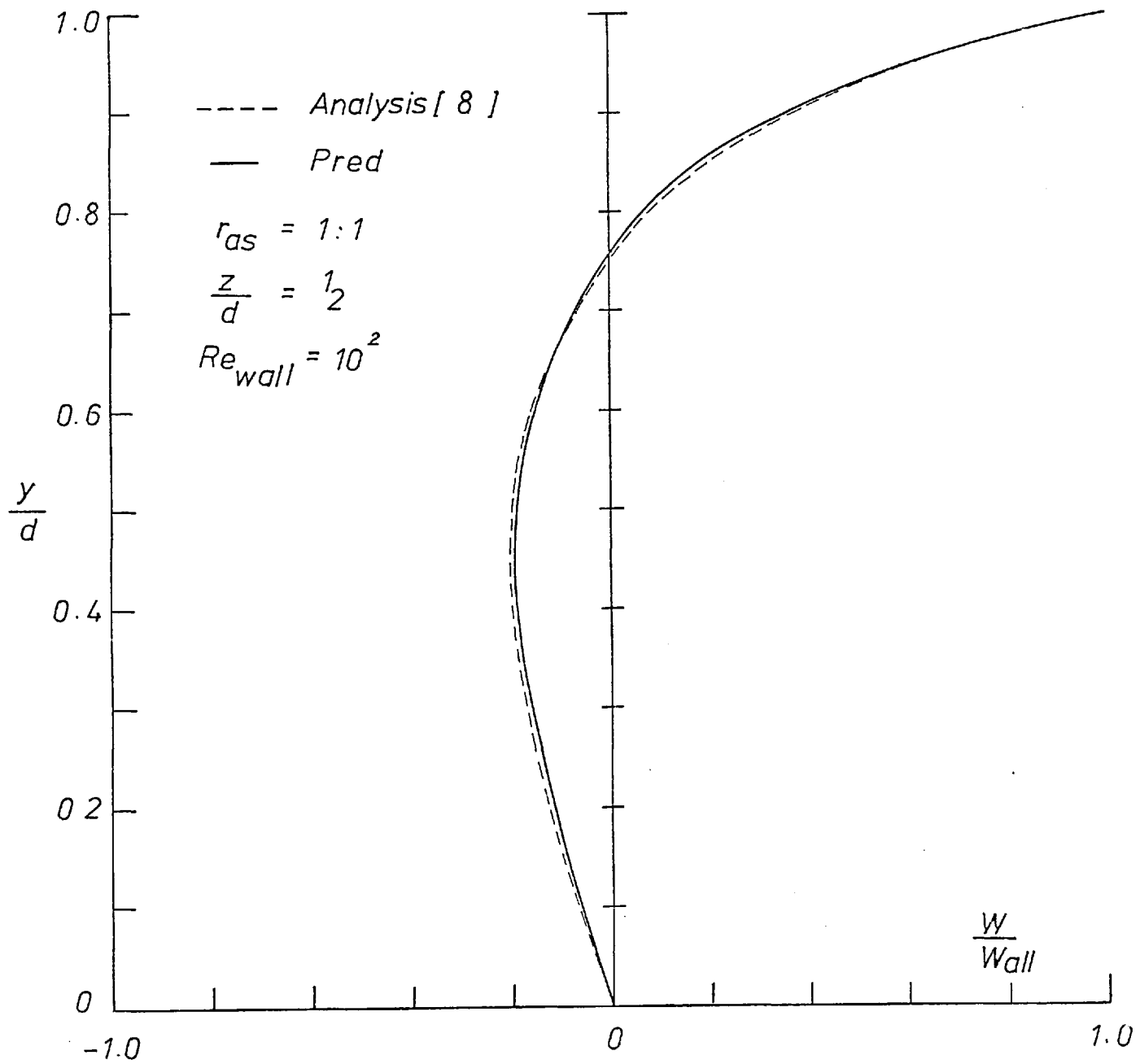
7.4   Some heat transfer calculations

7.4.1   Four walls heated to uniform temperature

In the first case, the situation of simultaneous development of flow and heat transfer is considered in rectangular-sectioned ducts with one moving wall wherein all four walls are heated to a uniform temperature.

Thus in Figure (7.4.1), the effect of the moving wall Reynolds number upon the bulk temperature rise can be clearly observed. The bulk fluid temperature at any axial position is defined as:

$$T_b \equiv \int_A \rho C_p \, UT \, dA \Big/ \int_A \rho C_p \, U \, dA \qquad \cdot \; (7.4.1)$$

The increase in mixing caused by increase in the moving-wall velocity causes an appreciable increase in temperature rise of the fluid. In Figure (7.4.2), the effect of aspect ratio upon bulk temperature rise may be observed. The greater the aspect ratio, the lower is this rise for a given distance (normalised with the shorter duct width). Also studied was the effect, upon the energy transferred to the flow, of the Prandtl number of the fluid. As is to be expected, Figure (7.4.3) shows the reduction in bulk-temperature rise with increase in Prandtl number. The three-dimensional nature of the temperature field dramatically represented in Figure (7.4.4.) where contours of temperature rise are indicated at three positions along the duct axis. The position of minimum temperature rise at $\left[\dfrac{x/d}{Re}\right]$ = 0.01 can be seen to be close to the point of maximum velocity (Fig. (7.3.7)).

7.4.2   Three adiabatic walls and heated moving wall

In this case, the moving wall is presumed heated to a steady, uniform temperature and the remaining three walls of the duct are presumed impervious to the transfer of heat. Figures (7.4.5) and (7.4.6) represent predictions similar to those presented above. In the former,

Fig.(7.4.1) Effect of moving wall on bulk-fluid temperature rise; Case 1.
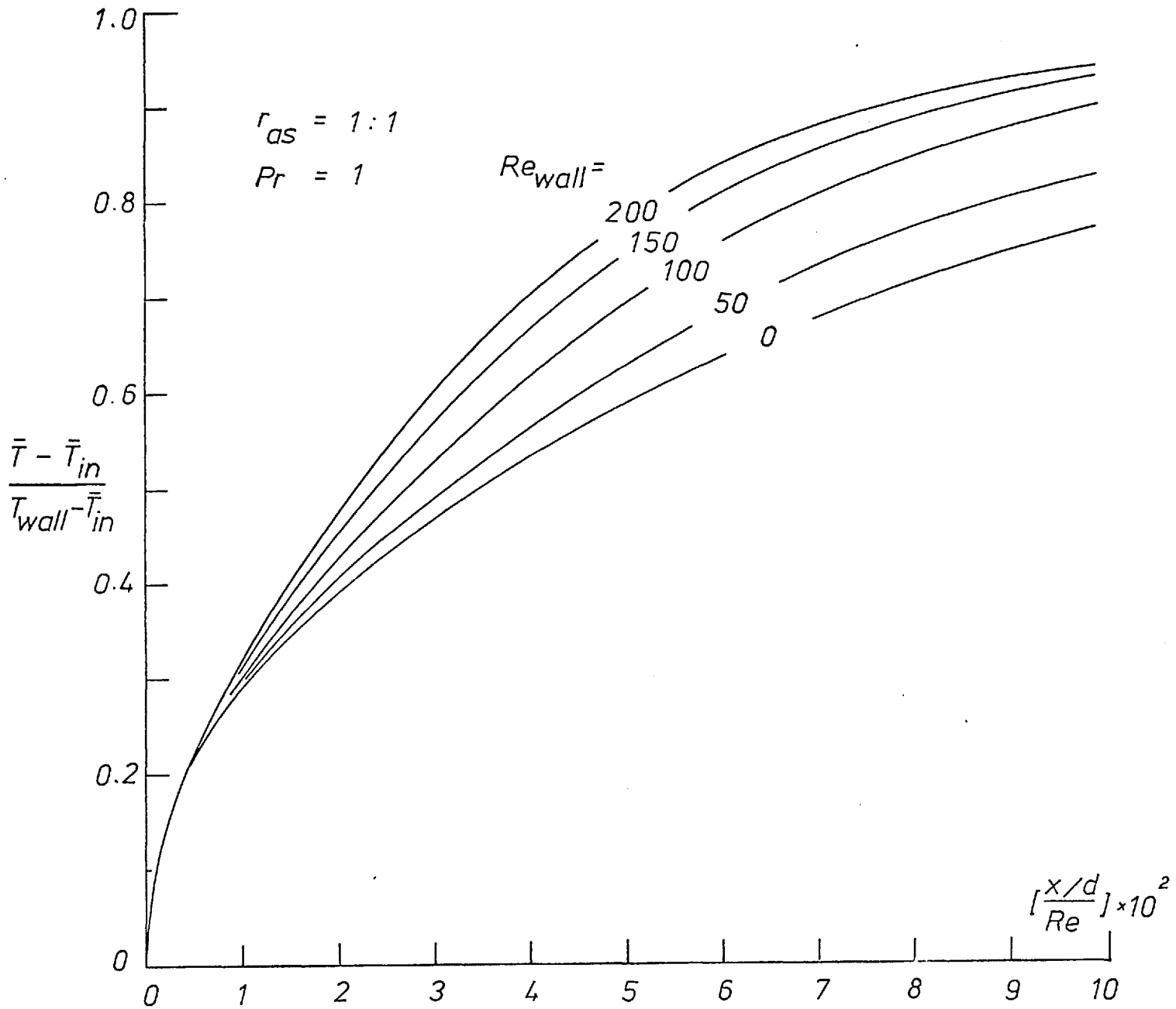
Fig.(7.4-2) Effect of aspect ratio on bulk-fluid temperature rise; Case1.

125
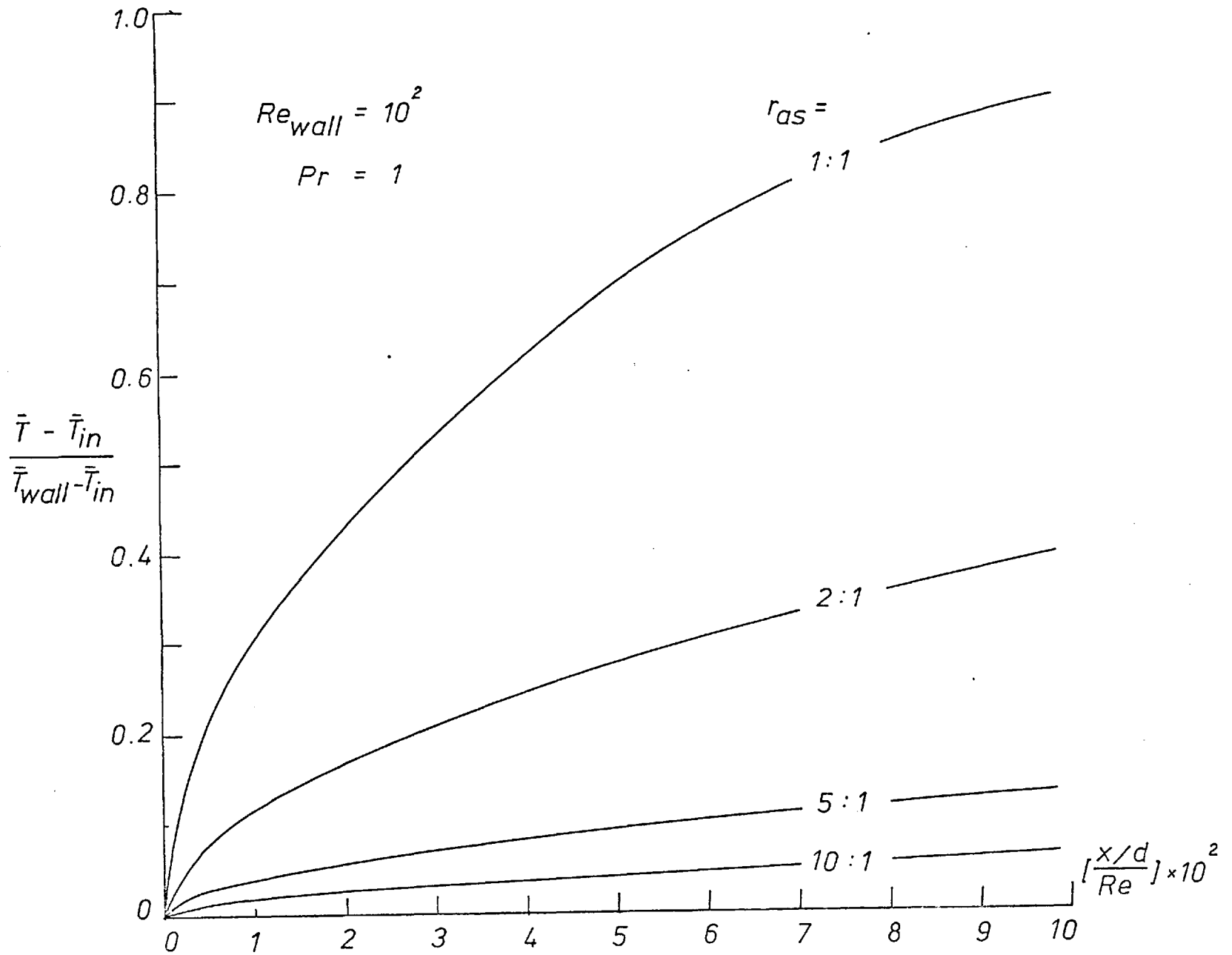
Fig.(7.4.3) Effect of Prandtl number on bulk-fluid temperature rise; Case 1.
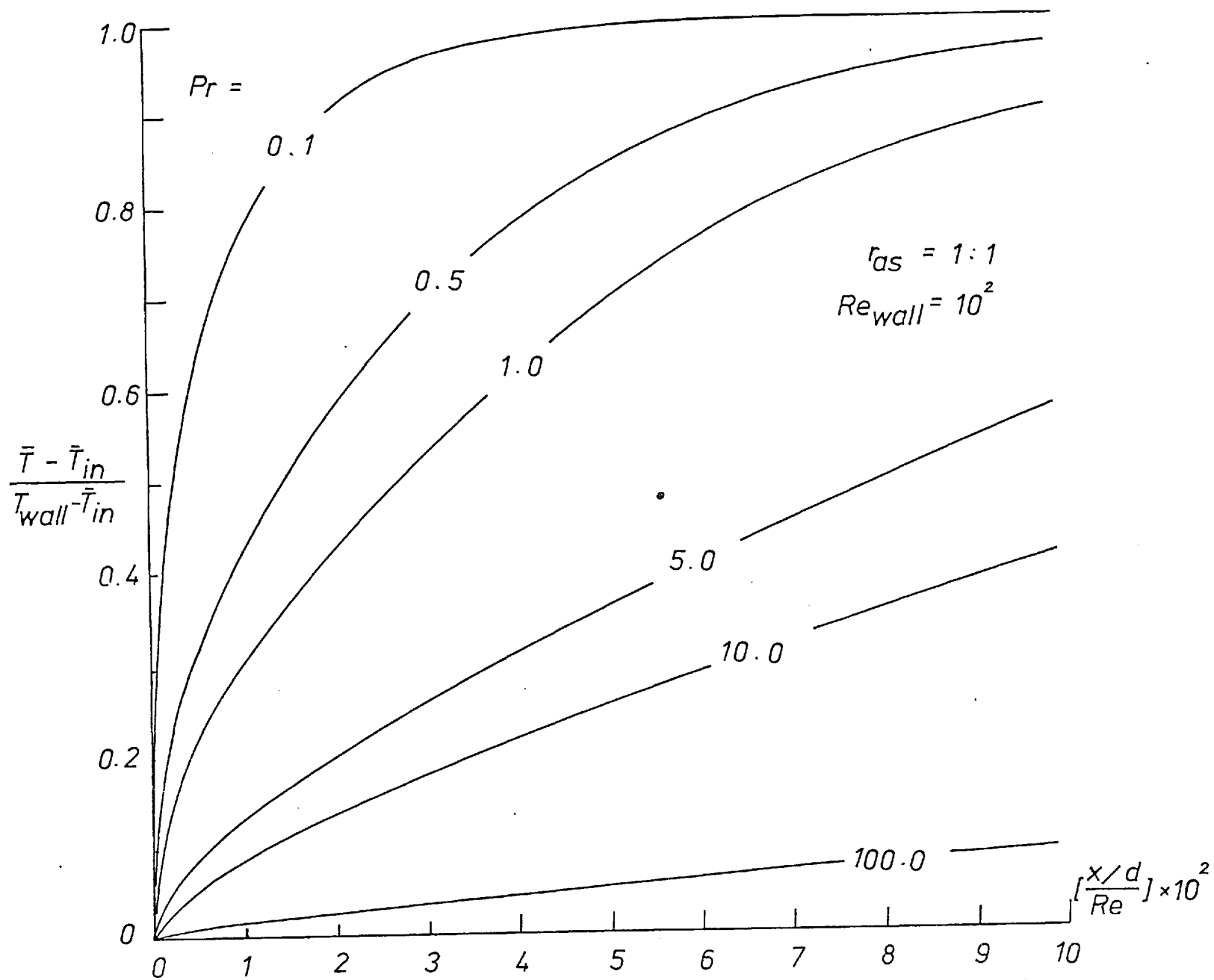
$Re_{wall} = 100$

$x/[d.Re] = 0.02$

$= 0.04$

$= 0.1$

0.5   0.8   0.9

0.5 0.8   0.9

0.8

0.9
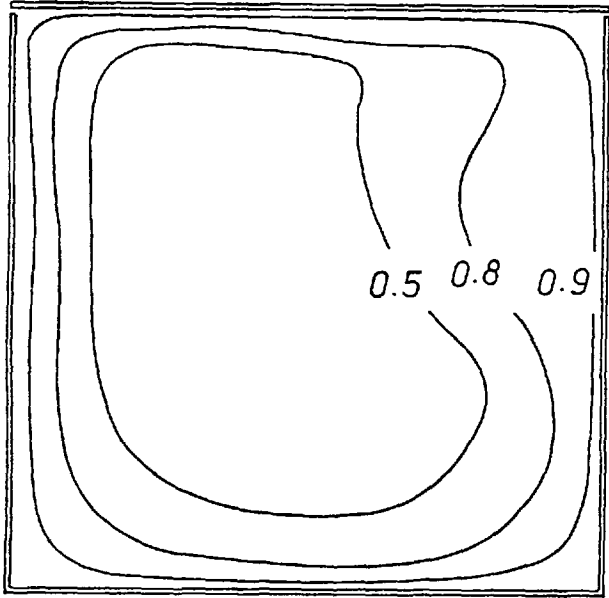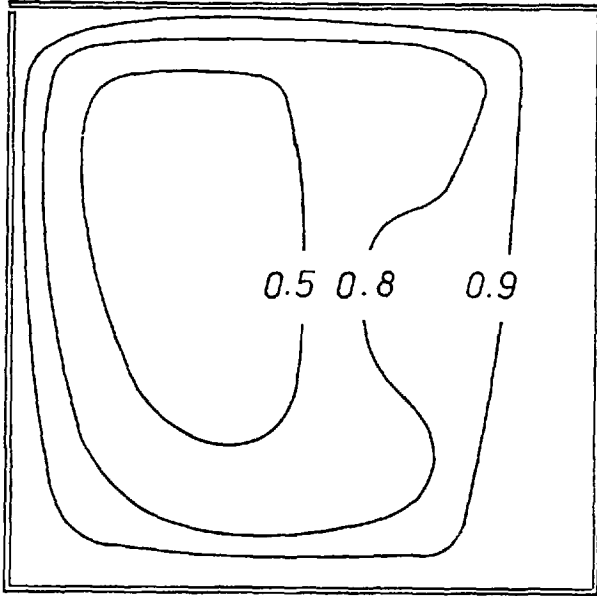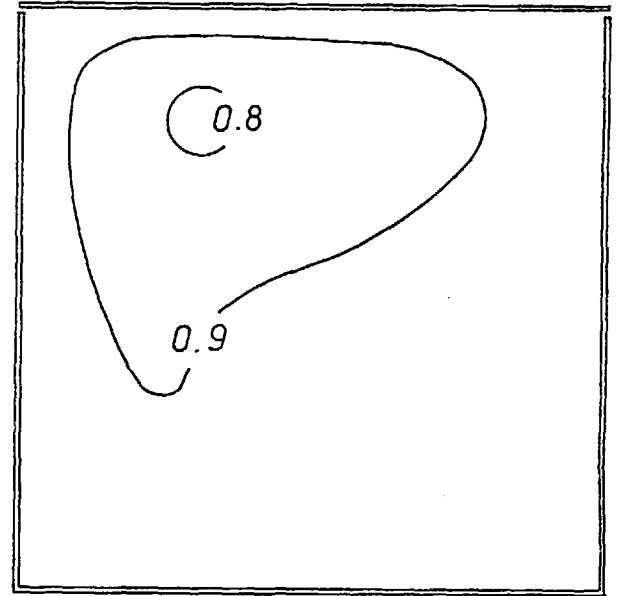
$r_{as} = 1 : 1$

$Pr = 1$

Fig.(7.4.4)   Effect of moving wall on temperature $(\dfrac{T - T_{in}}{T_w - T_{in}})$ contours.   Case 1.
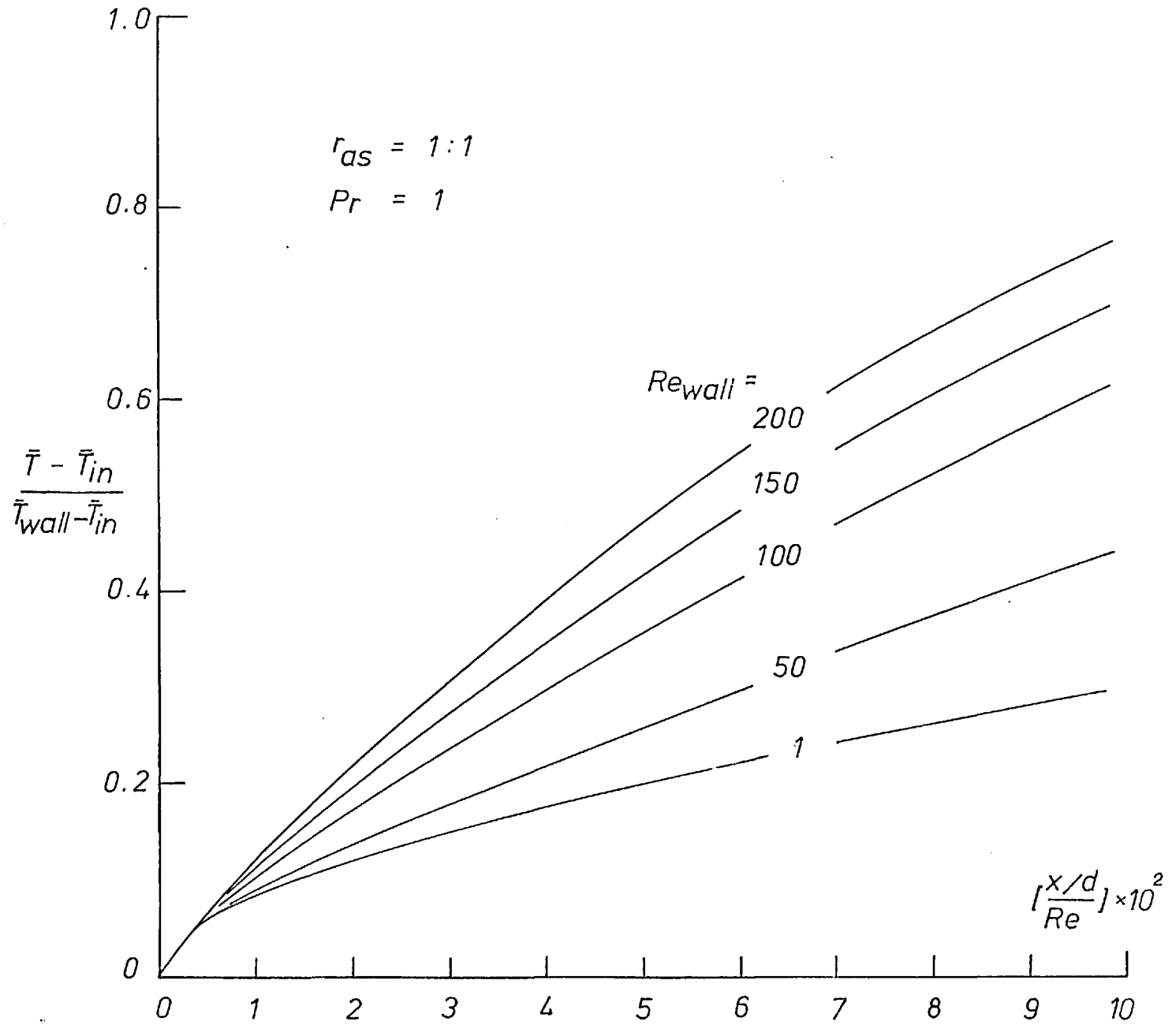
Fig. (7.4.5) Effect of wall-Reynolds number upon bulk temperature
rise. Case 2.
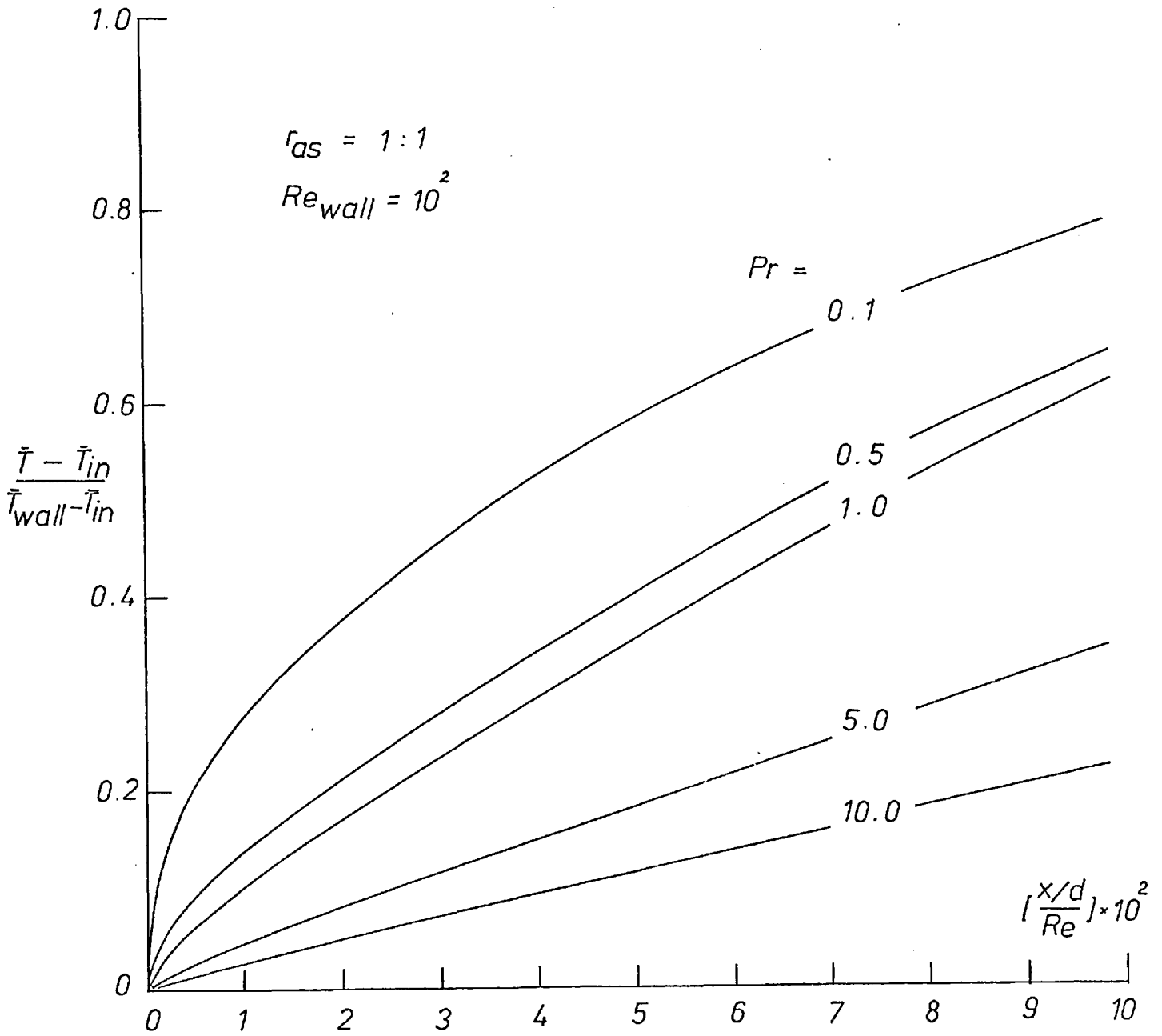
Fig. (7.4.6)   Effect of Prandtl number upon bulk temperature rise.
Case 2.

the effect of increasing the moving-wall velocity and in the latter, that of fluid Prandtl number upon bulk temperature rise can be observed. Finally in Figure (7.4.7), the effect upon temperature-rise contours at a given axial position, of the moving-wall Reynolds number, is represented. The 'cold-centre' of the fluid is moved further and further away from the vortex centre (Fig. (7.3.7)) as this quantity is increased.

7.5   Concluding remarks

In this chapter, predictions of a variety of laminar flow situations have been reported. Comparisons of these with analytical and experimental information, have indicated reasonably good agreement. It is thus concluded that the calculation procedure reported in Chapter 3 is reasonably accurate, flexible and, as can be seen from the tables in Appendix A3, economical to use.

$Re_{wall} = 1$ $= 100$ $= 200$
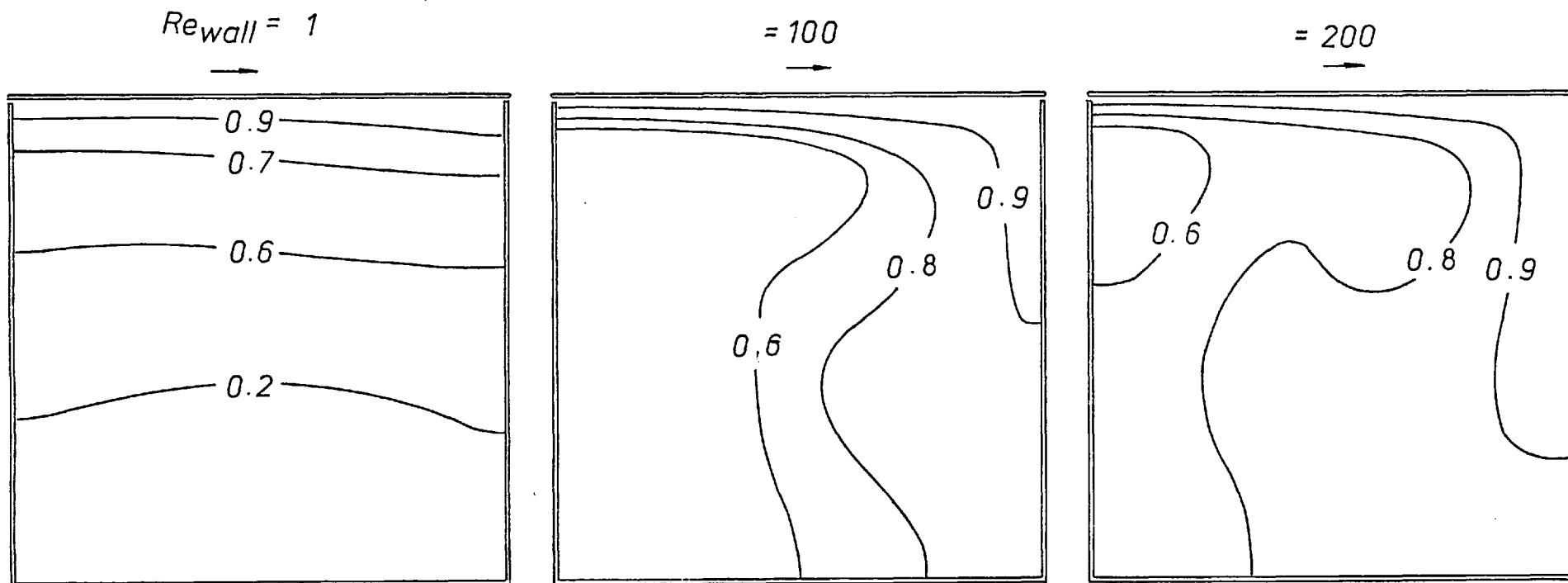
$r_{as} = 1 : 1$, $[\dfrac{x/d}{Re}] = 0.1$.

$Pr = 1.0$,

Fig.(7.4.7)   Effect of moving wall on temperature $(T - T_{in})/(T_w - T_{in})$ contours.   Case 2.

CHAPTER 8

PREDICTIONS OF TURBULENT, DIFFUSER FLOWS

8.1   Introduction

The numerical solution procedure described in Chapter 3 in con-
junction with the turbulence models described in Chapter 4, has been
used to obtain predictions of turbulent flow development in rectangular-
sectioned ducts and diffusers. It is the purpose of this chapter to
present these predictions and compare them with experimental data and
theoretical analyses wherever available. The experimental data used for
purposes of comparisons, include those obtained in the present investi-
gation, those reported in the literature and some unpublished work.

Details associated with the computational aspects of the afore-
mentioned predictions, are provided in Appendix A3.

8.2   Parameters investigated

The flow pattern in and performance of rectangular-sectioned
diffusers, forms the subject matter of this chapter. In all the cases
examined, the diffuser walls are smooth and impermeable to matter. When
known, the temperature and heat-flux distribut ions on these walls are
supplied to the numerical calculation procedure. Since attention is re-
stricted to unstalled flows in diffusers, the effects of conditions at
the outlet to diffusers upon the flow within them are negligible and
are not included in the present study. The effects of the following para-
meters are however, examined.

Inlet aspect ratio. Aspect ratio is here defined to be the ratio of the
larger to the smaller widths of the diffuser walls at inlet, without
reference to whether two or more walls are sloped to form the diffuser.
Additional information on the manner of formation of the diffuser ge-
ometry is provided in each case. Figure (8.2.1) illustrates the no-
menclature used in representing the diffuser geometry, and in defining

the aspect and area ratios.

$$r_{as} = \frac{b}{d}$$

$$r_{ar} = \frac{b_o d_o}{b d}$$
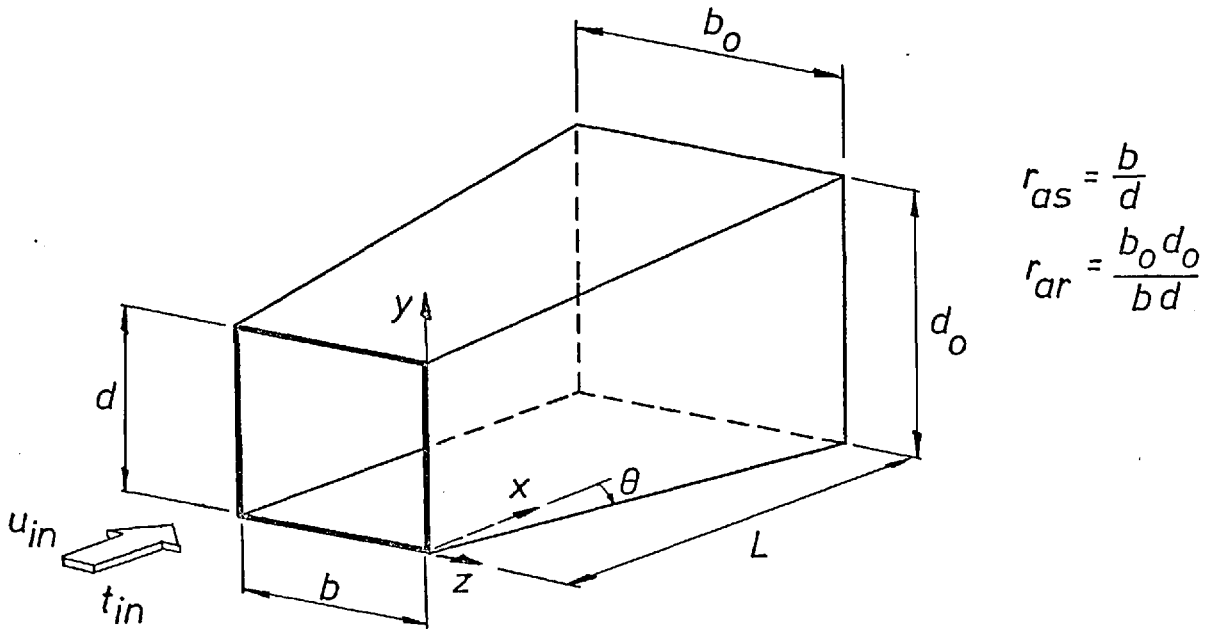
Fig.(8.2.1)   Illustration of diffuser geometry and nomenclature

Reynolds number. Reynolds number at the inlet of a diffuser is defined in terms of an average velocity at that cross-section and the minimum spacing between the two pairs of walls, d . Unless otherwise specified, this minimum width is also used as the reference width in normalising distance along the diffuser axis.

Included angle. The included angle between the diverging walls of a diffuser is the primary factor which governs the geometric configuration and largely performance of the diffuser. When the walls of the diffuser are not straight or when the walls of a rectangular-sectioned diffuser diverge in asymmetric fashion, the geometric configuration is more conveniently expressed as an area ratio factor as a function of diffuser length. Only those included angles or area ratios which allow unstalled flow in diffusers are considered in this chapter. Figure (8.2.1) illustrates the definition of area ratio.

Inlet conditions. Conditions at the inlet to diffusers affect the flow
pattern and pressure rise, often critically, in diffusers. The effects
of a variety of inlet conditions upon diffuser performance, are con-
sidered here. In a large number of situations considered here, such con-
ditions consist of distributions of axially-directed velocity components.
In some situations, where the velocity distrib ution across the diffuser
inlet plane is essentially uniform, measured values of the boundary-
layer momentum thickness δ^*/d on all four walls are used to approximate
the velocity profiles between pairs of parallel walls. Such approximations
corresponding to four values of momentum thickness are indicated in
Figure (8.2.2). Inlet velocity profiles, both experimentally-observed
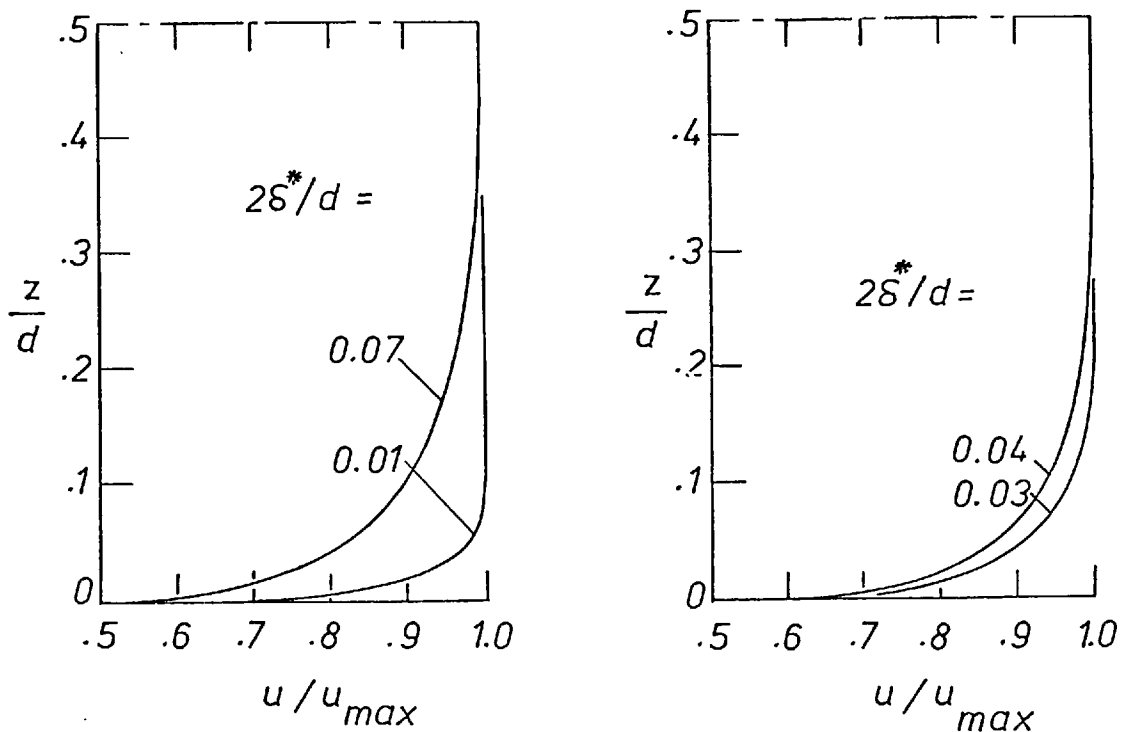
Fig.(8.2.2) Inlet velocity profiles of specific boundary –
layer thicknesses.

and approximated values are supplied to the prediction procedure in the
form of smooth curves, obtained in the former instance by simple least-
squares curve fitting. Such smooth curves enabled predictions with suc-
cessively refined grid dispositions to be obtained with ease.

For two cases considered in this chapter, measured values of inlet turbulence intensities are used to arrive at distributions of turbulence energy. In all other cases, estimates of energy level are used. Inlet turbulence intensities, under normal conditions, were found to be of minor influence upon predicted diffuser performance.

8.3 Prediction of diffuser flows

The predictions of turbulent flows in diffusers are obtained in the following manner. The geometric and fluid property information for each situation are first supplied to the computer program embodying the prediction procedure. The grid distribution in the $\eta \sim \xi$ plane is then chosen so as to suit the inlet distributions of velocity, temperature and other dependent variables. When the inlet conditions are uniform, a uniform spacing between grid nodes suffices for initial tests. When inlet conditions are unknown, an estimate is made in accordance with realism and information concerning the gross features of the flow. Calculations are then made over the entire length of the diffuser. Advantage is taken wherever possible, of the existence of planes of symmetry in the flow and calculations are restricted to domains bounded by such planes. Calculations are then repeated with successively refined grid dispositions (i.e. increased number of grid nodes, as well as reductions in spacing between grid nodes located in regions where steep gradients of velocity occur). When the results of these calculations, in detailed respects, show variations with grid size of less than 2 %, the grid-depending tests are terminated and the predictions then compared with experimental data. Checks are made to ensure that overall balances of momentum and other conserved properties are maintained by the calculation procedure.

In many instances, predictions obtained with the simple turbulence model coincided with those obtained with the two-equation model. Comparisons of the two models are indicated only when differences greater than 2 % are observed in the predictions. Thus, unless otherwise stated, predictions reported in this chapter are those obtained with the two-equation model.

8.3.1 Two-dimensional diffuser flows

Flows in diffusers of large inlet aspect ratio are termed two-dimensional. However, the influence of the short sides of such diffusers, may increase with distance downstream since the aspect ratio, in one configuration, approaches unity sufficiently far from the diffuser inlet. Consequently, the flow-field becomes increasingly three-dimensional with distance; a fact which makes the attainment of truely two-dimensional flow extremely difficult. The purpose of the predictions reported in this Section is to test the procedure in a relatively simple situation while simultaneously verifying the two-dimensionality assumption.

Accordingly, a calculation turbulent flow in a diffuser of aspect ration 6 : 1 and included angle 4.45° at a Reynolds number of 1.5×10^{5} is presented in Figure (8.3.1). This figure illustrates the pressure-rise coefficient $C_{p,x}$ as a function of axial distance compared with experimental data and analytical results. The experimental data are those reported by Carlson [10] . The analyses include inviscid calculations shown dashed, and momentum-integral calculations due to Cocanower et. al. [15] shown by a chain line. The former analytical result shows a pressure rise considerably in excess of measured values; the latter, while constituting a definite improvement over the former, being essentially a prediction procedure for two-dimensional flows, does not account for the frictional influence of the shorter sides of the diffuser. Hence the calculated value of $C_{p,x}$ is higher than the measured values. The present procedure however, by taking account of three-dimensional effects, predicts a pressure rise remarkably close to experimental value. It is observed from this example, that important three-dimensional influences persist even in large-aspect ratio diffuser flows which are conventionally classified as two-dimensional.

A second set of predictions of turbulent flow in an even larger aspect-ratio diffuser $(r_{as}=16.07:1)$ is presented in Figures (8.3.2a) and (8.3.2b). The former shows predicted values of pressure-rise coefficient and decay of centreline velocity which are compared with experimental data of Ellison [17] and the results of inviscid calculations. The latter figure illustrates the friction factor along the
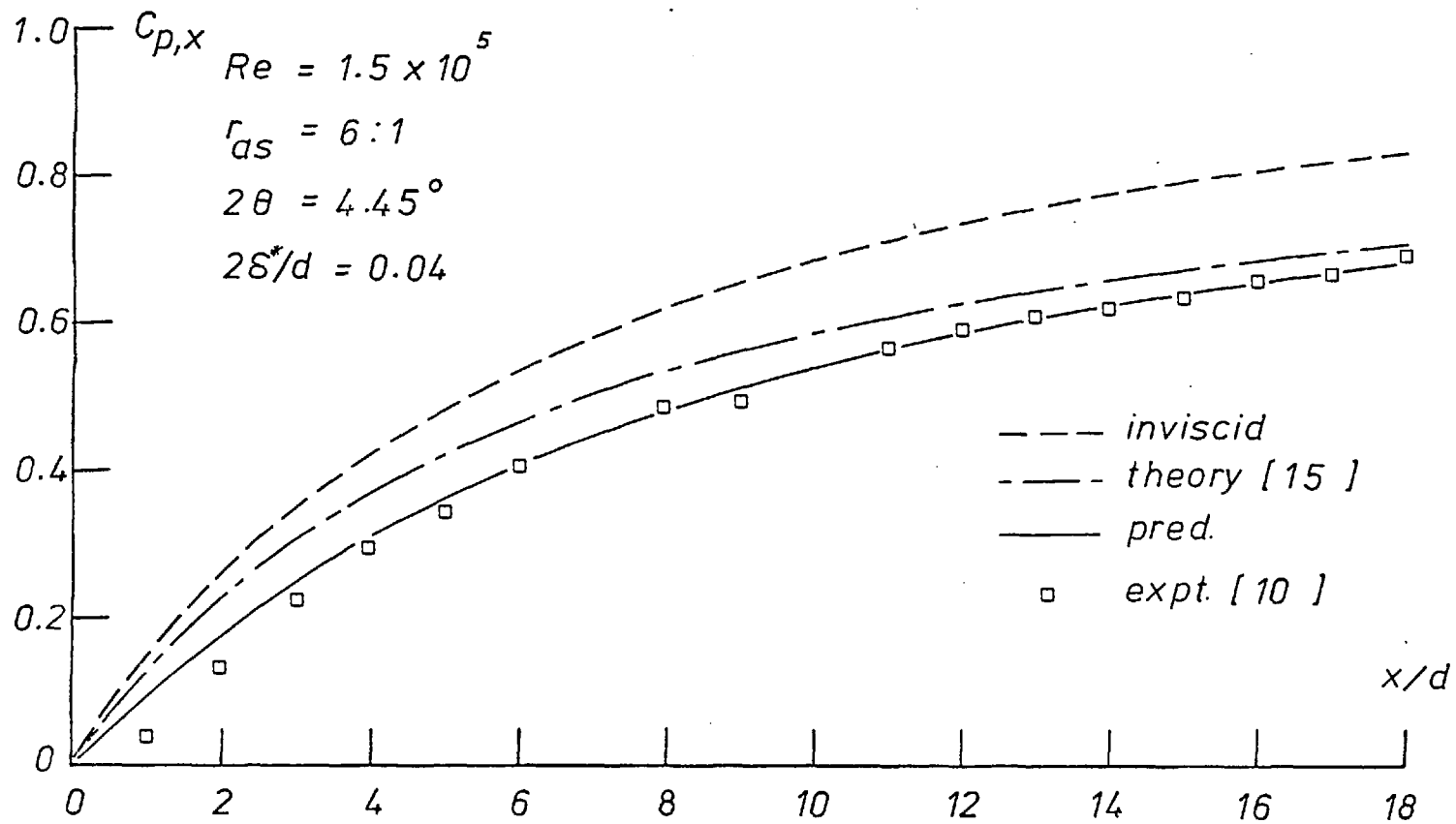
Fig.(8.3.1)   Pressure-rise coefficient vs distance in a large aspect ratio diffuser.
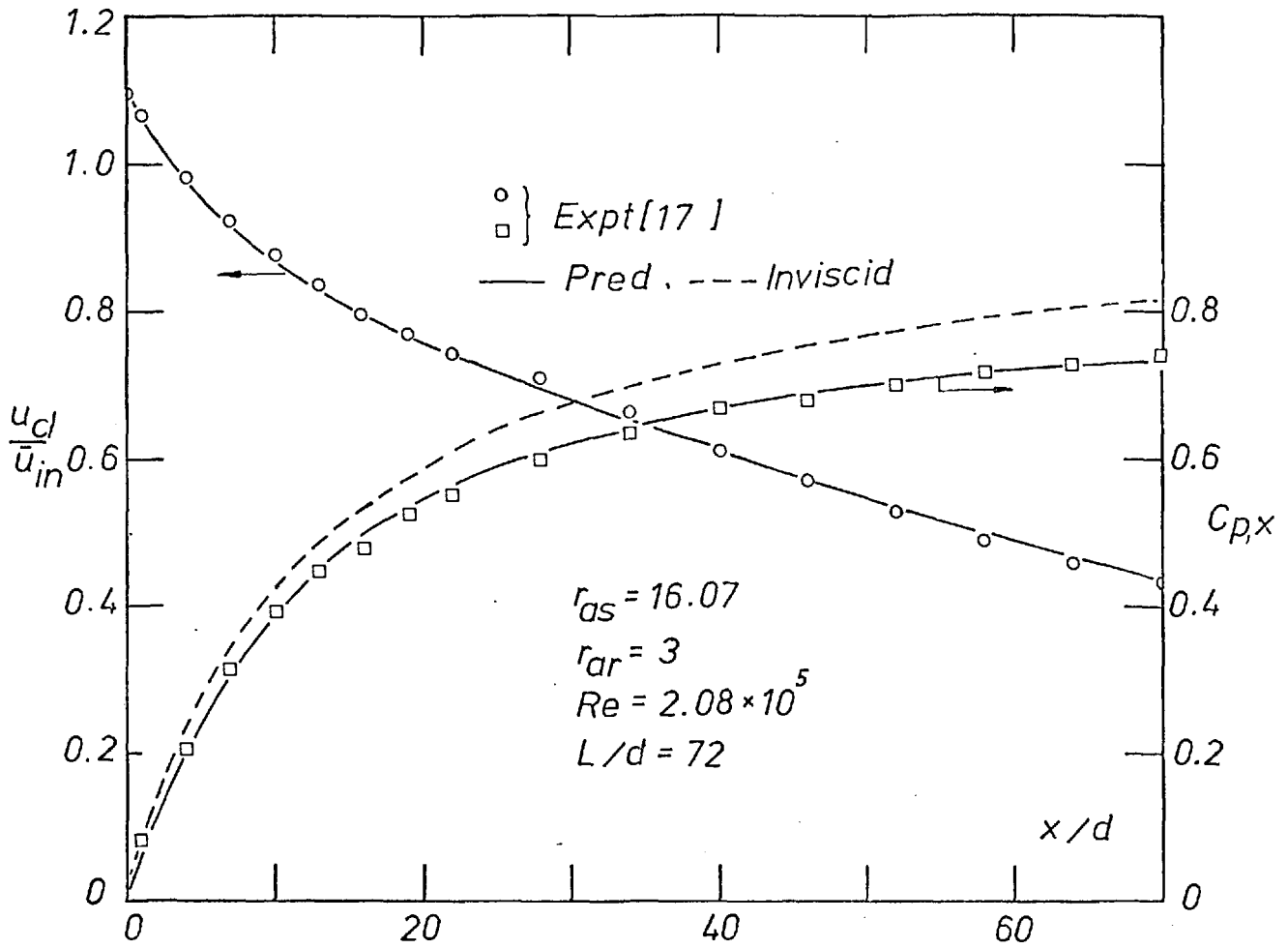
Fig.(8.3.2) (a) Pressure rise and velocity decay in a large
aspect ratio diffuser.
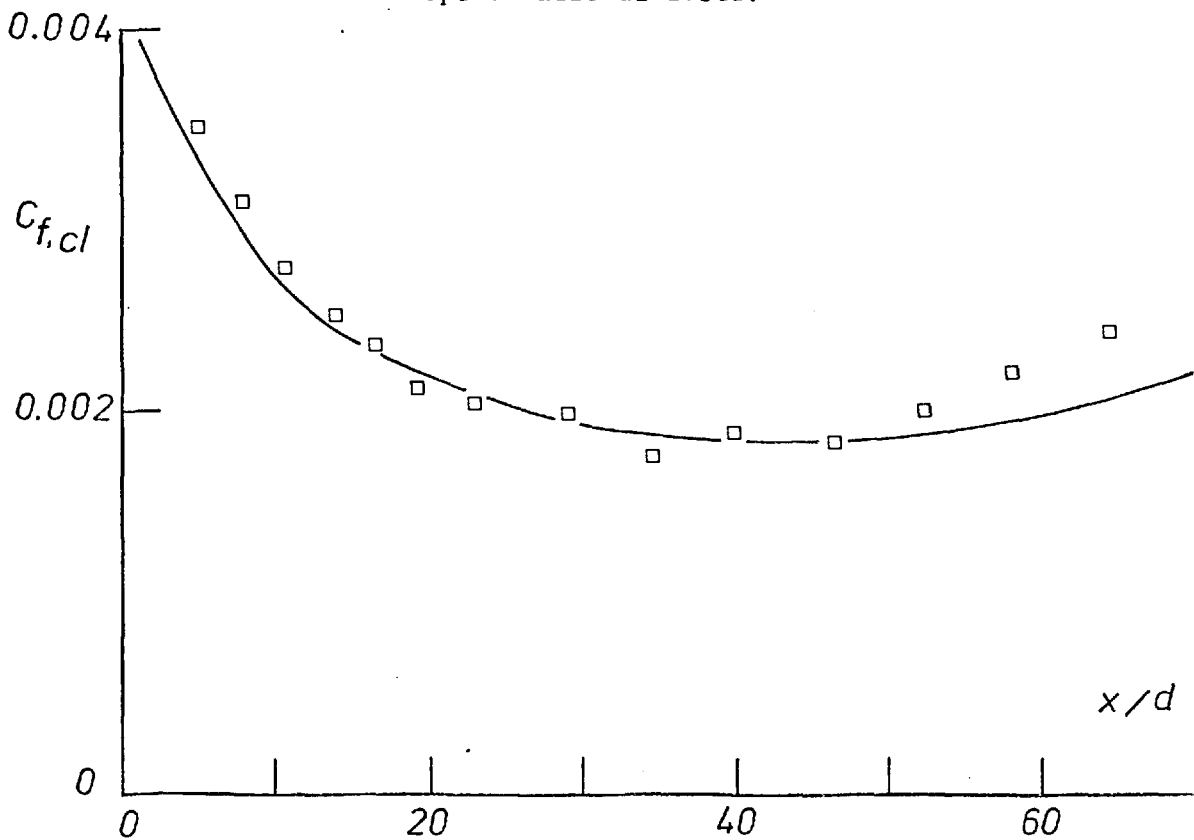
Fig.(8.3.2) (b) Shear stress coefficient in a large aspect ratio
diffuser.

centreline of the sloping walls of the diffuser again compared with
Ellison's data obtained by the Preston-tube method. In both figures the
predicted results are seen to compare favourably with experimental ob-
servations. Other analytical results were not available for comparison.
However, the nature of the comparisons made, validates the capability
of the prediction procedure in taking account of three-dimensional
effects within large aspect ratio diffusers, in detailed respects.

8.3.2 Effect of aspect ratio

Systematic and detailed measurements of turbulent flow in diffusers to determine the effect of aspect ratio upon performance under otherwise identical conditions do not appear to have been reported. However, a compilation of experimental information on pressure rise has been made by Reneau et. a. [47] ; a plot of this is shown in Figure (8.3.3). Also shown is a curve representing the present predictions.
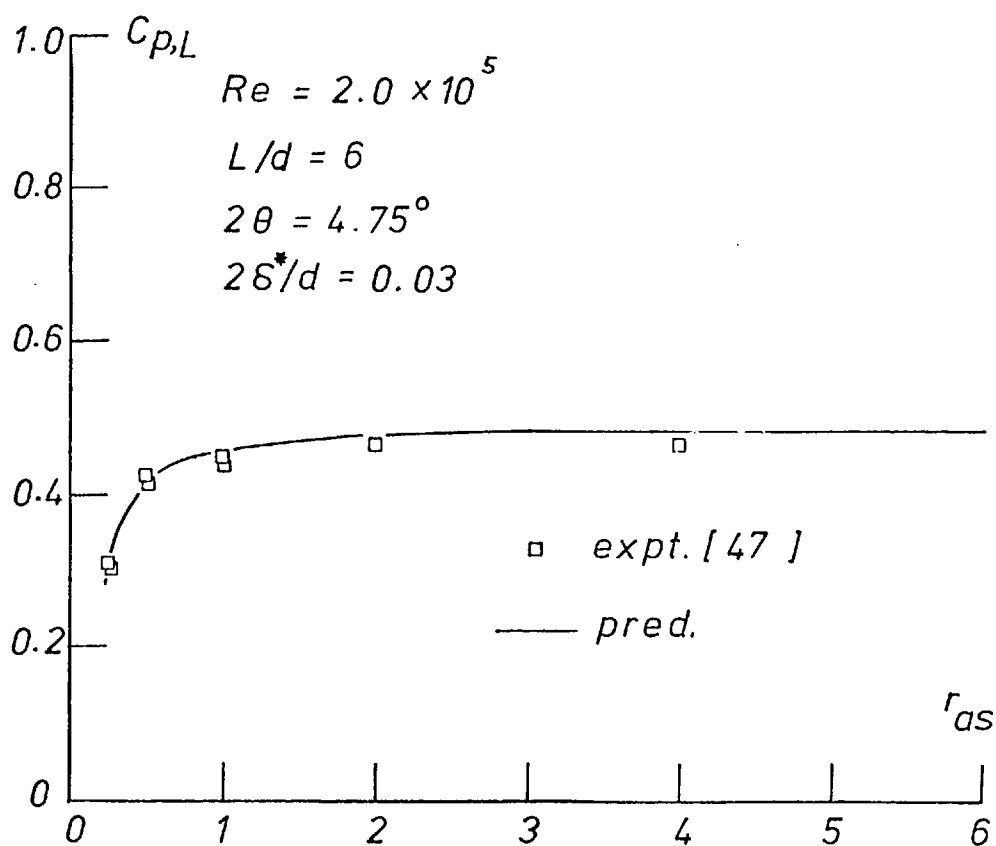
Fig.(8.3.3) Effect of aspect ratio on diffuser
performance at L/d = 6.

It does appear from this curve that performance is virtually unaffected by aspect ratio beyond a value of 3. It is emphasized here that the geometric configuration in this situation was such that two walls of the diffuser were kept parallel while the other two were sloped. Furthermore, the reference width was defined to be the spacing between the sloping walls at inlet. Thus, it is by varying the spacing between the parallel walls that the aspect ratios ranging from $\frac{1}{4}$ to 4 could be accounted for in the prediction procedure. Figure (8.3.4) provides a better picture of the effect of aspect ratio upon performance; it is
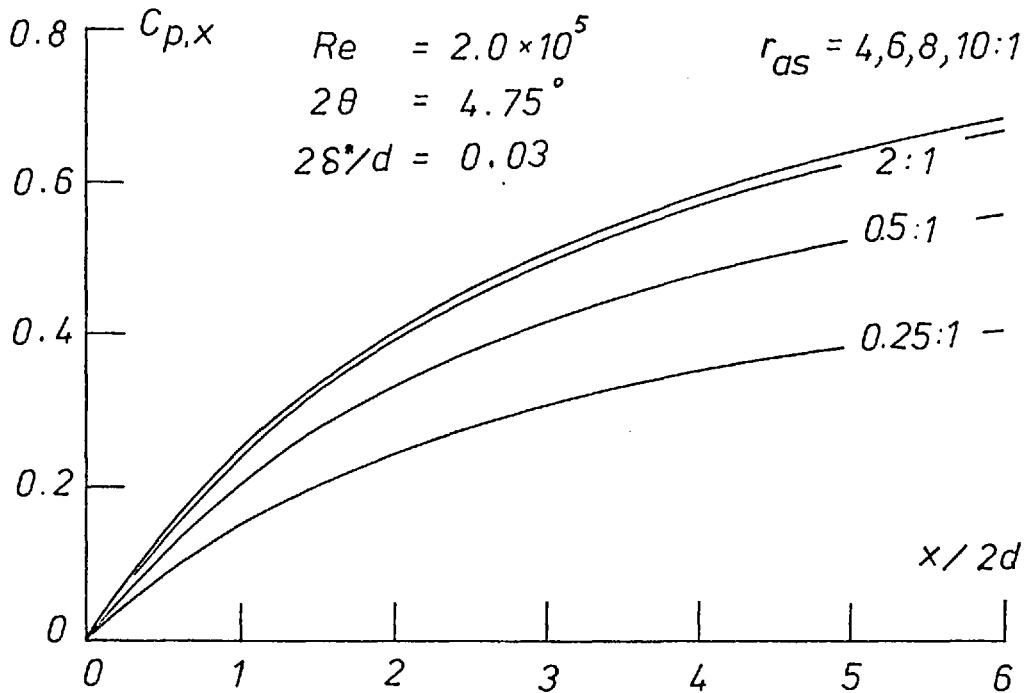
Fig.(8.3.4)   Effect of aspect ratio on pressure rise in rectangular – sectioned diffusers.

from the predictions shown in this figure that the values indicated in Fig. (8.3.3) were plotted. Diffuser performance is clearly seen to be improved as the parallel walls are spaced further and further apart; the flow rate of course being different in each case.

8.3.3 Effect of Reynolds number

As in the case of laminar flows, the effect of Reynolds number on flow behaviour in ducts of rectangular cross-sections has been experimentally determined (e. g. Hartnett et. al. [29]). In the case of fully-developed flow in ducts of constant cross-sections, friction factors over a range of Reynolds numbers is reasonably well predicted by the present procedure. This is illustrated in Figure(8.3.5).
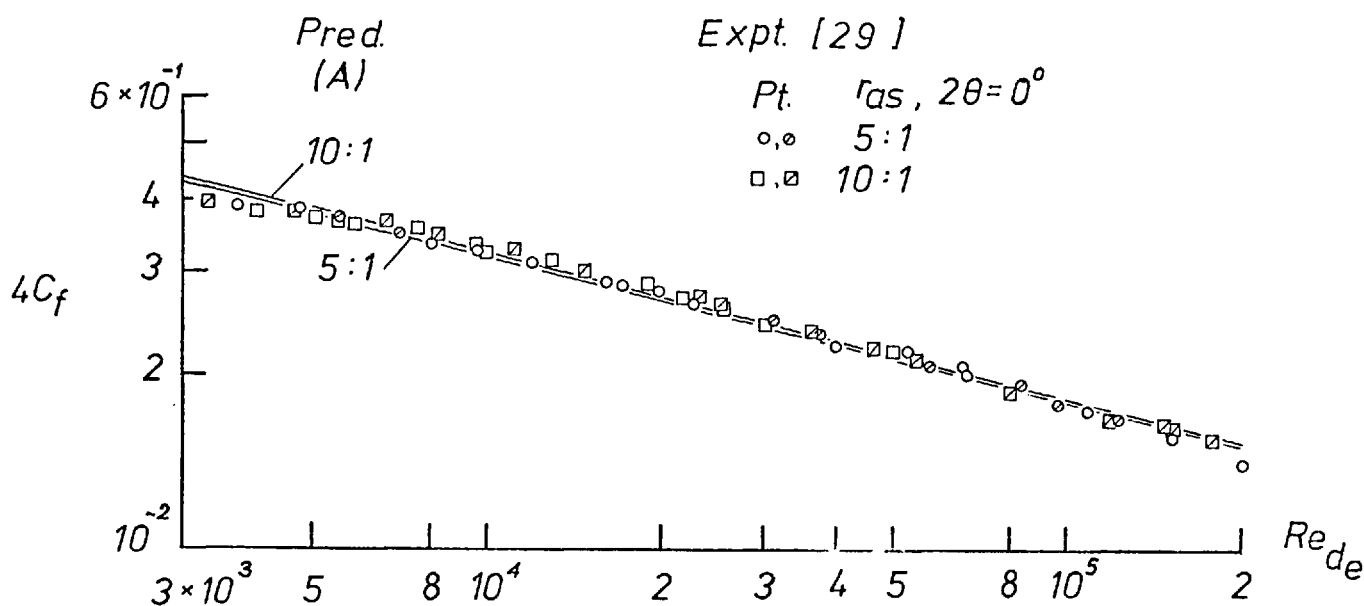
Fig.(8.3.5) Friction factor vs Reynolds number for fully-developed flow in rectangular-sectioned ducts.

As expected, the friction factor C_f decreases with increasing Reynolds number. Friction factors in rectangular-sectioned diffusers do not appear to have been reported. However, the effect of Reynolds number upon the pressure-rise coefficient in diffusers of aspect ratio 1 : 1, measured in the present investigation, is illustrated in Figure (8.3.6). Unfortunately, the range of Reynolds numbers covered in this investigation is limited. Within this range, as can be seen in Figure (8.3.6), appreciable Reynolds number dependence cannot be detected. The predictions, while agreeing reasonably well with the experimental data,

reveal a small dependence; diffuser performance increasing with in-
creasing Reynolds number in the range $/.0 \leq Re \times /0^{-5} \leq /.73$ by a small
amount.
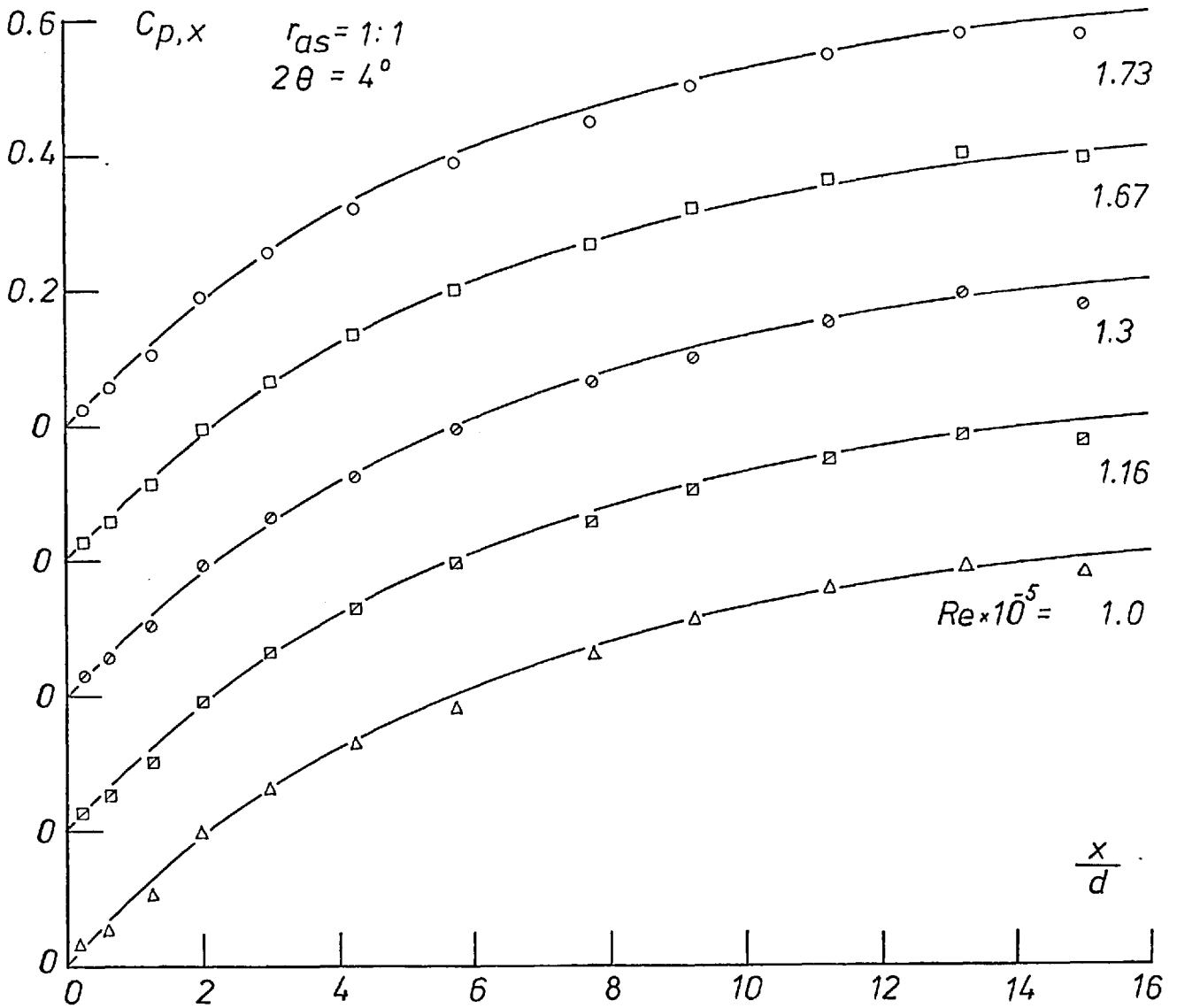
Fig.(8.3.6)   Effect of Reynolds number on pressure recovery.

8.3.4 Effect of diffuser included angle

a) Zero-angle diffusers or duct flows

As a preliminary to the study of flows in diffusers, predictions made of duct flows with uniform conditions at inlet, over a range of aspect ratios are reported in this Section. In figure (8.3.7), the predicted pressure-drop in a duct of square cross-section at a Reynolds number of 1.4×10^5, can be observed.
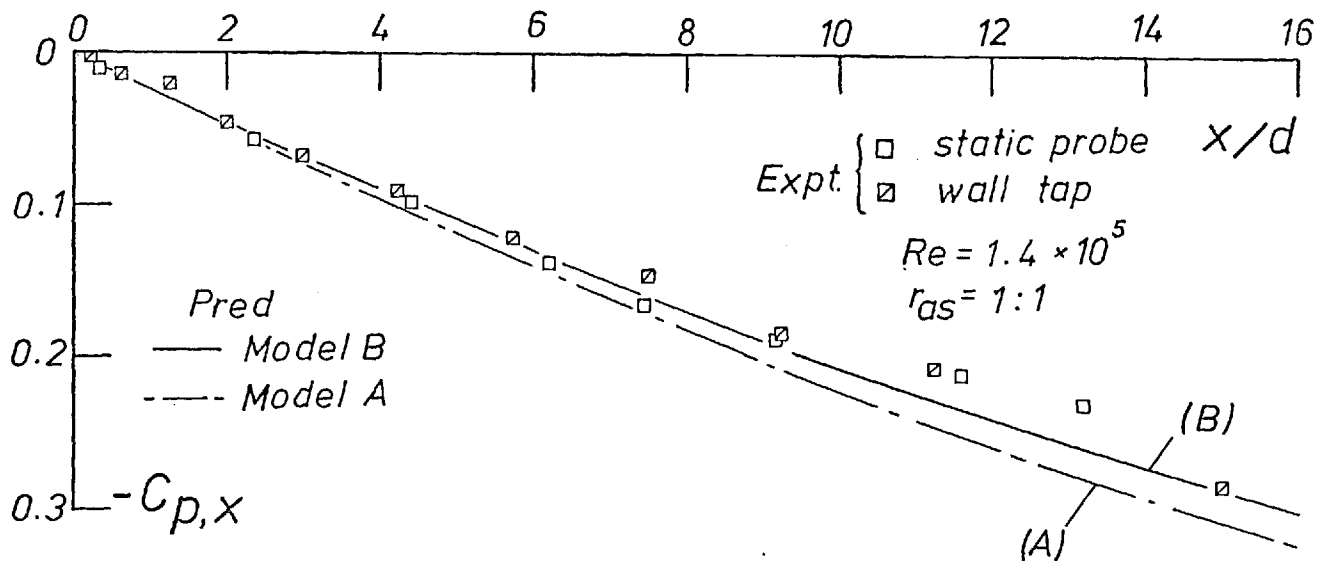
Fig.(8.3.7)   Pressure drop in the inlet region of a square-sectioned duct.

The prediction made with the simple turbulence model (A) indicates a pressure drop greater than that predicted with the two-equation model (B). Within the scatter of the experimental data obtained in the present investigation, also shown in the figure, the model (B) predicts the pressure drop with greater accuracy than (A), is accompanied by a correspondingly larger turbulent mixing than that experimentally observed. This is indeed the case as can be observed in Figure (8.3.8). The predicted increase in mixing can be seen to cause a retardation in the development of centreline velocity. Model B moreover predicts, centreline velocity development greater than A; however, the difference is not significant when compared with the experimental uncertainties.

$$\left[\frac{u_{cl}}{\bar{u}_{in}}\right] - 1$$

$Re = 1.4 \times 10^5$

$r_{as} = 1:1$

$2\theta = 0^\circ$

Model (B)

Model (A)

$\frac{x}{d}$
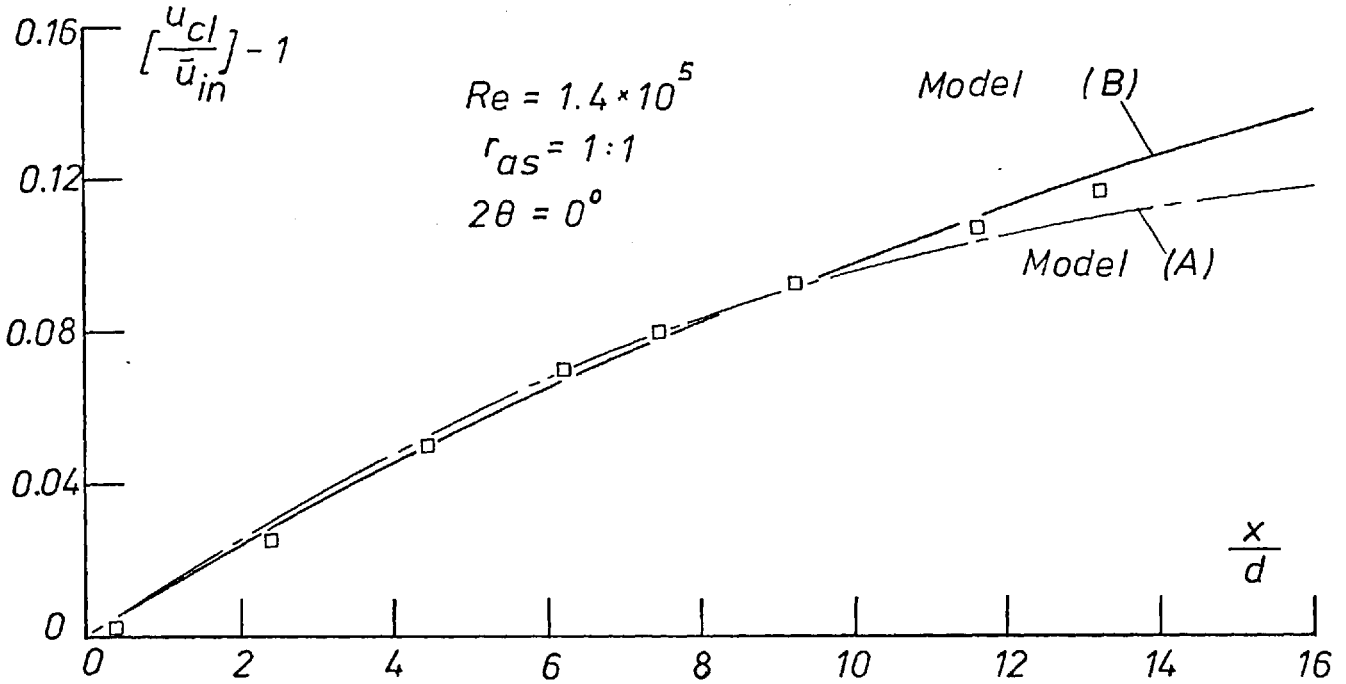
Fig.(8.3.8)   Development of centreline velocity in a square-sectioned duct.

An alternative formulation in the modelling the turbulent stresses, with particular reference to the turbulent normal stresses $-\rho\overline{u_i u_j}$, has been applied by Tatchell [60] to the prediction of developing flow in a square-sectioned duct. This method has permitted the prediction of turbulence-generated secondary flows, when the primary or axially-directed flow is otherwise fully-developed. However, in the developing region of the flow, no appreciable difference in the predicted values of pressure drop or centreline velocity increase, is observable between this method and the present two-equation model upto an L/d ratio of 16 : 1. It is thus concluded that the importance of separate and special modelling of the turbulence normal stresses is minimal in this region. This is borne out by the agreement between predicted values of velocity-profile development and corresponding experimental observations. The comparison is illustrated in Figure (8.3.9). The experimental data is that measured by the author in the present investigation. The velocity profiles are those corresponding to the vertical, i.e. $Z/d = \frac{1}{2}$) centreplanes. Similar results obtain for the horizontal centreplaces as well.
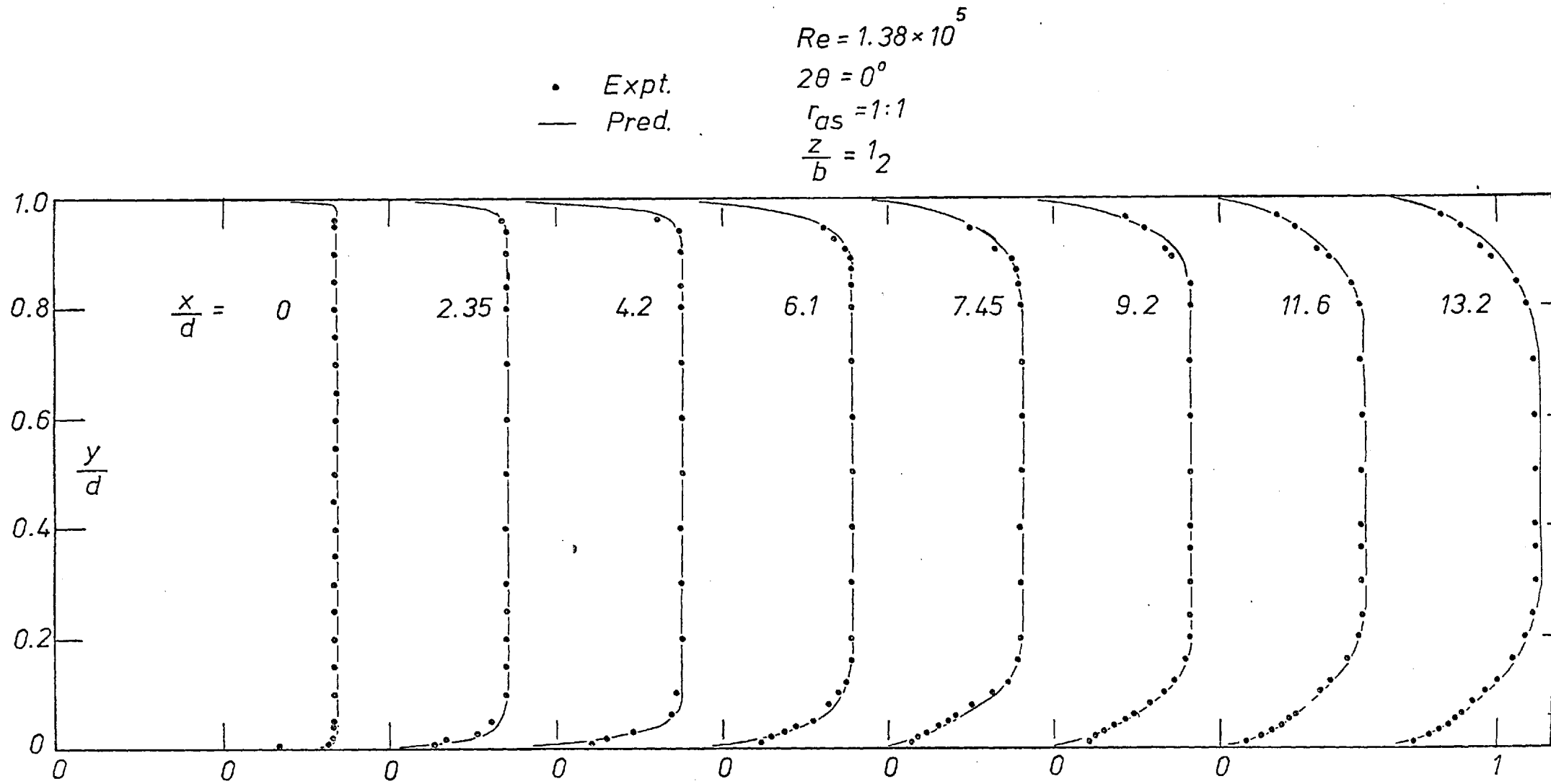
Fig.(8.3.9) Development of velocity (U/U_{in}) profiles accross the vertical centreplane of a duct of $r_{as} = 1 : 1$.

It was pointed out in Chapters 2 and 3, that the mathematical nature of three-dimensional boundary-layer flows required a special treatment of the pressure-gradient appearing in the ξ-direction momentum equation. Also, a method of obtaining this pressure-gradient was described; in the absence of other information it was assumed that the pressure-gradient was uniform across the duct/diffuser cross-section. One of the secondary objectives of the experimental program, was the validation of this assumption. That this has been satisfactorily achieved can be observed in Figure (8.3.10), where the predicted static pressure coefficient $-C_{p,x}$ is compared with measured values. A discrepancy is discernable at two axial stations. This is due to the fact, that, at these stations which were located at the downstream end of the test-section, the experimental results are adversely affected by the sudden expansions resulting from the connection to the tail-end diffuser.

Figures (8.3.11a) and (8.3.11b) show predictions of velocity profiles in a duct of aspect ratio 2 : 1, the same configuration for which laminar-flow results were described in Chapter 7. These profiles are compared with unpublished experimental data obtained by Masuda [37] . The comparisons show remarkably good agreement between the two.
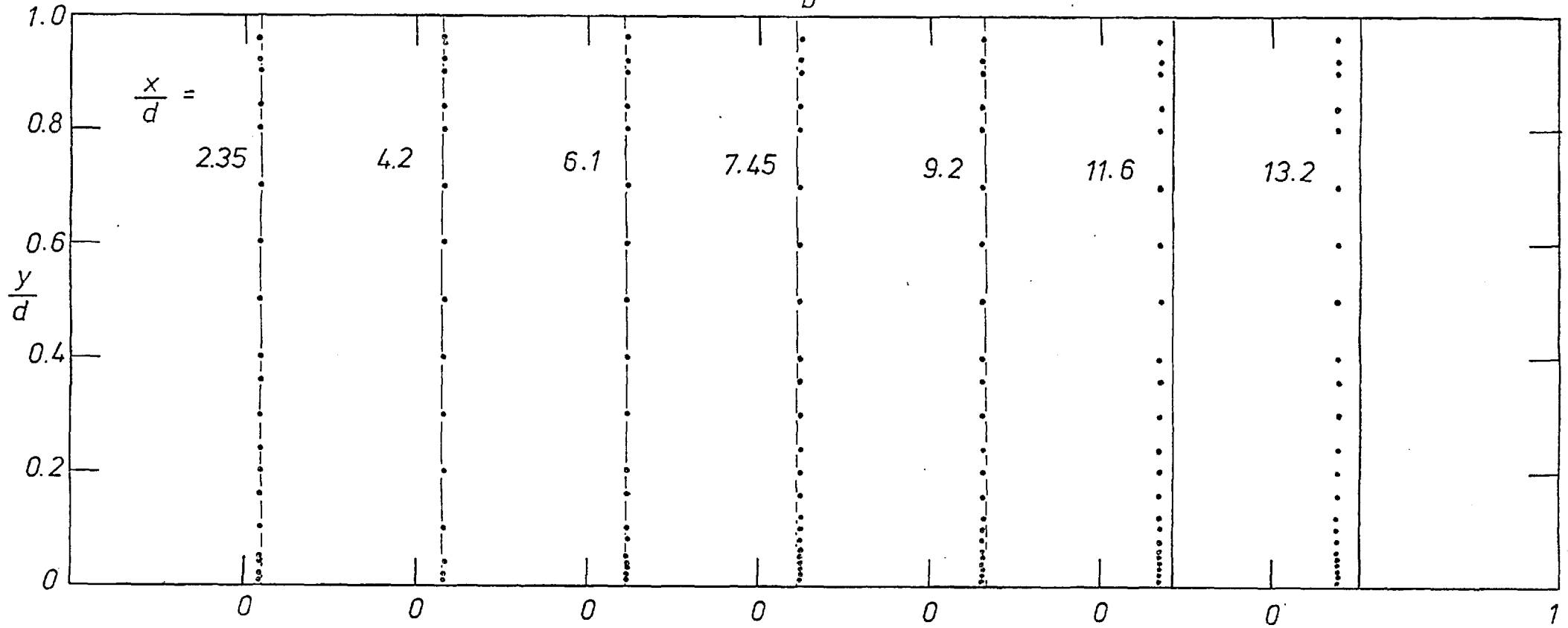
Fig.(8.3.10) Profiles of static pressure $(-C_{p,x})$ across the vertical central plane of a duct of r_{as} = 1 : 1.

case A

○ Expt.[37] $2\theta = 0°$
— Pred. $r_{as} = 2:1$
                $Re = 1.5 \times 10^5$
                $\frac{z}{b} = \frac{1}{2}$
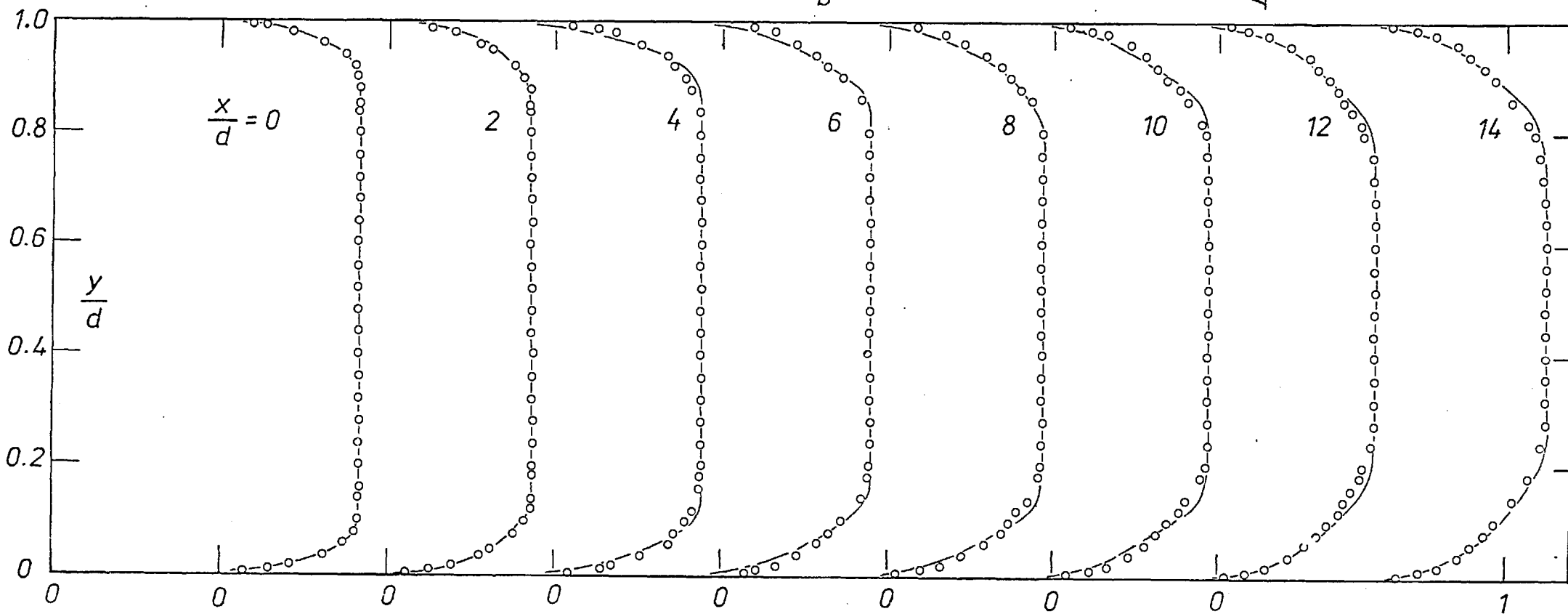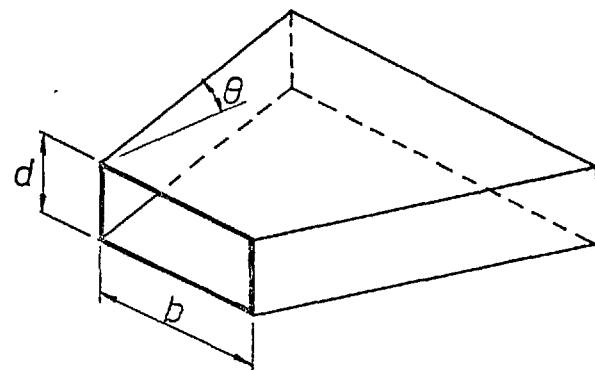
Fig.(8.3.11) (a)   Development of velocity (U/U_{in}) profiles across the vertical centreplanes of a duct of r_{as} = 2 : 1.

case A
∘ Expt.
— Pred.

$\dfrac{b}{d} = 2$

$\dfrac{y}{d} = \dfrac{1}{2}$

$\dfrac{x}{d} =$ 0   2   4   6   8   10   12   14

$\dfrac{z}{b}$
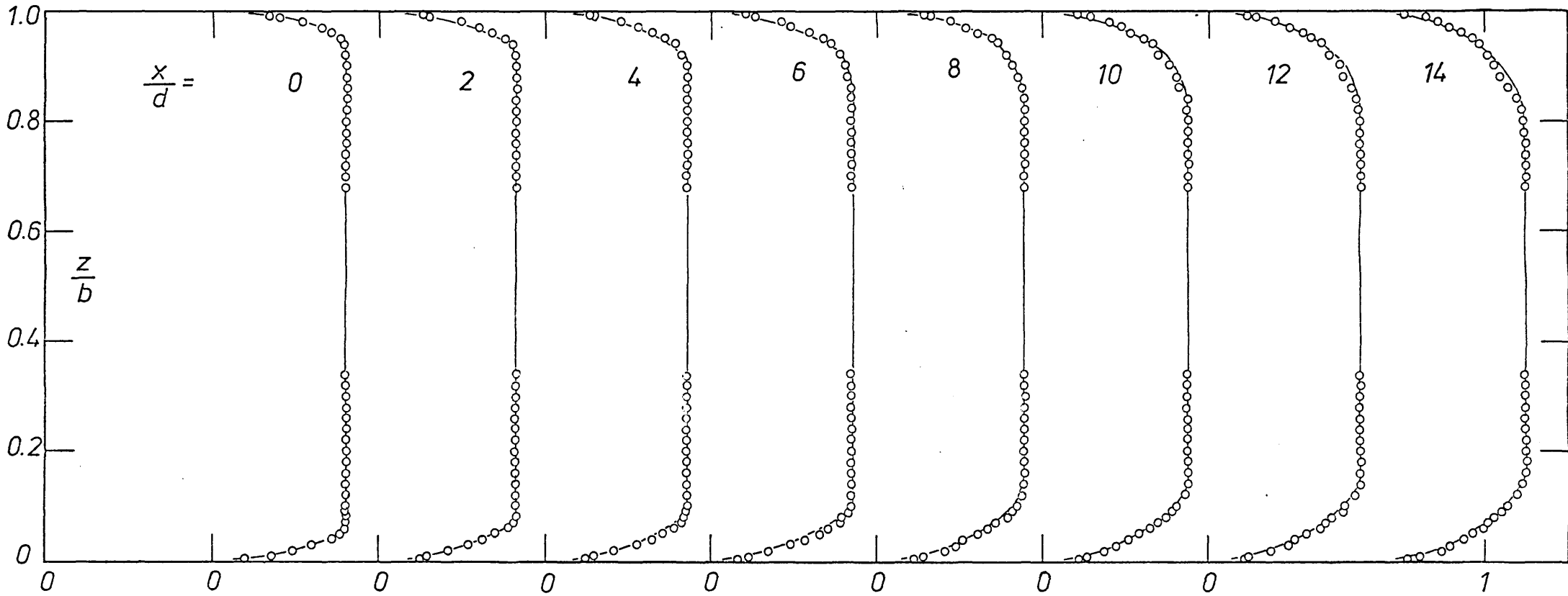
Fig.(8.3.11) (b) Development of velocity profiles across horizontal centreplanes of a duct of $r_{as} = 2 : 1$.

b) <u>Diffuser angles greater than zero</u>

Predictions made of flows in rectangular-sectioned diffusers, of several included angles (i.e. and area ratios) with uniform inlet conditions, are reported in this Section. Figure (8.3.12) shows predictions of pressure-rise coefficients within diffusers, of inlet aspect ratio 1 : 1and having two walls sloping at four different included angles. Also shown are experimental data measured in the present investigation. The open points represent values measured from static
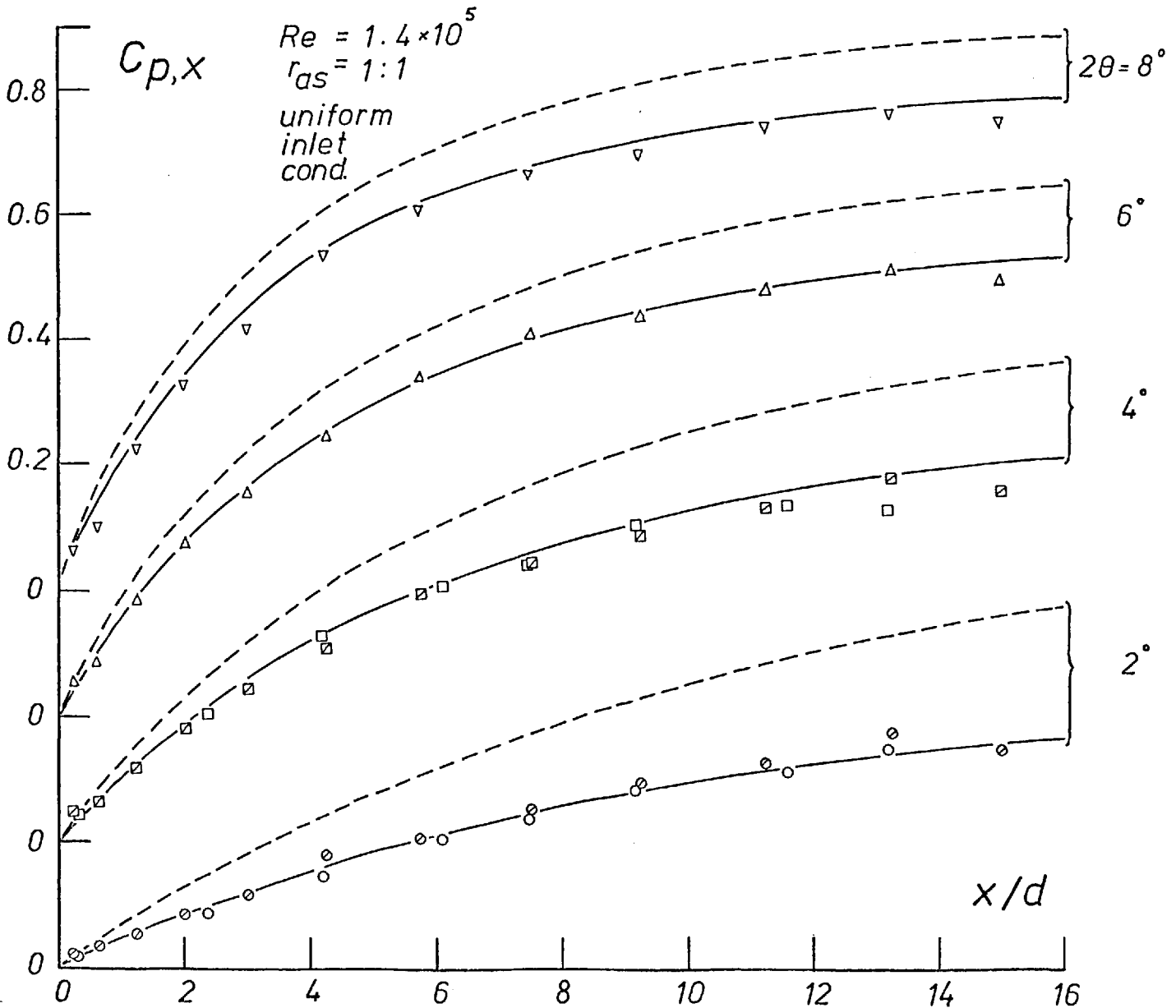
Fig.(8.3.12)   Effect of included angle on pressure recovery for uniform inlet conditions.

pressure probes traversed along the diffuser centreline and the slashed points represent values registered at wall static pressure taps. The predictions show good agreement with data; both indicate performance, at all four angles, well below that predicted by an inviscid analysis. For two of these situations, i.e. included angles 2° and 4°, Figures (8.3.13) and (8.3.14a) show profiles of axial velocity across vertical centreplanes at nine axial stations. The measured velocity distribution at station I (i.e. $x/d=0$) is supplied, as usual, as the initi al condition to the prediction procedure. Again, the agreement between data and prediction, for this relatively simple situation, is good. Figures (8.3.13b) and (8.3.14b) show similar profiles for the corresponding horizontal planes. Values indicated are at four stations at which experimental data were obtained in the present instance. Results are indicated, for convenience, as a function of normalised diffuser width at each station; the corresponding actual widths (and, in this case, the area ratios) are also indicated. For similarly uniform conditions at inlet, predictions of velocity profile in an 8° diffuser of aspect ratio 2 : 1 at inlet, are shown in Figures (8.3.15a) and (8.3.15b) the former being across vertical planes and the latter, horizontal planes. The predictions are compared with the data of Masuda [37] who also measured, for this circumstance, distributions of turbulence intensities at inlet to the diffuser. Values of turbulence energies derived from this are used as inlet conditions to the two-equation model of turbulence. The influence of this "free-stream" turbulence at inlet, upon predictions, is shown by tests to be a minor one.

As in the previous instances, the static pressure distribution remained uniform over the diffuser cross-sections over the entire length. This can be observed in Figure (8.3.16), where measured values of static pressure across the vertical centreplane of a 4° diffuser are compared at eight axial positions, with predicted values. With the exception of two such positions where the influence of tail-end connections have permeated upstream, the experimental data are in close agreement with predictions.

$$\bullet \ Expt. \qquad Re = 1.38 \times 10^5$$
$$— \ Pred. \qquad 2\theta = 2^\circ$$
$$r_{as} = 1:1$$
$$\frac{z}{b} = \frac{1}{2}$$
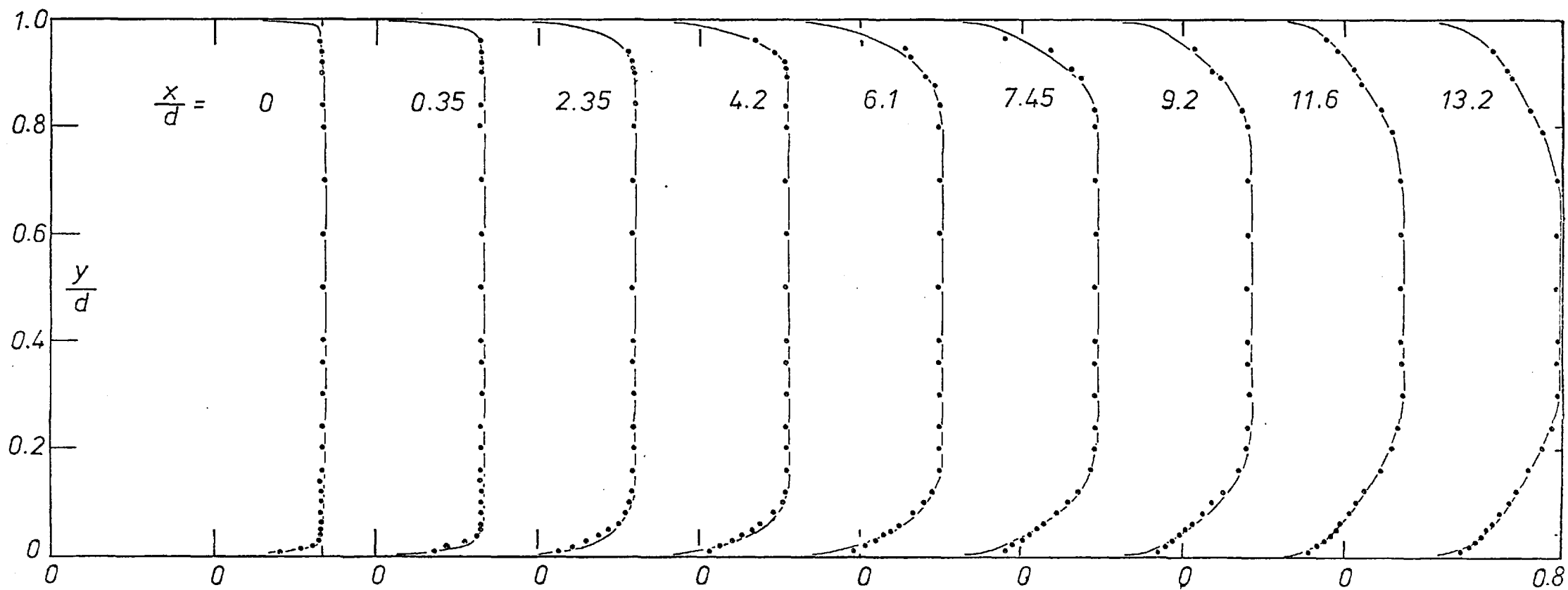
Fig.(8.3.13) (a) Development of velocity (U/U_{in}) profiles across the vertical centreplanes of a 2 deg. diffuser.
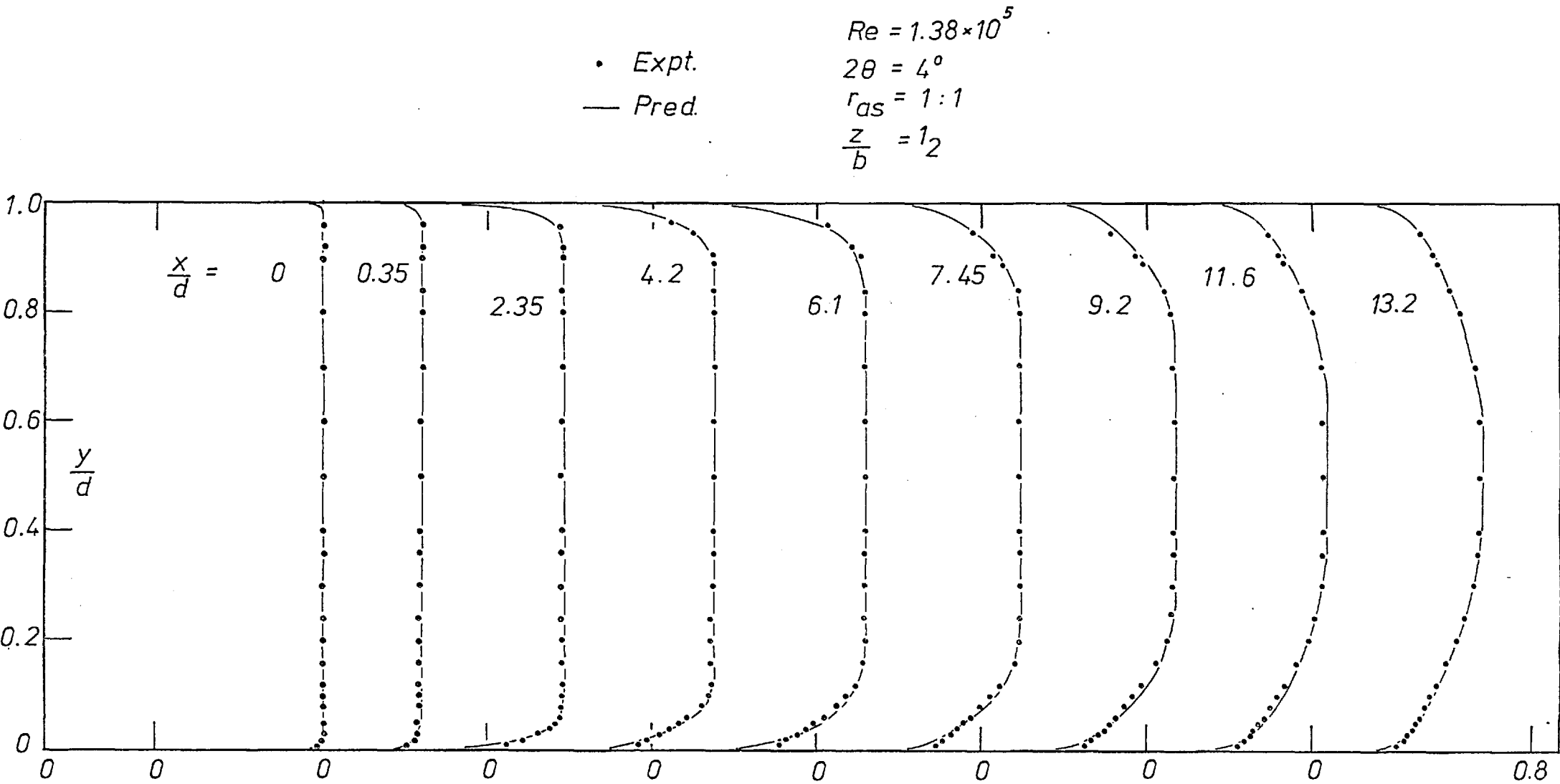
Fig.(8.3.14) (a) Development of velocity (U/U_{in}) profiles across the vertical centreplane of a 4 deg. diffuser.
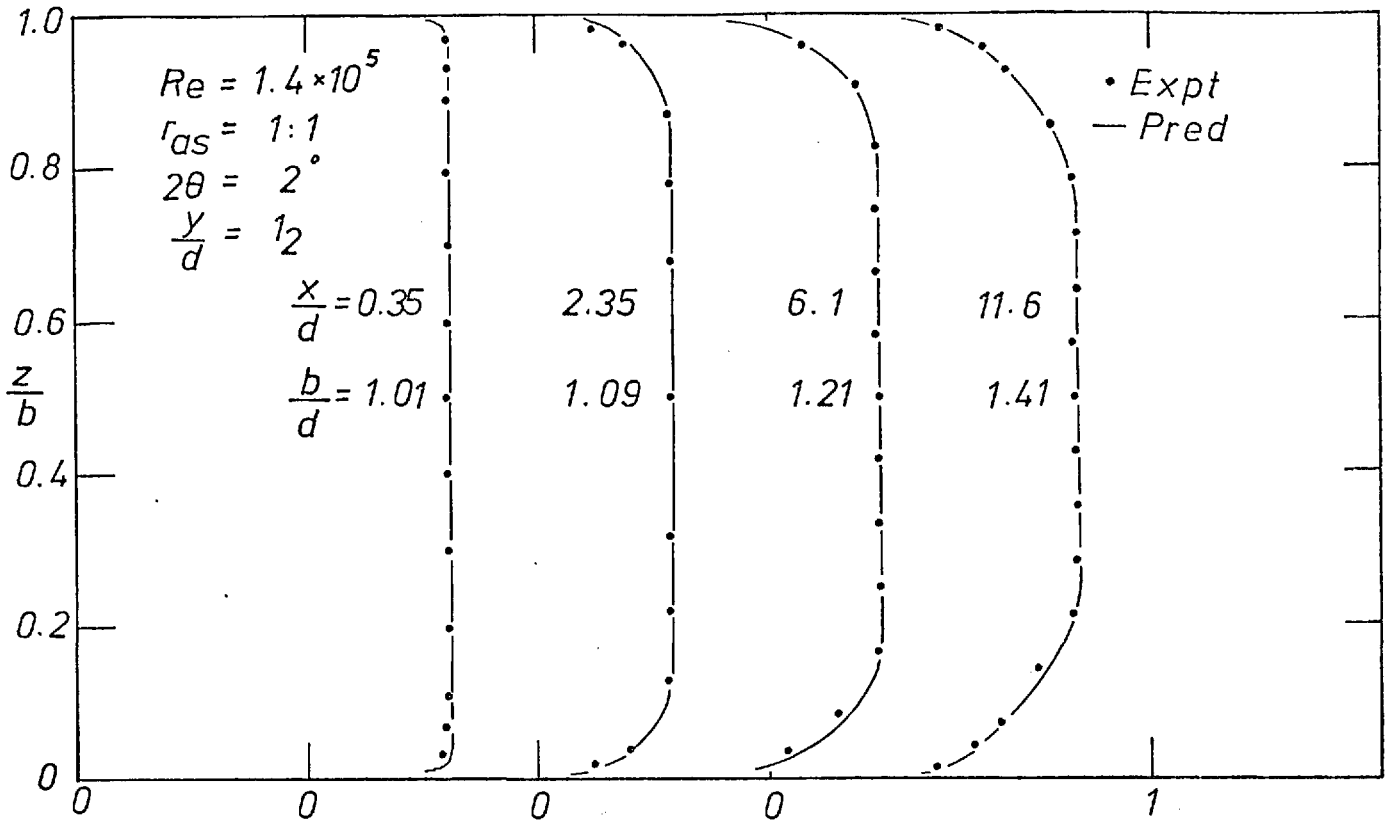
Fig.(8.3.13) (b) Profiles of velocity (U/U_{in}) across the horizontal centreplane of a 2 deg. diffuser.
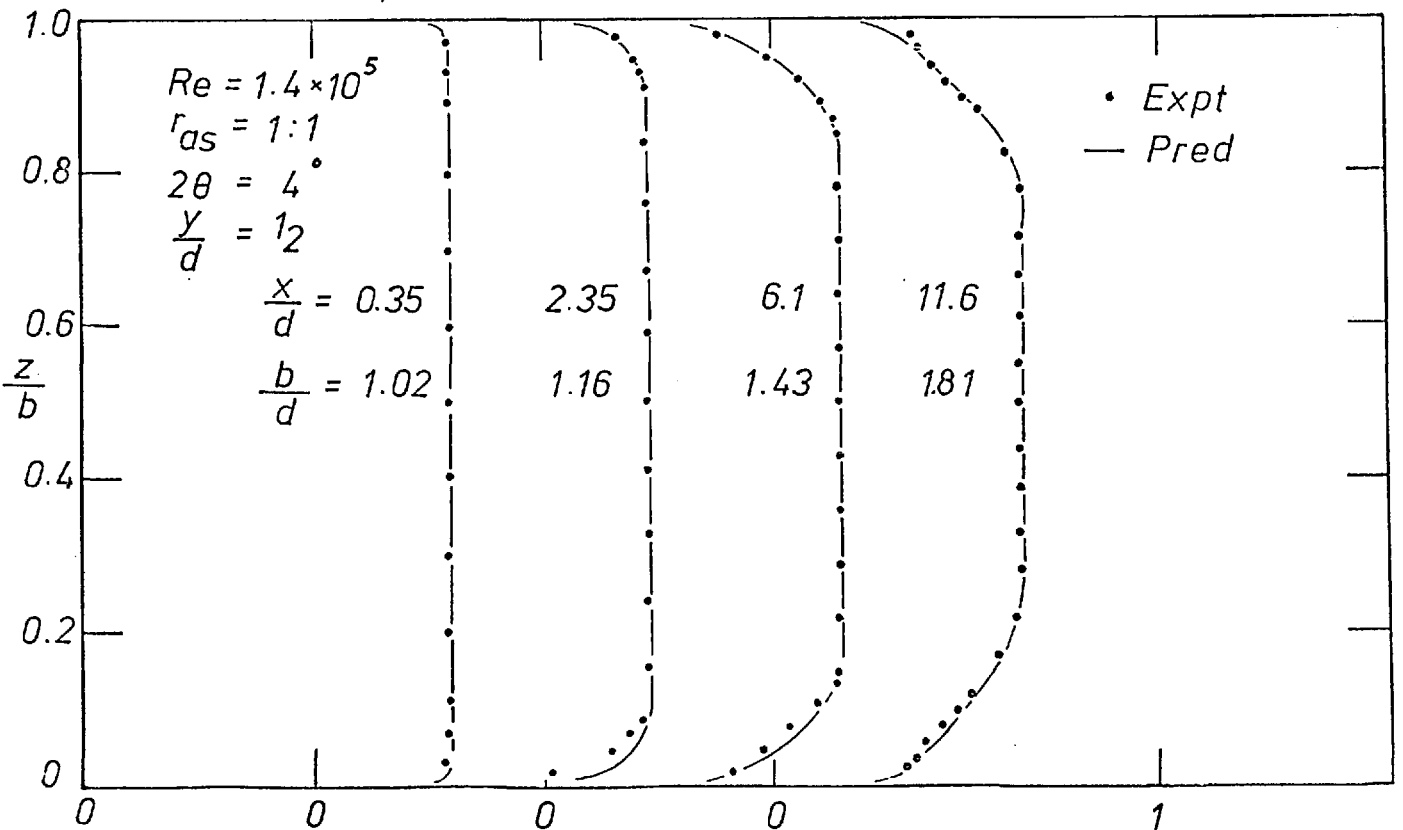
Fig.(8.3.14) (b) Profiles of velocity (U/U_{in}) across the horizontal centreplane of a 4 deg. diffuser.

case C $2\theta = 8^o$
  ○ Expt. [37] $r_{as} = 2:1$
  — Pred. $Re = 1.5 \times 10^5$
            $\frac{z}{b} = \frac{1}{2}$
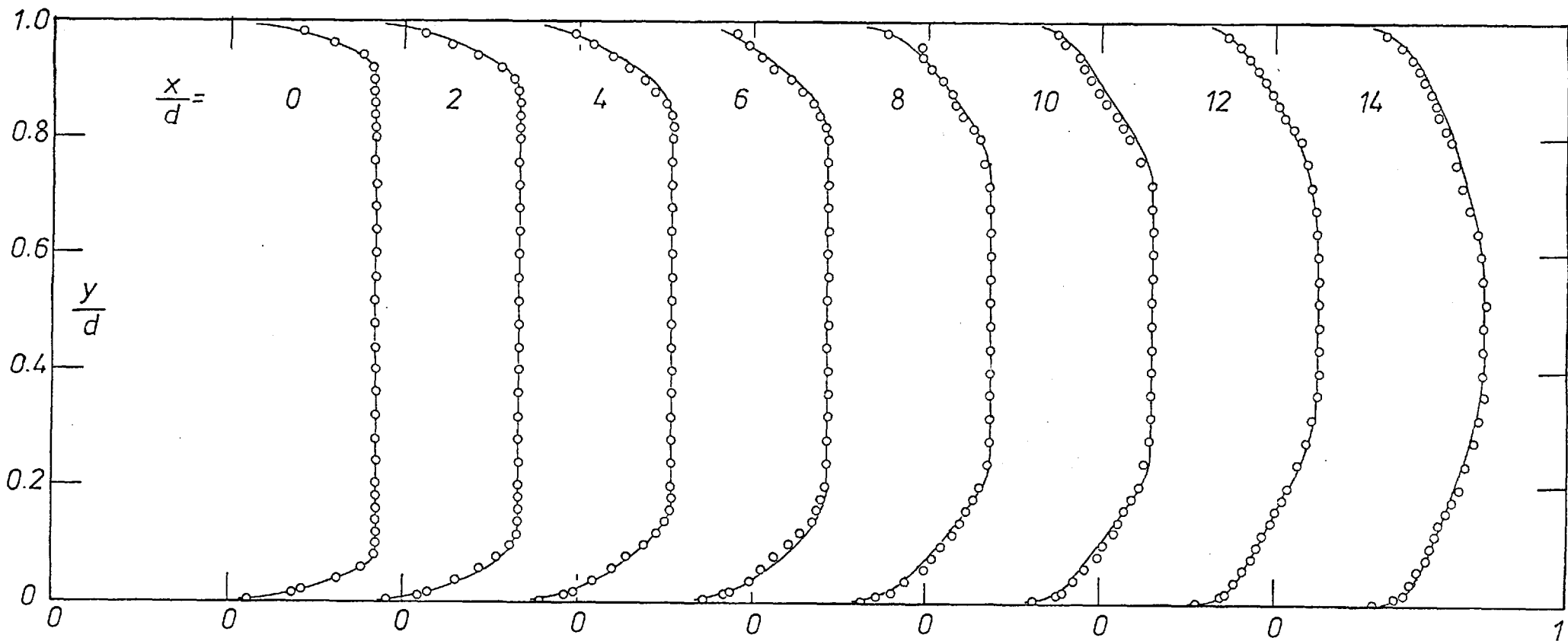
Fig.(8.3.15) (a)   Development of velocity (U/U_{in}) profiles across the vertical centreplane of an 8 deg. diffuser.

case C

○ Expt.
— Pred.

$\dfrac{y}{d} = \dfrac{1}{2}$

$\dfrac{x}{d} =$ 0   2   4   6   8   10   12   14

$\dfrac{b}{d} =$ 2.078   2.358   2.638   2.918   3.198   3.48   3.76   4.04

$(\dfrac{z}{b})_x$
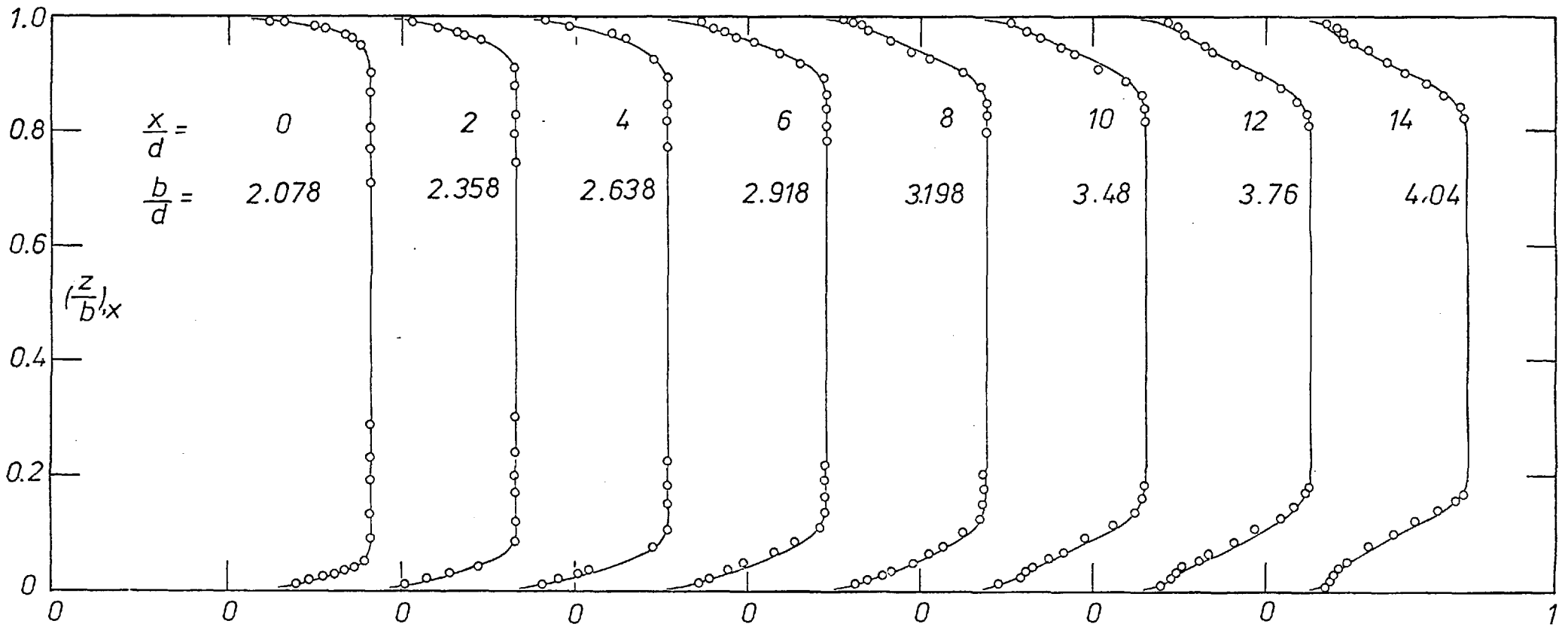
Fig.(8.3.15) (b)   Development of velocity profiles across the horizontal centreplane of an 8 deg. diffuser.
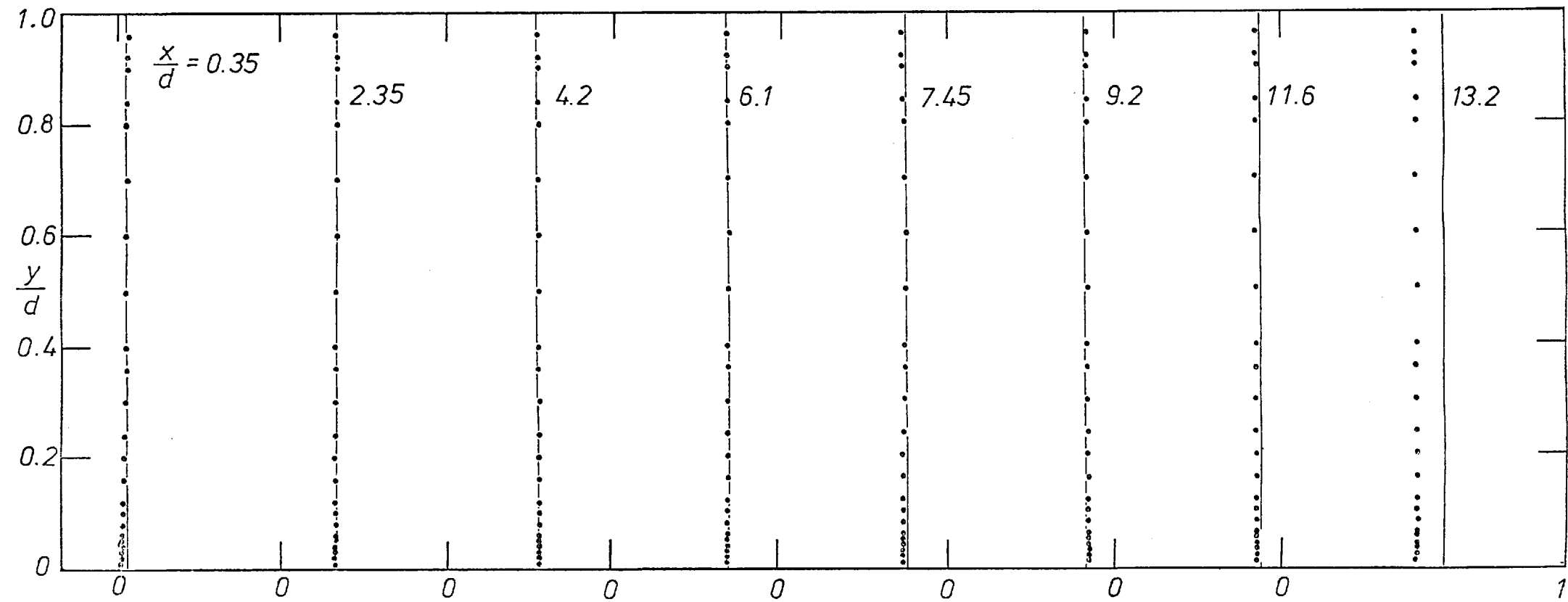
Fig.(8.3.16)   Profiles of static pressure ($-C_{p,x}$) across the vertical centreplane of a 4 deg. diffuser.

8.3.5   Effect of inlet conditions

It is long been recognised that diffuser performance is strongly influenced by conditions that prevail at the inlet (e.g. Bradley and Cockrell [5]). Generally speaking, performance is improved by reductions in boundary-layer thickness at inlet. Investigations conducted with the present prediction procedure using both the simple and the two-equation turbulence models indicated that this was indeed so. One result of this investigation is shown in Fig. (8.3.17). Two types of
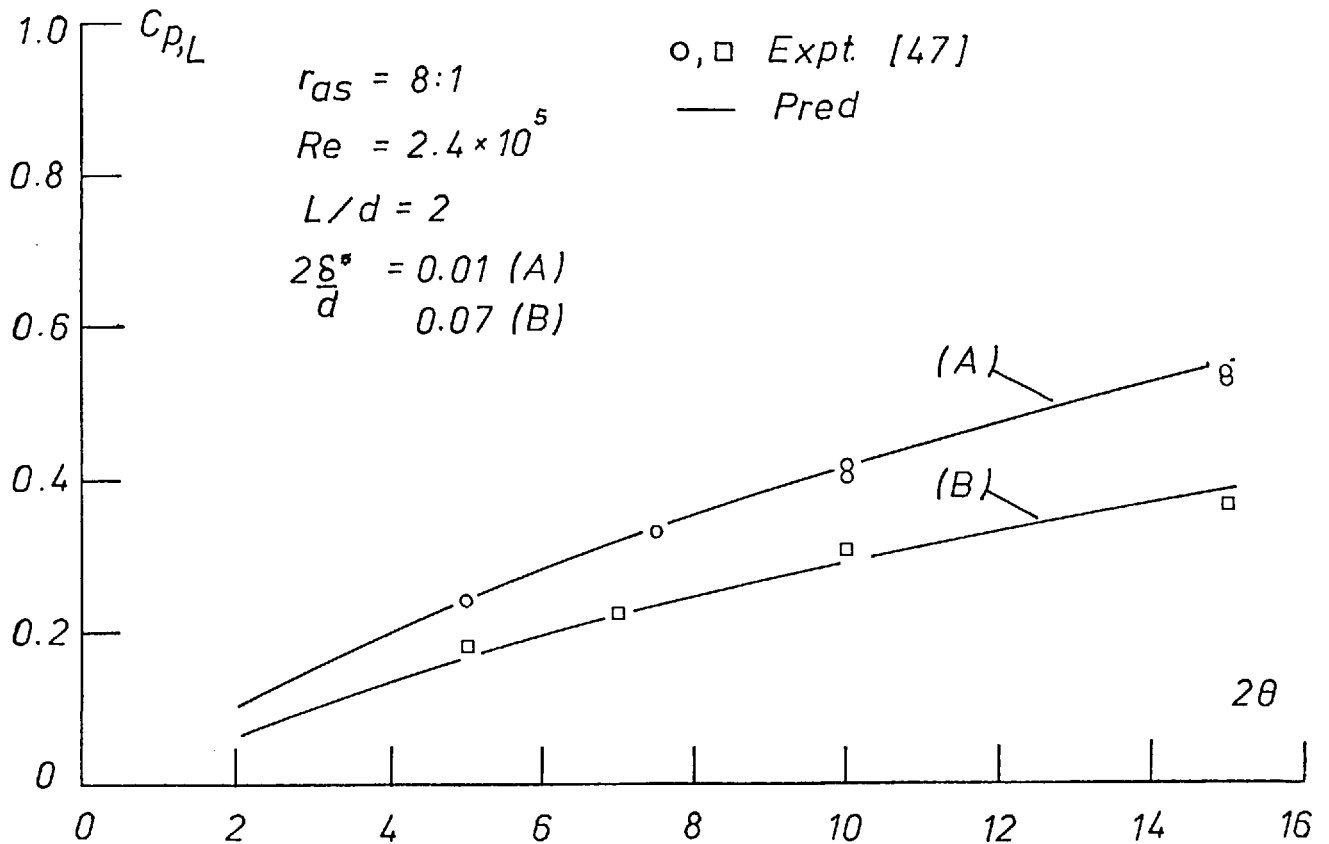
Fig.(8.3.17)   Effect of inlet boundary - layer thickness on pressure rise ina rectangular - sectioned diffuser.

velocity profile, both essentially uniform but possessing different boundary-layer thicknesses, are supplied as inlet conditions, across the vertical plane, to a large (8 : 1) aspect ratio diffuser over a range of included angles. At a given axial position (L/d=2)the predicted

performance with a thin inlet boundary-layer thickness is seen to be an improvement over that with a thick inlet boundary layer. Moreover, predicted performance compares favourably with measured values due to Reneau et. al. [47] . Some uncertainty must remain unresolved with these results, since the shape of the boundary layer profiles on the side walls is not reported; for this reason estimated thicknesses are used in the predictions.

Since diffusers in engineering practice, are often preceded by other devices, severe distortions occur in distributions of velocity at their inlet. It is interesting to observe the effects of such distortions upon diffuser performance. Accordingly, predictions were made of flows in a diffuser of aspect ratio 2 : 1, under shear flow conditions at inlet. Figure (8.3.18) shows velocity profiles predicted by both models of turbulence described in Chapter 4. Model A fails to predict the decay of shear rate with axial position, that is exhibited by the experimental data of Masuda et. al. [38] . Model B however, capable of accounting for the energy redistributions of shear flows, does prove an improvement over Model A. The performance of this diffuser under identical inlet conditions, for a range of included angles, is indicated in Fig. (8.3.19). Again, an inviscid analysis is seen to predict performance considerably in excess of that measured and predicted by the present procedure. An increase in shear-rate, causing greater mixing and, correspondingly pressure loss, is expected to reduce performance under otherwise similar conditions. That this is indeed so may be observed in Fig. (8.3.20). Here, for a diffuser of 6° included angle, predicted values of performance are compared with the experimental data of Masuda et. al., for three diferent rates of shear λ at inlet. This quantity is defined as follows:

$$\lambda \equiv \left\{\frac{\partial U}{\partial y}\right\}_{\mathcal{C}} \cdot \frac{d}{U_{in}} \qquad . (8.2.1)$$

Predictions of performance in the 16° diffuser indicated some interesting results. Stall, i.e. reverse flow along the diffuser axis was predicted at the corners of the diffuser cross-section, commencing at stations beyond an X/d of 4. The experimental data measured with wall static pressure taps, do not of course record this stall. However, it was de-
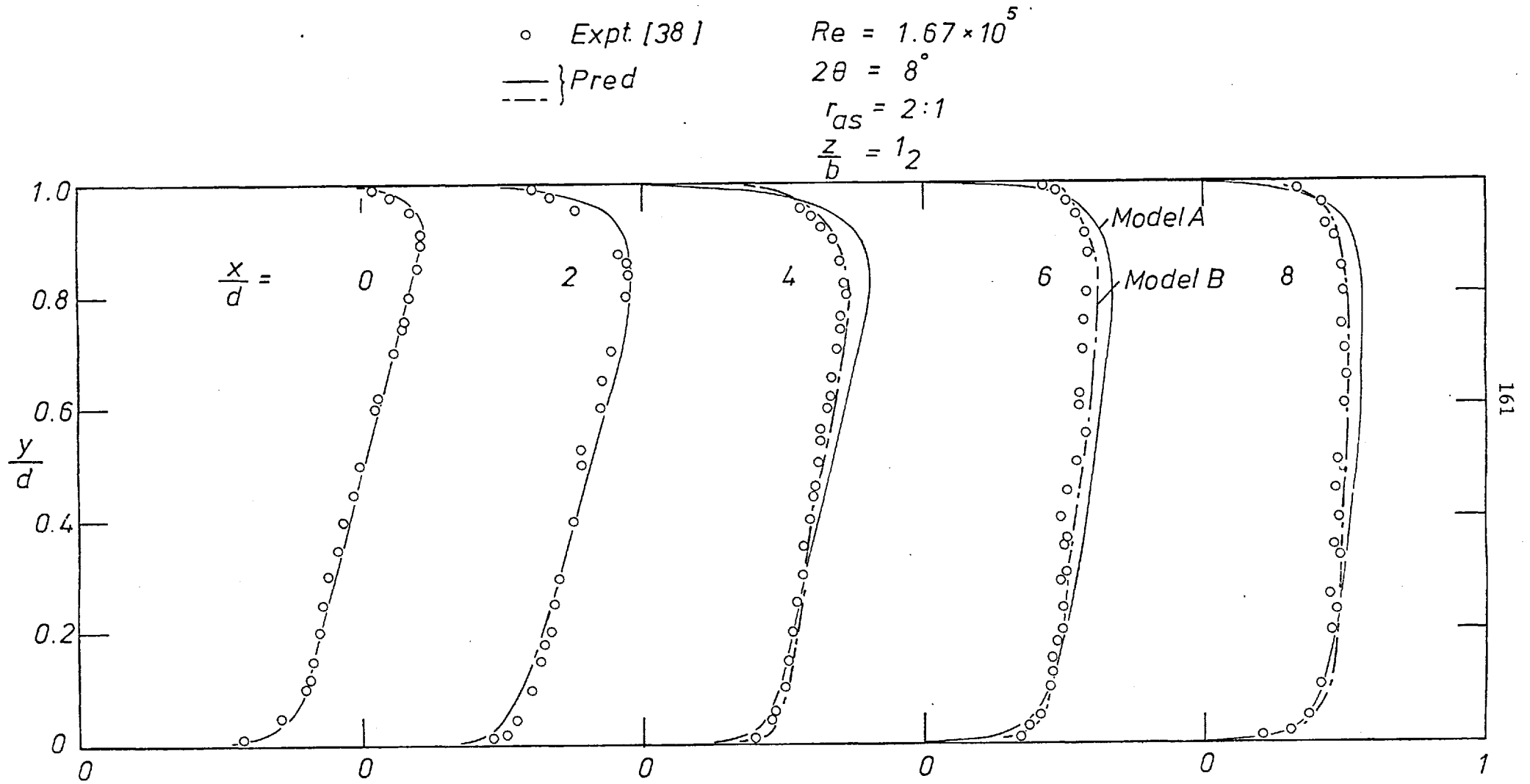
Fig.(8.3.18)   Development of velocity (U/U_{in}) profiles across the vertical centreplane of an 8 deg. diffuser. Non – uniform inlet conditions.
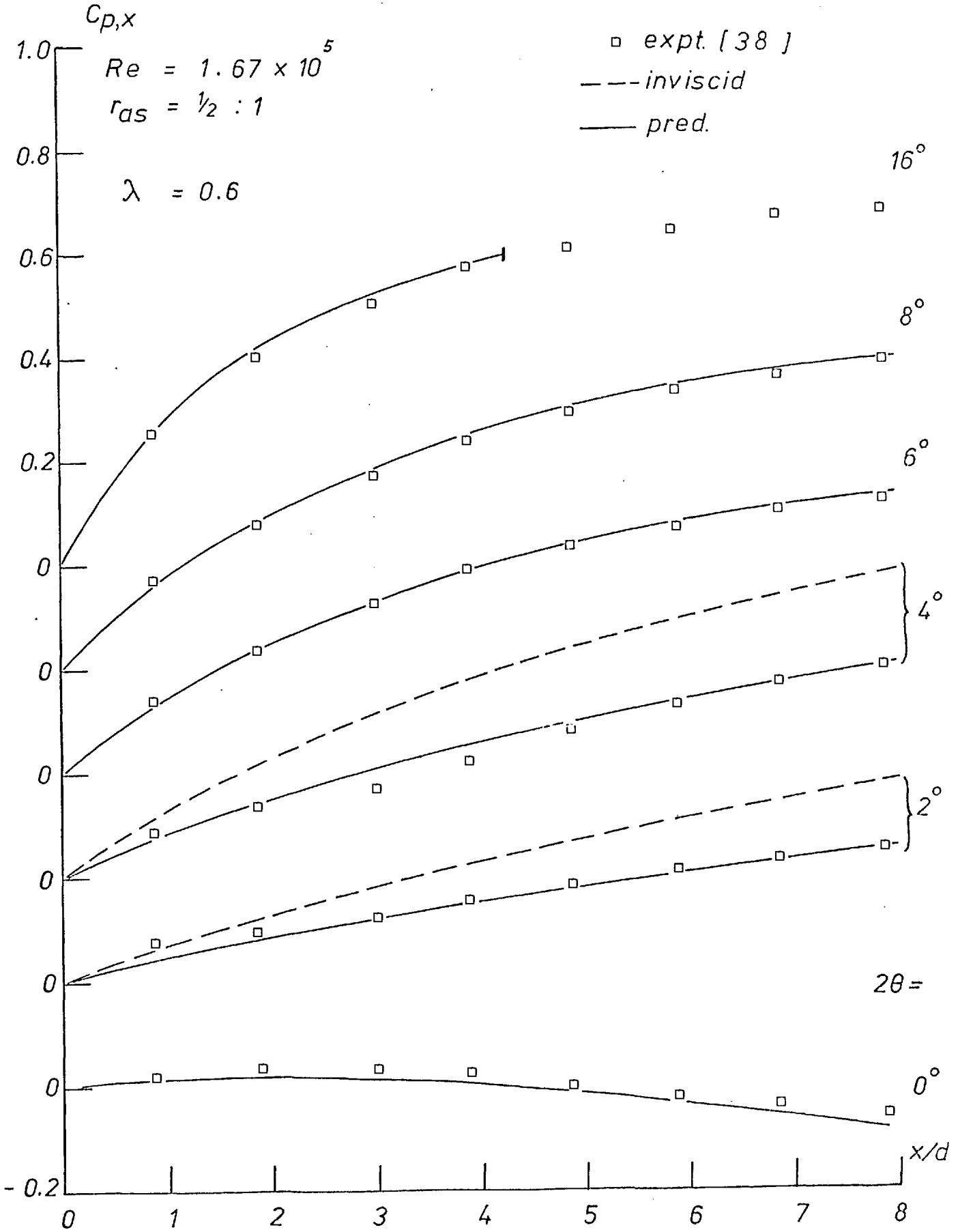
Fig.(8.3.19)   Effect of included angle on diffuser performance.   Non -
uniform inlet conditions.

termined later (Masuda [37]), that a state of incipient stall did exist at the corners, over the second half of the diffuser length.
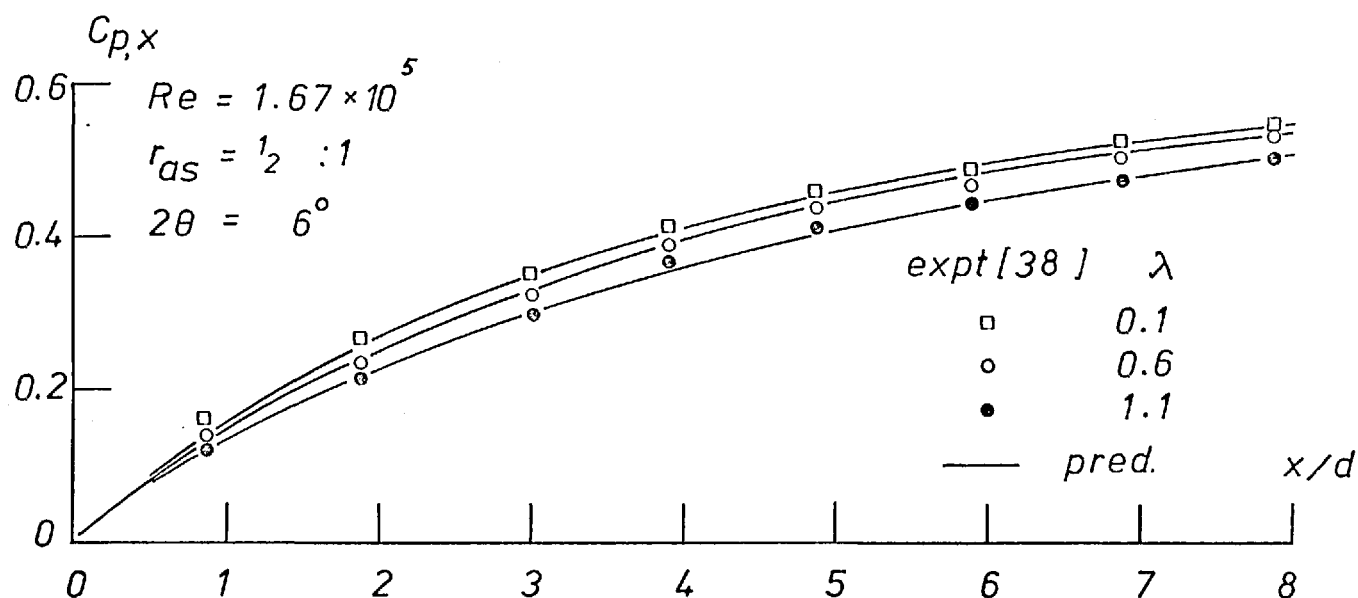
Fig.(8.3.20)   Effect of shear flow at inlet on the performance of a rectangular - sectioned diffuser.

Detailed measurements of axial velocity profiles in an 8° diffuser of inlet aspect ratio 2 : 1 provided by Masuda [37] are used to compare with predictions of the three-dimensional flow-field existing under these circumstances. The comparisons are illustrated in Figures (8.3.21a) and (8.3.21b). The decay-rate of 'free-stream' shear is seen to be reasonable well predicted.

The effect of inlet conditions upon diffuser performance was experimentally determined by Wolf and Johnstone [65] . They performed tests in a diffuser of aspect ratio 4 : 1 at inlet, with four different types of inlet conditions over a range of area ratios (i.e. included angles). In Figure (8.3.22), the geometric configuration used in these tests as well as the four types of velocity profiles across the vertical

case B

○ — Expt. [37] $2\theta = 0^{0}$
—— Pred. $r_{as} = 2:1$
$Re = 1.5 \times 10^{5}$
$\dfrac{z}{b} = \dfrac{1}{2}$

$\dfrac{x}{d} = 0$ 2   4   6   8   10   14

164
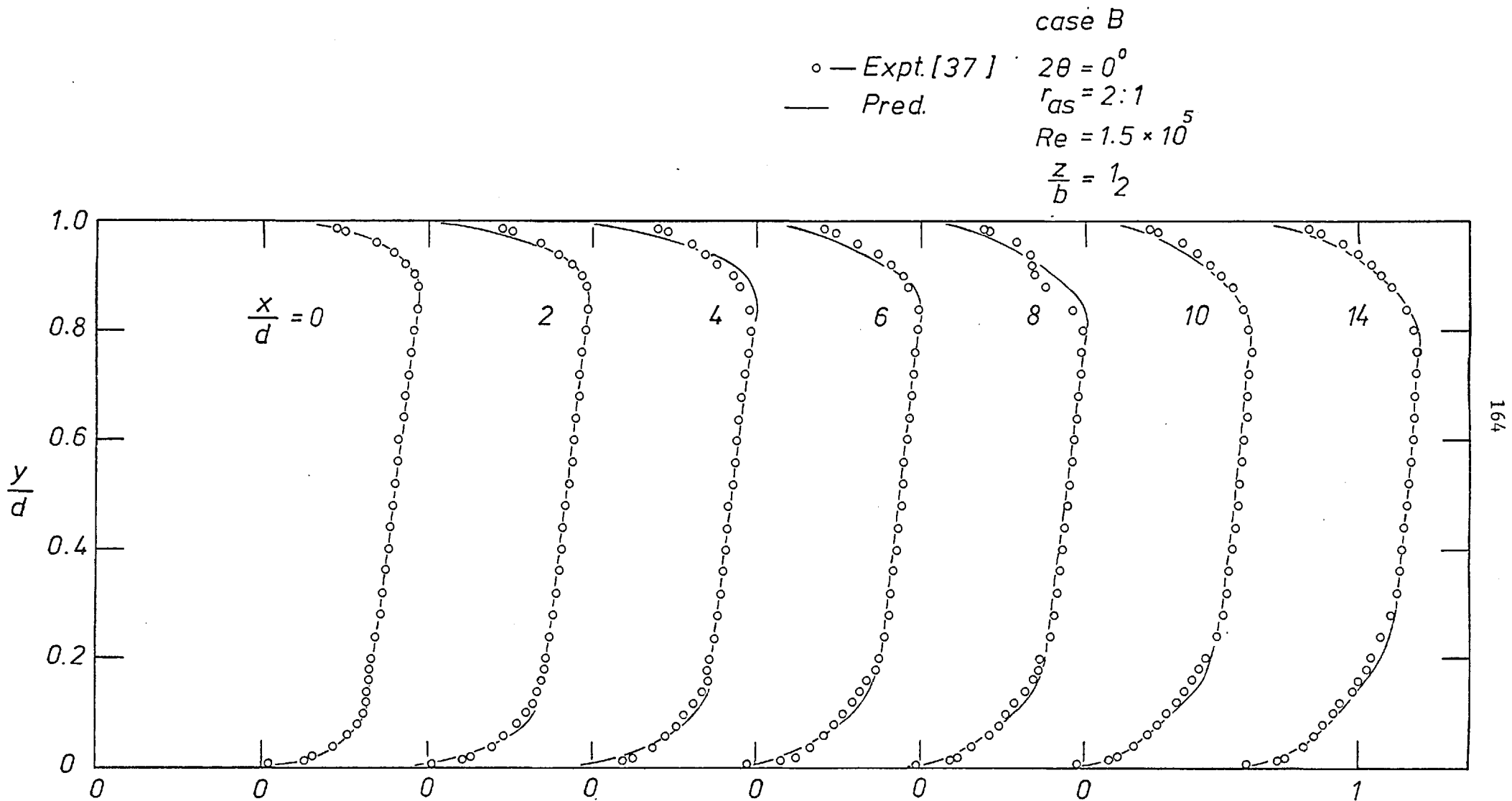
Fig.(8.3.21) (a)   Development of velocity (U/U_{in}) profiles across the vertical centreplane of a duct of $r_{as} = 2 : 1$. Non - uniform inlet conditions.

case B $\frac{b}{d} = 2$

o Expt.

— Pred. $\frac{y}{d} = \frac{1}{2}$

$\frac{x}{d} =$ 0   2   4   6   8   10   12   14

$\frac{z}{b}$
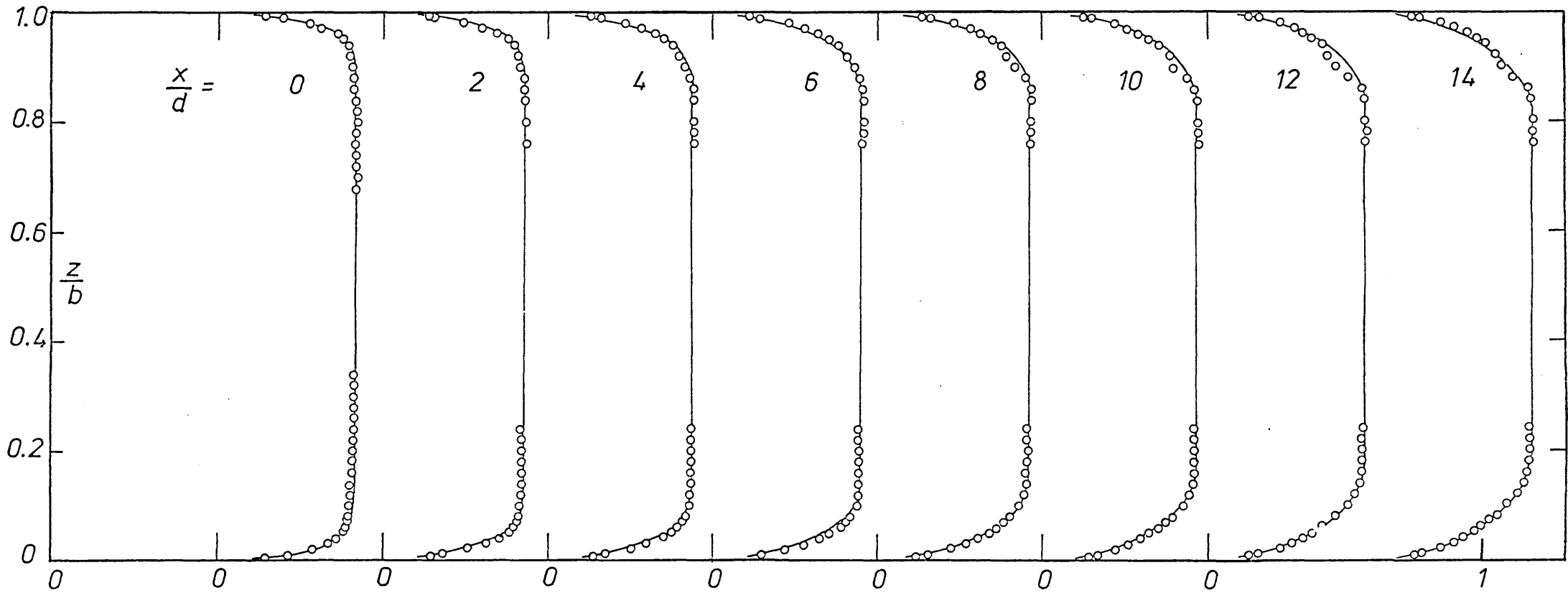
Fig.(8.3.21) (b) Development of velocity profiles across the horizontal centreplanes of a duct of r_{as} = 2 : 1.
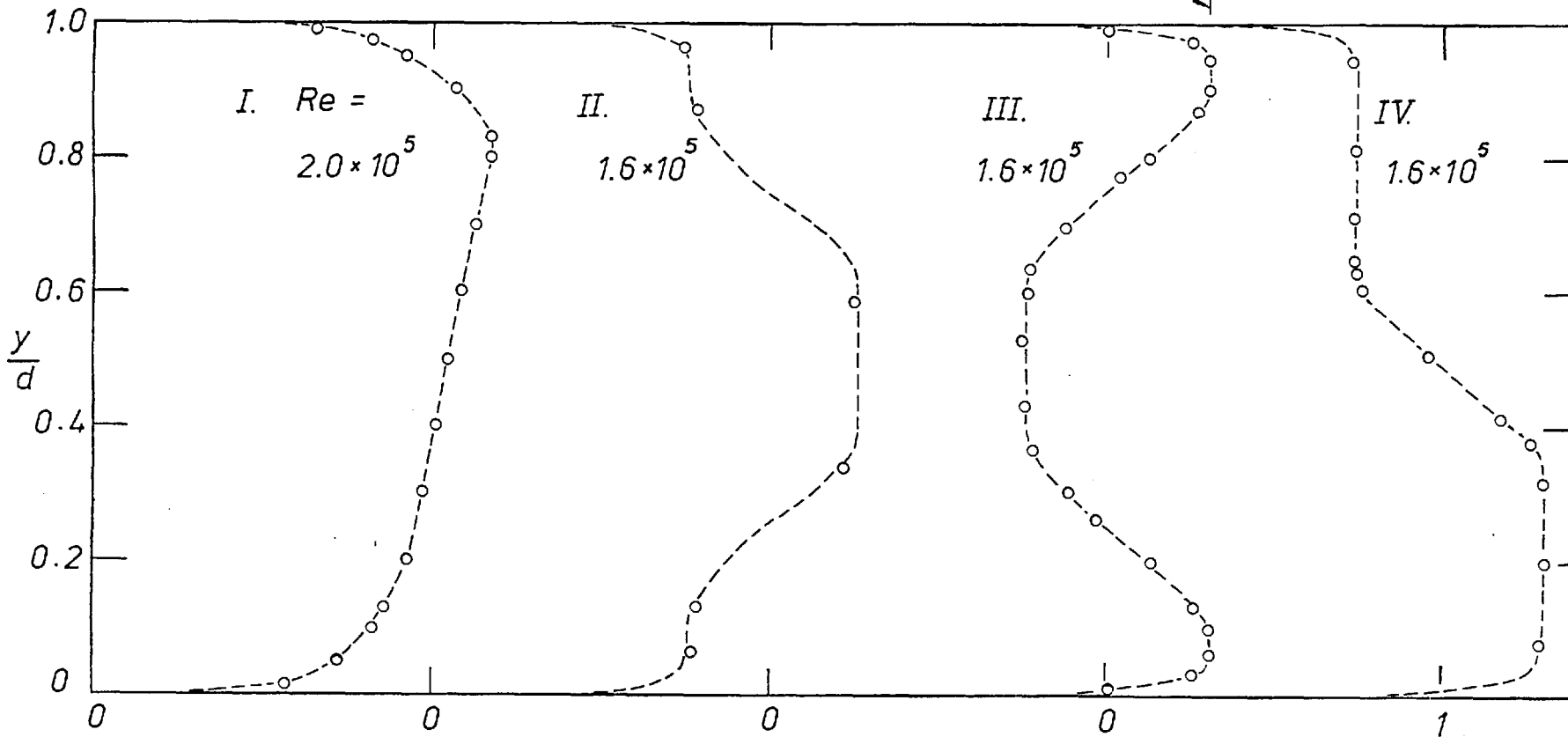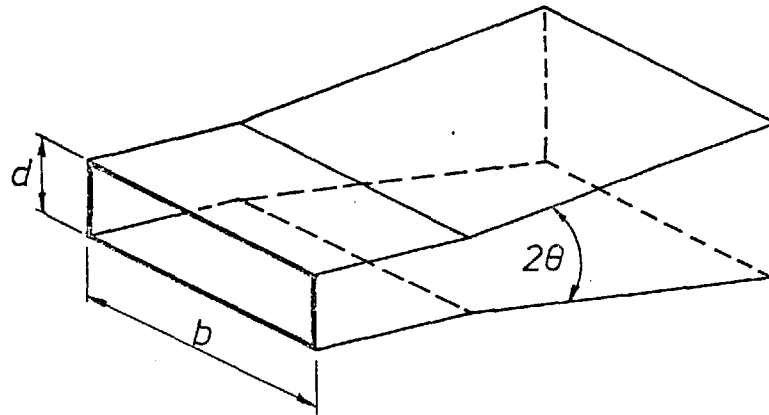
Fig.(8.3.22)   Measured profiles of velocity (U/U_{in}) across the vertical centreplane at inlet to a
duct/diffuser system; Wolf & Johnstone [65]   .

plane at inlet, are illustrated. These types consist of linear shear, jet, wake and step shear velocity profiles numbered in that order. Predictions made for the zero-included angle (i.e. duct) cases are represented in Figures (8.3.23), (8.3.24), (8.3.25) and (8.3.26). A faster rate of velocity profiles is predicted in cases II, III and IV, than those observed experimentally. This is attributed to the uncertainty in the distribution of velocity in the neighbourhood of the side walls. This distribution is presumed, for the sake of the predic tions, to be uniform except for thin $(2\delta^*/d \approx 0.04)$ boundary layers on the side walls. Within the limitations of this presumption, the pressure-drop is predicted reasonably well for all four cases considered. The four parts of Figure (8.3.27) represent predictions of diffuser performance in all four cases over area ratios ranging from 1.2 to 2.1; other conditions remain as represented in Figure (8.3.22). Nothwithstanding uncertainties regarding the measurements, made with wall static pressure taps on both diverging walls, the predicted performance compares favourably with the data. Finally, predictions of the effect of shear flow upon the performance of an 8° diffuser of inlet aspect ratio 2 : 1 are presented in Figures (8.3.28a) and (8.3.28b). It can be observed that the shear velocity profile does not become uniform downstream of the inlet. Across the horizontal plane however, the velocity distribution retains its uniformity over a large proportion of the cross-section.

It is thus apparent that predictions of the effects of inlet conditions upon diffuser performance are in reasonably close agreement, qualitatively and quantitatively, with experimental measurements.

8.3.6   Effect of wall shape

Although rectangular-sectioned diffusers, with straight axes are considered in this Thesis, investigations are made of the effects of wall shape upon diffuser performance. Predictions of flow in a diffuser of aspect ratio 1 : 1 and uniform conditions at inlet with one pair of walls flared out in a trumpet shape are presented in Figure (8.3.29). These predictions are compared with an inviscid analysis and experimental data obtained by Norbury [42] . Both qualitative and quantitative agreement between prediction and data is observed. As before, the inviscid analysis indicates a greater pressure rise and centreline velocity
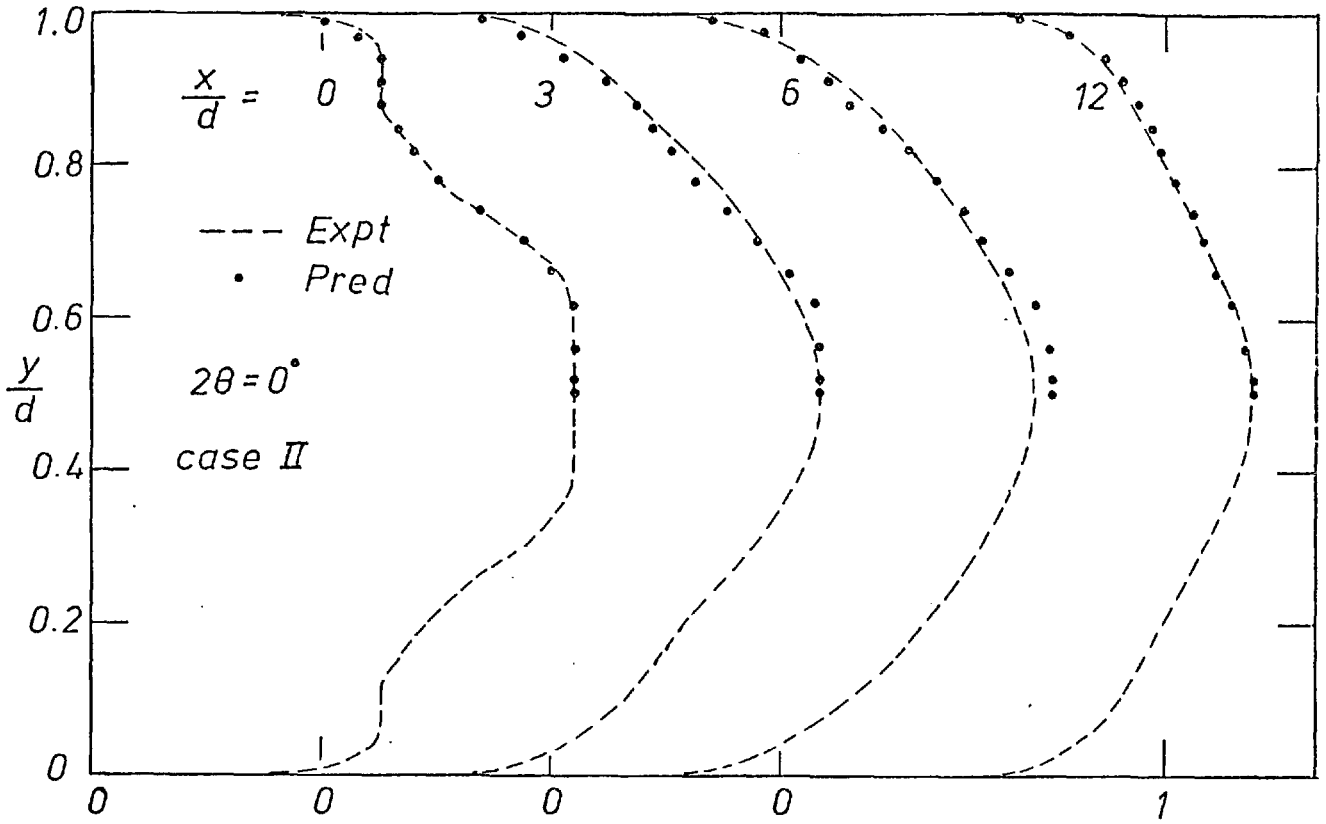
Fig.(8.3.23)   Development of velocity (U/U_{in}) profiles across the vertical
centreplane of a duct of $r_{as} = 4 : 1.$; Case II.
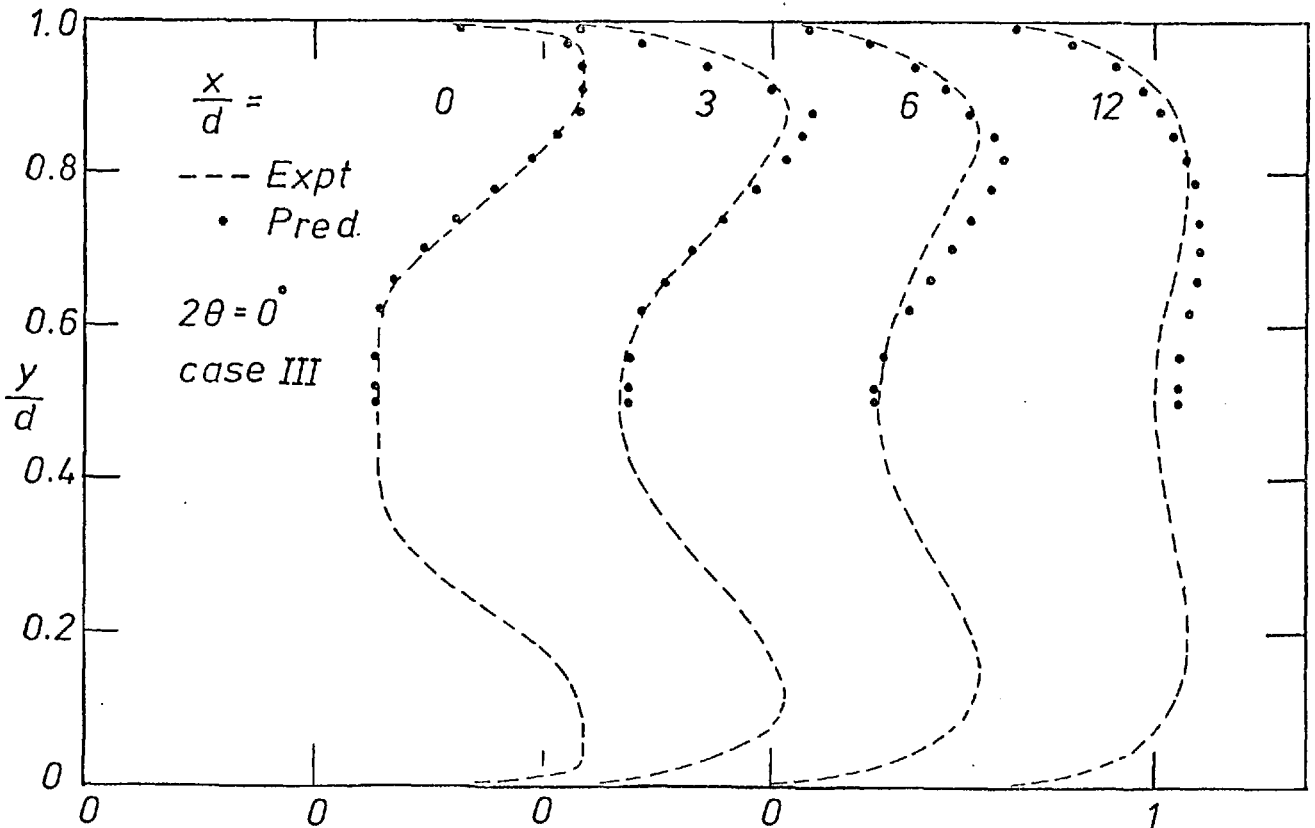
Fig.(8.3.24)   Development of velocity (U/U_{in}) profiles across the vertical
centreplane of a duct of $r_{as} = 4 : 1$; Case III.
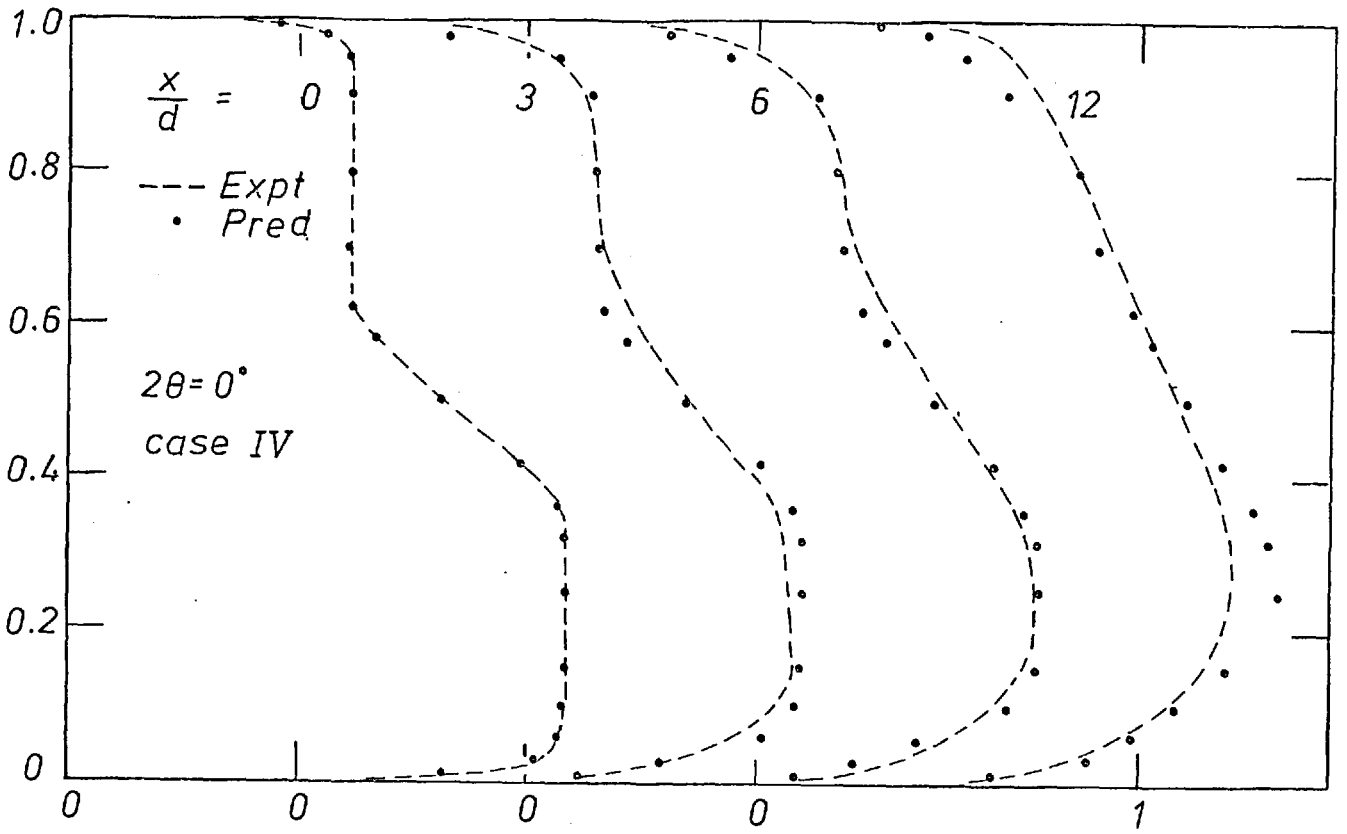
Fig.(8.3.25) Development of velocity (U/U_{in}) profiles across the vertical centreplane of a duct of r_{as} = 4 : 1; Case IV.
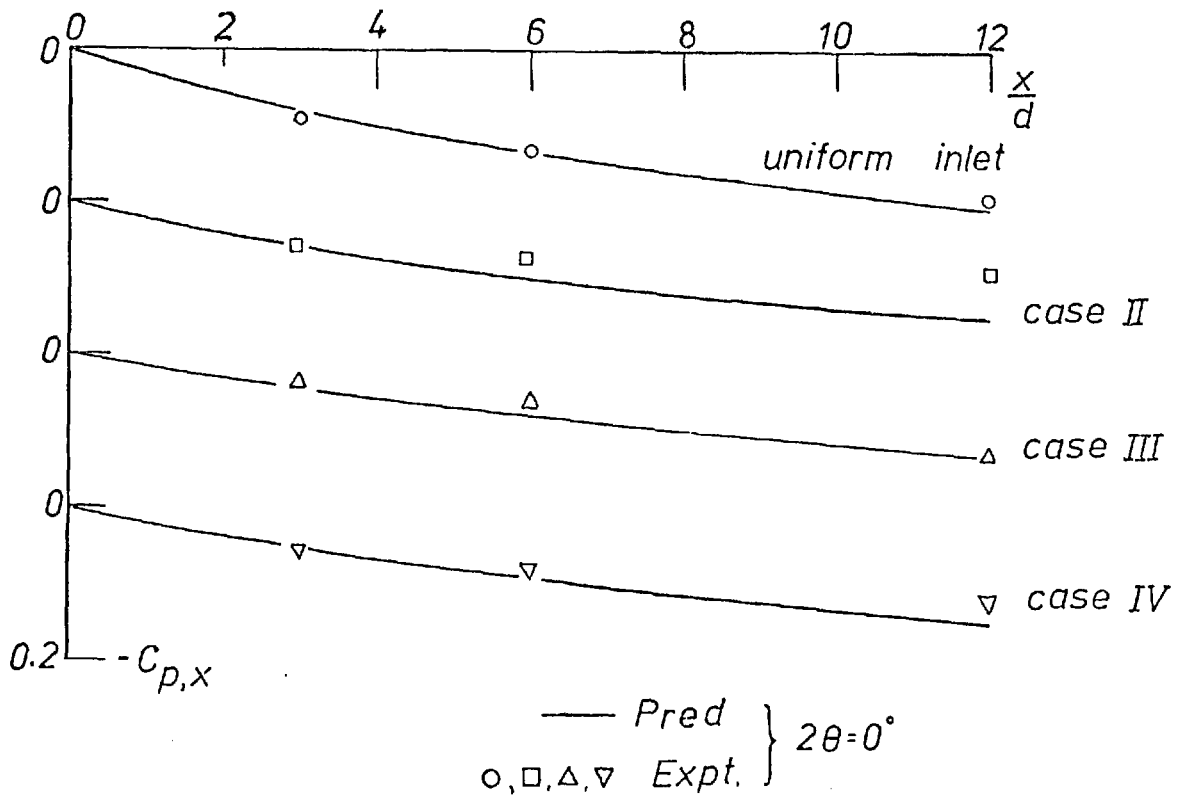
Fig.(8.3.26) Effect of inlet velocity distribution on pressure drop in a duct of r_{as} = 4 : 1.
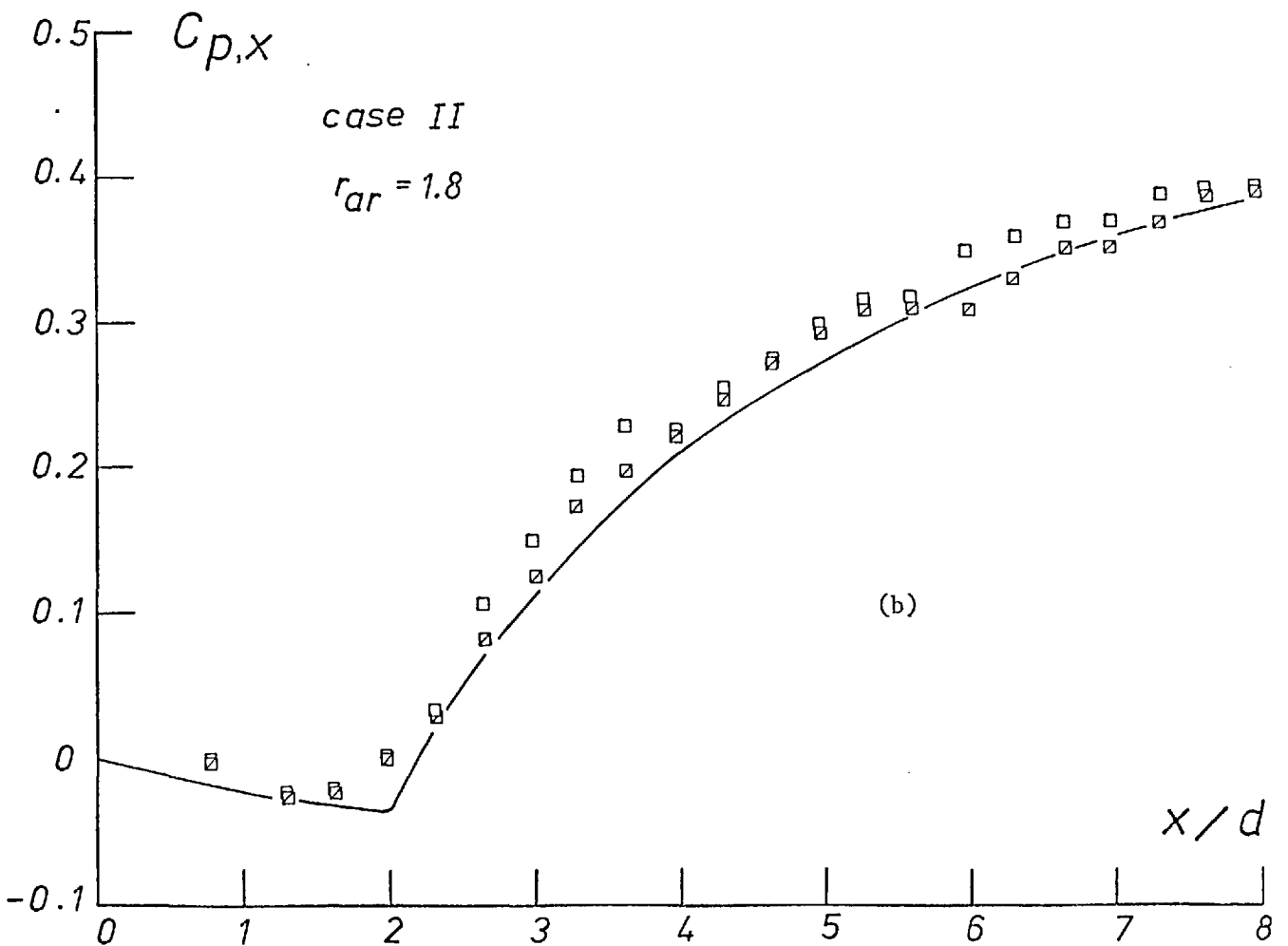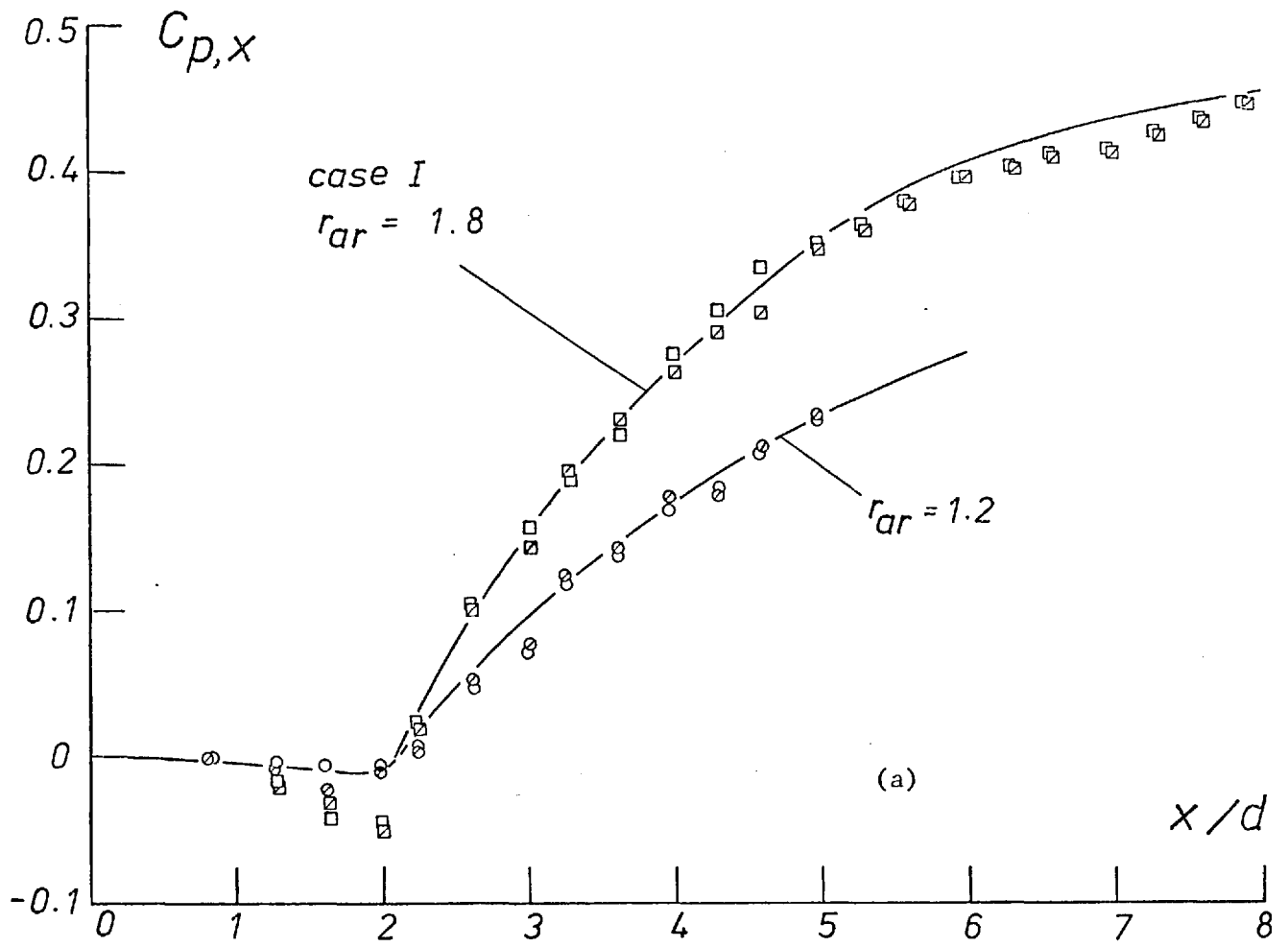
Fig.(8.3.27) Effect of inlet conditions on diffuser performance.
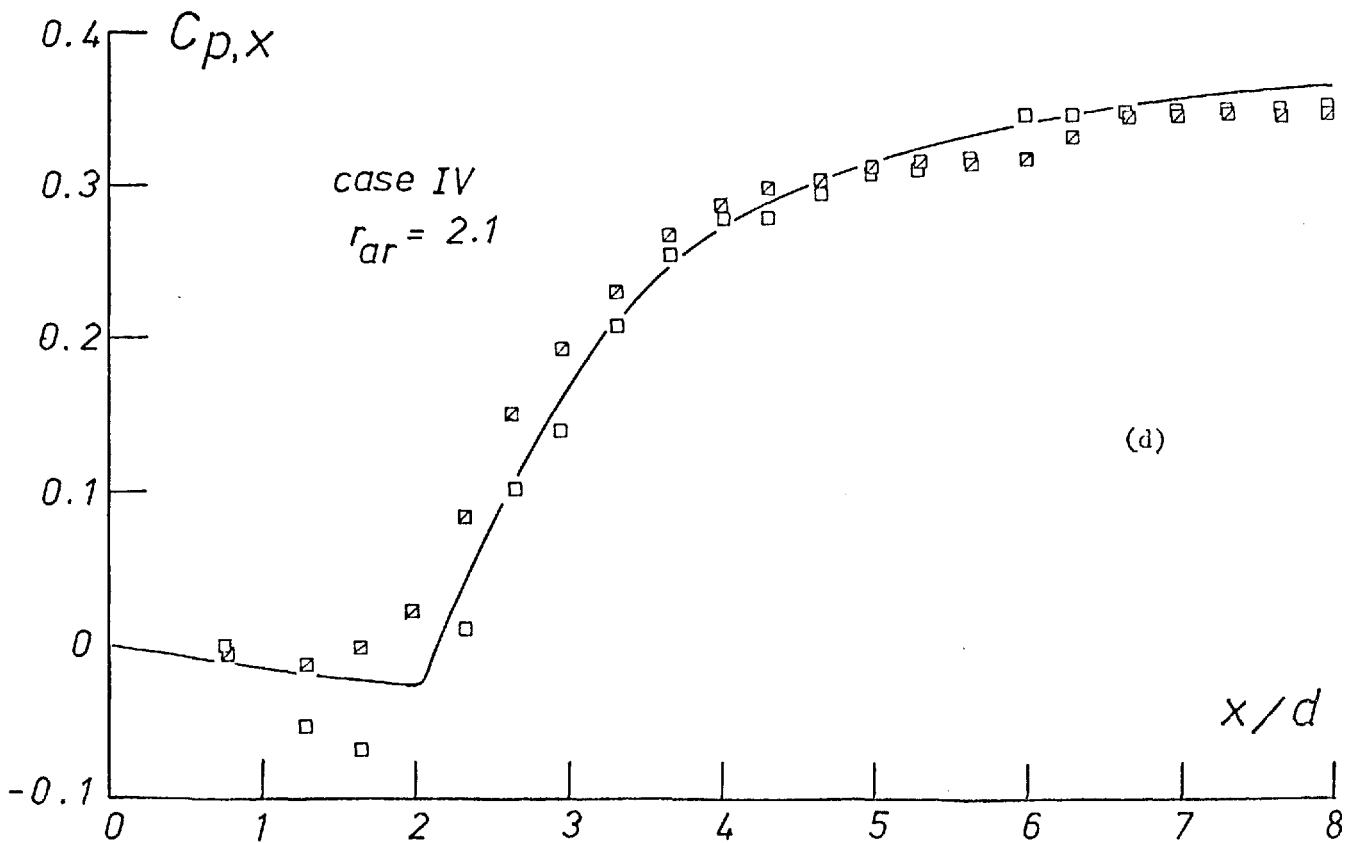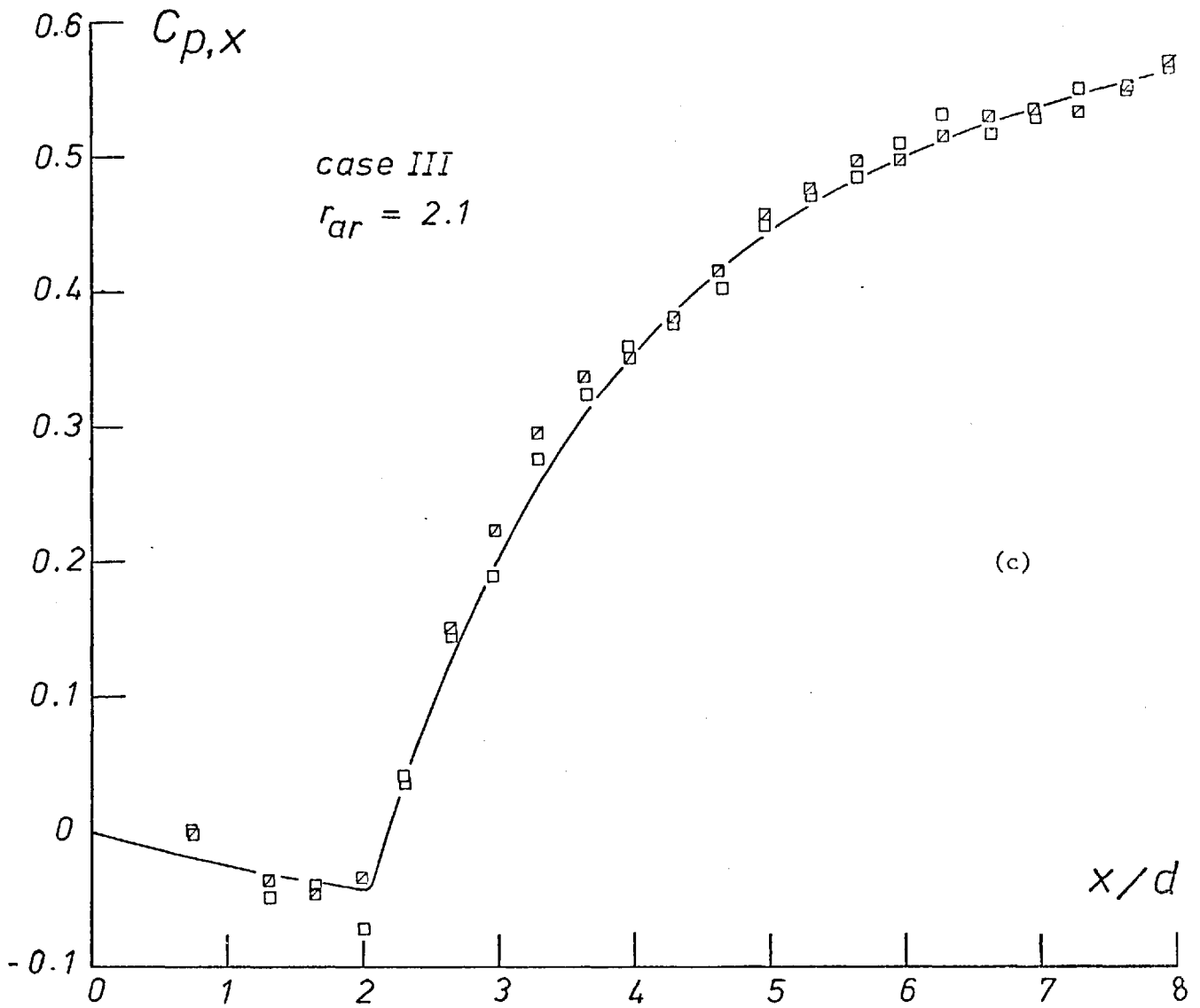
Fig.(8.3.27) Contd.
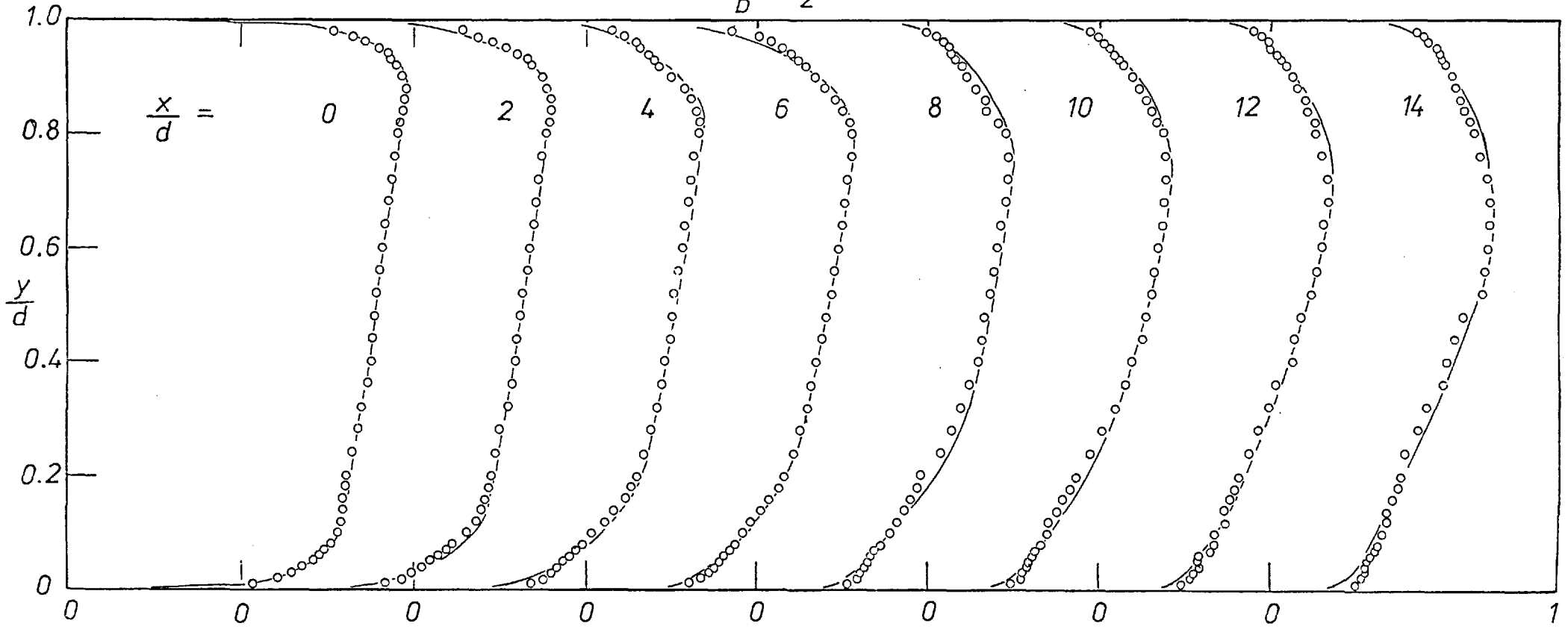
Fig.(8.3.28) (a) Development of velocity (U/U_{in}) profiles across the vertical centreplane of an 8 deg. diffuser. Non - uniform inlet conditions.

case D
o Expt.
— Pred.

$\frac{y}{d} = \frac{1}{2}$

$\frac{x}{d} =$ 0   2   4   6   8   10   12   14

$\frac{b}{d} =$ 2.078   2.358   2.638   2.918   3.198   3.48   3.78   4.04

$(\frac{z}{b})_{,x}$
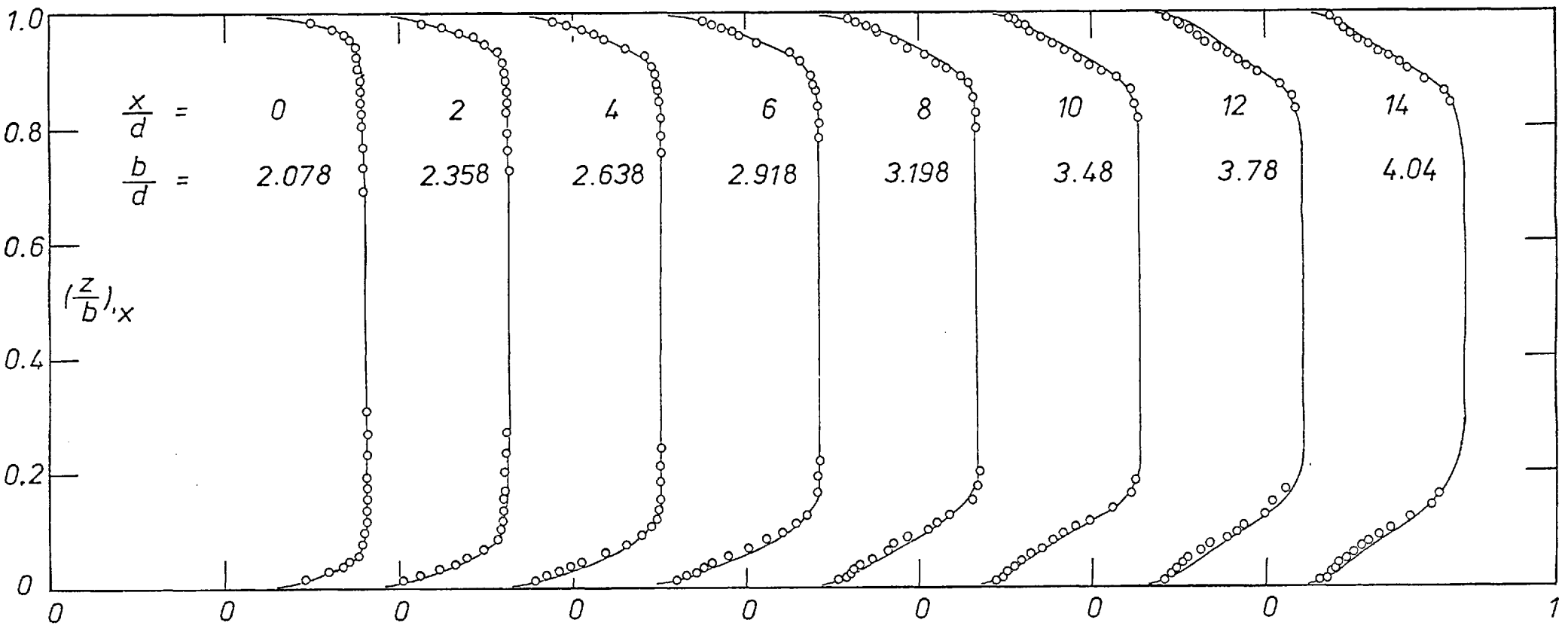
Fig.(8.3.28) (b) Development of velocity profiles across the horizontal centreplane of an 8 deg. diffuser.
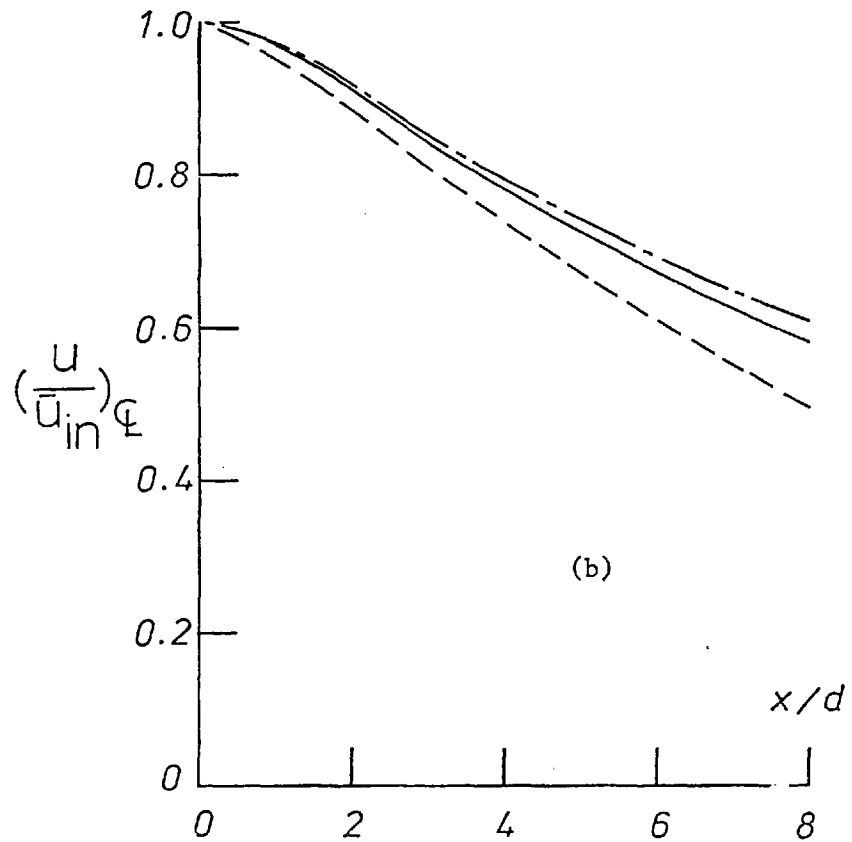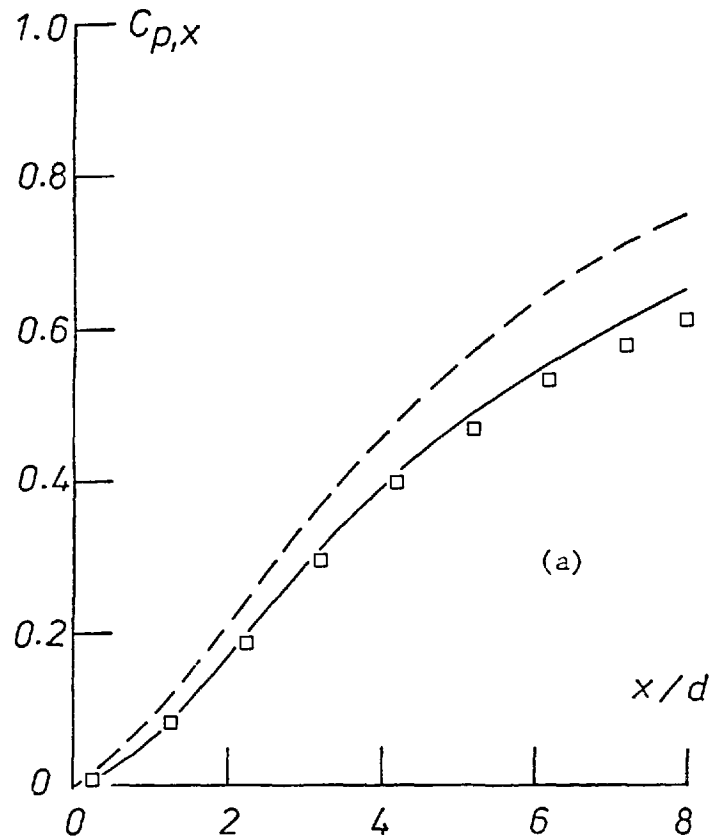
Fig.(8.3.29) Effect of wall shape on pressure rise and centreline velocity decay in a rectangular - sectioned diffuser.

decay rate than that predicted by the present procedure.

8.4   Heat transfer in diffusers

Unlike the hydrodynamic situation, heat transfer in diffusers has been sparingly reported. Ellison [17] obtained measurements of Stanton numbers in a large aspect ratio, small included angle diffuser over a limited range of Reynolds numbers. Only one wall was heated, at a specified rate. The measured distribution of wall temperatures for this situation is shown in Figure (8.4.1a). The thermal state of the other three walls was not reported. In view of this uncertainity, the following assumptions are made in order to obtain predictions of heat transfer:

a) The heated wall is smooth and non-conducting in
    the axial direction.

b) The other three walls are adiabatic.

c) The inlet temperature distribution is uniform
    and identical to that of ambient air.

With these assumptions, the predictions obtained with the present procedure are presented in Figures (8.4.1a) and (8.4.1b). In the former, the predicted temperature excess along the diffuser centreline, though small, is seen to be greater than that measured. It would be reasonable to presume that this is due to assumption b) above. In the latter predicted figure, Stanton numbers are in qualitative agreement with experimental data, for three Reynolds numbers. However, in view of the uncertainty about the experimental conditions, further conclusions cannot be drawn.

Similar results can be observed in Figure (8.4.2) where predictions of heat transfer in a large aspect ratio, 4° diffuser are presented. These results are compared with friction factor and Stanton number data obtained by Hool as reported by Carmichael and Pustintsev [12] whose analysis is also indicated in the figure. This analysis is based upon a two-dimensional momentum-integral method.
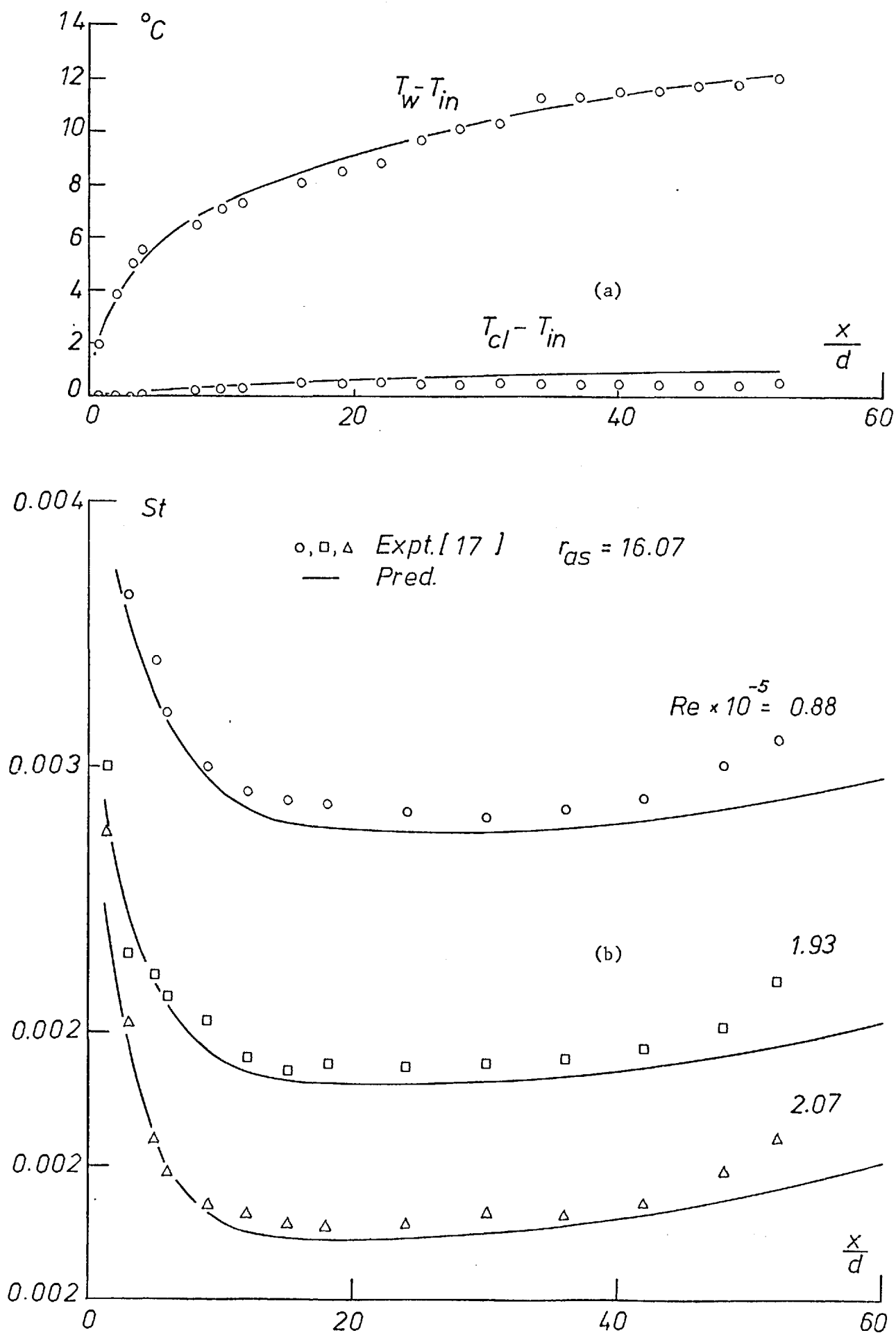
Fig.(8.4.1)   Heat transfer in a rectangular - sectioned diffuser
with one heated wall.
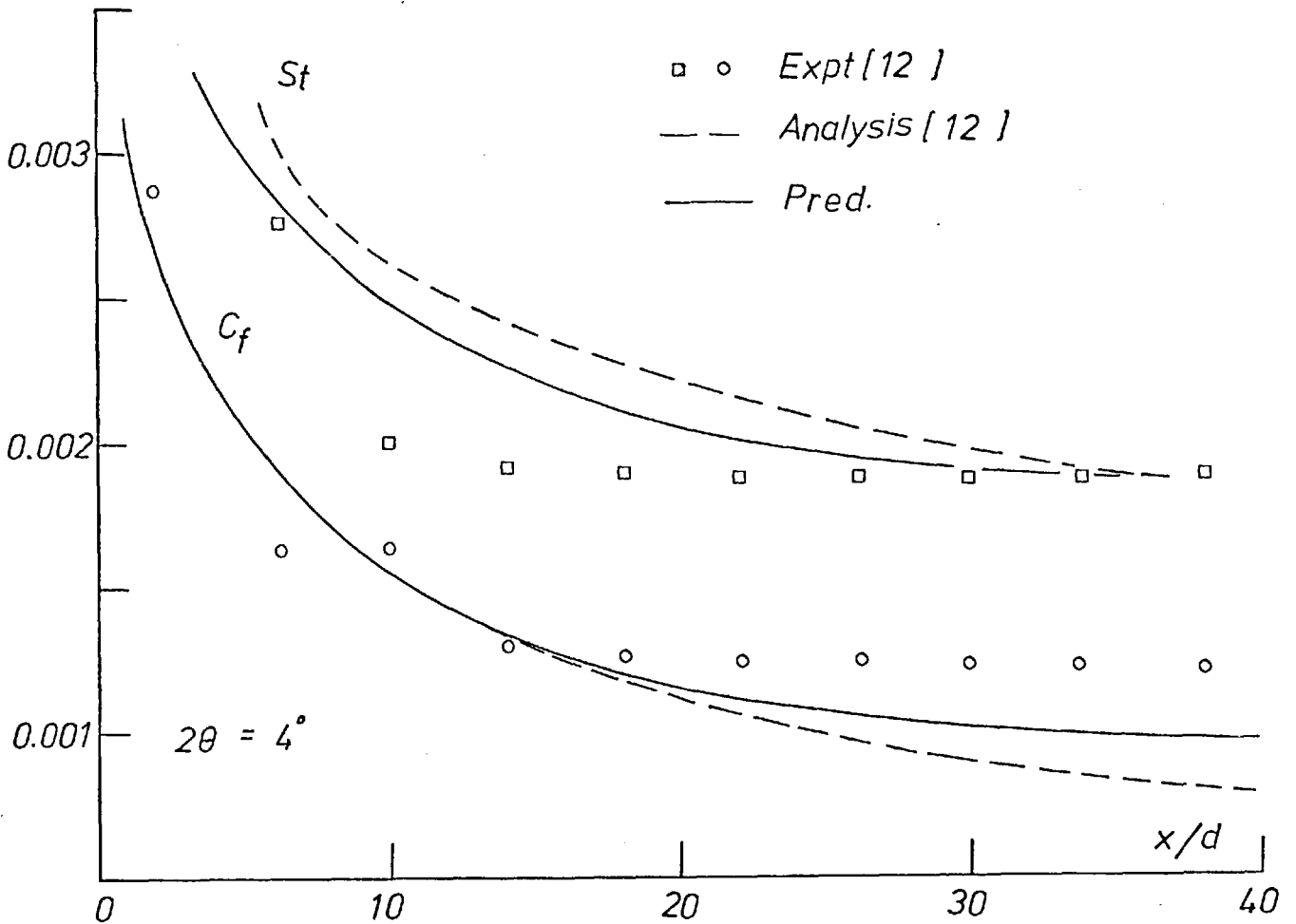
Fig.(8.4.2) Friction factor and heat transfer in a large aspect - ratio
diffuser.

8.5   Concluding remarks

In this chapter predictions of turbulent flow in rectangular-
sectioned ducts and diffusers have been reported. Detailed comparisons
with experimental evidence have been provided over a range of conditions.
The capability of the numerical prediction procedure in taking account
of the three-dimensional character of the flow field in rectangular-
sectioned diffusers has been validated. In these validation exercises,
experimentally-determined conditions at the inlet to diffusers have been
supplied, wherever possible, to the prediction procedure. For example,
when measurements of turbulence intensities were available (e.g. Figure
(8.5.1)), values of turbulence energies were derived from these and used
as initial conditions for the k-ε model of turbulence.

In the absence of such information, an estimation of the inlet
conditions, like the axial-velocity distribution in the corner regions
of diffusers, was made. This estimation was based upon the diffuser geo-
metry and the type of experimental rig used. When such estimations were
made, the resulting uncertainties in predictions did not permit detailed
conclusions to be drawn. The availability of detailed information on
inlet conditions permitted satisfactory predictions to be obtained. For
example, Figure (8.5.2) illustrates predicted pressure rise in diffusers
which are compared with Masuda's data [37] corresponding to conditions
in Figure (8.5.1).

The effects of several parameters upon diffuser performance
have been studied. The predictions have indicated a three-dimensional
flow field in large aspect ratio diffusers classified in the literature
as two-dimensional. The effects of distortions to the inlet velocity
distribution upon the flow pattern and pressure rise in diffusers have
been studied in detail. It is believed that the prediction procedure
will provide a clearer understanding of flow patterns in rectangular-
sectioned diffusers than hitherto possible.

For example, in Fig. (8.5.3) the performance of a diffuser of
aspect ratio 1 : 1 over a range of included angles, is presented. For
long, the data obtained by Vedernikoff [61] , represented in the figure
by squared points, remained unresolved. Two-dimensional diffuser-per-
formance charts failed to account for the rather low performance, re-
corded by Vedernikoff; an estimation based upon modifications to per-
formance chart values to account for three-dimensional effects, due to
Reneau et. al. [47] , failed likewise. Computational experiments
made with the present prediction procedure for the above-mentioned
situation, indicates that the reduced performance can indeed be attri-
buted to a rather thick inlet boundary-layer thickness on all four walls
of the diffuser. The prediction indicated on the figure corresponds to
a boundary layer thickness $2\delta^*/d$ of approximately 0.07. Further cor-
roboration of this explanation is provided by data obtained in the
present investigation with thin inlet boundary-layer thicknesses, and
the corresponding predictions, both of which are also indicated in
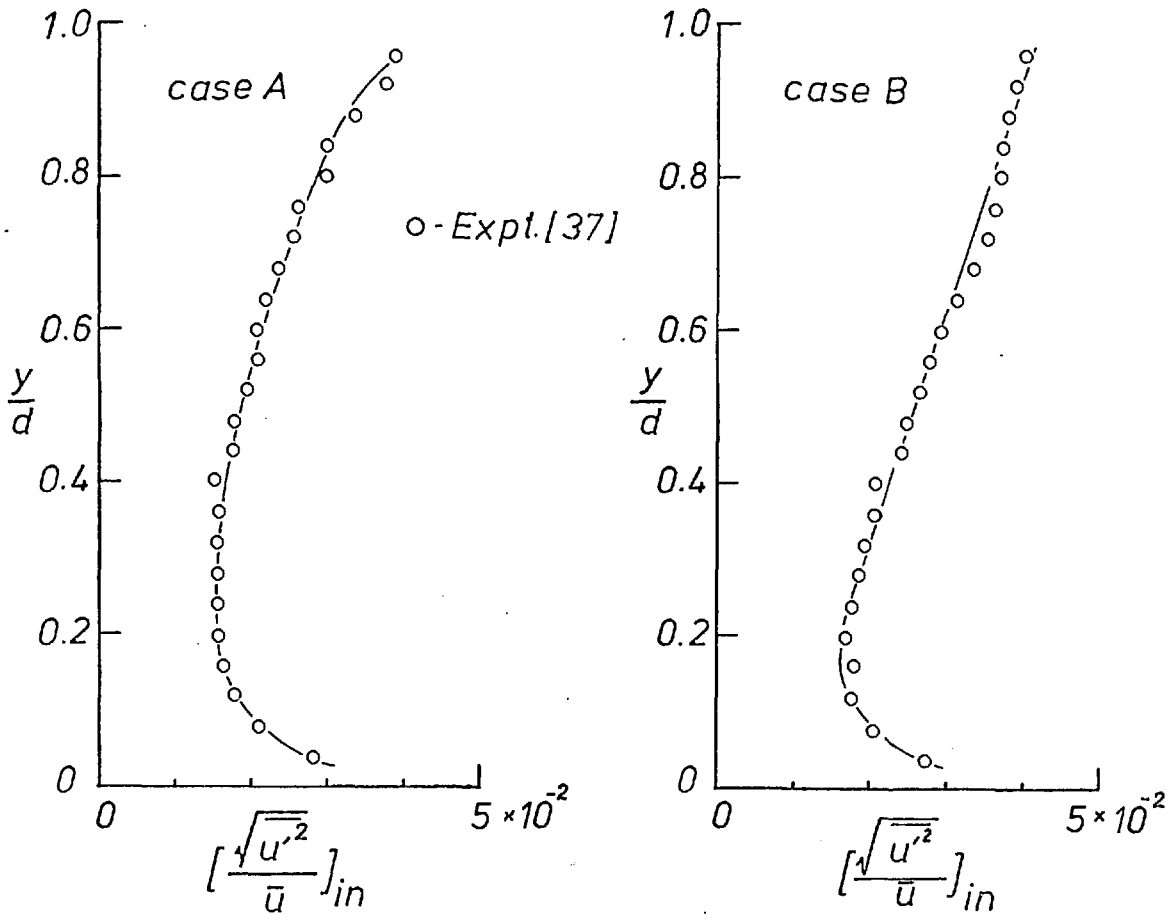
Fig.(8.5.1) Measured values of turbulence intensities at diffuser
inlet; Masuda [37] .
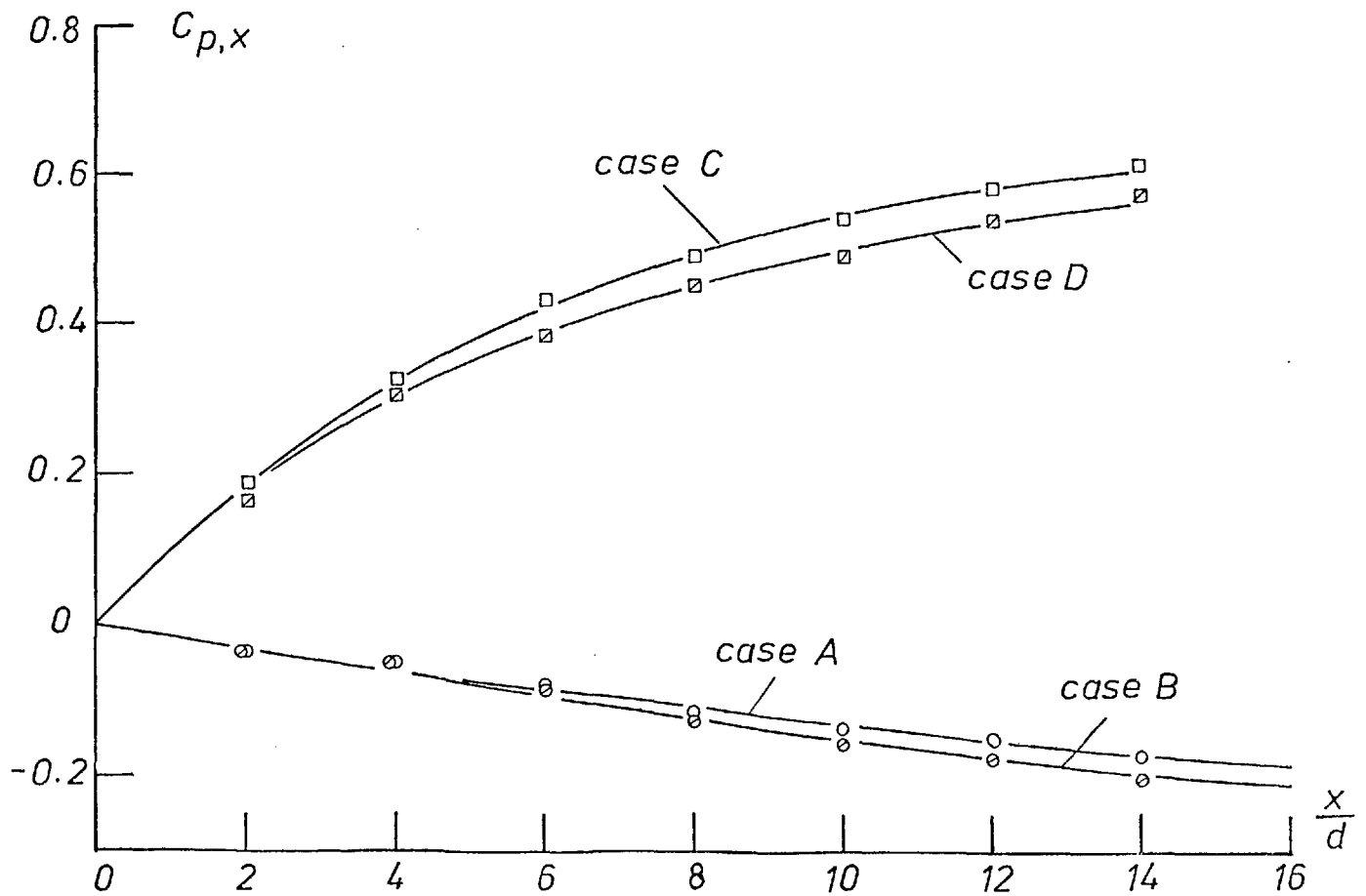
Fig.(8.5.2) Variation of static pressure in ducts and diffusers (r_{as} = 2 : 1)
under non - uniform inlet conditio-s

figure (8.5.3).
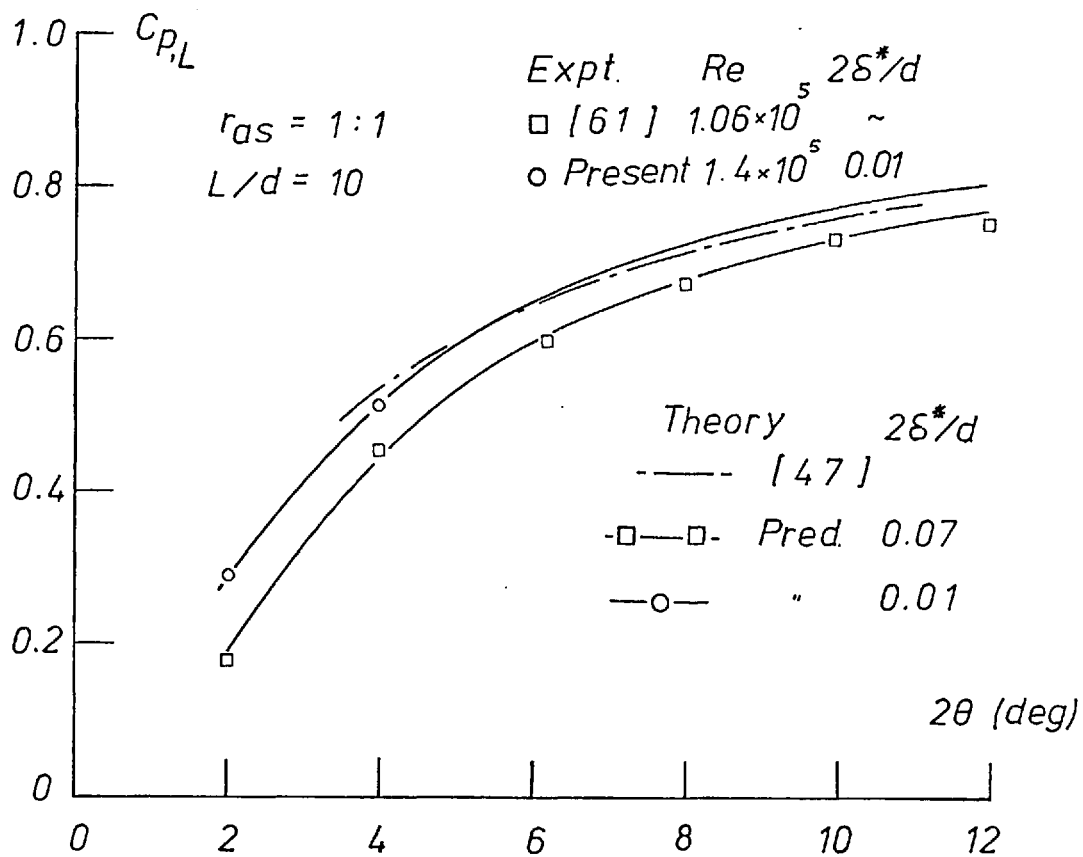
Fig.(8.5.3)   Effect of inlet conditions on the performance
of a diffuser of r_{as} = 1 : 1.

CHAPTER 9

CONCLUDING REMARKS

9.1 Review of work reported in this Thesis

1)   In Part I of this Thesis an outline was provided, of the physical and mathematical description of three-dimensional boundary layers confined within ducts. The physical description highlighted the characteristic features of such flow situations. The mathematical description utilized these features in arriving at the partial differential equations which govern the transport of mass, momentum and energy in such situations. The differential equations were represented in a system of curvilinear, quasi-orthogonal co-ordinates. Such a representation permitted the description of flows within ducts whose cross-sectional area varied with axial position. A procedure for the discretization of the differential equations and the solution of the resulting linearized algebraic equations, was then described. Two hypotheses for the mathematical modelling of turbulence in confined, three-dimensional, boundary-layer flows were presented.

2)   In Part II, the program of experimental investigations of flows in rectangular-sectioned diffusers was reported. This program included the design and fabrication of various elements of a rig, as well as measuring devices used in the investigations. The central element of the rig was a test-section, of inlet aspect ratio 1 : 1, capable of being adjusted to form diffusers of varying included angles upto a maximum of 12°. The measuring devices were of a simple nature and were used to record distributions of static pressure and axial velocity at several positions along diffusers of three different included angles. The results of these measurements were presented, along with assessments of the reliability and accuracy of data so obtained.

3)   Validation of the prediction procedure formed the subject of Part III of this Thesis. Calculations of both laminar and turbulent flows were reported. Detailed comparisons of the calculated results with a body of experimental and analytical evidence, over a wide range of

182

conditions were presented,

9.2   Attainment of objectives – an assessment

The results presented in Chapters 7 and 8 are used here to examine the extent to which the objectives of the research program, were attained.

1)   Predictions of two classes of laminar flows in straight, rectangular-sectioned ducts, were successfully obtained. The approximations made in arriving at the mathematical descriptions of such flows, were thus proved valid.

2)   The predictions of turbulent diffuser flows, presented in Chapter 8, indicate that the numerical procedure proved reasonably successful in handling confined flows in ducts of axially-varying area, i.e. diffusers.

3)   The results reported in Section 8.3.5 of Chapter 8, show that the simple model of turbulence, while proving adequate for diffuser flows with simple inlet conditions, proved insufficient for more complex situations. These situations were successfully predicted with the two-equation turbulence model.

4)   The experimental program was successfully completed. The data obtained from this program provided additional validation of the predictive procedure, as can be seen in Section 8.3.4, in several respects. These data, tabulated in Appendix A4, augment the existing experimental information on low-aspect ratio diffusers.

9.3   Limitations and capabilities of prediction procedure

The capabilities and limitations of the prediction procedure are summarised as follows:

1)   The prediction procedure comprising the calculation procedure described in Chapter 3, and the two-equation turbulence model described

in Chapter 4, is capable of predicting successfully, turbulent three-dimensional flows in straight, rectangular-sectioned ducts with cross-sectional areas varying along the axis in a prescribed manner.

2)   The limits within which the cross-sectional area is permitted to vary, are such as to ensure that the flows retain their boundary-layer character. This implies, for example, that the procedure in its present form is applicable only to the unstalled flow regime within diffusers.

3)   The two-equation turbulence model used in this work is restricted in its application to fully-turbulent flows wherein large variations in fluid property do not occur. Modifications to the model would be required, for example, to render it applicable to flows subjected to strong buoyancy forces.

9.4   Suggestions for future work

A review of the prediction procedure described in this Thesis, suggests the following areas of future work.

1)   In a number of engineering situations, small regions of recirculating flow occur in flows which are otherwise directed predominantly in one direction. In such regions, the boundary-layer approximations are rendered invalid, and the differential equations governing the flow are elliptic in nature. The ellipticity of these equations does not permit marching-integration procedures and the resulting economy in computer storage, to be used. Consequently iterative schemes, with the requisite increase in computer storage, have to be resorted to and become for the situations described above unnecessarily wasteful. A useful future task would thus be to extend the capability of three-dimensional, boundary-layer flow prediction procedures in handling small regions of flow recirculation.

2)   The numerical procedure described in this Thesis, needs to be tested in its ability to take account of the following:streamline curvature along the predominant flow direction, caused by curved geometries;

the presence of body forces; and, variations from the regular rectangular geometries treated in the present work.

3)   Furthermore, the effects of body forces upon the turbulence structure in three-dimensional, confined boundary layers, require suitable formulation.

4)   Modelling of the interfacial region between two immiscible fluids requires to be devised. Such modelling would then permit the prediction, for example, of river flows wherein heat and mass transfer occur across the free surface.

5)   Validation of the prediction procedure for situations other than those reported in this Thesis, needs to be speedily performed.

PART IV

Supplementary Information

REFERENCES

1. AHMED, S. (1971): "Turbulent flow in non-circular ducts".
    Ph.D. Thesis, University of Waterloo, Waterloo, Ontario,
    Canada.

2. AHMED S. and J. BRUNDRETT (1971): "Turbulent flow in non-
    circular ducts. Part I Mean flow properties in the devel-
    oping region of a square duct". Int. J. Heat & Mass Trans-
    fer 14, (3), pp. 365 - 375.

3. AMSDEN A.A. and F.H. HARLOW (1970): "The SMAC method: a
    numerical technique for calculating incompressible fluid
    flows". Los Alamos Sci. Lab. Rep. LA-4370, Los Alamos,
    California, USA.

4. BEAVERS, G.S., E.M. SPARROW and R.A. MAGNUSON (1970):
    "Experiments on hydrodynamically developing flow in rec-
    tangular ducts of arbitrary aspect ratio". Int. J. Heat&
    Mass Transfer 13, (6), pp. 689 - 703.

5. BRADLEY, C.I. and D.J. COCKRELL (1971): "The response of
    diffusers to conditions at their inlet". Paper 5, Section A,
    Symposium on internal flows, University of Salford, UK,
    April 1971.

6. BRADSHAW, P. and R.C. PANKHURST (1964): "The design of low-
    speed wind tunnels". Prog. Aero. Sci. 5, pp. 1 - 69.

7. BULEEV, N.I. (1962): "Theoretical model of the mechanism of
    turbulent exchange in fluid flows". Teploperedacha, USSR
    Academy of Sci., Moscow, pp. 64 - 69, Translation J.J. Cornish,
    UKAEA Res. Group, AERE, Harwell, UK.

8. BURGGRAF, O. (1966): "Analytical and numerical studies of
    steady separated flows". J. Fluid Mech. 24, pp. 113 - 151.

9. CARETTO, L.S., R.M. CURR and D.B. SPALDING (1972): "Two nu-
    merical methods for three-dimensional boundary layers".
    Comp. Methods App. Mech. and Eng. 1, pp. 39 - 57.

10. CARLSON, J.J. (1965): "The effect of wall shape on flow
    regimes and performance in straight two-dimensional diffusers".
    Eng. Thesis, Thermosciences Div., Mech. Eng. Dept., Stanford
    Univ., Stanford, California, USA.

11. CARLSON J.J., J.P. JOHNSTONE and C.J. SAGI (1967): "Effects
    of wall shape on flow regimes and performance in straight
    two-dimensional diffusers". J. Basic Eng. (ASME), 89, (1),
    pp. 151 - 160.

12. CARMICHAEL, A.D. and G.N. PUSTINTSEV   (1966):   "The prediction
     of turbulent boundary layer development in conical diffusers".
     J. Mech. Eng. Sci., $\underline{8}$, (4), pp. 426 - 436.

13. CHORIN, A.J.   (1967:   "A numerical method for solving incom-
     pressible viscous flow problems".   J. Comp. Phy. $\underline{2}$, pp. 12 - 26.

14. CHUI, G. and S.J. KLINE   (1967):   "Investigation of a two-dimen-
     sional, fully-stalled turbulent flow-fluid".   Rep. MD-19,
     Thermosciences Div., Mech. Eng. Dept., Stanford Univ., Stanford,
     California, USA.

15. COCANOVER, A.G., S.J. KLINE and J.P. JOHNSTONE   (1965):   "A
     unified method for predicting the performance of subsonic dif-
     fusers of several geometries".   Rep. PD-10, Thermosciences
     Div., Mech. Eng. Dept., Stanford Univ., Stanford, California,
     USA.

16. CURR, R.M., DEVRAJ SHARMA and D.B. TATCHELL   (1972):   "Numerical
     predictions of some three-dimensional boundary layers in ducts".
     Comp. Methods App. Mech. & Eng., $\underline{1}$, pp. 143 - 158.

17. ELLISON, G.M.   (1970):   "Flow and heat transfer in a straight
     sided diffuser".   MSc Thesis, Mech. Eng. Dept., University of
     Manchester, Institute of Technology, Manchester, U.K.

18. FAN, L.T. and C.L. HWANG   (1966):   "Bibliography of hydrodynamic
     entrance region flow".   S. Rep. 67, Kansas State University
     Bull, $\underline{50}$, (3), Manhatten, Kansas, USA.

19. FIEDLER R.A. and F.B. GESSNER   (1972):   "Influence of tangential
     fluid injection on the performance of two-dimensional diffusers".
     J. Basic. Eng. (ASME), $\underline{94D}$, (3), pp. 666 - 674.

20. FLEMING, D.P. and E.M. SPARROW   (1969):   "Flow in the hydro-
     dynamic entrance region of ducts of arbitrary cross-section".
     J. Heat Transfer (ASME) $\underline{91}$, Paper 69-HT-1.

21. FOX, R.W. and S.J. KLINE   (1960):   "Flow regime data and design
     methods for curved subsonic diffusers".   Rep. PD-6, Thermo-
     sciences Div., Mech. Eng. Dept., Stanford Univ., Stanford,
     California, USA.

22. FURUYA, F., T. FUJIMOTO, E. YAMAZATO, I. TSUZUKI and I. NISHIURA
     (1970):   "Performance of the two-dimensional diffuser with
     suction at entrance".   Bull. JSME $\underline{13}$, (56), pp. 264 - 271.

23. GOLDSTEIN, R.J. and D.K. KREID   (1967):   "Measurements of lami-
     nar flow development in a square duct using a Laser-Doppler
     flow meter".   J. App. Mech. (ASME) $\underline{34}$, (4), pp. 813 - 818.

24. GOSMAN, A.D., W.M. PUN, A.K. RUNCHAL, D.B. SPALDING and M. WOLFSHTEIN
     (1969):   Heat and Mass Transfer in recirculating flows.   Aca-
     demic Press, London & New York.

25. HAN, L.S. (1960): "Hydrodynamic entrance lengths for incompressible laminar flow in rectangular ducts". J. App. Mech. (ASME) 27, (3), pp. 403 - 409.

26. HARLOW, F.H. (1973), Editor: "Turbulence transport modelling". AIAA Selected reprint series, XIV.

27. HARLOW, F.H. and P.I. NAKAYAMA (1967): "Turbulence transport equations". Phy. Fluids, 10, (11), pp. 2323 - 2332.

28. HARLOW, F.H. and J. E. WELCH (1965): "Numerical calculation of time-dependent viscous incompressible flow of fluid with free surface". Phy. Fluids 8, (9), pp. 2182 - 2189.

29. HARTNETT, J.P., J.C.Y. KOH and S.T. McCONAS (1962): "A comparison of predicted and measured friction factors for turbulent flow through rectangular ducts". J. Heat Transfer (ASME), 84, (1), ppg. 82 - 88.

30. HINZE, J.O. (1959): Turbulence. McGraw-Hill Book Co. Ltd., New York.

31. HORLOCK, J.H. and R.I. LEWIS (1961): "Shear flows in straight-sided nozzles and diffusers". Int. J. Mech. Sci., 2, pp. 251 - 266.

32. JOHNSTONE, J.P. and C.A. POWARS (1967): "Effects of aspect ratio on the performance of straight-walled, two-dimensional diffusers". Rep. PD-13, Thermosciences Div., Mech. Eng. Dept. Stanford Univ., Stanford, California, USA.

33. LAUNDER, B.E. and D.B. SPALDING (1971): "Turbulence models and their application to the prediction of internal flows". Invited lecture, A Symposium on internal flows, Salford, U.K., April 1971.

34. LAUNDER, B.E. and D.B. SPALDING (1972): Mathematical models of turbulence. Pergamon Press, London & New York.

35. LIVESEY, J.L. and J.T. TURNER (1964): "The effect of velocity profile decay on shear-flow in diffusers". Int. J. Mech. Sci., 6, pp. 371 - 379.

36. LUNDGREN, T.S., E.M. SPARROW and J.B. STARR (1964): "Pressure drop due to the entrance region of ducts of arbitrary cross-section". J. Basic Eng. (ASME) 86, (3), pp. 620 - 626.

37. MASUDA, S. (1972): Private communication.

38. MASUDA, S., I. ARIGA and I. WATANABE (1971): "On the behaviour of uniform shear flow in diffusers and its effects on diffuser performance". J. Eng. Power (ASME), 93A, (3), pp. 377 - 385.

39.   McCOMAS, S.T.   (1967):   "Hydrodynamic entrance lengths for ducts
       of arbitrary cross-sections".   J. Basic Eng. (ASME) 89, (4),
       pp. 847 - 850.

40.   McMILLAN, O.J. and J.P. JOHNSTONE   (1970):   "Performance of low-
       aspect ratio diffusers with fully-developed turbulent inlet
       flows".   Rep. PD-14, Thermosciences Div., Mech. Eng. Dept.
       Stanford Univ., Stanford, California, U.S.A.

41.   MILLER, J.A.   (1971):   "Laminar incompressible flow in the en-
       trance region of ducts of arbitrary cross-section".   J. Eng.
       for Power (ASME), 93, (1), pp. 113 - 118.

42.   NORBURY, J.F.   (1959):   "Some measurements of boundary-layer
       growth in a two-dimensional diffuser".   J. Basic Eng. (ASME),
       81D, (3), pp. 285 - 296.

43.   PATANKAR, S.V.   (1971):   "On available calculation procedures
       for steady, three-dimensional boundary layers".   Rep. BL/TN/A/44,
       Heat Transfer Section, Dept. of Mech. Eng., Imperial College,
       London, U.K.

44.   PATANKAR, S.V. and D.B. SPALDING   (1970):   Heat and Mass Transfer
       in Boundary Layers.   International Textbook Co., Ltd., U.K.

45.   PATANKAR, S.V. and D.B. SPALDING   (1972):   "A calculation pro-
       cedure for heat, mass and momentum transfer in three-dimensional
       parabolic flows".   Int. J. Heat Mass Transfer 15, (10), pp.1787-
       1806.

46.   PRANDTL, L.   (1925):   "Ueber die ausgebildete Turbulenz".
       ZAMM, 15 , pp. 136.

47.   RENEAU, L.R., J.P. JOHNSTONE and S.J. KLINE   (1964):   "Diffuser
       design manual - Parts I and II".   Rep. PD-8, Thermosciences
       Div., Mech. Eng. Dept. Stanford Univ., Stanford, California,
       U. S. A.

48.   ROCKWELL, D.O.   (1972):   "Flow-fields in a two-dimensional dif-
       fuser with extraction of fluid on the diverging walls".
       J. Eng. Power (ASME), 94A, (3), pp. 226 - 232.

49.   RODI, W.   (1972):   "The prediction of free turbulent boundary
       layers by use of a two-equation model of turbulence".
       PhD Thesis, Univ. London.

50.   ROSENHEAD, L.   (1963), Editor: Laminar Boundary Layers
       Oxford University Press, pp. 409 - 488.

51.   SAGI, S.J. and J.P. JOHNSTONE   (1967):   "The design and per-
       formance of two-dimensional curved diffusers - Parts I and II".
       J. Basic Eng. (ASME), 89D, (4), pp. 715 - 731.

52. SAGI, C.J., J.P. JOHNSTONE and S.J. KLINE (1965): "The design and performance of two-dimensional, curved, subsonic diffusers. - Diffuser Design Manual Part II". Rep. PD-8, Thermosciences Div.,Mech. Eng. Dept.,Stanford Univ., Stanford, California, U.S.A.

53. SAKURAI, T. (1972): "Study on the flow in diffusers for centrifugal turbomachinery - Rep. 3 : Effects of circumferential non-uniformity of inlet flow". Bull JSME, 15, (85), pp. 848-857.

54. SHAH, R.K. (1971): "Laminar flow forced convection Heat Transfer and flow friction in straight, and curved ducts - a summary of analytical solutions". PhD Thesis, Dept. of Mech. Eng. Stanford Univ., Stanford, California, U.S.A.

55. SHARMA, D. and D.B. SPALDING (1971): "Laminar flow heat transfer in rectangular-sectioned ducts with one moving wall". First National Conference on Heat & Mass Transfer, Madras, India.

56. SMITH, C.R. and S.J. KLINE (1971): "An experimental investigation of the transitory stall regime in two-dimensional diffusers including the effects of periodically disturbed inlet conditions". Rep. PD-15, Thermosciences Div., Mech. Eng. Dept., Stanford Univ., Stanford, California, U.S.A.

57. SOVRAN, G. and E.D. KLOMP (1967): "Experimentally-determined optimum geometries for rectilinear diffusers with rectangular, conical or annular cross-section". From 'Fluid mechanics of internal flow' - Ed. G. Sovran, Elsevier Publishing Co., Amsterdam.

58. SPALDING D.B. (1972): "A novel finite-difference formulation for differential expressions involving both first and second derivatives". Int. J. Num. Methods in Eng., 4, pp. 551 - 559.

59. SPARROW, E.M., C.W. HIXON and G. SHAVIT (1967): "Experiments on laminar flow development in rectangular ducts". J. Basic Eng. (ASME) 89, (1), pp. 116 - 124.

60. TATCHELL, D.G. (1974): "Convective processes in confined three-dimensional boundary layers". PhD Thesis, London University, to be published.

61. VEDERNIKOFF, A.N. (1944): "An expermimental investigation of the flow of air in a flat broadening channel". NACA T.M. 1059.

62. WAITMAN, B.A., L.R. RENEAU and S.J. KLINE (1960): "Effects of inlet conditions on performance of two-dimensional diffusers". J. Basic Eng. (ASME) 81D, (3), pp. 285 - 295.

63. WHEELER, A.J., J.P. JOHNSTONE (1971): "Three-dimensional turbulent boundary layers - an assessment of prediction methods". Rep. MD-30, Thermosciences Div., Mech. Eng. Dept., Stanford Univ., Stanford, California, U. S. A.

64.   WIGINTON, C.L. and C. DALTON   (1970):   "Incompressible laminar
           flow in the entrance region of a rectangular duct".   J. App.
           Mech. (ASME), 37, (3), pp. 854-856.

65.   WOLF, S. and J.P. JOHNSTONE   (1966):   "Effects of non-uniform
           inlet velocity profiles on flow regimes and performance in
           two-dimensional diffusers".   Rep. PD-12, Thermosciences Div.,
           Mech. Eng. Dept., Stanford Univ., Stanford, California, U.S.A.

66.   YU, H.S. and E.M. SPARROW   (1970):   "Flow development in a
           channel having a longitudinally-moving wall".   J. App. Mech.
           (ASME), Paper No. 70-W.A/APM-11.

67.   SCHLICHTING, H.   (1960):   Boundary layer theory.   McGraw-Hill
           Cook Co. Inc., New York

NOMENCLATURE

Symbol	Meaning	Location of first occurance
A	area	Eq. (7.4.1)
A_i	coefficient of reduced discretized eq.	Eq. (3.3.6)
A_i'	coefficient of discretized eq.	Eq. (3.2.4)
A,B	turbulence model identification	Fig. (8.3.9)
b	width of duct/diffuser	Fig. (7.2.5)(a)
c	friction-factor constant	Table (7.2.1)
c_D	constant in Prandtl/Kolmogorov formula	Eq. (4.4.1)
C_f	friction factor $\left(\equiv -\left[\frac{dp}{dx}\right]\frac{d}{\rho \bar{U}_{in}^2} ; \ \tau_w/\frac{1}{2}\rho \bar{U}_{in}^2\right)$	Fig. (7.2.2)
C_j^i	convective terms in discretized eq.	Eq. (3.2.1)
C_p	specific heat	Eq. (7.4.1)
$C_{p,x}$	pressure-rise coefficient $\left(\equiv (\bar{p}-\bar{p}_{in})/\frac{1}{2}\rho \bar{U}_{in}^2\right)$	Fig. (3.5.1)
C_μ	turbulence length-scale constant	Eq. (4.3.3)
C_1, C_2	turbulence model constants	Eq. (4.4.4)
d	characteristic width of duct/diffuser	Fig. (3.5.1)
d_e	equivalent diameter of duct/diffuser	Fig. (7.2.2)
D	domain of integration	Eq. (4.3.3)
D	downstream calculation plane	Fig. (3.2.2)
D^U, D^V, D^W	coefficient of pressure gradient terms	Eq. (3.3.2)
D_j^i	diffusion terms in discretized equations	Eq. (3.2.1)
e	Location in grid	Fig. (3.2.6)
E	grid location East of point P	Eq. (2.2.8)
E	constant in semi-logarithmic law-of-the-wall	Eq. (4.6.1)
G	generation of turbulence energy	Eq. (4.4.4)
G_j^i	mass velocity	Eq. (3.2.2)
$-J_{\emptyset,i}$	flux of $\emptyset$ in i^{th} direction	Eq. (2.2.3)
k	turbulence energy	Eq. (4.3.1)
ℓ	turbulence length scale	Eq. (4.3.2)
L	length of duct/diffuser	Fig. (8.3.17)
$\dot{m}_P$	mass source at P	Eq. (3.3.10)
$\dot{m}^*$	mass flow based on 'starred' velocity-field	Eq. (3.3.15)

n	location on grid	Fig. (3.2.6)
N	grid location <u>N</u>orth of point P	Fig. (2.2.1)
$p, \bar{p}$	static pressure	Eq. (2.2.4)
P	location on grid	Fig. (3.2.1)
$P_\emptyset$	function on semi-logarithmic law	Eq. (4.6.4)
$Pr_\emptyset$	laminar Prandtl/Schmidt number for diffusion of $\emptyset$	Eq. (2.2.6)
$Pr_{t,\emptyset}$	turbulent Prandtl/Schmidt number for diffusion of $\emptyset$	Eq. (4.5.2)
r_{as}, r_{ar}	ratio aspect and area ratios	Fig. (8.2.1)
r, R	radii of curvature	Eq. (4.3.1)
Re	Reynolds number	Fig. (3.5.1)
s	location on grid	Fig. (3.2.6)
S	grid location <u>S</u>outh of P	Fig. (2.2.1)
$s^\emptyset$	source/sink term for $\emptyset$	Eq. (2.2.3)
$S^\emptyset$	integrated form of source/sink term	Eq. (3.2.1)
St	Stanton number	Fig. (8.4.1)
T	temperature	Table (4.5.1)
T_a	ambient temperature	Section (A4.1)
T_b	bulk temperature	Eq. (7.4.1)
u_i	fluctuating component of velocity along i^{th} direction	Fig. (3.2.2)
U	denoting upstream station	Eq. (4.2.2)
U	ξ-direction velocity component	Eq. (2.2.11)
U_i	velocity component along i^{th} direction	Eq. (2.2.1)
V	η-direction velocity component	Eq. (2.2.11)
υ	volume	Eq. (A3.1.1)
w	location on grid	Fig. (3.2.6)
W	grid location <u>W</u>est of point P	Fig. (2.2.1)
W	ζ-direction velocity component	Eq. (2.2.11)
x, y, z	Cartesian co-ordinates	Eq. (2.2.1), (2.2.8)

194

Greek Symbols

α	slopes of diffuser walls	Eq. (4.3.5)
δ	characteristic distance	Eq. (4.6.1)
δ, Δ	difference of	Fig. (3.2.6)
δ^*	boundary-layer momentum thickness	Fig. (8.3.17)
$\delta_{i,j}$	Kronecker-delta $(= 1 \text{ for } i=j; = 0 \text{ for } i \neq j)$	Eq. (2.2.4)
ε	dissipation rate of turbulence	Eq. (4.4.1)
Γ_ϕ	diffusion coefficient for ϕ	Eq. (2.2.5)
ξ, η, ζ	quasi-orthogonal co-ordinates	Eq. (2.2.8)
θ	half diffuser included angle	Fig. (5.3.4)
λ	velocity gradient in shear flow	Eq. (8.2.1)
κ	semilog-law constant	Eq. (4.6.1)
μ	laminar viscosity	Eq. (2.2.4)
μ_t	turbulent viscosity	Eq. (4.3.1)
μ_{eff}	effective viscosity	Eq. (4.5.1)
ρ	fluid density	Eq. (2.2.1)
σ_{ij}	stress tensor	Eq. (2.2.2)
τ_w	wall shear stress	Eq. (4.6.2)
ϕ	general dependent variable	Eq. (2.2.2)
$\dot{\phi}_w''$	wall-flux of ϕ	Eq. (4.6.4)
Ω	angular direction	Eq. (4.3.3)

Subscripts

$\mathcal{C}$	centreline	Fig. (3.5.2)
e	location - e	Eq. (3.2.1)
i,j	location i,j	Eq. (2.2.1)
in	inlet	Eq. (3.5.2)
o	outlet	Fig. (7.3.6)
max	maximum value	Fig. (8.2.1)
τ	shear	Eq. (4.6.1)
w	wall	Eq. (4.6.1)
ϕ	variable	Eq. (2.2.3)

Superscripts

ϕ	variable - ϕ	Eq. (3.2.1)
i	direction - i	Eq. (3.2.1)
$*$	"starred" values	Eq. (3.3.8)
$'$	"primed" values	Eq. (3.3.11)
o	outlet	Fig. (8.2.1)
$\left.\begin{array}{c} E, W, \\ N, S \end{array}\right\}$	relating to boundaries	Fig. (2.2.1)

APPENDIX A1

DIFFERENTIAL EQUATIONS GOVERNING THREE-DIMENSIONAL BOUNDARY LAYERS

A1.0 Introduction

In this Appendix the partial differential equations governing three-dimensional boundary-layers flows are listed. The equations are expressed with reference to the quasi-orthogonal co-ordinate system described in Chapter 2. The diffusion coefficient as well as the sources and sinks of each dependent variable of the above equations are then tabulated.

A1.1 Differential equations

Continuity

$$\frac{\partial(\rho U)}{\partial \xi} + \frac{\partial}{\partial \eta}\left\{\rho V - \rho U\left[\frac{dy_s}{dx} + \eta \frac{d(y_N - y_s)}{dx}\right]\right\}\frac{1}{(y_N - y_s)}$$

$$+ \frac{\partial}{\partial \zeta}\left\{\rho W - \rho U\left[\frac{dz_W}{dx} + \zeta \frac{d(z_E - z_W)}{dx}\right]\right\}\frac{1}{(z_E - z_W)}$$

$$= 0 \qquad . \ (A1.1.1)$$

ξ - direction momentum

$$\frac{\partial(\rho U U)}{\partial \xi} + \frac{1}{(y_N - y_s)}\cdot\frac{\partial}{\partial \eta}\left[\left\{\rho V - \rho U\left[\frac{dy_s}{dx} + \eta \frac{d(y_N - y_s)}{dx}\right]\right\}U\right]$$

$$+ \frac{1}{(z_E - z_W)}\cdot\frac{\partial}{\partial \zeta}\left[\left\{\rho W - \rho U\left[\frac{dz_W}{dx} + \zeta \frac{d(z_E - z_W)}{dx}\right]\right\}U\right]$$

$$= \mathcal{S}^U + \frac{1}{(y_N - y_s)^2}\frac{\partial}{\partial \eta}\left[\Gamma_U \frac{\partial U}{\partial \eta}\right] + \frac{1}{(z_E - z_W)^2}\frac{\partial}{\partial \zeta}\left[\Gamma_U \frac{\partial U}{\partial \zeta}\right]$$

$$\cdot \ (A1.1.2)$$

η -direction momentum

$$\frac{\partial(\rho UV)}{\partial \xi} + \frac{1}{(y_N - y_S)} \frac{\partial}{\partial \eta}\left[\left\{\rho V - \rho U\left[\frac{dy_S}{dx} + \eta \frac{d(y_N - y_S)}{dx}\right]\right\}V\right]$$

$$+ \frac{1}{(z_E - z_W)} \frac{\partial}{\partial \zeta}\left[\left\{\rho W - \rho U\left[\frac{dz_W}{dx} + \zeta \frac{d(z_E - z_W)}{dx}\right]\right\}V\right] = \mathcal{S}^V$$

$$+ \frac{1}{(y_N - y_S)^2} \frac{\partial}{\partial \eta}\left[\Gamma_V \frac{\partial V}{\partial \eta}\right] + \frac{1}{(z_E - z_W)^2} \frac{\partial}{\partial \zeta}\left[\Gamma_V \frac{\partial V}{\partial \zeta}\right]$$

. (A1.1.3)

ζ -direction momentum

$$\frac{\partial(\rho UW)}{\partial \xi} + \frac{1}{(y_N - y_S)} \frac{\partial}{\partial \eta}\left[\left\{\rho V - \rho U\left[\frac{dy_S}{dx} + \eta \frac{d(y_N - y_S)}{dx}\right]\right\}W\right]$$

$$+ \frac{1}{(z_E - z_W)} \frac{\partial}{\partial \zeta}\left[\left\{\rho W - \rho U\left[\frac{dz_W}{dx} + \zeta \frac{d(z_E - z_W)}{dx}\right]\right\}W\right] = \mathcal{S}^W$$

$$+ \frac{1}{(y_N - y_S)^2} \frac{\partial}{\partial \eta}\left[\Gamma_W \frac{\partial W}{\partial \eta}\right] + \frac{1}{(z_E - z_W)^2} \frac{\partial}{\partial \zeta}\left[\Gamma_W \frac{\partial W}{\partial \zeta}\right]$$

. (A1.1.4)

Turbulence energy

$$\frac{\partial(\rho Uk)}{\partial \xi} + \frac{1}{(y_N - y_S)} \frac{\partial}{\partial \eta}\left[\left\{\rho V - \rho U\left[\frac{dy_S}{dx} + \eta \frac{d(y_N - y_S)}{dx}\right]\right\}k\right]$$

$$+ \frac{1}{(z_E - z_W)} \frac{\partial}{\partial \zeta}\left[\left\{\rho W - \rho U\left[\frac{dz_W}{dx} + \zeta \frac{d(z_E - z_W)}{dx}\right]\right\}k\right] = \mathcal{S}^k$$

$$+ \frac{1}{(y_N - y_S)^2} \frac{\partial}{\partial \eta}\left[\Gamma_k \frac{\partial k}{\partial \eta}\right] + \frac{1}{(z_E - z_W)^2} \frac{\partial}{\partial \zeta}\left[\Gamma_k \frac{\partial k}{\partial \zeta}\right]$$

. (A1.1.5)

Energy dissipation rate

$$\frac{\partial(\rho U \varepsilon)}{\partial \xi} + \frac{1}{(y_N - y_S)} \frac{\partial}{\partial \eta}\left[\left\{\rho V - \rho U\left[\frac{dy_S}{dx} + \eta\frac{d(y_N - y_S)}{dx}\right]\right\}\varepsilon\right]$$

$$+ \frac{1}{(z_E - z_W)} \frac{\partial}{\partial \zeta}\left[\left\{\rho W - \rho U\left[\frac{dz_W}{dx} + \zeta\frac{d(z_E - z_W)}{dx}\right]\right\}\varepsilon\right] = b^\varepsilon$$

$$+ \frac{1}{(y_N - y_S)^2} \frac{\partial}{\partial \eta}\left[\Gamma_\varepsilon \frac{\partial \varepsilon}{\partial \eta}\right] + \frac{1}{(z_E - z_W)^2} \frac{\partial}{\partial \zeta}\left[\Gamma_\varepsilon \frac{\partial \varepsilon}{\partial \zeta}\right]$$

$$. \quad (A1.1.6)$$

Energy

$$\frac{\partial(\rho U c_p T)}{\partial \xi} + \frac{1}{(y_N - y_S)} \frac{\partial}{\partial \eta}\left[\left\{\rho V - \rho U\left[\frac{dy_S}{dx} + \eta\frac{d(y_N - y_S)}{dx}\right]\right\}c_p T\right]$$

$$+ \frac{1}{(z_E - z_W)} \frac{\partial}{\partial \zeta}\left[\left\{\rho W - \rho U\left[\frac{dz_W}{dx} + \zeta\frac{d(z_E - z_W)}{dx}\right]\right\}c_p T\right] = b^T$$

$$+ \frac{1}{(y_N - y_S)^2} \frac{\partial}{\partial \eta}\left[\Gamma_T \frac{\partial T}{\partial \eta}\right] + \frac{1}{(z_E - z_W)^2} \frac{\partial}{\partial \zeta}\left[\Gamma_T \frac{\partial T}{\partial \zeta}\right]$$

$$. \quad (A1.1.7)$$

A1.2 Γ_ϕ and $\mathcal{S}^\phi$ for each dependent variable

No	ϕ	Γ_ϕ	$\mathcal{S}^\phi$
1	U	μ_{eff}	-
2	V	μ_{eff}	$\dfrac{1}{(y_N-y_S)^2}\dfrac{\partial}{\partial\eta}\left\{\mu_{eff}\dfrac{\partial V}{\partial\eta}\right\}$ $+\dfrac{1}{(y_N-y_S)(z_E-z_W)}\dfrac{\partial}{\partial\zeta}\left\{\mu_{eff}\dfrac{\partial W}{\partial\eta}\right\}$
3	W	μ_{eff}	$\dfrac{1}{(y_N-y_S)(z_E-z_W)}\dfrac{\partial}{\partial\eta}\left\{\mu_{eff}\dfrac{\partial V}{\partial\zeta}\right\}$ $+\dfrac{1}{(z_E-z_W)^2}\dfrac{\partial}{\partial\zeta}\left\{\mu_{eff}\dfrac{\partial W}{\partial\zeta}\right\}$
4	k	$\dfrac{\mu_{eff}}{Pr_{t,k}}$	$\mu_t\left[2\left\{\dfrac{1}{(y_N-y_S)^2}\left(\dfrac{\partial V}{\partial\eta}\right)^2+\dfrac{1}{(z_E-z_W)^2}\left(\dfrac{\partial W}{\partial\zeta}\right)^2\right\}+\right.$ $\dfrac{1}{(y_N-y_S)^2}\left(\dfrac{\partial U}{\partial\eta}\right)^2+\dfrac{1}{(z_E-z_W)^2}\left(\dfrac{\partial U}{\partial\zeta}\right)^2+$ $\left.\left\{\dfrac{1}{(y_N-y_S)}\left(\dfrac{\partial W}{\partial\eta}\right)+\dfrac{1}{(z_E-z_W)}\left(\dfrac{\partial V}{\partial\zeta}\right)\right\}^2\right]-\rho\varepsilon$
5	ε	$\dfrac{\mu_{eff}}{Pr_{t,\varepsilon}}$	$C_1\dfrac{\varepsilon}{k}\cdot\mu_t\left[2\left\{\dfrac{1}{(y_N-y_S)^2}\left(\dfrac{\partial V}{\partial\eta}\right)^2+\dfrac{1}{(z_E-z_W)^2}\left(\dfrac{\partial W}{\partial\zeta}\right)^2\right\}+\right.$ $\dfrac{1}{(y_N-y_S)^2}\left(\dfrac{\partial U}{\partial\eta}\right)^2+\dfrac{1}{(z_E-z_W)^2}\left(\dfrac{\partial U}{\partial\zeta}\right)^2+$ $\left.\left\{\dfrac{1}{(y_N-y_S)}\left(\dfrac{\partial W}{\partial\eta}\right)+\dfrac{1}{(z_E-z_W)}\left(\dfrac{\partial V}{\partial\zeta}\right)\right\}^2\right]$ $-C_2\rho\dfrac{\varepsilon^2}{k}$
6	T	$\dfrac{\mu_{eff}}{Pr_{eff,\phi}}$	0

A1.3   Constants of the k-ε turbulence model

No	$\emptyset$	$Pr_{t,\emptyset}$
1	U	1.0
2	V	1.0
3	W	1.0
4	k	1.0
5	ε	1.3
6	T	0.9

C_D	C_1	C_2
0.09	1.44	1.92

APPENDIX A2

SOME CONSEQUENCES OF THE TURBULENT-VISCOSITY HYPOTHESIS

A2.0 Introduction

In this Appendix a brief derivation is provided of the set of equations that is obtained as a consequence of the turbulent viscosity assumption. This derivation is independent of the manner in which the effective viscosity is arrived at.

A2.1 Effective form of complete stress tensor

Consider first, the general form of the momentum equations in tensor form:

$$\frac{\partial (\rho U_i U_j)}{\partial x_i} - \rho U_j = - \frac{\partial \sigma_{ij}}{\partial x_i} \qquad \cdot (A2.1.1)$$

For the purposes of this Appendix, attention is confined to the right hand side of equation (A2.1.1).

The complete stress tensor in turbulent flow can be expressed as:

$$- \sigma_{ij} = - P \delta_{ij} + \mu \left\{ \frac{\partial U_i}{\partial x_j} + \frac{\partial U_j}{\partial x_i} \right\} + \overline{\rho u_i u_j} \qquad , (A2.1.2)$$

where: $p \equiv$ the conventional static pressure,

and $\mu \equiv$ molecular viscosity of fluid.

If the expression for Reynolds stresses (4.3.1) is substituted into equation (A2.1.2), we have:

$$-\sigma_{ij} = - p \delta_{ij} + \mu \left\{ \frac{\partial U_i}{\partial x_j} + \frac{\partial U_j}{\partial x_i} \right\} + \rho \nu_t \left\{ \frac{\partial U_i}{\partial x_j} + \frac{\partial U_j}{\partial x_i} \right\} + \frac{2}{3} k \delta_{ij} \quad ,$$

$$= - \left(p + \frac{2}{3} \right) \delta_{ij} + \left(\mu + \rho \nu_t \right) \left\{ \frac{\partial U_i}{\partial x_j} + \frac{\partial U_j}{\partial x_i} \right\} \qquad ,$$

$$= -p_o \, \delta_{ij} \quad + \quad \mu_{eff} \left\{ \frac{\partial U_i}{\partial x_j} + \frac{\partial U_j}{\partial x_i} \right\} \qquad , \quad (A2.1.3)$$

where, $p_o \equiv p + \frac{2}{3}k$, is the "effective" static pressure, used throughout the text with the subscript removed for convenience,

and $\mu_{eff} \equiv \mu + \rho \nu_t$, is the "effective" viscosity, i.e. transport coefficient of turbulent momentum.

A2.2 Simplifying assumptions

As described in Chapter 2, not all stresses in equation (A2.1.3) are of equal magnitude, when the flow considered is of the three-dimensional, boundary-layer variety. In particular, stresses along the PFD and on planes normal to it are negligible in comparison with those in the other two directions. The mathematical consequences of neglecting such stresses are listed below. .

The diffusion-of-momentum terms alone are, in cartesian co-ordinates:

x - direction:

$$\frac{\partial}{\partial x}\left(\mu_{eff} \frac{\partial U}{\partial x}\right) \quad + \quad \frac{\partial}{\partial y}\left(\mu_{eff} \frac{\partial U}{\partial y}\right) \quad + \quad \frac{\partial}{\partial z}\left(\mu_{eff} \frac{\partial U}{\partial z}\right)$$

$$+ \quad \frac{\partial}{\partial x}\left(\mu_{eff} \frac{\partial U}{\partial x}\right) \quad + \quad \frac{\partial}{\partial y}\left(\mu_{eff} \frac{\partial V}{\partial x}\right) \quad + \quad \frac{\partial}{\partial z}\left(\mu_{eff} \frac{\partial W}{\partial x}\right), \quad (A2.2.1)$$

y - direction:

$$\frac{\partial}{\partial x}\left(\mu_{eff} \frac{\partial V}{\partial x}\right) \quad + \quad \frac{\partial}{\partial y}\left(\mu_{eff} \frac{\partial V}{\partial y}\right) \quad + \quad \frac{\partial}{\partial z}\left(\mu_{eff} \frac{\partial V}{\partial z}\right)$$

$$+ \quad \frac{\partial}{\partial x}\left(\mu_{eff} \frac{\partial U}{\partial y}\right) \quad + \quad \frac{\partial}{\partial y}\left(\mu_{eff} \frac{\partial V}{\partial y}\right) \quad + \quad \frac{\partial}{\partial z}\left(\mu_{eff} \frac{\partial W}{\partial y}\right), \quad (A2.2.2)$$

Z — direction:

$$\frac{\partial}{\partial x}\left(\mu_{eff}\frac{\partial w}{\partial x}\right) \quad + \quad \frac{\partial}{\partial y}\left(\mu_{eff}\frac{\partial w}{\partial y}\right) \quad + \quad \frac{\partial}{\partial z}\left(\mu_{eff}\frac{\partial w}{\partial z}\right)$$

$$+ \quad \frac{\partial}{\partial x}\left(\mu_{eff}\frac{\partial U}{\partial z}\right) \quad + \quad \frac{\partial}{\partial y}\left(\mu_{eff}\frac{\partial V}{\partial z}\right) \quad + \quad \frac{\partial}{\partial z}\left(\mu_{eff}\frac{\partial w}{\partial z}\right).$$

$$(A2.2.3)$$

Examination of equations (A2.2.1) to (A2.2.3) reveals that:

• Neglecting stresses along the PFD implies that all terms of the form:

$$\frac{\partial}{\partial x}\left(\mu_{eff}\frac{\partial U_i}{\partial x_j}\right) \qquad \text{, can be set to zero.}$$

• Neglecting stresses on planes normal to PFD implies that terms of the form:

$$\frac{\partial}{\partial x_j}\left(\mu_{eff}\frac{\partial U_i}{\partial x}\right) \qquad \text{, can be set to zero.}$$

A2.3   Resulting terms representing diffusion

It can be observed that the effective-viscosity approach leads to diffusion terms identical to terms appropriate to incompressible, laminar flows, with molecular viscosity being replaced by effective viscosity, thus:

$$\frac{\partial}{\partial x_i}\left(\mu_{eff}\frac{\partial U_j}{\partial x_i}\right) \qquad . \quad (A2.3.1)$$

In addition, the transport of momentum in the y- and z-directions involve additional terms containing μ_{eff}. In the present work, these have been expressed as additional sources or sinks of the appropriate momenta. For completeness, these terms are listed below:

$$\phi^V = \frac{\partial}{\partial y}\left\{\mu_{eff}\frac{\partial V}{\partial y}\right\} + \frac{\partial}{\partial z}\left\{\mu_{eff}\frac{\partial w}{\partial y}\right\} \qquad , \quad (A2.3.2)$$

and,

$$\mathscr{b}^W \;=\; \frac{\partial}{\partial y}\left(\mu_{eff}\,\frac{\partial V}{\partial z}\right) \;+\; \frac{\partial}{\partial z}\left(\mu_{eff}\,\frac{\partial W}{\partial z}\right) \qquad , \quad (A\ 2.3.3)$$

which are expressed in quasi-orthogonal co-ordinates as follows:

$$\mathscr{b}^V \;=\; \frac{1}{(y_N - y_S)^2}\,\frac{\partial}{\partial \eta}\left\{\mu_{eff}\,\frac{\partial V}{\partial \eta}\right\} \;+\; \frac{1}{(y_N - y_S)(z_E - z_W)}\,\frac{\partial}{\partial \zeta}\left\{\mu_{eff}\,\frac{\partial W}{\partial \eta}\right\}, \quad (A\ 2.3.4)$$

and,

$$\mathscr{b}^W \;=\; \frac{1}{(y_N - y_S)(z_E - z_W)}\,\frac{\partial}{\partial \eta}\left\{\mu_{eff}\,\frac{\partial V}{\partial \zeta}\right\} \;+\; \frac{1}{(z_E - z_W)^2}\,\frac{\partial}{\partial \zeta}\left\{\mu_{eff}\,\frac{\partial W}{\partial \zeta}\right\} . \quad (A2.3.5)$$

A2.4   Effective viscosity in the mixing-length model

Using Equation (4.2.3), the general expression for, effective viscosity is rewritten as:

$$\nu_t \;=\; \ell^2 \left[\left\{\frac{\partial U_i}{\partial x_j} + \frac{\partial U_j}{\partial x_j}\right\}\frac{\partial U_i}{\partial x_j}\right]^{\frac{1}{2}} \qquad , \quad (A2.4.1)$$

It is reiterated here, that, as a consequence of the boundary-layer approximations:

$$\frac{\partial}{\partial x}\left(U_i\right) \;<<\; \frac{\partial}{\partial y}\left(U_i\right) \;\; and \;\; \frac{\partial}{\partial z}\left(U_i\right)$$

and hence terms of this nature may be dropped from the expression (A4.2.1). This done, the expression for effective viscosity, becomes:

$$\nu_t \;=\; \ell^2 \left\{ 2\left[\left(\frac{\partial V}{\partial y}\right)^2 + \left(\frac{\partial W}{\partial z}\right)^2\right] + \left(\frac{\partial U}{\partial y}\right)^2 + \left(\frac{\partial W}{\partial y} + \frac{\partial V}{\partial z}\right)^2 \right.$$

$$\left. + \left(\frac{\partial U}{\partial z}\right)^2 \right\}^{\frac{1}{2}} \qquad , \quad (A2.4.2)$$

and in terms of the quasi-orthogonal co-ordinates:

$$
\nu_t = \ell^2 \left\{ 2 \left[\frac{1}{(y_N - y_S)^2} \left(\frac{\partial V}{\partial \eta}\right)^2 + \frac{1}{(z_E - z_W)^2} \left(\frac{\partial W}{\partial \zeta}\right)^2 \right] \right.
$$

$$
+ \frac{1}{(y_N - y_S)^2} \left(\frac{\partial U}{\partial \eta}\right)^2 + \frac{1}{(z_E - z_W)^2} \left(\frac{\partial U}{\partial \zeta}\right)^2
$$

$$
\left. + \left(\frac{1}{(y_N - y_S)} \frac{\partial W}{\partial \eta} + \frac{1}{(z_E - z_W)} \frac{\partial V}{\partial \zeta} \right)^2 \right\}^{\frac{1}{2}}
\qquad . \quad (A2.4.3)
$$

A 2.5   The generation term in the $k \sim \varepsilon$ model

The general expression for the generation of turbulence energy is (see Rodi [49]):

$$
G = - \rho \overline{u_i u_j} \cdot \frac{\partial U_i}{\partial x_j}
\qquad . \quad (A2.5.1)
$$

If, into this, the expression for the turbulence stress Equation (3.2.1), is substituted, one obtains,

$$
G = \rho \nu_t \left\{ \frac{\partial U_i}{\partial x_j} + \frac{\partial U_j}{\partial x_i} \right\} \frac{\partial U_i}{\partial x_j}
\qquad . \quad (A2.5.2)
$$

Using identical arguments to that in the previous section, this expression for three-dimensional boundary-layer flows is reduced to:

$$
G = \rho \nu_t \left\{ 2 \left[\left(\frac{\partial V}{\partial y}\right)^2 + \left(\frac{\partial W}{\partial z}\right)^2 \right] + \left(\frac{\partial U}{\partial y}\right)^2 + \left(\frac{\partial U}{\partial z}\right)^2 \right.
$$

$$
\left. + \left(\frac{\partial W}{\partial y} + \frac{\partial V}{\partial z} \right)^2 \right\}
\qquad , \quad (A2.5.3)
$$

or, in terms of the quasi-orthogonal co-ordinates:

$$
G = \rho \nu_t \left\{ 2 \left[\frac{1}{(y_N - y_S)^2} \left(\frac{\partial V}{\partial \eta}\right)^2 + \frac{1}{(z_E - z_W)^2} \left(\frac{\partial W}{\partial \zeta}\right)^2 \right] + \frac{1}{(y_N - y_S)^2} \left(\frac{\partial U}{\partial \eta}\right)^2 \right.
$$

$$
\left. + \frac{1}{(z_E - z_W)^2} \left(\frac{\partial U}{\partial \zeta}\right)^2 + \left(\frac{1}{(y_N - y_S)} \frac{\partial W}{\partial \eta} + \frac{1}{(z_E - z_W)} \frac{\partial V}{\partial \zeta} \right)^2 \right\} \cdot (A2.5.4)
$$

A2.6   Concluding remarks

Were the Boussinesq hypothesis (4.2.1) to be an exact relation-
ship, the expressions derived above would be exact within the framework
of the boundary-layer approximations. However, there is strong evidence
to suggest that the hypothesis breaks down under certain conditions as
for example in the following situations.

a) Turbulent stresses $-\overline{\rho u_i u_j}$ are known, through
experimental evidence to be non-zero, even though
the time-averaged or macroscale velocity gradients
are identically zero, (e.g. Launder and Spalding
[34]).

b) Turbulent normal stresses, i.e. $-\overline{\rho u_i u_i}$ can but
be positive; the relationship (4.2.1) would imply
however, that they are dependent upon the sign of
the velocity gradients.

It has been presumed, that, for the situations described in this work,
the effect of neglecting these factors is negligible, and that methods
developed to overcome the defects of equation (4.2.1) (e.g. Tatchell
[60]) are not required to be used. Results presented in Chapter 8,
would appear to substantiate this.

APPENDIX   A3

SOME COMPUTATIONAL DETAILS

A3.0   Introduction

This Appendix contains information relating to the use of the numerical procedure used for the predictions reported in Chapter 7 and 8. The grid dispositions used, as well as matters associated with the use of the computer program incorporating the numerical procedure are described.

A3.1   Discretization of source terms

In Chapter 3, it was mentioned that the discretized form of the source (and/or sink) term for each variable ϕ , was linearized. The discretized balance equation having being obtained by integration of the differential equation over the control volume for each ϕ , the linearized terms involve volumetric quantities. Thus:

$$\int_{\mathcal{V}} s^{\phi}\, d\mathcal{V} \;=\; S_U^{\phi} \;+\; S_P^{\phi}\, \phi_P \qquad\qquad , \;(A3.1.1)$$

where, $\mathcal{V}$ here represents the volume of the control volume for ϕ.

Whatever the nature of the grid-disposition (i.e. uniform or highly non-uniform spacing between grid nodes) used, the value of ϕ_P in (A3.1.1) is presumed to be the average value of ϕ for that control volume. The consequence of the linearization with the above presumption, is an increase in implictness of the discretized ϕ-equation. This may be observed from the following.

The coefficients of the algebraic equation representing the balance of ϕ over the control volume having been assembled in the manner detailed in Chapter 3, the balance equation may be expressed as:

$$\left\{ \sum_{i = E,W,N,S,P_U} A_i^{\phi\prime} - S_P^{\phi} \right\} \phi_P = \sum_{i = E,W,N,S} A_i^{\phi\prime} \phi_i + S_U^{\phi} \qquad \cdot (A3'.2)$$

Then, the coefficient of ϕ_P becomes

$$A_P^{\phi\prime} = \sum_{i = E,W,N,S,P_U} A_i^{\phi\prime} - S_P^{\phi} \qquad \cdot (A3'.3)$$

The enlargement of $A_P^{\phi\prime}$ by S_P^{ϕ} (this quantity itself being always arranged to be negative) helps the coefficients of the reduced form of (A3.1.2), i.e.

$$\phi_P = \sum_{i = E,W,N,S} A_i^{\phi} \phi_i + S_U^{\phi} \qquad ,(A3.1.4)$$

to satisfy the condition,

$$\sum_{i = E,W,N,S} A_i^{\phi} \leqslant 1 \qquad (A3.1.5)$$

with even more certainty than before. Since criterion (A3.1.5) is known[*] to increase the stability of the discretized balance equation (A3.1.4), linearization of source terms is seen to promote stability. Hence, where-ever possible, the source terms detailed in Appendix A1, are expressed in linearized form.

A3.2   The near-wall treatment

The application of wall-functions to the near-wall region, is considered here in discretized form. In Fig. (A3.2.1) below:

---

[*]
See for example Gosman et. al. [24] .
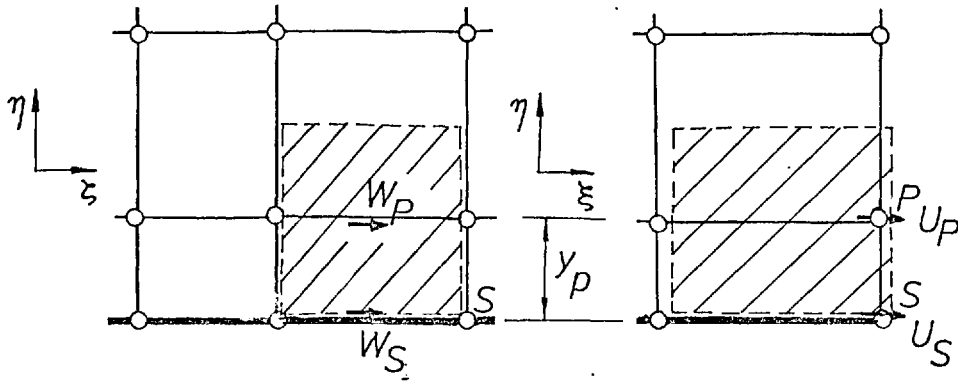
Fig. (A3.2.1)

attention is confined to the control volume associated with grid node. The steep gradients occurring in the region of the wall are accounted for by the use of wall-flux relationships in the following manner. The appropriate flux at the wall is expressed in terms of an appropriate diffusion coefficient at the wall and a ϕ-gradient, with the usual presumption of linear ϕ- variation between grid nodes. Thus,

$$\dot{\phi}_S^{\,\prime\prime} = \Gamma_\phi^S \cdot \left\{ \frac{\phi_P - \phi_S}{y_P} \right\} \qquad , \qquad (A3.2.1)$$

Since this is identical to the form in which diffusion at the interface between adjacent control volumes is calculated in the rest of the calculation domain, the problem reduces to finding an appropriate value of Γ_ϕ^S . Two examples of so doing are described below.

a)   Laminar flow

The region adjacent to wall boundaries is likened to a "Couette-flow" region where the velocity at the boundary away from the fixed wall is prescribed by reference to the solutions to flow-field equations. Thus, the simplified momentum equation in the x-direction,

$$0 = -\frac{\partial \bar{p}}{\partial x} + \frac{\partial}{\partial y}\left\{ \mu\, \frac{\partial U}{\partial y} \right\} \qquad ,(A3.2.2)$$

is used to arrive at diffusion coefficient Γ_ϕ^s in (A3.2.1):

$$\Gamma_U^s = \mu - \left(\frac{d\bar{p}}{dx}\right)\left\{\frac{y_P^2}{U_P - U_s}\right\} \qquad \cdot (A3.2.3)$$

When pressure gradients are absent, this relation reduces to the use of laminar viscosity at the wall boundary. The relation(A3.2.3) moreover, may be used either explicitly using upstream values for calculating terms on the right-hand side or iteratively at any given downstream station. Similar practices may be adopted for all velocity components parallel to wall boundaries. The effect of inclusion of wall-functions upon pressure drop is illustrated in Figure (A3.2.2).

b)   Turbulent flow

Equation (4.5.1) is used to illustrate the practices adopted for turbulent flow. The value of U_τ computed from the $k \sim \varepsilon$ model is used in this illustration.

The wall-shear stress is computed as:

$$\tau_w = \Gamma_U^s (U_P - U_s)/y_P \qquad , (A3.2.4)$$

using the relation (4.5.1) and the definition

$$\tau_w \equiv \rho U_\tau^2 \qquad , (A3.2.5)$$

the following expression is arrived at:

$$\Gamma_U^s = \frac{\rho_P C_D^{\frac{1}{4}} k_P^{\frac{1}{2}} y_P}{\frac{1}{\kappa} \ln\left[E C_D^{\frac{1}{4}} k_P^{\frac{1}{2}} y_P \rho_P / \mu_P\right]} \qquad \cdot (A3.2.6)$$

The underlying assumption behind this expression is the fact that the grid disposition is so chosen that the point p always lies in the fully-turbulent region of the boundary layer where the semi-log law (4.5.1) applies.

As mentioned in Chapter 4, the boundary conditions for the equations governing the transport of k and ε in the two-equation turbulence model, are prescribed in an empirical manner. The practice adopted in the present work is described below.

It is presumed that in the vicinity of wall boundaries to fluid flow, there exists a constant shear-stress region. It is observed that in this region there is near-balance between the generation and dissipation of turbulence energy, k, and its diffusion is negligible (see, for example, Rodi [49]). In the calculation procedure this region is represented by the computational control volumes adjacent to the boundary. The kinetic energy at the grid node corresponding to such control volumes, is calculated from

$$k_P = \frac{\tau_w / \rho}{C_D^{\frac{1}{2}}}$$

$$= \frac{U_\tau^2}{C_D^{\frac{1}{2}}} \qquad , \text{(A3.2.7)}$$

where U_τ is obtained by re-arrangement of equation (4.6.1).

In the constant shear-stress layer, by presuming the length scale to vary linearly with distance from the wall, the dissipation rate ε is calculated from

$$\varepsilon_P = U_\tau^2 \left. \frac{\partial U}{\partial y} \right|_P$$

$$= \frac{U_\tau^3}{\kappa y_P} \qquad . \text{(A3.2.8)}$$

This completes the turbulence modelling of near-wall regions.
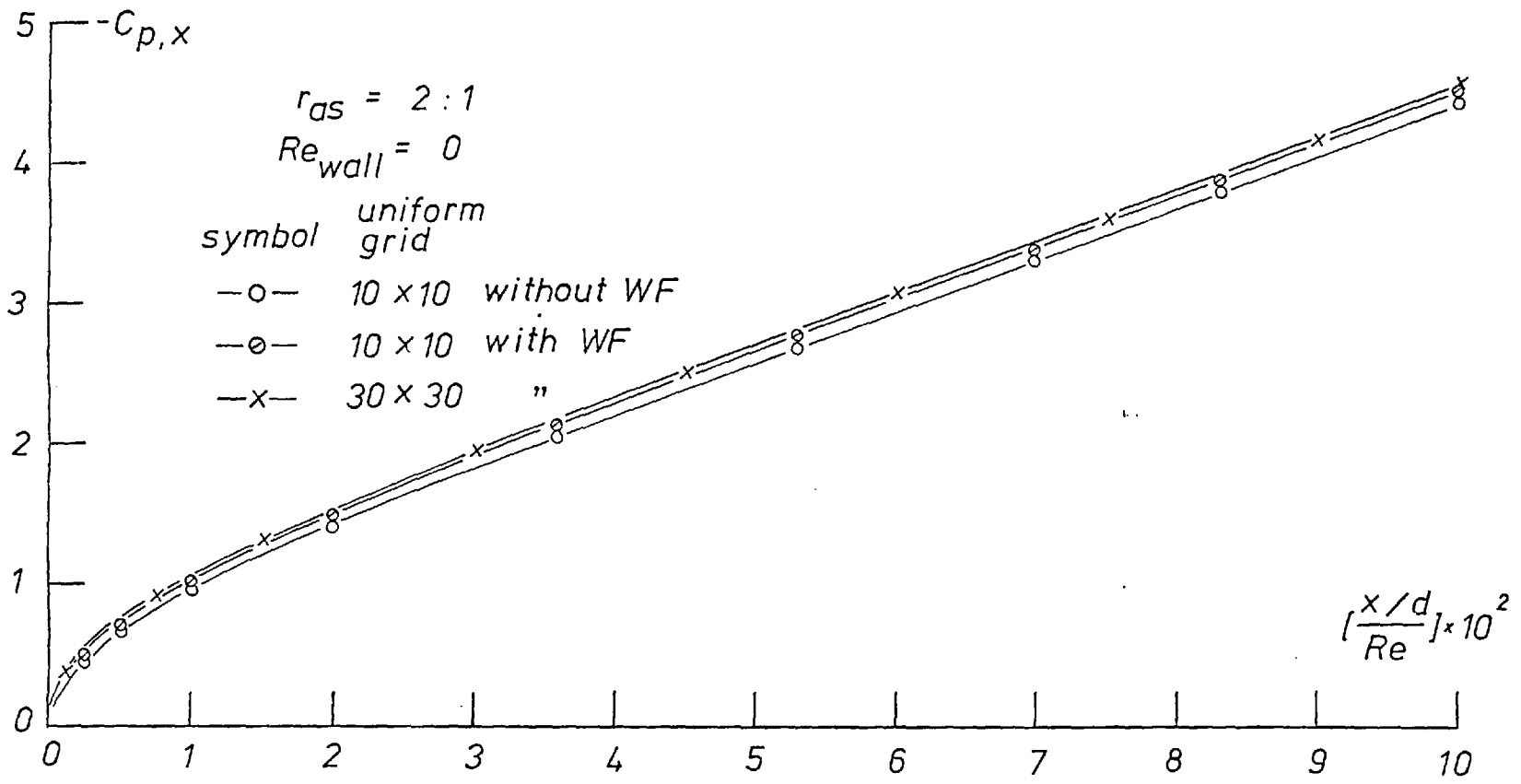
Fig.(A3.2.2) Effect of including wall functions. Laminar
flow in a rectangular - sectioned duct.

A3.3 Grid disposition

As mentioned earlier, a series of grid-dependency tests was conducted for each of the cases for which predictions are reported in Chapters 7 and 8. In most cases, the grid dispositions used are non-uniform; the spacing being grid nodes are so adjusted that a greater proportion of such nodes are disposed in regions of the calculation domain where steep gradients of dependent variables occur, than in regions where such gradients are relatively small.

A3.3.1 Grid in the $\eta \sim \zeta$ plane

The maximum number of grid lines in each of the η and ζ directions, used in the prediction procedure varied from problem to problem. For the prediction of laminar flows reported in Chapter 7, a 20 x 20 system of uniformly spaced grid lines has been found sufficient in obtaining grid-independent solutions.

In the prediction of turbulent flows described in Chapter 8 non-uniform grid spacings were used; a number of grid nodes in the neighbourhood of 400 being used in the $\eta \sim \zeta$ plane. The number of such grid dispositions actually used is too great to catalogue here; however, table (A3.3.1) lists a few examples of grids used predicting the data of Masuda [37] and of Wolf and Johnstone [65] . These examples illustrate the manner in which known distribtuions of velocity are used to choose the grid dispositions supplied to the prediction procedure.

Such dispositions resulted for turbulent flow calculations, in the first grid node away from the wall in each direction lying in the $C_D^{\frac{1}{4}} k^{\frac{1}{2}} y_p \rho_p / \mu_p$ range 50 to 120, (ref. Figure (4.6.1)).

Case No	Data of	Calculation domain	No of calc. planes	Grid size	Grid co-ordinates
1	Masuda [37]		210	18 × 12	η = 0.0,0.01,0.03,0.06,0.1, 0.15,0.23,0.35,0.5,0.65, 0.77,0.84,0.88,0.92,0.95, 0.97,0.99,1.0 ζ = 0.0,0.1,0.3,0.45,0.55, 0.65,0.75,0.85,0.92,0.96, 0.99,1.0
2	Wolf & Johnstone [65] Case II		125	16 × 12	η = 0.0,0.04,0.12,0.24,0.32, 0.4,0.48,0.56,0.64,0.7, 0.76,0.82,0.88,0.94,0.98,1.0 ζ = 0.0,0.05,0.15,0.25,0.35, 0.45,0.55,0.65,0.75,0.85, 0.95,1.0
3	Norbury [42]		150	12 × 12	η = 0.0,0.05,0.15,0.25,0.35, 0.45,0.55,0.65,0.75,0.85, 0.95,1.0 ζ = 0.0,0.05,0.15,0.25,0.35, 0.45,0.55,0.65,0.75,0.85, 0.95,1.0
4	Wolf & Johnstone [65] Case IV		130	20 × 12	η = 0.0,0.01,0.03,0.06,0.1,0.15, 0.25,0.32,0.36,0.42,0.5, 0.58,0.62,0.7,C.8,0.9,0.95, 0.98,0.995,1.0 ζ = 0.0,0.05,0.15,0.25,0.35, 0.45,0.55,0.65,0.75,0.85, 0.95,1.0

Table (A3.3.1)

A3.3.2 Forward step sizes

The marching-integration scheme used in this work permits the choice of variable forward-step sizes, with position along the predominant flow direction. In all cases reported here, the first forward step from the diffuser inlet section was chosen to be in the range of 0.5 to 10 % of the characteristic width, d . This was increased by a constant factor at each subsequent forward step, until a specified maximum value was reached, whereupon this value was kept constant for subsequent steps in the marching procedure. The constant increment factor, used in the present work, lay in the range 1.02 to 1.15 and the maximum value of forward step size in the range 20 % to 100 % of the characteristic width,

A3.4 Computer times

Computations were performed, with a program written in FORTRAN IV* on a CDC 6600 computer. Economy was affected by storing a major portion of the program in compiled form and specifying merely the input information for each run in source form. Compilation times, using an FTN, Version 4.0 compiler, were of the order of 20 secs. Execution times varied considerably from run to run, depending upon the grid sizes used, the turbulence model etc. A typical computational time for a case where integrations were performed at 200 axial stations, until an L/d of about 15 was covered, was 75 secs.

A3.5 Concluding remarks

The information provided in this Appendix indicates that the numerical procedure is flexible and computations are economical to perform.

_____

*This program named STABLE (for Steady Three-dimensional Analyser of Boundary-Layer Equations), is a property of Combustion, Heat and Mass Transfer Limited, 2 Vineyard Hill Road, London SW19.

APPENDIX A4

TABULATED VALUES OF EXPERIMENTAL DATA

A4.0   Introduction

In this Appendix experimental data obtained in the experimental program described in Chapter 5, are presented in tabulated form. The data consist of axial-velocity and static pressure profiles, suitably normalised, across the vertical and horizontal central planes at eight axial stations. Static pressure values obtained from wall static-pressure taps at twelve axial stations are also presented.

A4.1   Effect of included angle on pressure rise
        Experimental conditions

$$r_{as} = 1 : 1; \quad \overline{U}_{in} = 38.5 \text{ m/s}; \quad T_a = 21^{\circ} \text{ C}.$$

No	x/d	$C_{p,x}$ (wall static-pressure tap values) $2\theta =$				
		0°	2°	4°	6°	8°
1	0.0	0.0	0.0	0.0	0.0	0.0
2	0.25	-0.003	0.024	0.049	0.053	0.061
3	0.625	-0.015	0.039	0.068	0.082	0.101
4	1.25	-0.022	0.055	0.118	0.184	0.228
5	2.0	-0.045	0.087	0.181	0.272	0.330
6	3.0	-0.066	0.116	0.245	0.354	0.420
7	4.25	-0.090	0.182	0.307	0.442	0.535
8	5.75	-0.120	0.208	0.394	0.541	0.606
9	7.5	-0.144	0.251	0.447	0.610	0.664
10	9.25	-0.183	0.295	0.489	0.638	0.699
11	11.25	-0.206	0.325	0.531	0.679	0.742
12	13.25		0.376	0.579	0.706	0.761
13	15.0	-0.283	0.348	0.558	0.694	0.750

A4.2   Effect of Reynolds number on pressure rise
        Experimental conditions

$$r_{as} = 1 : 1; \quad 2\theta = 4^{\circ}; \quad T_a = 20.5^{\circ} \text{ C}.$$

No	x/d	$C_{p,x}$ (wall static-pressure tap values) $Re \times 10^{-5} =$				
		1.0	1.16	1.30	1.67	1.73
1	0.0	0.0	0.0	0.0	0.0	0.0
2	0.25	0.029	0.028	0.029	0.029	0.026
3	0.625	0.051	0.051	0.053	0.059	0.058
4	1.25	0.102	0.100	0.103	0.112	0.107
5	2.0	0.198	0.195	0.197	0.198	0.191
6	3.0	0.262	0.260	0.261	0.267	0.257
7	4.25	0.330	0.327	0.327	0.336	0.335
8	5.75	0.380	0.393	0.393	0.403	0.390
9	7.5	0.460	0.455	0.456	0.468	0.458
10	9.25	0.510	0.506	0.498	0.519	0.508
11	11.25	0.558	0.549	0.553	0.564	0.548
12	13.25	0.587	0.582	0.587	0.600	0.584
13	15.0	0.583	0.577	0.579	0.592	0.577

A4.3 Static-pressure traverses: $2\theta = 0^{\circ}$ $(-C_{p,x})$

Experimental conditions

$$r_{as} = 1 : 1; \quad \bar{U}_{in} = 40.1 \text{ m/s}; \quad T_a = 20\,^{\circ}C; \quad z/d = 0.5.$$

No	x/d = y/d =	2.35	4.20	6.10	7.45	9.20	11.6	13.2
1	0.01	0.055	0.0974	0.1380	0.162	0.185	0.206	0.230
2	0.02	"	0.098	"	"	0.186	0.207	0.231
3	0.03	"	"	"	"	"	0.208	0.232
4	0.04	"	"	"	"	0.187	0.209	"
5	0.05	"	"	"	"	"	"	"
6	0.06	"	"	"	"	"	"	"
7	0.08	"	"	"	"	"	"	"
8	0.1	"	"	"	0.163	"	0.210	"
9	0.12	"	"	"	"	"	"	"
10	0.16	"	"	"	"	"	"	0.231
11	0.2	"	"	"	"	"	0.209	"
12	0.24	"	"	"	"	0.186	"	"
13	0.3	"	"	"	"	"	"	"
14	0.36	"	0.099	0.139	"	"	"	0.230
15	0.4	"	0.099	"	"	"	"	"
16	0.5	"	"	"	0.164	"	0.208	"
17	0.6	"	"	0.138	"	"	"	"
18	0.7	"	0.098	"	"	"	"	"
19	0.8	"	"	"	"	"	"	"
20	0.83	"	"	"	0.163	"	"	"
21	0.88	"	"	"	"	0.185	"	0.231
22	0.91	"	"	"	"	"	"	"
23	0.94	"	0.097	"	"	"	0.206	0.232
24	0.96	"	"	"	"	"	"	"

A4.4 Static pressure traverses: $2\theta = 2°$ $(C_{p,x})$

Experimental conditions

$r_{as} = 1 : 1$; $\bar{U}_{in} = 38.5$ m/s; $T_a = 20°$ C; $z/d = 0.5$.

No	x/d = y/d =	0.0	0.35	2.35	4.2	6.1	7.45	9.2	11.6	13.2
1	0.01	-0.011	0.017	0.087	0.146	0.202	0.236	0.278	0.307	0.349
2	0.02	-0.01	"	"	"	"	"	0.277	"	0.345
3	0.03	-0.01	"	"	0.145	"	"	"	"	0.346
4	0.04	"	"	"	"	"	"	"	"	"
5	0.05	"	0.016	"	"	"	0.235	"	"	"
6	0.06	"	"	"	0.144	"	"	"	"	"
7	0.08	"	"	0.086	"	0.203	"	"	"	0.345
8	0.1	"	"	"	"	"	0.236	"	"	"
9	0.12	"	"	"	0.145	0.204	"	0.278	"	"
10	0.16	"	"	"	"	0.205	"	0.279	0.308	"
11	0.2	"	"	"	"	0.206	0.237	"	"	0.346
12	0.24	"	"	0.087	"	0.205	"	0.280	"	"
13	0.3	"	"	"	"	"	"	"	"	0.347
14	0.36	"	"	"	"	"	"	"	0.309	"
15	0.4	"	"	"	0.146	0.206	0.238	0.281	"	0.346
16	0.5	"	"	"	0.147	"	"	"	0.308	"
17	0.6	"	"	0.088	0.148	"	"	"	"	"
18	0.7	"	0.017	"	"	"	0.239	"	"	"
19	0.8	"	"	"	0.147	0.207	"	"	0.307	"
20	0.83	"	0.018	"	"	"	0.238	0.280	"	"
21	0.88	"	0.017	"	"	"	0.237	0.279		"
22	0.91	"	"	0.087	"	0.206	"	0.278	"	"
23	0.94	"	"	"	0.146	"	0.236	0.277	"	"
24	0.96	"	0.016	0.086	"	0.207	"	"	-	-

A4.5 Static pressure traverses: $2\theta = 4°$ $(C_{p,x})$

Experimental conditions

$r_{as} = 1 : 1;$ $\bar{U}_{in} = 40.1$ m/s; $T_a = 21°$ C; $z/d = 0.5.$

No	y/d =	x/d = 0.0	0.35	2.35	4.2	6.1	7.45	9.2	11.6	13.2
1	0.01	0.00	0.014	0.176	0.304	0.383	0.415	0.484	0.487	0.462
2	0.02	"	0.016	"	"	"	"	0.483	0.486	"
3	0.03	"	0.017	"	0.305	"	"	0.481	"	0.461
4	0.04	"	0.018	0.177	0.306	0.384	"	"	0.485	"
5	0.05	"	"	"	0.305	0.383	0.416	"	"	"
6	0.06	"	"	"	"	"	"	"	"	"
7	0.08	"	0.019	"	"	"	"	0.480	"	"
8	0.1	"	"	"	0.306	"	0.417	"	"	"
9	0.12	"	"	"	"	"	0.418	"	"	"
10	0.16	"	0.021	"	0.305	0.384	"	"	"	"
11	0.2	"	0.022	"	"	"	"	"	"	0.462
12	0.24	"	0.025	"	"	0.385	0.420	"	"	"
13	0.3	"	"	0.178	"	"	"	"	0.486	0.463
14	0.36	"	0.026	"	0.306	"	0.422	"	"	0.464
15	0.4	"	0.027	0.179	"	"	"	"	0.487	"
16	0.5	"	0.029	0.180	"	0.386	0.426	"	0.488	0.466
17	0.6	"	0.030	"	"	0.387	0.427	0.481	"	"
18	0.7	"	0.030	0.181	"	0.389	0.425	"	"	0.465
19	0.8	"	0.032	0.182	"	"	"	0.482	"	0.464
20	0.84	"	0.034	"	"	0.390	0.423	"	0.487	0.463
21	0.88	"	0.036	0.181	0.305	"	0.421	0.481	0.486	0.462
22	0.91	"	0.038	0.180	"	0.388	0.418	"	0.485	0.461
23	0.94	"	"	"	"	0.387	0.416	0.480	0.485	"
24	0.96	"	–	–	"	"	–	–	–	–

A4.6 Values of $(U/\bar{U}_{in})$ across the vertical centreplane

Experimental conditions

$2\theta = 0^{\circ}$; $r_{as} = 1 : 1$; $\bar{U}_{in} = 41.2$ m/s; $T_a = 22^{\circ}$ C; $z/d = 0.5$.

No	y/d =	x/d = 0.35	2.35	4.2	6.1	7.45	9.2	11.6	13.2
1	0.01	0.610	0.762	0.731	0.736	0.727	0.715	0.699	0.706
2	0.02	0.796	0.800	0.773	0.775	0.744	0.768	0.741	0.750
3	0.03	0.990	-	-	0.821	0.777	0.808	0 783	0.789
4	0.04	-	0.919	0.869	0.860	0.818	0.841	0.817	0.820
5	0.05	0.992	0.961	-	0.924	0.857	0.870	0.846	0.846
6	0.06	-	-	-	-	0.888	0.897	0.871	0.869
7	0.08	-	-	-	0.977	0.942	0.947	0.917	0.912
8	0.1	0.994	1.016	1.033	1.019	0.990	0.987	0.959	0.950
9	0.12	-	1.016	-	1.048	1.029	1.024	0.996	0.986
10	0.16	0.995	1.017	-	1.064	1.070	1.073	1.057	1.045
11	0.2	0.996	1.017	1.046	1.065	1.076	1.086	1.093	1.091
12	0.24	0.996	1.018	-	1.067	1.077	1.088	1.102	1.111
13	0.3	0.997	1.019	1.047	1.068	1.077	1.089	1.104	1.115
14	0.36	0.998	-	1.048	1.068	1.078	1.090	1.105	1.116
15	0.4	0.999	1.023	1.049	1.068	1.079	1.090	1.106	1.116
16	0.5	1.005	1.025	1.05	1.070	1.080	1.092	1.107	1.118
17	0.6	1.008	1.026	1.05	1.071	1.081	1.093	1.109	1.119
18	0.7	1.010	1.025	1.051	1.071	1.081	1.093	1.110	1.101
19	0.8	1.010	-	1.052	1.072	1.082	1.094	1.104	1.059
20	0.84	1.000	-	1.05	1.073	1.081	1.087	1.073	0.976
21	0.88	0.997	-	1.05	1.072	1.074	1.014	0.986	0.942
22	0.91	0.993	-	1.05	1.043	1.054	0.976	0.951	0.870
23	0.94	0.989	-	0.961	1.003	0.930	0.886	0.869	0.822
24	0.96	0.986	-	0.890	0.966	-	0.830	0.817	-

A4.7 Values of $(U/\bar{U}_{in})$ across the vertical centreplane

Experimental conditions

$2\theta = 2°$; $r_{as} = 1 : 1$; $\bar{U}_{in} = 41.5$ m/s; $T_a = 19.5°$ c; $z/d = 0.5$.

No	y/d =	x/d = 0.0	0.35	2.35	4.2	6.1	7.45	9.2	11.6	13.2
1	0.01	0.849	0.812	0.678	0.636	0.579	0.537	0.511	0.473	0.439
2	0.02	0.887	0.855	0.723	0.678	0.616	0.566	0.535	0.500	0.466
3	0.03	0.921	0.931	0.778	0.724	0.651	0.602	0.565	0.526	0.489
4	0.04	0.965	0.975	0.825	0.758	0.683	0.633	0.590	0.549	0.511
5	0.05	0.991	0.987	0.865	0.793	0.713	0.659	0.612	0.568	0.529
6	0.06	0.994	"	–	0.824	0.740	0.683	0.632	0.584	0.544
7	0.08	0.996	"	–	0.876	0.788	0.729	0.670	0.619	0.574
8	0.1	0.996	"	0.938	0.908	0.830	0.770	0.708	0.648	0.605
9	0.12	0.997	"	0.943	0.918	0.865	0.806	0.743	0.675	0.630
10	0.16	0.997	"	0.949	0.920	0.890	0.857	0.801	0.730	0.680
11	0.2	"	"	"	"	0.891	0.866	0.833	0.774	0.724
12	0.24	"	"	0.950	0.921	"	0.867	0.838	0.799	0.761
13	0.3	"	0.988	0.952	0.920	"	"	0.840	0.807	0.781
14	0.36	"	"	0.947	"	0.888	0.866	0.839	0.805	0.783
15	0.4	0.989	0.989	0.944	"	"	."	0.838	"	0.785
16	0.5	1.000	0.990	0.946	"	0.890	0.867	"	0.806	0.784
17	0.6	1.001	0.991	0.948	"	"	"	0.839	0.807	"
18	0.7	1.001	0.992	0.952	0.919	0.886	0.866	0.838	"	0.782
19	0.8	1.000	0.993	0.954	0.922	0.888	0.874	0.837	0.775	0.736
20	0.84	0.998	0.990	0.955	0.924	0.884	"	0.819	0.738	0.686
21	0.88	0.997	0.989	0.958	0.926	0.872	0.821	0.739	0.661	0.622
22	0.91	0.996	–	0.950	"	0.840	0.787	0.707	0.637	0.601
23	0.94	0.994	–	0.940	0.876	0.777	0.705	0.641	0.580	0.551
24	0.95	0.991	–	–	0.815	0.764	0.634	–	0.536	–

A4.8 Values of $(U/\bar{U}_{in})$ across the vertical centreplane

Experimental conditions

$2\theta = 4°$; $r_{as} = 1 : 1$; $\bar{U}_{in} = 41.7$ m/s; T_a 20° C; $z/d = 0.5$.

No	y/d =	x/d = 0.35	2.35	4.2	6.1	7.45	9.2	11.6	13.2
1	0.01	0.911	0.675	0.550	0.473	0.442	0.386	0.344	0.318
2	0.02	0.943	0.729	0.582	0.498	0.457	0.406	0.361	0.337
3	0.03	0.947	0.784	0.631	0.533	0.487	0.431	0.379	0.351
4	0.04	0.948	0.826	0.667	0.564	0.511	0.451	0.394	0.366
5	0.05	"	0.852	0.703	0.589	0.533	0.470	0.409	0.379
6	0.06	"	0.864	0.734	0.624	0.554	0.487	0.421	0.391
7	0.08	"	0.867	0.782	0.668	0.595	0.518	0.445	0.413
8	0.1	"	"	0.810	0.709	0.631	0.551	0.475	0.431
9	0.12	0.949	0.868	0.816	0.743	0.667	0.581	0.505	0.449
10	0.16	0.950	"	0.817	0.772	0.721	0.637	0.541	0.485
11	0.2	"	0.870	"	0.776	0.737	0.679	0.584	0.523
12	0.24	"	"	0.818	0.776	0.740	0.693	0.614	0.557
13	0.3	0.952	"	0.824	"	"	0.695	0.636	0.589
14	0.36	0.954	0.872	"	"	"	0.696	0.637	0.602
15	0.4	"	0.871	"	0.776	0.738	"	0.637	0.605
16	0.5	0.955	0.872	"	0.775	0.736	"	0.638	"
17	0.6	0.958	"	0.825	0.777	0.735	"	0.641	0.606
18	0.7	0.960	0.871	0.826	0.776	0.738	0.697	"	0.597
19	0.8	0.963	0.873	0.827	"	0.739	0.688	0.597	0.532
20	0.84	0.965	0.875	"	0.777	0.735	0.659	0.561	0.505
21	0.88	0.966	"	0.830	0.759	0.671	0.588	0.501	0.455
22	0.91	"	"	0.825	0.720	0.644	0.565	0.478	0.442
23	0.93	"	0.873	0.751	0.645	0.573	0.466	0.446	0.405
24	0.95	0.950	0.861	0.683	–	–	–	–	–

A4.9 Profiles of $(U/\bar{U}_{in})$ across horizontal planes

a) Experimental conditions

$2\theta = 0^{\circ}$, $r_{as} = 1 : 1$; $\bar{U}_{in} = 39.5$ m/s; $T_a = 22^{\circ}$ c; x/d = 6 : 1.

No	z/d = y/d =	0.05	0.15	0.25	0.35	0.45	0.55
1	0.05	0.763	0.851	0.859	0.877	0.904	0.905
2	0.15	0.788	1.028	1.063	1.061	1.064	1.063
3	0.25	0.790	1.022	1.066	1.064	1.067	1.064
4	0.35	0.810	1.031	1.067	1.065	1.068	1.066
5	0.45	0.819	1.048	1.068	1.067	1.070	1.068
6	0.55	0.825	1.054	1.070	1.068	1.071	1.070
7	0.65	0.811	1.055	1.071	1.070	1.071	1.070
8	0.75	0.810	1.056	1.071	1.071	1.071	1.071
9	0.85	0.789	1.052	1.071	1.071	1.071	1.071
10	0.95	0.798	0.968	0.966	0.976	0.966	0.966

b) Experimental conditions

$2\theta = 0^{\circ}$; $r_{as} = 1 : 1$; $\bar{U}_{in} = 39.5$ m/s; $T_a = 22^{\circ}$ C; x/d = 11.6;
y/d = 0.5.

No	$\frac{z}{d}$	$\frac{U}{\bar{U}_{in}}$	No	$\frac{z}{d}$	$\frac{U}{\bar{U}_{in}}$
1	0.03	0.705	13	0.36	1.102
2	0.04	0.749	14	0.4	1.105
3	0.05	0.759	15	0.5	1.107
4	0.06	0.802	16	0.6	1.106
5	0.07	0.829	17	0.7	1.105
6	0.09	0.882	18	0.8	1.099
7	0.11	0.925	19	0.84	1.068
8	0.13	0.962	20	0.90	0.971
9	0.16	1.030	21	0.92	0.935
10	0.2	1.079	22	0.95	0.845
11	0.24	1.097	23	0.96	0.785
12	0.3	1.101	–	–	–

A4.10   Profiles of $(U/\bar{U}_{in})$ across horizontal planes

Experimental conditions

$2\theta = 2^{\circ}$; $r_{as} = 1 : 1$; $\bar{U}_{in} = 40.5$ m/s; $T = 21^{\circ}$ C

a) $b/d = 1.0862$; $x/d = 2.35$

No	z/b = \ y/d =	0.05	0.1	0.16	0.2	0.3	0.4	0.5
1	0.019	0.669	0.725	0.735	0.738	0.737	0.747	0.750
2	0.038	0.737	0.801	0.809	0.810	0.807	0.831	0.834
3	0.130	0.772	0.904	0.942	0.937	0.941	0.942	0.944
4	0.223	0.839	0.938	0.953	0.941	0.945	0.943	0.945
5	0.315	0.855	0.941	0.957	0.944	0.947	0.944	"
6	0.5	0.865	0.938	0.949	0.949	0.950	0.949	0.944
7	0.685	0.885	0.934	0.948	0.940	0.942	0.940	"
8	0.777	0.867	0.931	0.943	0.935	0.939	0.938	0.942
9	0.870	0.806	0.922	0.940	0.930	0.937	"	0.944
10	0.962	0.693	0.791	0.798	0.784	0.823	0.820	0.840
11	0.981	0.637	0.700	0.705	0.718	0.738	0.730	0.751

b) $b/d = 1.2130$; $x/d = 6.1$

No.	z/b = \ y/d =	0.1	0.3	0.5
1	0.038	0.656	0.636	0.646
2	0.088	0.751	0.758	0.784
3	0.170	0.774	0.882	0.885
4	0.253	0.799	0.888	0.886
5	0.335	0.810	0.890	0.887
6	0.418	0.817	0.891	0.889
7	0.500	0.829	0.891	0.888
8	0.582	0.832	0.892	0.884
9	0.665	0.827	0.887	0.883
10	0.747	0.793	0.882	0.883
11	0.830	0.776	0.878	0.883
12	0.912	0.760	0.803	0.830
13	0.962	0.670	0.690	0.685

(A4.10 continued)

c) $b/d = 1.405$; $x/d = 11.6$

No	z/b	y/d = 0.1	0.3	0.5	No	z/b	0.1	0.3	0.5
1	0.016	0.456	0.433	0.441	10	0.571	0.646	0.798	0.800
2	0.044	0.574	0.521	0.546	11	0.642	0.645	0.798	0.801
3	0.073	0.599	0.584	0.601	12	0.714	0.616	0.794	0.802
4	0.144	0.602	0.716	0.725	13	0.785	0.608	0.788	0.799
5	0.215	0.628	0.795	0.796	14	0.856	0.604	0.716	0.742
6	0.286	0.642	0.805	0.801	15	0.927	0.592	0.584	0.625
7	0.358	0.632	0.807	0.801	16	0.956	0.553	0.528	0.568
8	0.429	0.644	0.803	0.802	17	0.984	0.448	0.427	0.454
9	0.500	0.646	0.801	0.803					

A4.11 Profiles of $(U/\bar{U}_{in})$ across horizontal planes

Experimental conditions

$2\theta=4^{o}$, $r_{as}=1:1$; $\bar{U}_{in}=40.5\text{m/s}$;
$T = 20^{o}C$.

a) $b/d=1.0244$, $x/d=0.35$, $y/d=0.5$

No	z/b	$(U/\bar{U}_{in})$	No	z/b	$(U/\bar{U}_{in})$
1	0.031	0.939	8	0.598	0.953
2	0.070	0.944	9	0.695	0.951
3	0.110	0.952	10	0.793	0.952
4	0.207	0.952	11	0.890	"
5	0.305	0.953	12	0.930	"
6	0.402	0.955	13	0.969	0.950
7	0.500	0.955			

b) $b/d=1.164$; $x/d=2.35$; $y/d=0.5$

No	z/b	$(U/\bar{U}_{in})$	No	z/b	$(U/\bar{U}_{in})$
1	0.019	0.619	10	0.586	0.870
2	0.053	0.773	11	0.672	0.869
3	0.070	0.824	12	0.758	0.866
4	0.088	0.854	13	0.844	0.867
5	0.156	0.866	14	0.912	0.866
6	0.242	0.867	15	0.930	0.864
7	0.328	0.870	16	0.947	0.846
8	0.414	0.872	17	0.981	0.699
9	0.500	0.872			

c) $b/d = 1.426$; $x/d = 6.1$, $y/d = 0.5$

No	z/b	$(U/\bar{U}_{in})$	No	z/b	$(U/\bar{U}_{in})$	No	z/b	$(U/\bar{U}_{in})$
1	0.023	0.486	10	0.430	0.775	19	0.921	0.669
2	0.051	0.570	11	0.500	"	20	0.949	0.591
3	0.079	0.640	12	0.570	0.771	21	0.977	0.458
4	0.107	0.709	13	0.640	0.770			
5	0.135	0.761	14	0.710	"			
6	0.149	0.769	15	0.781	0.769			
7	0.219	0.774	16	0.851	"			
8	0.290	0.775	17	0.865	0.765			
9	0.360	0.774	18	0.893	0.728			

(A4.11 continued)

d) <u>b/d = 1.810, x/d = 11.6, y/d = 0.5</u>

No	z/b	$(U/\bar{U}_{in})$	No	z/b	$(U/\bar{U}_{in})$
1	0.025	0.339	14	0.555	0.639
2	0.036	0.360	15	0.611	0.640
3	0.058	0.388	16	0.666	"
4	0.080	0.430	17	0.721	"
5	0.102	0.471	18	0.776	0.639
6	0.124	0.508	19	0.832	0.602
7	0.169	0.580	20	0.876	0.533
8	0.224	0.634	21	0.898	0.494
9	0,279	0,640	22	0.920	0.454
10	0.334	0.642	23	0.942	0.413
11	0.390	0.641	24	0.964	0.376
12	0.445	0.638	25	0.975	0.357
13	0.500	0.638			